Author:
Kristnama, Ashwin R

Title:
Effect of high velocity oblique impacts on carbon/epoxy laminates

Effect of high velocity oblique impacts on carbon/epoxy laminates

By

Ashwin Rao KRISTNAMA

A dissertation submitted to the University of Bristol in accordance with the requirements for award of the degree of DOCTOR OF PHILOSOPHY in the Faculty of Engineering.

SEPTEMBER 2019

Word count: 49842

Abstract

The ingestion of small hard body particles at high velocities leads to Foreign Object Damage (FOD), against which composite structures are required to be resilient as the development of failure modes and their interactions can result in considerable loss in mechanical performance. Extensive knowledge of the damage process in composites and advanced numerical simulation tools can help to improve FOD resistance at an early design stage. In this work, the behaviour of carbon/epoxy laminates subjected to high velocity oblique impacts is studied. Impact tests at the edge and centre of quasi-isotropic IM7/8552 laminates using a 3 mm steel cube projectile have been conducted over a range of velocities. The extent of impact damage, characterised in terms of fibre failure and delamination area, was observed to increase with increasing impact energy. Beyond the velocity at which laminate perforation was observed, the delamination area decreased with increasing impact energy. To predict the dynamic response of the carbon/epoxy laminates, a Hi-Fidelity Finite Element Method was employed, which combines failure criteria based on Weibull theory and maximum stress, where multiple split paths and delamination were modelled using a cohesive interaction, together with an automated unit cell meshing technique. The results from the baseline impact model were in good agreement with the experimental results for some impact energies. The baseline impact model was further investigated by changing the orientation of the projectile before impact and by varying the number and position of cohesive layers. While the extent of fibre failure was significantly affected by changes in projectile orientation, the extent of delamination was observed to be more dependent on the number of cohesive layers utilised.

The combination of high velocity impacts using small and light projectiles and the subsequent reduction in tensile strength has not received much attention, this research aims at investigating the residual tensile strength of impacted laminates and the damage development due to tension. The tensile strength of the impacted laminates was observed to be strongly dependent on the extent of fibre failure. The contribution of impact-induced delamination to the residual strength has been discussed. Impacted laminates under tension have also been analysed numerically, where the failure stress is strongly reliant on the length of 0° splits. To find a simpler and quicker way to assess the effect of impact damage, this work takes a new approach in comparing machined notches as a potential equivalent for impact damage. As the impact velocity increases, edge machined notches are a very good equivalent for edge-impacted laminates. Generally, all composite structures are shielded for protection against impacts and/or erosion, and to this extent, an experimental high velocity impact study has been conducted on carbon/epoxy laminates with an edge shield. At high impact velocities, the edge shield was observed to significantly reduce the extent of impact damage and the resulting tensile strength.

Acknowledgements

The author acknowledges the support from Rolls-Royce plc for this research through the Composites University Technology Centre (UTC) at the University of Bristol and from the Engineering and Physical Sciences Research Council (EPSRC) through the Centre for Doctoral Training in Advanced Composites at the University of Bristol (Grant no.EP/G036772/1).

I would like to extend my deepest gratitude to my supervisors, Professor Michael R Wisnom and Professor Stephen R Hallett, who have always supported me and have patiently guided me through this research, and their contributions have raised the quality of this thesis.

I am deeply grateful to Dr Xiaodong Xu, who has provided invaluable discussion and support on damage characterisation and modelling. I am genuinely appreciative of Professor David Nowell for his supervision and support during this research. The author also acknowledges the technical staff in the Engineering workshop at the University of Bristol and at the Department of Engineering Science at the University of Oxford for access to testing facilities, their continuous support and expertise.

A special mention to Mr Jun LIU and Professor John Dear, of Imperial College London, for access to the gas gun facility and their precious support. My thankfulness to Dr Oliver Nixon-Pearson at the University of Bristol for carrying out the CT scanning of impacted laminates.

Finally, this would not have been possible without the love and never-ending support from my Mum, Dad, Family, Samantha & friends. Thank you all.

Author's Declaration

I declare that the work in this dissertation was carried out in accordance with the requirements of the University's *Regulations and Code of Practice for Research Degree Programmes* and that it has not been submitted for any other academic award. Except where indicated by specific reference in the text, the work is the candidate's own work. Work is done in collaboration with, or with the assistance of, others, is indicated as such. Any views expressed in the dissertation are those of the author.

Name: Ashwin R KRISTNAMA

Signed: ……..

Date: 19/9/2019

Table of Contents

List of *Figures*

List of *Table*s

List of Abbreviations

CFRP – Carbon Fibre Reinforced Plastics

GLARE – Glass Laminate Aluminium Reinforced Epoxy

FOD – Foreign Object Damage

CT – Computed Tomography

FEM – Finite Element Method

FE – Finite Element

VCCT – Virtual Crack Closure Technique

CZM – Cohesive Zone Modelling

CDM – Continuum Damage Mechanics

FEA – Finite Element Analysis

EIM – Equivalent Inclusion Model

DIC- Digital Image Correlation

CAI – Compression After Impact

LE – Leading edge of laminate

TE – Trailing edge of laminate

CNC – Computer Numerical Control

C.V – Coefficient of Variance (%)

NCC – National Composite Centre

Hi-FEM – High Fidelity Finite Element Method

CLT – Classical Laminate Theory

SCF – Stress Concentration Factor

FMC – Full-Matrix capture

TFM – Total Focussing Method

TSL – Traction-Separation Law

ERR – Energy Release Rate

M1 – Method 1, M2 – Method 2

SPC – Single Point Constraint

RoI – Region of Interest

List of Symbols

ε_c – failure strain

V_s (m/s) – speed of sound

v_{trans} (m/s) – transition velocity

t (mm) – thickness of laminate

P (N)– threshold force / applied load

w (mm) – width of broken fibres

E_D (J)– energy absorbed by laminate through delamination

k – number of delaminated interfaces

A_D (mm^2) – delamination area

G_I (N/mm) – energy release rate in Mode I

G_{II} (N/mm) – energy release rate in Mode II

G_{IC} (N/mm) – critical energy release rate in Mode I

G_{IIC} (N/mm) – critical energy release rate in Mode II

E_F (J) – Energy consumed in breaking fibres

E_{lm} (J) – Linear momentum transfer

E_K (J) **–** Incident kinetic energy of projectile

ρ (kg/m^3)– material density

E (GPa) – Young's modulus

G (GPa) – Shear modulus

v – Poisson's ratio

σ_I (MPa)– Mode I stress

σ_I^* (MPa) – Mode I strength

σ_{II} (MPa) – Mode I stress

σ_{II}^* (MPa) – Mode II strength

η – enhancement factor

α – empirical parameter

σ_{ij} – stress tensor components

X_T (MPa) – strengths of the composite laminate in tension

S_{12} (MPa) – strength of laminate under in-plane shear

σ_i (MPa) – elemental stress

V_i (m^3) – elemental volume

σ_{unit} (MPa) – tensile strength of a unit volume of material

m – Weibull modulus

$e_{f,c}^2$ – failure criteria

X_C (MPa) – compressive strength

σ_{I}^{max} (MPa) – Peak traction in normal direction

σ_{II}^{max} (MPa) – Peak traction in tangential direction

m_p (g)– mass of projectile

v_p (m/s) – velocity of projectile

ε_y – axial strain wave

σ (MPa) – tensile failure stress

$P_{failure}$ (N) – average peak load recorded at failure

A_{total} mm^2 – total cross-sectional area of the laminate

A_{net} mm^2 – net cross-sectional area

A_{ff} mm^2 – area of fractured fibres

D (mm) – damage zone size

c (mm) – Fibre fracture width

f – geometrical parameter for finite width

σ_g (MPa) – applied gross section stress

List of Units

g – gram

ml – millilitres

mm – millimetre

m – metre

µm - micrometre

m/s – metre per second

ms – milliseconds

µs - microseconds

J – Joules

MPa - megapascals

kV – kilovolts

µA – microamperes

° - degrees

Hz – hertz

MHz – megahertz

N – newtons

kN – kilonewtons

1. Introduction

Driven by economics, logistics and expectations of society, innovation in composites is facilitated by the developments in materials, processing methods and design tools. Despite the application of flax fibre composite in secondary aircraft structures of military aircraft during the 1930s, aluminium alloys have been the material of choice until recently. After several years since the first carbon fibre was patented in 1961, the development of better matrix systems and carbon fibres has propelled fibre reinforced plastics to a level where they could compete with metallic airframe structures and perform even better. Research and innovation from the past few decades has allowed the transition from secondary civil aircraft components manufactured from glass, carbon or aramid fibre reinforced composites to large primary aerodynamic structures built from carbon fibre composites, such as the vertical and the horizontal stabilizers in the A320 family in the late 1980s. Since then, there has been an increasing usage of carbon fibre reinforced plastics (CFRP) in civil aircraft replacing aluminium in many primary structures. *Figure 1.1* shows the mass fraction of composite materials in Airbus aircraft generations [1], where composites have overtaken the usage of metals and account for more than half of the structural weight.

Fibre composites are known for their ability to tailor the material to the required properties. Their excellent weight-specific stiffness and strength values allow for lighter structures and higher load capacity, and hence reduced fuel consumption. CFRP usage in primary and secondary aircraft structures allow weight reductions of up to 10% and 20% respectively, as compared to aluminium alloys [2]. While these benefits are gained with

higher material costs, replacing large amount of parts riveted together with fully integrated composite structures, the lower assembly costs can counterbalance the higher material costs.

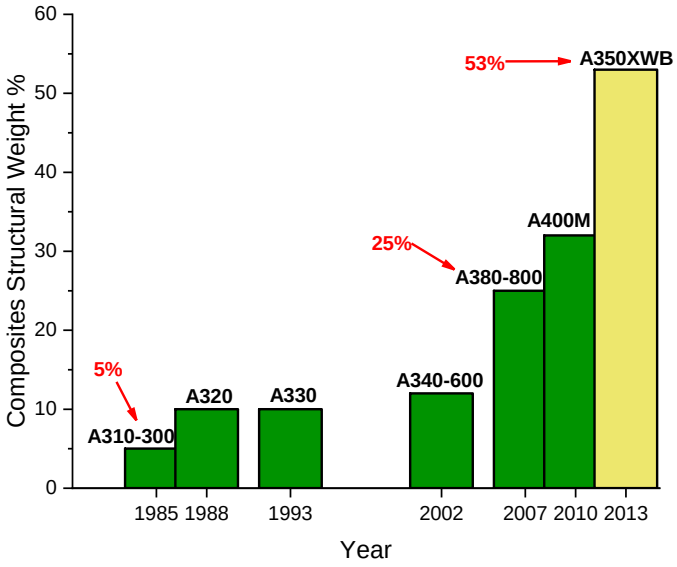

Figure 1.1: Composite structural mass of Airbus aircraft over the years [1].

In the design process of fibre reinforced structures, it is more complex to predict the strength and failure behaviour than for metallic structures. In the development process of an aircraft, many tests are carried out on various structural levels, as shown in *Figure 1.2* [3]. Using reliable computer models which provide robust and trustworthy simulations, the costs of development can be reduced by reducing the number of experimental tests done. The aim is to conduct tests on smaller coupons and verify that the models are reliable, hence tests can be eventually replaced with simulations on a higher structural level.

Despite their distinct advantages over more conventional engineering materials, composite materials do suffer some serious limitations. They have a dramatically lower

impact resistance compared to traditional metallic structures. Impact resistance is defined as the ability of a material to absorb and dissipate energies under an impact loading, where the responses can range from localised damage to total disintegration. In comparison to metals, composite materials behave differently to impact loading and dissipation of the incident kinetic energy of the projectile. For low impact energies, metals absorb energy through elastic and plastic deformation [4]. Even though plastic deformation may cause some permanent structural deformation, its consequences on the load-carrying capability of the component is usually small [5]. Higher incident energies may cause target perforation and while such damage will significantly affect the load-bearing ability of the structure, its effects can be predicted using fracture mechanics principles [6]. In composites, however, the ability to undergo plastic deformation is likely to be restricted resulting in large areas of fracture with reductions in strength and stiffness [7, 8]. As the damage zone is more complex and thus difficult to characterise, it is even more difficult to predict the post-impact load-bearing capability of a damaged composite structure.

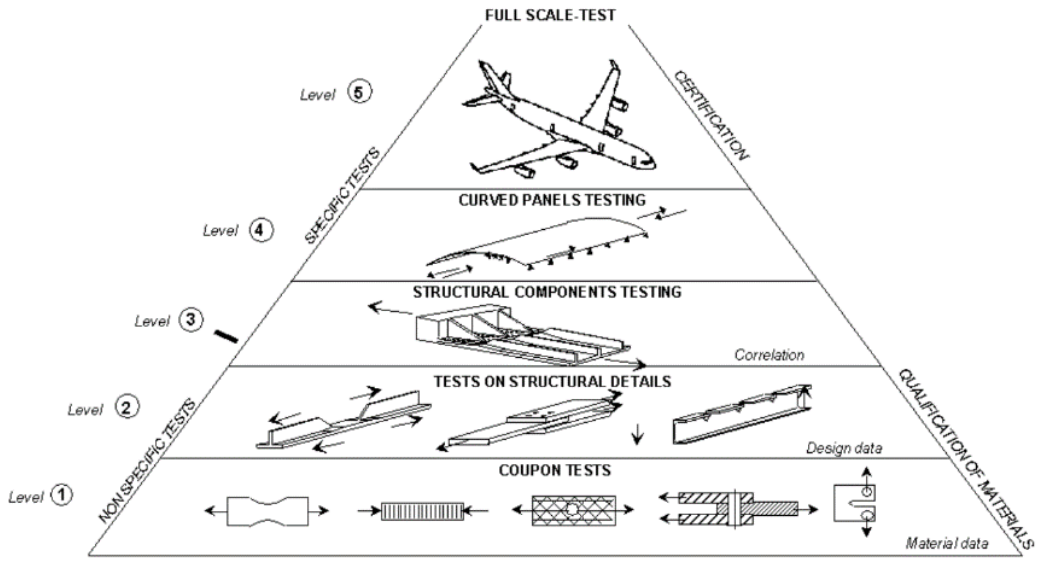

Figure 1.2: Testing pyramid for airframe development [3].

Foreign Object Damage (FOD) is a significant threat to aircraft components, especially in a gas turbine engine, where high rotational speeds can lead to very high velocity impacts. Under an impact, the material properties and structural behaviour are significantly influenced, which can lead to catastrophic failures and low performance. It is therefore important to understand the effect of FOD on component strength and structural integrity. While extensive research has been conducted on high velocity impacts using larger and heavier projectiles, smaller and lighter projectiles that are representative of small, hard and sharp-edged fragments have not been thoroughly researched. Studying the literature also revealed that most studies have either focused on damage development under high velocity impacts or residual strength of impacted laminates separately. While Compression After Impact (CAI) has been the standardised strength measurement of post-impact, tension after impact is equally important for any engine components which can undergo high tensile forces and there has been very little research carried out to investigate the residual tensile strength of thin laminates impacted at high velocities. In the early design stages, the associated development costs for numerous high velocity impact tests can be very high. Therefore, with a good understanding of impact damage mechanisms and powerful simulation tools, it would be possible to reduce multiple coupon level tests at the bottom of the testing pyramid and move to high-fidelity modelling without the need of conducting impact tests.

The research presented here looks at the failure mechanisms in carbon/epoxy laminates when impacted at high velocities using a small and light projectile and addresses the effect of impact damage on the residual tensile strength. The objectives of this work are:

- To conduct high velocity impacts on thin carbon/epoxy laminates using a gas gun, and characterise the impact damage using X-ray Computed Tomography (CT)
- To develop Finite Element models to simulate the dynamic behaviour of thin laminates under high velocity impacts and to predict residual strength of impacted laminates under quasi-static tension
- To investigate similarities to machined notches in terms of residual strength, in order to find a quicker way of assessing impact damage, reduce the number of tests and to improve design
- To assess the importance of an edge shield under high velocity impacts.

An overview of publications studying high and low velocity impacts as well as a summary of published papers on numerical models to predict impact damage is presented in *Chapter 2*. An experimental investigation on the damage mechanisms in carbon/epoxy laminates due to high velocity oblique impacts over a range of velocities is presented in *Chapter 3*. Impact tests are carried out at two different locations on the target as it is of interest to investigate the extent of impact damage close to the edge and away from the edge. The dynamic behaviour of carbon/epoxy laminates subjected to high velocity oblique impacts is then studied in *Chapter 4*, where a Finite Element model is developed and validated against the impact damage observed during the tests. Post-impact, the laminates are tested for residual tensile strength and the results are presented in *Chapter 5*. The residual tensile strength of machined notches is also determined to investigate if they offer a simpler and quicker way to assess the effect of impact damage. In terms of quasi-static tensile modelling, two approaches are considered in *Chapter 6* – creating a finite element model incorporating the characterised impact

damage from *Chapter 3* and employing the impact model from *Chapter 4* for tensile predictions. The residual tensile strength is predicted over a range of impact velocities and the results are compared against experimental results from *Chapter 5*. In addition, the predicted residual strengths of machined notches are compared to impacted laminates, and the results are detailed in *Chapter 6*. The threat of FOD on structural components found in gas turbine engine is investigated experimentally by carrying out high velocity oblique impacts on laminates which have a thin layer of protection on the edge. This study is presented in *Chapter 7*, where the effect of the edge shield on the damage development and residual strength is studied. Concluding remarks and future works are the presented in *Chapter 8*.

2. Literature Review

Composite materials have become popular over the last few decades due to their advantages over other materials in terms of strength, stiffness, low weight, design flexibility, corrosion and chemical resistance. When aircraft structures and aerofoils are subjected to FOD under harsh operating environments, they become vulnerable to various failure modes [9]. Matrix damage, delamination and fibre failure evolve and interact with each other, and these damages can significantly reduce the residual strength of an impacted structure. The response of composite structures to various impact loading scenarios has been reviewed by several authors over the years, e.g. [9-14].

In commercial aircraft, in-flight collisions with birds or hailstones, engine blade loss, runway debris or tool drops are most likely to cause dynamic transverse loading conditions [15]. The structural response is dependent on impact conditions and can vary from elastic impacts without any material damage through barely visible damage to catastrophic failure of the structure [15, 16]. Composite materials have low transverse strength and are more likely to develop significant damage under an impact loading. The impact response of a structure causes different damage behaviour based on the impact velocity. High velocity impacts result in damage localised around the point of impact, while low velocity impacts cause structural deformation under the load of the impactor and the resulting damage can spread to a large area around the impact point [16].

The velocity range from which impacts are classified as ‘high velocity’ or ‘low velocity’ is not clear in the literature. Some sources defined a maximum impact velocity irrespective of the impacted structure. While *Cantwell and Morton* [13] defined low

velocity as impact speed of up to 10 m/s, *Abrate* [10] drew the line at a significantly higher level of 100 m/s. *Liu and Malvern* [17] and *Joshi and Sun* [18] classified the velocity range as a result of the resulting damage. While impact velocity was classified as high when penetration damage occurred, delamination and matrix cracks resulted from low velocity impacts. In contrast, *Choi* [19] reported that high velocity and low velocity impact responses were very similar as long as the energies were the same. Another classification was based on the structural response of the impacted structure. High velocity or ballistic impacts resulted in localised material damage, caused mainly by through thickness stress waves (illustrated in *Figure 2.1* [14]). On the other hand, low velocity impacts were at impact speeds with a long contact duration between the impactor and the target such that the structure is deformed in phase with the impactor. *Davies and Robinson* [20] defined low velocity impacts as impact speeds at which stress wave propagation in the through thickness direction does not influence the resulting damage process. They were able to calculate the transition between low velocity and high velocity impacts for a material assuming the stress wave propagates at the speed of sound. Thereby, for a material with a compressive strain ε_c and speed of sound V_s, the transition velocity is given by:

$$\varepsilon_c = \frac{v_{trans}}{Vs} \tag{2.1}$$

Using typical failure strains between 0.5% and 1%, and V_s = 2000 m/s (for common epoxy composites) [20], the transition velocity between low and high velocity impacts for typical epoxy composites is between 10 m/s and 20 m/s.

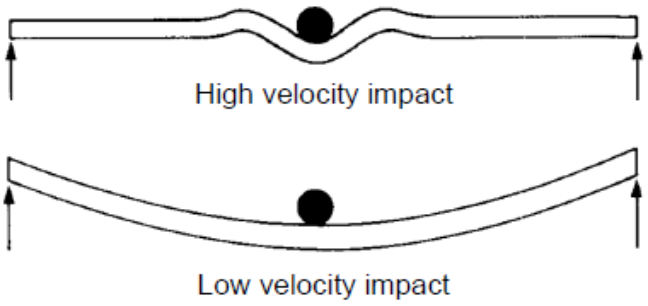

Figure 2.1: Schematic representation of impact response under high and low velocity [14].

2.1 Impact damage description

Complex damage mechanisms in composites, such as delamination and intra-laminar damage, can result from both high and low velocity impacts. The damage initiation and growth are dependent on several factors [21] which include:

(i) Impact source properties such as shape, mass, stiffness and impact velocity;

(ii) composite laminate in terms of stacking sequence, ply moduli, ply orientation and fracture toughness;

(iii) fibre and matrix interactions;

Typically for low velocity impacts, damage is driven by delamination with some fibre breakage while complete perforations are likely to occur under high velocity impacts. Fibre failure in plies and the debonding between plies are the two main mechanisms from which structural failure originates. In addition, the final failure is also affected by other subcritical degradations. A typical impact damage is schematically shown in *Figure 2.2* [22].

2.1.1. Matrix cracking

Under an impact event, the composite structure undergoes complex loading conditions where the bottom of a laminate is in tension with shear stresses between the plies and contact stress at the impact region [23]. Matrix cracking is an early damage mechanism usually observed before delamination. *Abrate* [24] identified two types of matrix cracks and they are illustrated in *Figure 2.3*. Cracks, observed in the bottom ply, were termed as *tensile-cracks*, and they were assumed to be induced by in-plane normal stresses due to flexural deformation of the laminate [25, 26]. The second kind of cracks, *shear cracks*, were observed near the centre ply, where the transverse shear stresses were maximum. Shear cracks were observed to be inclined at approximately 45° around the impact region, where they can also be initiated due to high contact stresses [25, 27].

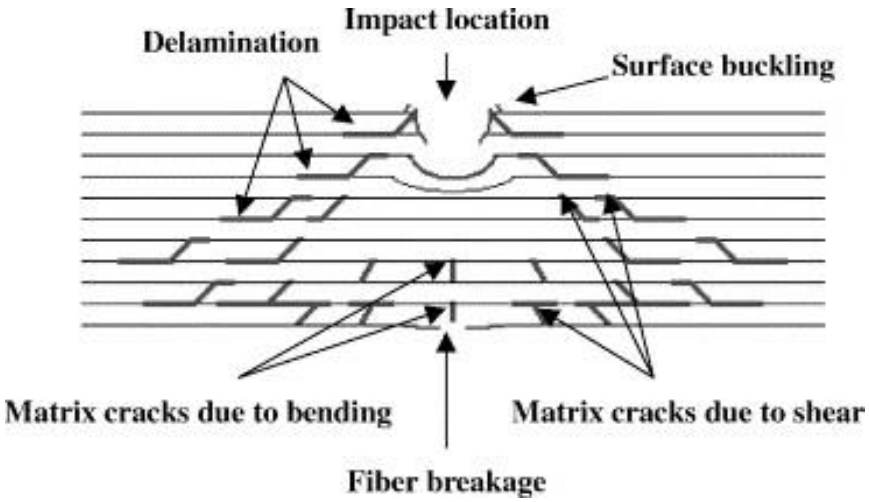

Figure 2.2: Schematic representation of typical impact damage mode for composite laminates [22].

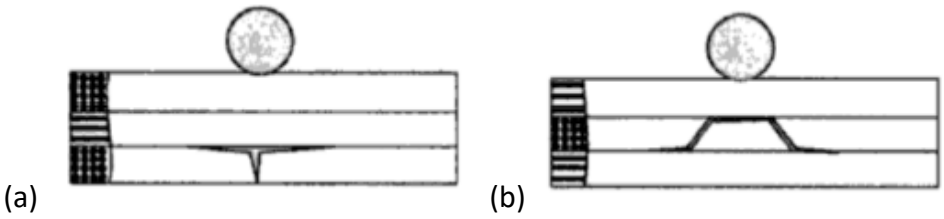

Figure 2.3: Types of matrix cracks: (a) shear crack, (b) tensile crack [24].

The relationship between a laminate's flexural deformation and matrix failure was assessed in several studies. *Cantwell and Morton* [14, 28] investigated high and low velocity impacts on carbon fibre laminates with different lay-ups. From their results, they concluded that the target stiffness is a dominant parameter and controls the mode of fracture. Matrix cracks can propagate from the impacted surface or the back surface towards the centre of the laminate, depending on the laminate's bending stiffness. Assuming that the global deflection of the impacted laminate is negligible, damage is expected to be ruled by contact forces leading to shear stresses within the laminate. Matrix failure can cause the crack to propagate through the upper ply until it is deflected at the interface, resulting in delamination. This interlaminar fracture is seen to extend considerably from the point of impact until it is deflected into a lower ply though matrix shear cracking. This represents a *pine tree* pattern of shear cracks which is developed at the impacted surface and propagates down into the laminate, as illustrated in *Figure 2.4a* [24]. Flexible targets respond primarily in a flexural mode as the bending stiffness is decreased. The high tensile stresses generated in the lowest ply cause cracks in the bottom layers to propagate upwards in an *inverse pine tree* pattern, as depicted in *Figure 2.4b* [24]. These pine tree patterns were confirmed by *Jih and Sun* [26] and *deFreitas et al.* [29] for carbon-epoxy laminates and by *Shyr and Pan* [30] for E-glass laminates, where

multiple 90° matrix cracks were observed to accumulate in the plies prior to complete matrix failure due to tensile loading. *Berthelot* [31] reported a maximum number of cracks per area, also called crack density, in glass and carbon fibre laminates. Damage in laminated composite materials was also described in terms of maximum crack density by *Puck and Schurman* [32] together with *Williams et al.* [33]. While the maximum matrix crack density is a material characteristic, its effect on the mechanical performance of the composite is quite small. However, matrix cracks play an important role in the formation and joining up of delaminations.

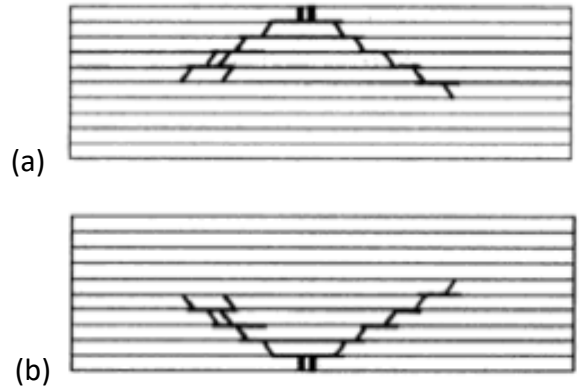

Figure 2.4: Crack patterns in impacted laminates (a) pine tree, (b) inverse pine tree [24].

2.1.2. Delamination

Delamination is of great concern among the several damage modes observed in impacted composite materials. Even small areas of delamination can yield a significant reduction in residual mechanical properties [10, 25]. Driven by interlaminar shear stress and the relatively low mechanical matrix properties, delamination initiates and spreads via matrix cracks [34,35]. While *Olsson* [36] observed delaminations in thin laminates at the mid-plane interface where the contact forces were quite small, *DeMoura and Goncalves* [37] observed delaminations close to the impact point in thick laminates. The bending stiffness mismatching between adjacent plies of different fibre orientations was

how *Liu* [38] explained the formation of delamination due to impact. He claimed that the adjacent plies of different fibre orientations have different bending rigidities, and the difference in rigidities causes delamination at the connective interface. With increasing fibre angle difference between adjacent plies, delamination area was reported to increase. *Olsson* [36], who also supported this claim, found cross-ply laminates to be most likely to delaminate. In 1981, *Takeda* [39] identified the interactions between matrix cracks and delaminations. While investigating [0,90,0] glass/epoxy laminates under impact, delaminations were seen to initiate from the through-thickness matrix cracks parallel to the 0° fibres. The close relation between matrix cracks and delaminations have been confirmed in multiple later papers [24, 30, 40-42].

2.1.3. Fibre failure

Fibre failure due to low velocity impacts was not extensively considered in the literature because most low energy impacts do not cause fibre failure. This damage mode only occurs for high impact energies [14]. Fibre failure is closely related to the final failure of a structure and typically occurs after the onset of delaminations and/or matrix cracks [14, 43]. In the bottom plies, fibre failure is due to the high bending stresses while in the top plies, fibres fail due to compression or shear stresses around the impact region [14, 22, 44]. Fibre failure in thin laminates affects more plies and is more significant as compared to fibre failure in thick laminates, thus pointing out the importance of membrane stresses for fibre failure initiation [44, 45]. Fibre failure is reported to significantly influence the impact response and post-impact behaviour as compared to matrix cracks or delaminations, as fibres are the major load carrying constituents in a laminate [46].

2.1.4. Damage threshold

There exists a certain threshold value for impact energy or contact force above which onset of damage occurs. *Takeda* [39] observed matrix crack formation in glass/epoxy cross-ply laminates for impact tests where the impact velocity exceeded a certain minimum value. *Choi and Chang* [24] also reported a threshold value for impact energy where only above this threshold could significant damage be observed. *Davies et al.* [46, 47] found a load threshold for delamination damage in quasi-isotropic carbon/epoxy laminates of different thicknesses and boundary conditions. Based on their observations of a sudden increase in delamination damage when a critical load was exceeded, an analytical calculation of the energy release rate for a circular delamination within an isotropic plate yielded an equation for delamination threshold load P_c:

$$P_c^2 = \frac{8\pi^2 E t^3 G_c}{9(1-\nu^2)} \tag{2.2}$$

Based on *Eq. (2.2)*, the damage initiation threshold force, P, varies with $t^{3/2}$, with t being the thickness of the laminate. *Cantwell et al.* [48] aimed to investigate the damage initiation threshold in glass fibre reinforced epoxy plates when impacted at low velocities. Experimental data was analysed based on energy and stress models, where the threshold force was observed to increase with increasing test temperature and projectile diameter. *Schoeppner and Abrate* [49] evaluated data from more than 500 impact experiments at the Air Force Research Laboratory (AFRL), however, they could not find evidence of an impact damage energy threshold as the experiments revealed that the damage size grew with increasing impact energy. Instead, they identified a load threshold for delamination onset.

2.1.5. Features influencing impact damage

In addition to impact velocity, impact energy and contact forces, laminate thickness and projectile shapes have been studied for their influences on impact damage. *Ahmadi et al.* [50] investigated the resistance of Glass Laminate Aluminium Reinforced Epoxy (GLARE) laminates with varying thickness subjected to high velocity impacts. The results showed widespread delamination between the glass/epoxy plies during the perforation process. The ballistic resistance of the laminate was evaluated by the specific perforation energy, which was shown to be highest for a thickness ratio glass/epoxy plies to aluminium sheet of 1.45. The findings also revealed that the ballistic resistance increased with an increase in the overall thickness of the target, and this increase in absorbed energy is due to more fibre fracture, bending and membrane stretching. The authors then compared the experimental results against analytical data, where they concluded with an overall agreement showing that 82% - 94% of energy absorbed goes into the global deformation of the aluminium sheets.

Gower et al. [51] carried out experimental and numerical studies on the impact response of laminated Kevlar at impact velocities ranging from 130 m/s to 250 m/s, velocities below the penetration limit of the panels. It was observed that upon impact, penetration of the first few plies occurred before delamination of subsequent layers. A comparative study on the projectile shape was carried out, where more plies underwent deformation with a conical projectile as compared to a hemispherical projectile. The influence of projectile shape on aluminium sandwich composite plates has been investigated both experimentally and numerically by *Kursun et al.* [52]. This was a low velocity impact carried out using steel conical, ogival, hemispherical and flat impactors.

Based on the experiments and a numerical model, the authors concluded that for an impactor with a larger contact surface, very large stress waves are distributed over the entire surface of the target, and thus cause a bigger damage area. A flat-shaped impactor produced a more brittle like damage with low deformation around the contact area, whereas plastic deformations with large damage sizes were observed with the other impactor shapes.

Fuoss et al. [53] conducted a parametric study to determine the effects of key stacking sequence parameters on the impact damage resistance of composite laminates. The three main parameters considered were interface angle, ply orientation relative to a fixed axis and ply grouping. Using a linear quasi-static finite element analysis, internal stress states in the laminate were investigated and delamination damage was predicted for low velocity/high-mass impact. The authors also stated some guidelines to assist designers in selecting stacking sequences to improve the impact resistance of composite structures. The proposed guidelines were to avoid ply grouping, to avoid stacking adjacent plies in similar orientations, particularly at interface angles below 45° and to avoid using multiple interface angles to stack plies. *Lopez-Puente et al.* [54] carried out experimental and numerical investigation on the normal and oblique (45°) responses of a 2.2 mm thick woven CFRP laminates. 90° and 45° impacts between 70 m/s and 531 m/s were conducted using a spherical steel projectile of diameter 7.5 mm with a mass of 1.73 g. Different energy absorption mechanisms were investigated, where the kinetic energy of the projectile was assumed to be absorbed in the form of matrix cracking and delamination below the ballistic limit. Above the ballistic limit, laminate perforation was observed with the extent of fibre failure corresponding to a cylindrical penetration path due to the shape of the projectile, As the impact velocity was increased, the damage

extension decreased. Above the ballistic limit, the authors observed larger extent of damage as impact obliquity is increased. In a more recent study conducted by *Cui et al.* [55], 90° and 45° impacts were conducted on 5 mm thick IM7/8552 composite plates using a 32.7 g steel ball of 20 mm diameter for a velocity range of 21 – 157 m/s. Whilst delamination was observed as the main failure mode for impact velocities of 59 m/s, fibre failure and splitting were dominant at higher velocities of 110 m/s.

Understanding the mechanism of foreign object damage in composite materials is vital to improve the tolerance and reliability of composite structures subjected to high velocity impacts. *Yashiro et al.* [56] characterised the impact damage induced in CFRP laminates due to high velocity impacts. High velocity impacts were carried out on Carbon Fibre Reinforced Polymer (CFRP) laminates with four different stacking sequences, namely a unidirectional laminate, two cross-ply laminates and a quasi-isotropic laminate. Detailed impact damage was observed using optical microscopy and soft X-ray radiography. All laminates revealed a delamination pattern consisting of pairs of fan-shaped delaminations symmetrical about the impact point and elongated delamination along matrix cracks in the bottom ply. Catastrophic ply failure was observed beneath the impact point in the off-axis plies, delaminations were seen to expand from the tips of matrix cracks and the projected damage surface area was found to be impact velocity dependent.

2.2 Numerical damage modelling

Impact has been studied using two-dimensional (2D) and three-dimensional (3D) finite element analyses. 2D modelling approaches provide significantly lower computational costs as compared to 3D analysis. Despite the ability of 2D analysis to

model through-thickness failure subject to the 2D simplification, complex 3D damage patterns cannot be modelled. *Davies and Zhang* [46] compared 2D and 3D approaches and stated that 2D models are valid provided that there are no stresses in the through-thickness direction, and recommended 3D models for impact simulations. *Kaerger et al.* [57, 58] also compared 2D and 3D models for damage prediction and they concluded that more detailed damage predictions, such as sub-laminate buckling, can only be obtained through 3D analysis.

With increasing demand for advanced and robust numerical models for virtual testing in industry and academia, the Finite Element Method (FEM) is employed to study and predict failure behaviour and damage mechanisms of laminated composites. Two approaches exist for impact-induced damage prediction: discrete and Continuum Damage Mechanics (CDM) approaches. The main difference between these two approaches is linked to damage being modelled as separate cracks and delaminations using the discrete approach rather than being distributed over the volume using the CDM approach. Using discrete models for damage, each layer in a composite material is assumed to be linear elastic up to a point at which a failure criterion is satisfied and beyond this point, the element loses its stress carrying capacity. Several discrete damage models have used maximum stress or strain as failure criteria, such as *Hashin* [59] and *Chang-Chang* [60] where the damage parameters for the failure modes of the laminates usually involve fibre fracture in tension, fibre buckling in compression and matrix cracking. On the other hand, the use of CDM consists of damage parameters for several failure modes which are considered as internal variables of the whole constitutive behaviour of the composite material. Thus, the coupling between strain and damage is modelled in a progressive manner and it is possible to mention LaRC04 [61] and *Martinez et al*. [62] among the

damage models using CDM. Interlaminar failure or delamination can be modelled using numerical techniques such as Virtual Crack Closure Technique (VCCT) [63-65] or the Cohesive Zone Modelling (CZM) [66-69].

2.2.1. Cohesive Zone Modelling

Implementation of interface elements with CZM formulations for interlaminar damage has become widespread, eventually leading to a standard feature in most FEA software packages. Cohesive elements are 3D interface elements representing the resin rich regions between the plies of a composite structure. The behaviour of the interface is established using damage mechanics and fracture mechanics, which allow displacement discontinuities across the interface. When the strength limit is exceeded, the stiffness of the interface elements is slowly reduced to zero. The fracture toughness represents the work required to split two adjacent layers [70]. The three different fracture modes, shown in *Figure 2.5* [71], with corresponding fracture energies are modelled. The degradation in all three modes is typically modelled using a bilinear softening constitutive law which relates the traction and separation of the cohesive element in a mixed mode fracture, with the area under the bilinear curve being the critical Energy Release Rate (ERR) [72], as shown in *Figure 2.6*. The main parameters in cohesive zone modelling are the interfacial strength at which damage initiates and the rate at which damage propagates. These material properties can be obtained through double cantilever beam tests for Mode I according to ASTM D5528 [73], end-notched flexure tests for Mode II according to ASTM D7905 [74] and mixed-mode bending tests for mixed-mode loading according to ASTM D6671 [75]. *Cui et al.* [55] who investigated oblique and normal impacts on IM7/8552 provided strength and fracture toughness data, where IM7/8552

material has been characterised at different strain rates with various combinations of stress conditions, including considerable dynamic studies using the split-Hopkinson bar test system. Detailed information of some experiments from the literature [76-83] has resulted in a relatively complete datasheet representing the rate-dependent failure envelope of IM7/8552 laminate [55].

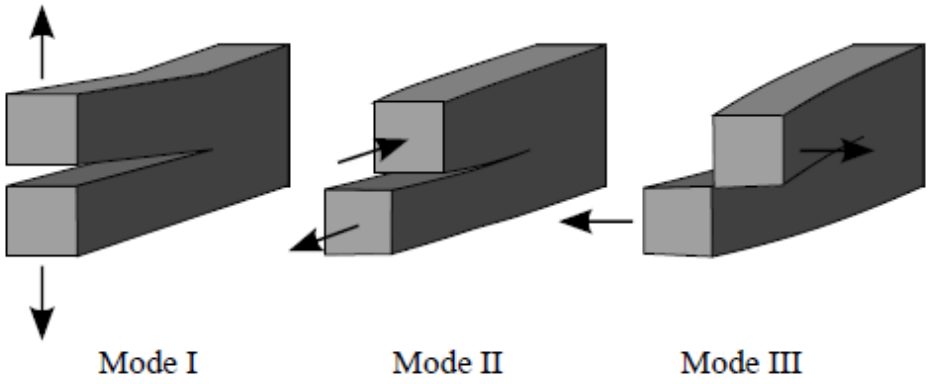

Figure 2.5: Fracture modes: Mode I – tension; Mode II – in-plane shear; Mode III – out-of-plane shear [71].

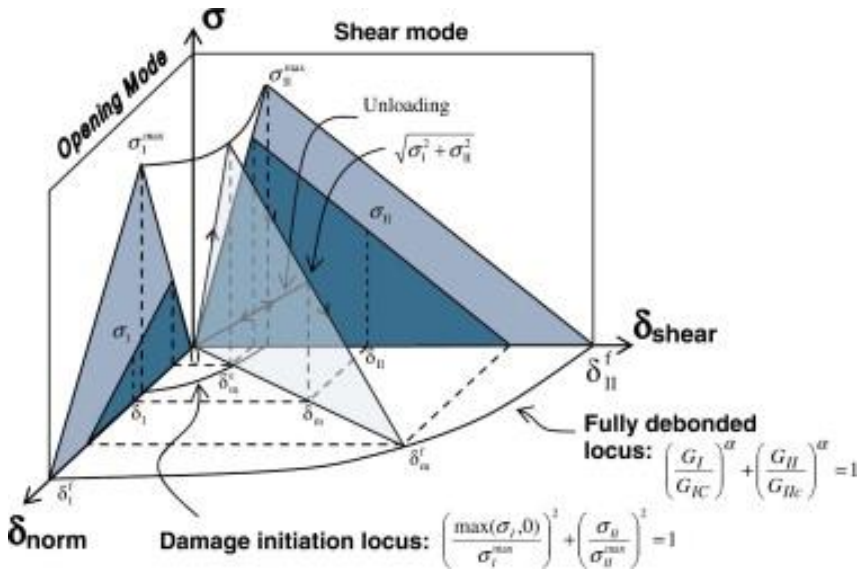

Figure 2.6: Mixed-mode traction displacement relationship for cohesive interface elements [72].

Hallett et al. [84] studied the advantages of using cohesive interface elements to simulate inter- and intra-laminar damage in scaled laminates loaded in tension, with good agreement in relation to experimental results. *Li et al*. [85] used a cohesive-layer model to simulate crack growth in specimens tested under static loading and low velocity impact. Based on available experimental results of load versus crack length response, critical strain-energy release rates were identified and used as input parameters in the model, which was then employed to trace the crack growth for given initial crack lengths. For a given impact load, the authors concluded that the cracks grow to a greater length under dynamic loading than for a quasi-statically applied load and this was due to the result of local vibrations that cause higher frequency oscillations of the crack-opening displacement.

The progressive damage evolution at notch tips using the explicit LS-DYNA code was studied by *Xu et al.* [72] on scaled centre-notched carbon/epoxy laminates. Fibre failure was accounted for by Weibull statistics and splits within plies and delaminations

between plies were simulated using cohesive interface elements. Potential intralaminar split paths were defined in the FE mesh, thus simulating the damage zone at the notch tips, which includes splitting, delamination and fibre breakage. The authors stated that the damage zone is energy-driven, where smaller notches have under-developed damage zones due to lower strain-energy release rates as compared to larger notches having higher strain-energy release rate.

Aymerich et al. [86] investigated the potential of cohesive interface elements for damage prediction in laminates under low velocity impact. The model was developed based on a bilinear cohesive law and was validated by simulation of fracture toughness tests, and then employed to model the impact response of cross-ply graphite/epoxy laminates. The finite element model was successful in predicting the sequence and location of the damage mechanisms under low velocity impact. By studying the influence of matrix cracks on the delamination growth, the authors obtained better delamination predictions when matrix cracks were modelled as well.

2.2.2. Impact modelling approaches

There exist many approaches for materials modelling and numerical simulation of the impact response of composite structures. Instead of using cohesive interface modelling, *Johnson et al.* [87,88] employed cohesive contact definitions with a stacked-shell approach in their impact damage model. The cohesive contact definition imposed traction forces between master surfaces of the lower ply and slave nodes of the upper ply. While the computational costs are drastically reduced as the number of elements used is significantly reduced, the interface properties are degraded based on a stress-displacement model dependent on fracture energies. The impact damage model

developed was successful in distinguishing between the different failure modes in the structure, but the authors concluded that the approach was not practical for larger structural applications. On the other hand, *Heimbs* [89] modelled bird strike on aircraft components and employed cohesive elements instead of a cohesive contact definition because the latter has proven to be much more expensive.

The simulation of high velocity impact on composite structures has been studied by *Schueler et al.* [90]. A modelling methodology was presented which captured intra- and inter- laminar damage and their interactions using shell element layers representing sub-laminates that are connected with cohesive interface layers to simulate delamination. Their work described numerical algorithms for implementing the Ladaveze continuum damage model for the plies and developed a method to derive delamination interface properties. The interface stiffness and cohesive material density were obtained by investigating the energy conversion during impact from simulations using different stacked shell configurations and linear elastic material laws for the sub-laminates and interface layers. The softening effect of the cohesive layers was quantified by comparing the internal energy of the cohesive layers to the intra-ply internal energy for configurations with two, four and eight interface layers for the 17-ply lay-up. Through the convergence study, the best compromise between modelling accuracy and simulation run time was found. The modelling accuracy was then assessed against experimental impact tests using a gas gun. The authors found that the predictive capabilities of the simulation approach were limited as the number and position of interface layers in the through thickness direction affected the damage patterns, where an increase in the interface layers does not result in an increase in modelling accuracy in comparison to the test results.

Xiao et al. [91] worked previously on relatively thin composite plates and developed a quasi-static penetration model for ballistic impacts. Their work was extended to develop a combined numerical and experimental methodology for modelling high velocity impact, damage and penetration mechanics of thick-section S-2 glass/SC15 laminates for a range of impact velocities [92]. The methodology was to use the finite element analysis code LS-DYNA together with the progressive composite damage model MAT_COMPOSITE_DMG_MSC (MAT162). MAT162 accounts for several different failure modes for the fibre and matrix phases of the composite material. Material property variations with strain rate may be included using simple logarithmic based functions included in the model [93]. A set of damage history variables is introduced in MAT162 to relate the onset and growth of damage to stiffness loss in the material. MAT162 uses four different softening parameters, i.e. AM1 and AM2 for fibre damage along material directions 1 and 2, AM3 for fibre shear and crush, and AM4 for matrix crack and delamination. The choice of a set of these four AM values is crucial as a poor choice may lead to prediction of either higher or lower energy absorption capabilities of the composite structure. Softening and element erosion parameters were determined through quasi-static punch shear tests. Validated FE parameters were then used for detailed analysis of impact, stress wave propagation, damage and penetration mechanics. Ballistic experiments over a range of velocities between 50 m/s to 1000 m/s were carried out and the 3D finite model was validated, which can also be extended to optimise laminated structures for maximum energy dissipation. However, the use of MAT162 requires a total of 34 material properties and computational modelling parameters, of which 9 are elastic constants and 10 are failure properties that require standard ASTM tests or composite laminate mechanics theories to be determined.

With less restrictions in mesh density in recent years, it is possible to model composite laminates with solid elements rather than single though-thickness layered shell elements, thus allowing to allocate failure criteria to the solid elements representing the fibres and matrix. *Pernas-Sanchez et al.* [94] developed a numerical methodology to predict the damage behaviour of composite unidirectional laminates subjected to high velocity impacts using a steel sphere of 7.5 mm diameter, and to analyse the influence of projectile's spherical radius. The results were validated against experimental tests in terms of residual velocity and the damage area. Inter- and intra- laminar failures were modelled through a cohesive interaction and stress-based damage criteria respectively, including fibre failure under tension and compression, matrix failure under compression and tension. The geometry of the projectile was found to significantly influence the impact process, where the residual velocity was seen to increase with the spherical radius for a given impact energy. However, the predicted delamination area was found to be smaller than the C-scan images. As delamination spreads via matrix cracks, the stress-based failure criterion for matrix failure is not enough to capture the matrix crack propagation.

Other works in the literature have taken novel approaches in simulating impact damage in composite structures. *Nishikawa et al.* [95] presented a numerical simulation of composite plates subjected to soft-body impact at high velocity for a bird-strike problem. They developed a new contact algorithm based on the Lagrange multiplier method to appropriately predict the impact forces applied to the plate, without causing severe numerical instabilities. The combination of a soft-body impactor and a contact algorithm allowed capturing the transition from global bending deformation due to low velocity impact to shear deformation localised around the impact point at higher impact

velocities. This damage mode transition allowed detecting the threshold velocity for extensive fibre failure and perforation, which can be referred to as a ballistic limit and is a useful indicator of the bird-strike impact resistance of the composite.

Xiao et al. [96] proposed an analytical method to predict the low velocity impact-induced damage area in composite laminates. The novelty of their work lies in the definition and analysis of the interlaminar shear strength to predict the interlaminar shear failure due to impact, where the interlaminar shear strength was predicted by a micromechanical model based on Eshelby's equivalent inclusion model (EIM), instead of carrying out interlaminar shear strength tests. The contact force was estimated based on an energy-balance model and a quasi-static assumption (isotropic and circular damage area), which allowed the relationship between delamination area and impact energy to be obtained. Good damaged area predictions were obtained in comparison to test data, however, as the impact energy was increased, large deviations from the test data were observed. The authors identified some limitations with their method, where the effect of the plate geometrical nonlinearity and energy absorbed in the form of matrix cracking and fibre failure were not considered in the analysis.

The damage initiation and progression in cross-ply CFRP has been experimentally and computationally investigated by *Topac et al.* [97]. The damage growth and strain fields in the through thickness direction were recorded using the Digital Image Correlation (DIC) technique and a high-speed camera. The matrix failure initiation and propagation were modelled via a CDM based failure approach proposed by *Christensen* [98], which assumes matrix crack initiation through the interactions between the tensile and compressive failure strengths of a ply in normal orthotropic directions and the absolute

values of transverse and longitudinal shear strengths. The authors found two different failure modes depending on the stacking sequence. For a $[0_7/90_4]_s$ lay-up, delamination initiates in the bottom 0°/90° interface followed by matrix cracks, which grow towards the impact point, thus causing delamination in the upper ply. For a $[90_7/0_4]_s$ lay-up, delamination of the lower interface occurs after vertical matrix cracks initiate on the lower 90° layers.

Studying the literature for high velocity impact modelling approaches, it is worth mentioning that none of the cohesive formulations employed takes into consideration the enhancement effect of the through-thickness compression on shear behaviour in order to correctly capture the Mode II behaviour under an impact loading. In addition, no papers were found on modelling potential split paths in laminates subjected to high velocity impacts. The use of potential split paths can be particularly interesting for high velocity impacts, where the impact damage zone behaviour can be accurately modelled together with different failure criteria for intra- and inter-laminar failure.

2.3 Residual strength

Composite materials offer numerous advantages over their metallic counterparts. However, they are prone to a wide range of defects and damage which may significantly reduce the residual strength. In the case of a composite structure, the damage caused by high velocity impacts involves delamination and fibre failure. Generally, the damage area extends to a significantly larger area than the visible damage area. Components found in aircraft engines can undergo compressive, tensile and cyclic loads, and it is of interest of investigate the residual strength of impacted structures which can be subjected to any of these loads.

In the early 90's, *Reifsnider et al.* [99] predicted the tensile strength after impact of composite laminates as a function of the damaged area caused by impact. The model developed in their work uses a closed-form solution for an infinite plate containing an elliptical inclusion given by *Lekhnitskii* [100] and an average stress criterion applied at ply level. The approach is based on the strength of the laminate being controlled by the stress concentration in the undamaged material around the impacted region. The size and shape of the damage were measured experimentally, and their values were used as an input to the stress analysis of an elastic inclusion and as an input to a ply-level failure criterion.

Dorey and Sidey [101] used a 6mm diameter steel projectile fired from an airgun with impact speeds up to 300 m/s to investigate ballistic response of carbon/epoxy composite laminates of thickness 3mm with quasi-isotropic layup. Residual tensile tests were conducted post impact. It was found that specimens impacted at a ballistic velocity of 60 m/s – 80 m/s showed maximum damage area and lowest residual strength compared to specimens impacted above the ballistic velocity. The residual tensile strength was observed to vary inversely proportionally with the impact energy at low impact speeds, until a critical value where it drops rapidly. Above the ballistic limit, relatively clean holes were punched and the residual strength was increased. *Horsfall et al.* [102] investigated the residual compressive strength of 10 mm E-glass/polyester laminates with ballistic impact damage. The projectile used was NATO standard 7.62 mm x 51 mm ammunition with muzzle speed of 841 m/s. The study showed that the reduction in residual strength was directly proportional to the amount of kinetic energy absorbed by the laminates, irrespective of whether the laminate was perforated or not.

Wang and Callinan [103] manufactured tensile, compression and shear specimens which were used for ballistic testing at impact velocities between 200 m/s and 1000 m/s. Various projectiles with 7.62 mm, 12.7 mm and 20.0 mm calibres were used. The results showed that above the ballistic limit, with the overall damage area being significantly larger than the projectile size, the residual strength of the specimen with ballistic damage is not significantly lower than that of a specimen with a machined hole of the same diameter as the projectile calibre. *Zhou* [104] conducted low velocity impact tests on thick glass fibre reinforced woven fabric laminates and investigated the residual compressive strength. Damage initiation was identified using damage force and the incident kinetic energy. The impacted panels failed by buckling and they retained between 20% - 30 % of the strength under compressive loading.

In the last decade, many works have focussed on the prediction of residual strength of composite structures after impact. For a low velocity impact, *Koo et al.* [105] looked at predicting the residual strength of composite structures with impact damage by using the characteristic length of the composite with the hole corresponding to the impact damage area. The prediction results using the corresponding hole diameter showed good agreement with experimental results. *Kannan et al.* [106] assessed the residual strength of completely and partially penetrated laminates due to impact loads by idealising the damage locations as holes and cracks [107]. For velocities leading to complete perforation, the residual strength was observed to be the same as the static strength of a laminate having the same diameter as the impactor. For impact velocities lower than the penetration velocity, an empirical relation was proposed to predict the residual strength based on the kinetic energy absorbed by the laminates.

To predict the residual strength of any impacted composite structure, it is important to model the continuous fibre breakage process under a specific loading, where the interactions among the different failure mechanisms within the impact damage zone can be simulated. Except for a numerical study on residual tensile strength of centre-notched laminates [72], there is no evidence found in the literature where the progressive damage development has been modelled to predict the residual tensile strength of high velocity impacted composite structures.

2.4 Conclusions

Over the years, there have been many experimental studies on high velocity impacts, where impact induced damage has been assessed using numerous techniques and has been quantified in terms of damage area, amount of fibre fracture, impact energy and residual velocity. A multitude of parametric studies have also been conducted. Furthermore, using commercial software packages available, high velocity impact simulations have been successful. Based on the two works found in the literature which focussed on normal and oblique impacts [54,55], the authors stated that obliquity significantly affects the impact damage. As such, this research will look at a combination of high velocity oblique impacts, impact damage assessment using non-destructive techniques and investigation on the residual strength. While previous studies have employed larger and heavier spherical projectiles, a steel cube projectile is chosen for this present study as it is more representative of small, hard and sharp-edged fragments which may be ingested in aircraft engines.

In terms of residual strength, the work in the literature mostly looked at low velocity impacts or Compression After Impact (CAI). While CAI has been the standardised

strength measurement for many composite structures subjected to high velocity impacts, it is equally important to investigate the tensile strength degradation for structural components subjected to high tensile forces. It is to be noted that carrying out high velocity impacts can be an expensive test programme in the early design stages. In terms of residual strength, there is no study in the literature comparing impacted laminates to laminates with machined notches under quasi-static tension. As such, this research takes a new approach in comparing machined notches as a potential equivalent for tension after impact tests. While all structural components susceptible to impact damage and/or erosion have a protective shield, it is of interest to investigate the effect of the shield on the impact damage and residual strength.

3. Impact study – Experimental

The effect of foreign object damage (FOD) on composite structures represents a high level of concern as damage can take various forms such as matrix cracks, delamination, fibre/matrix debonding, pull-out and fibre fracture. Since catastrophic structural failure arises from a combination of these factors, composite components are required to be resilient against FOD induced by localised high velocity impact events. To this extent, it is important to understand the mechanisms behind FOD in composite materials in order to improve FOD resistance at an early design stage.

This section describes the experimental works carried out on thin carbon/epoxy laminates. Initially, a parametric study was conducted during the *Extended Project* [108] to investigate different impact scenarios in terms of damage induced. Impact tests were carried out at high velocity using a gas gun and the damage post-impact was studied using Ultrasonic C-scan. Then, a second set of impact tests was conducted for two different oblique impact configurations over a range of velocities and the damage process was characterised using X-ray Computed Tomography (CT) scans.

3.1 Initial Impact study

The high impact velocity considered was around 300 m/s, where impacted laminates revealed varying damage extent for different configurations considered. As such, it was possible to study the effect of thickness, impact position and impact angles on thin composite laminates.

3.1.1 Material and procedure

The material used is Hexcel HexPly® IM7/8552 carbon-epoxy pre-preg with ply thickness of 0.125 mm. Quasi-isotropic stacking sequences $[-45/0/45/90]_s$ and $[-45/0/45/90]_{2s}$ were chosen for the laminates and after curing, the laminates have a nominal fibre volume fraction of about 60% according to the manufacturer's specifications. The nominal overall thicknesses are 1 mm and 2 mm, which are very close to the actual specimen thickness. *Table 1* summarises the test matrix for both high velocity impact events. Non-impacted laminates of 1 mm and 2 mm thicknesses were used as baselines. The laminates, 140 mm x 20 mm, were hit on the two edges at different angles, using a 3mm steel cube of mass 0.22 g as the projectile. A cube projectile was chosen for this study as it is more representative of small sharp-edged particles ingested in aircraft engines, as compared to other previous studies which employed larger and heavier projectiles [54,55,109]. The edges of impact points were referred to as the leading edge (LE) and trailing edge (TE), as depicted in *Figure 3.1*. The arrows in *Figure 3.1* represent the impact angle.

The gas gun available at University of Oxford, as depicted in Figure 3.2 [110], was used for carrying out the high velocity impact tests. The gas gun consists of a compressed gas reservoir, a breech, a pair of clamps, a 1.3 m long barrel of 12.5 mm diameter, a sabot arrester and a target support. A cylindrical sabot manufactured in the workshop is used to support projectile during its acceleration along the barrel. Once the sabot and projectile are positioned and clamped inside the breech, the sabot is accelerated by releasing the clamps after reaching the desired level of pressure. A sabot arrester, positioned at the end of barrel, stops the sabot and allows the projectile to travel by inertia. The projectile

strikes the target, which is supported at its base as a cantilever. The boundary condition imposed

Table 3-1:Test matrix for impact tests.

Number of specimens	Thickness/ mm	Impact position	Impact angle/ °
5	1	-	-
5	1	LE	90
5	1	LE	45
5	1	TE	45
5	2	-	-
5	2	LE	90
5	2	LE	45
5	2	TE	45

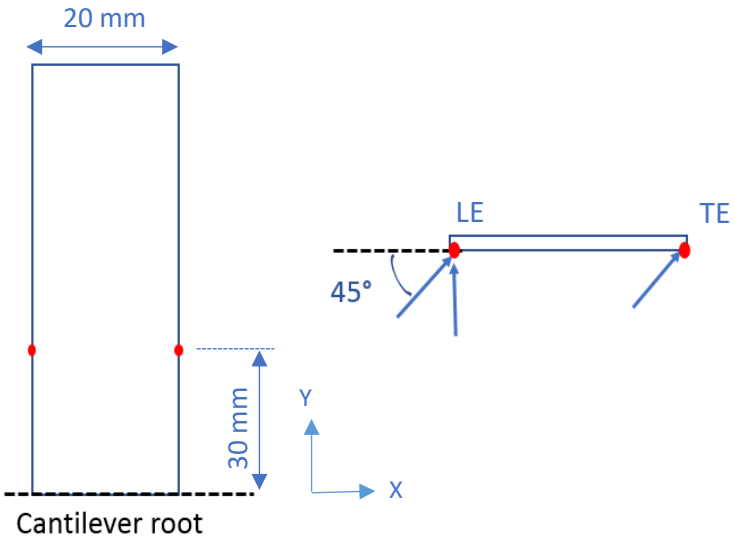

Figure 3.1 :Schematic of specimen and impact configurations, where the front view is shown on the left and the top view on the right. The red dot represents impact locations.

on one end of the target was achieved through a mechanical fixture. The fixture can rotate about the longitudinal specimen axis (Y axis) and translate perpendicular to the gun axis (X axis). It can also be adjusted for height (Y axis). Therefore, the laminate can be positioned at the required angle and position in front of the barrel. The target is clamped over a length of 40 mm from one end onto the mechanical fixture, which is rigidly fixed during the tests.

Two optical sensors placed 50 mm apart along the barrel read the time as the sabot passes these two points. The velocity of the projectile was recorded at 300 m/s (C.V. 2.0 %). Previous work has shown negligible rotation of the sabot and projectile in the barrel of the gun [98], however it was not possible to control the rotation of the cube once it leaves the sabot. A high-speed video camera (Photron Ultima APX-RS) was employed to record the impact process. A lamp was used to ensure enough lighting and the camera was configured to obtain 30000 fps. *Figure* 3.3 shows an example of a video sequence observed from 45° impacts to the LE and TE at 300 m/s. Visually, an impact to the LE results in a larger extent of fibre failure compared to an impact at the TE. In the present study, the residual velocity of the projectile was not determined.

Post-impact, ultrasonic C-scans were conducted on one impacted laminate for each configuration to investigate the internal damage. This type of scan captures reflections coming back from the sample after a wave is emitted from the probe. A probe frequency of 10 Hz and focal length of 76 mm was used. Measuring the amplitude and the time along the waveform allows gathering information about the internal damage of the impacted laminates.

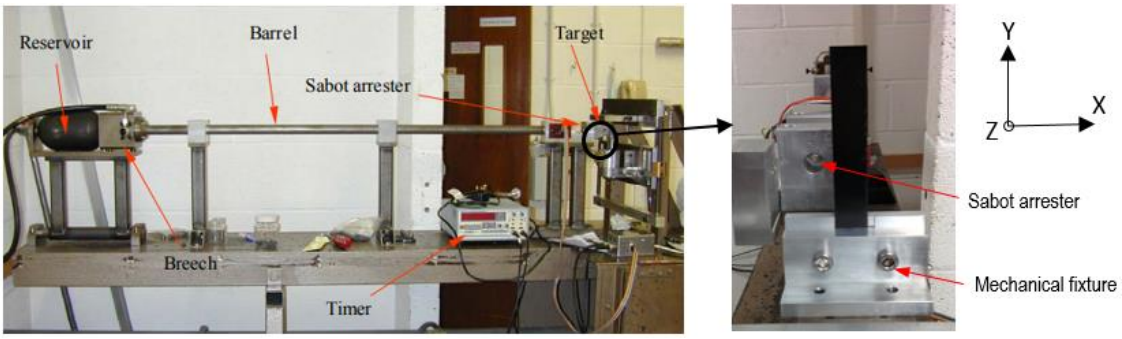

Figure 3.2: High speed impact test setup [110].

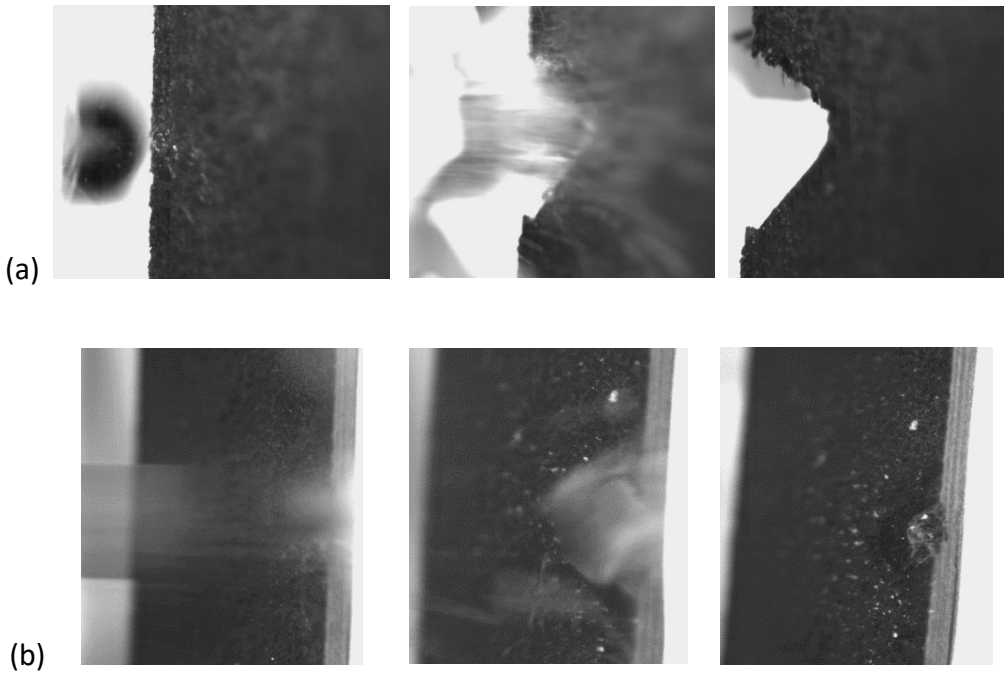

Figure 3.3: Impact sequences for (a) 45° impact to the LE and (b) 45° impact to the TE.

3.1.2 Effect of thickness

The effect of thickness on high velocity impacted laminates can be investigated from the internal damage seen in the C-scans as shown in *Figures 3.4a* and *3.4b*. The variations in colour around the impact point represent the extent of internal damage, i.e delamination. The dark blue background in *Figure 3.3a* and the orange background in *Figure 3.4b* represent the back surface of the laminate. The delaminated interfaces, represented by different colours, are also indicated in *Figure 3.4.* A direct comparison

between the two C-scan images in *Figure 3.4* shows that the 1 mm thick specimen has a larger propagated delamination area than the 2 mm thick specimen, as represented by the white boundaries. Under an impact event, delamination migrates via tensile cracks that form towards the back surface of the laminate due to bending. As thinner laminates are less stiff than thicker laminates, delamination propagates to a larger extent.

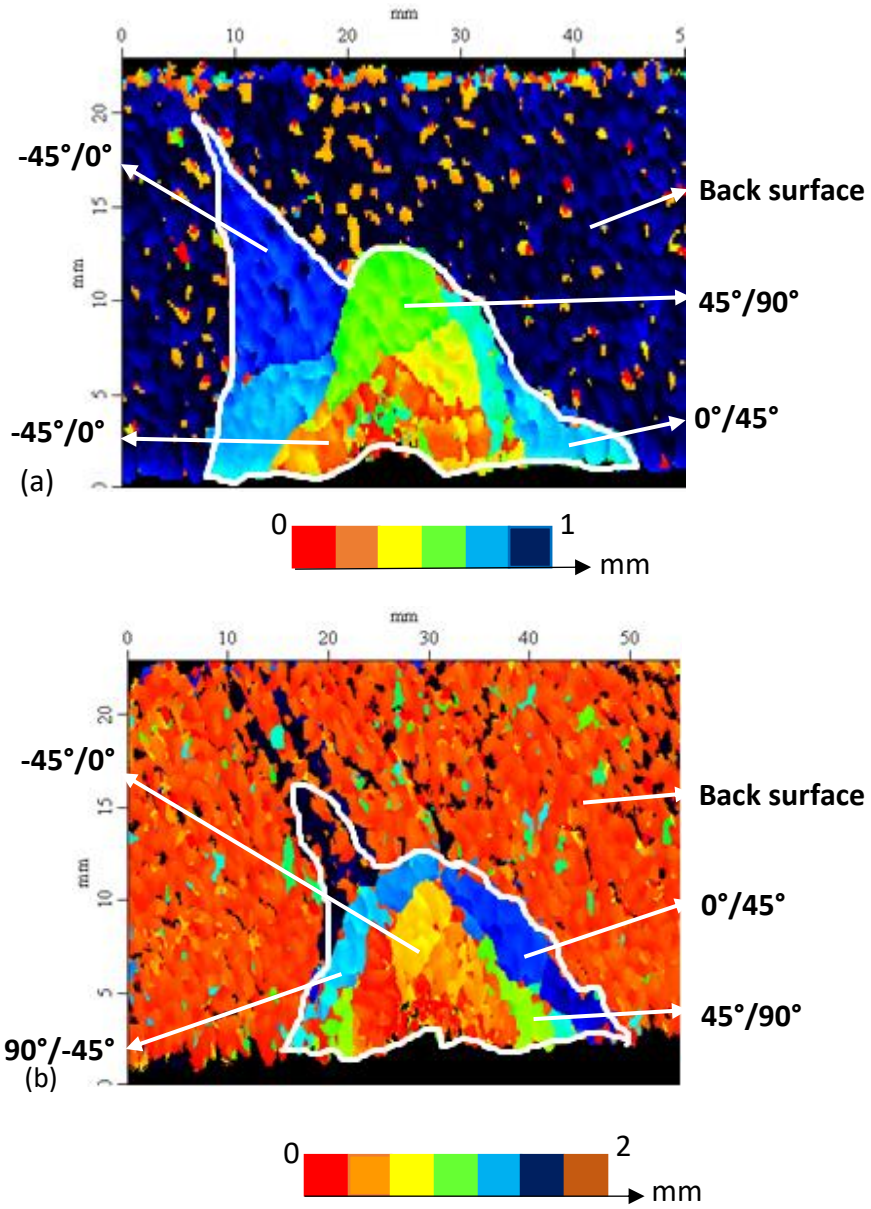

Figure 3.4: C-scan images for high velocity impacted laminates (a) 1 mm thick (b) 2 mm thick with impacts at 90° to the leading edge (LE).

3.1.3 Effect of impact position

The effect of impact position on the internal damage can be examined from *Figures 3.5(a-d).* 1 mm thick laminates subjected to high velocity impacts at 45° to the leading edge (LE) and the trailing edge (TE) are considered. For both LE and TE impacts, the closest and furthest surfaces of the laminate from the probe are analysed. For the case of LE impact, the projectile strikes the edge of the laminate at an angle and perforates the full thickness until it leaves the laminate. For impact at the TE, the projectile impacts the edge of the laminate, but only perforates a fraction of the thickness before leaving the laminate. This difference is shown by the size of the void present at the edges in *Figure 3.5a* and *3.5c*. A leading edge impact showed a larger amount of fibre fracture as compared to a trailing edge impact and the extent of delamination is also larger in the laminate impacted at 45° to the LE, as depicted in *Figures 3.5b* and *3.5d*.

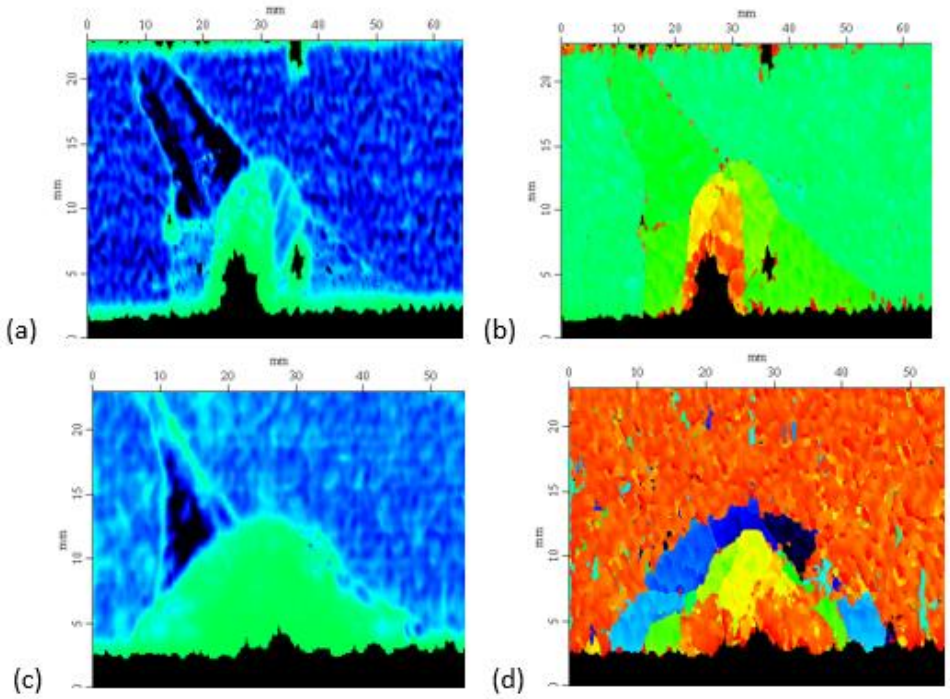

Figure 3.5: C-scan images for high velocity impacted laminates. Laminates are 1mm thick and hit at the LE (a, b) and at the TE (c, d) at an angle of 45°

3.1.4 Effect of impact angle

To investigate the effect of normal and oblique impacts on the damage extent, microscopic images of the high velocity impacted laminates are shown in *Figures 3.6a* and *3.6b*. Oblique impacts to the edge of the laminates revealed a larger extent of fibres broken as compared to impacts normal to the edge. Visually, this is confirmed by the size of the void at the edge of the laminate in *Figure 3.6*. For normal impacts, the projectile strikes the laminate and promotes a damage area equal to the void present at the edge in *Figure 3.6a*. For oblique impacts, the trajectory of the projectile promotes a damage area equal to the semi-elliptical void present at the edge, where the edge represents the minor axis of the ellipse. The schematic shown in *Figure* 3.7 illustrates the effect of obliquity on the laminate. The extent of impact damage is strongly dependent on the

trajectory of the projectile, where the laminate is expected to experience more fibre failure when impacted at 45°.

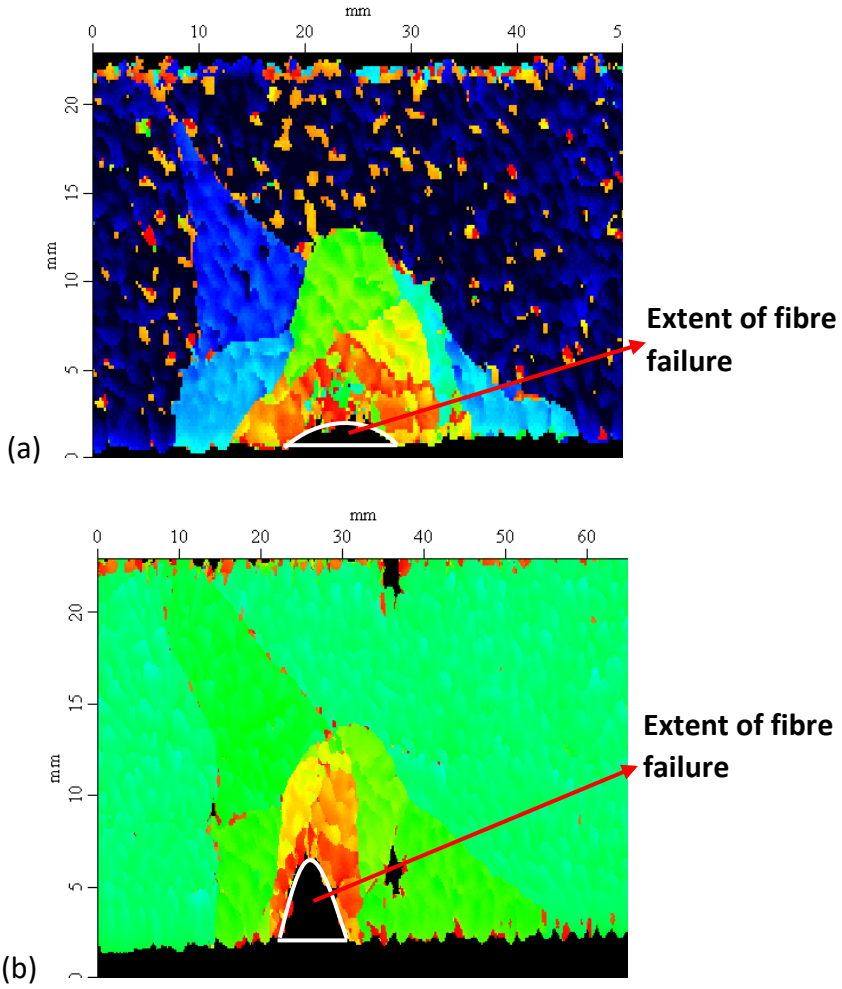

Figure 3.6: 1mm thick laminate impacted at (a) LE at an angle of 90° and (b) LE at an angle of 45°.

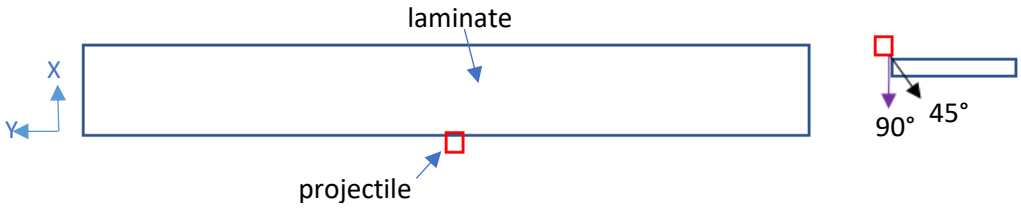

Figure 3.7: Sketch of the impact on composite laminate – (a) plan view of laminate and projectile, (b) side view showing impact at 90° (purple arrow) and 45° (black arrow).

3.2. High velocity impact

Following the initial impact study on thin laminates, a second study on high velocity impacts was conducted using the previously described gas gun [111]. The velocity considered for this study varies from 100 m/s to 350 m/s, at intervals of 50 m/s. Using the ultrasonic C-scan machine to study impact induced damage, it was not possible to investigate every interface within the laminate independently. For this study, X-ray Computed Tomography (CT) was employed to obtain detailed analysis and characterisation of the impact damage. Oblique (45°) impacts were carried out at two impact positions. Impact induced damage was characterised in terms of amount of fibres broken and delamination area, and the effect of impact position on the impact damage zone was also studied.

3.2.1 Materials and procedure

Quasi-isotropic Hexcel HexPly® IM7/8552laminates with $[45/90/-45/0]_{2s}$ stacking sequence was used. Due to a range of impact velocities for this second study, it was desirable to double the laminate's width as delamination can extend in the transverse direction. Consequently, for reasonable ratios of gauge length and width to size of impact damage, the dimensions of the laminates are: 250 mm x 40 mm x 1.9 mm, with the nominal overall thickness very close to the actual specimen thickness. In this experimental study, it is of interest to study the extent of impact damage close to the edge of the target and far away from the edge, which is why high velocity impacts were made at an angle of 45° to the edge and centre of the laminates, as shown in *Figure 3.8*. For edge impacts, the projectile was aimed to hit the target at a point which is 1.5 mm from the edge, to ensure contact between the projectile and the target. For centre

impacts, the projectile was aimed to hit the target exactly at the centre of the laminate's width. The test matrix for this high velocity impact study is summarised in *Table 3.2*. The recorded velocities from each impact configuration are shown in *Table* 3.2, where the consistency of the impact tests can be confirmed by the low C.V values (0.5 – 5.4 %). A high-speed camera, configured to obtain 30000 fps, was employed to capture the impact process. However, on post-processing the camera footage it was not possible to clearly capture the projectile before and after impact.

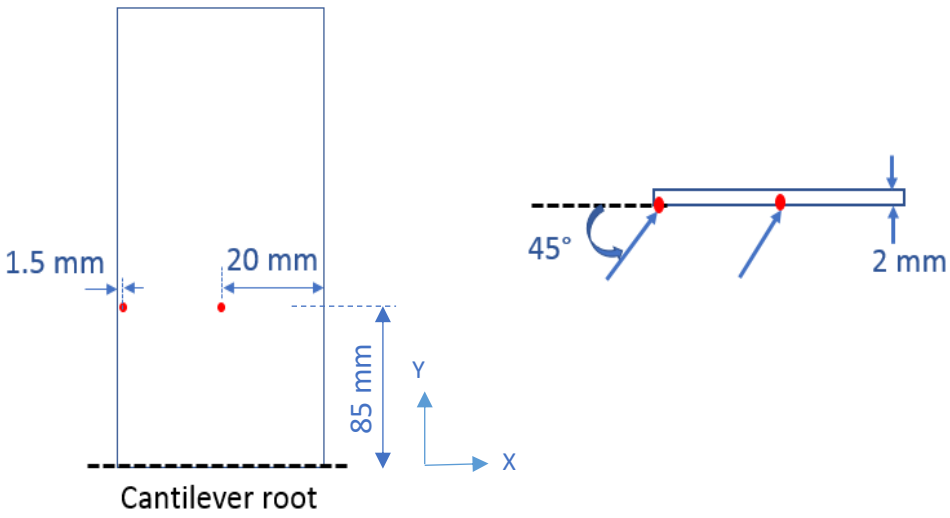

Figure 3.8: Oblique impact positions illustrated by the red dots. The image on the left is the front view and the image on the right is the plan view [111].

Table 3-2: Test matrix for second high velocity impact study [111].

Edge Impacts		**Centre Impacts**	
No. of specimens	Recorded impact velocity (m/s) (C.V %)	No. of specimens	Recorded impact velocity (m/s) (C.V %)
4	98.0 (4.3)	5	101 (5.4)
4	150 (1.4)	4	152 (1.1)
4	201 (3.5)	5	202 (0.7)
4	256 (2.5)	5	252 (0.5)
5	308 (2.2)	5	301 (1.2)
4	351 (3.3)	5	350 (1.2)

Composite structures are more reliable when the complex mechanisms of impact damage are well understood. Because such impact damage can severely degrade the structure's residual strength, characterisation of impact damage is valuable for clarifying the energy absorption mechanism and damage states. Over the years, numerous techniques have been developed to assess damage within a composite laminate, and these non-destructive methods include acoustic emissions, ultrasonic C-scan, scanning electron microscopy, X-ray Computed Tomography (CT) and optical techniques [112-1115]. While the resolution associated with acoustic emission and C-scan may be limited and it can be difficult to identify the damage mechanisms, 3D analysis is not possible with surface methods such as electron and optical microscopy. X-ray CT has emerged as a key imaging tool in material characterisation, which allows 3D visualisation of an object non-destructively as well as enabling the monitoring of damage accumulation. The use of X-

ray tomography for analysis and identification of damage and microstructures in composites has attracted increasing attention recently [116,117]. This is because sample characterisation is carried out in a non-destructive way where there are no preparation issues associated with it and the integrity of the sample can be preserved. Secondly, it allows capturing a three-dimensional view of the complex morphology of microstructures and damage, where the interaction of matrix cracking, fibre failure, fibre/matrix debonding or delamination can be studied.

For this second study on high velocity impacts, X-ray CT was chosen for extensive damage characterisation of all impacted laminates. A single specimen from each impact configurations was considered. 3D mapping of a given sample was achieved through CT reconstruction and this allowed identifying several features such as delamination, fibre failure and matrix cracks. To enhance X-ray contrast, all impacted laminates were soaked in X-ray dye penetrant over a period of 24 hours. The penetrant consists of 250 g zinc iodide, 80 ml distilled water, 80 ml isopropyl alcohol and 1ml kodak photoflo®. Zinc iodide is relatively non-toxic and is reasonably X-ray opaque, which is why it was used [118].

X-ray CT was performed at the National Composites Centre (NCC) using a Nikon XTH225ST 320 kV electron beam machine [118] with a 3 µm focal spot size. One specimen was scanned for each impact configuration. Each specimen was mounted on the rotation stage and positioned between the X-ray source and the panel detector. The target emits a cone of X-rays which travel through the specimen to the detector. During the scan, the specimen is rotated through 360° with small increments, and projections are collected at each orientation. Employing a filtered back-projection reconstruction algorithm, the individual sets of projections are reconstructed into a 3D volume. The scanning voltage

was 55 kV and current 145 µA, with an exposure time for each radiograph was 700 ms. The Metris CT Pro software was used to reconstruct each scan volume with manipulation and analysis performed using the VG Studio® Max 2.1 and Avizo®7 software packages [118]. Through visualisation as a 3D map, the local X-ray absorption coefficient of the material is represented by the grey scale value. The solid material (fibres and matrix) and air (matrix cracks, delamination, voids and other defects) are identified by the two peaks on the histogram of the grey scale intensity. Hence, the matrix cracks and delaminations could be segmented around the appropriate grey scale values [119].

3.2.2 Impact damage characterisation

In the event of high velocity impact, composite laminates experience different complex failure mechanisms, namely fibre failure, delamination, fibre/matrix debonding and matrix cracking. Previous works on high velocity impacts found in the literature mainly investigated the extent of damaged area as a function of impact velocity or energy absorbed. In this work, emphasis is laid upon impact damage characterisation in terms of fibre fracture and delamination area. The amount of fibre failure in impacted laminates is an important feature to analyse because it is expected that the residual tensile strength of impacted laminates will be strongly dependent on the extent fibre fracture. In *Chapter 5*, the residual tensile strength of impacted laminates is investigated and the relationship between extent of impact damage and residual strength is studied. Taking this into consideration and the fact that the post-impact tensile load is mostly carried by the 0° plies, the width over which the fibres are broken in the 0° plies were measured. CT scan images for edge-impacted laminates at 200 m/s and 350 m/s are shown in *Figure 3.9* and CT scan images for centre-impacted laminates at 200 m/s and 350 m/s are illustrated in

Figure 3.10. The widths, *w*, of broken 0° fibres are also shown in *Figures 3.9* and *3.10*. CT scanning images were uploaded to the ImageJ® software. The image width is 175 pixels, corresponding to 40 mm. By drawing a horizontal line corresponding to *w,* the length of the line was obtained in terms of its number of pixels, after which the equivalent length of w, in mm, was determined. From the CT scan images, the definition of *w* was made by considering the light patches, which represent the extent of fibre failure and can be easily identified from the surrounding dark patches. The dark areas around the light patches represent remaining fibres around the impact point, and were not considered when measuring *w*. The impact induced fibre failure, termed as fibre fracture width, is determined as the widths of broken fibres in each of the 0° plies averaged over the number of 0° plies broken [111]. *Table 3.3* provides details on the number of broken 0° plies and the fibre fracture widths for both edge- and centre-impacted laminates.

Through the thickness, there is a double 0° ply block at the central symmetry plane, but outboard only single 0° plies. For an edge-impacted laminate at 100 m/s, fibre failure was observed only in the top outboard 0° ply. Fibre failure in all 0° plies was observed when the impact velocity was increased to 200 m/s. As the impact velocity was further increased to 300 m/s, complete laminate perforation was noticed. For centre impacts at 100 m/s and 150 m/s, none of the 0° plies showed fibre failure. With further increase in impact velocity up to 300 m/s, three out of the four 0° plies showed fibre failure. At 350 m/s, the centre-impacted laminates exhibited broken fibres in all four 0° plies and laminate perforation was also observed. As the impact velocity was increased above 200 m/s, the extent of fibre failure determined in both edge- and centre-impacted laminates were significantly larger than the dimensions of the projectile. This is because of the oblique trajectory of the projectile during penetration which promotes a larger

extent of fibre failure. In addition, the multiple ply orientations, the local bending and the development of different damage modes around the impact site cause a larger extent of fibre failure than just the area under the impactor [111].

Although fibre fracture width was determined by inspecting CT scan images of 0° plies, which is a much quicker way to characterise the extent of impact damage, the extent of broken fibres in all plies was analysed as it becomes relevant for cases when the applied load post-impact is not aligned with the 0° plies. Using the same method of measuring the distance of fibres broken and averaging over the total number of plies broken, the fibre fracture widths for edge- and centre-impacted laminates were calculated, and the results are presented in *Table 3.4*. The extent of fibre fracture for both edge- and centre-impacted laminates increases with impact velocity and beyond the velocity at which a more pronounced shape of the projectile penetrating through the specimen is observed, the extent of fibre failure is expected to reach a constant value. Detailed measurements of broken fibres in all plies for all impact configurations can be found in *Appendix A*. For edge impacts in *Table 3.4*, the method of considering only 0° plies broken for fibre fracture width determination results in larger fibre fracture widths with an average difference of 3.4 % when compared to the fibre fracture widths determined by considering all plies in the laminate. For centre impacts, a direct comparison between the two methods used to determine fibre fracture widths show that considering only 0° plies broken leads to smaller fibre fracture widths with an average difference of 4.3 %. With reasonably low percentage differences and the fact that the 0° plies which carry most of the subsequent tensile loading, considering only 0° broken fibres to determine the fibre fracture width is suitable and time efficient.

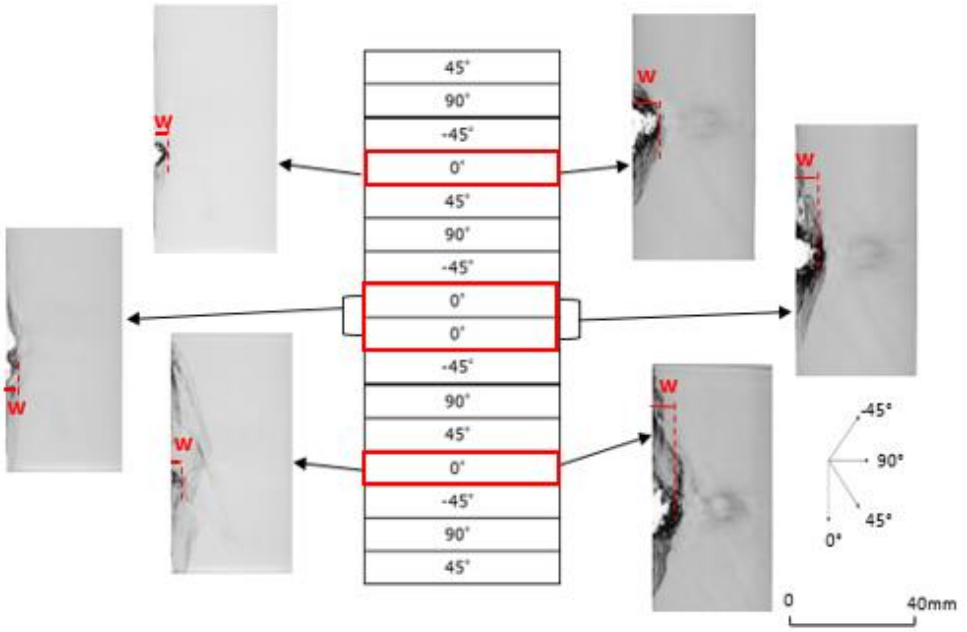

Figure 3.9: Extent of broken fibres in edge-impacted laminates at 200 m/s (left) and 350 m/s (right) [111].

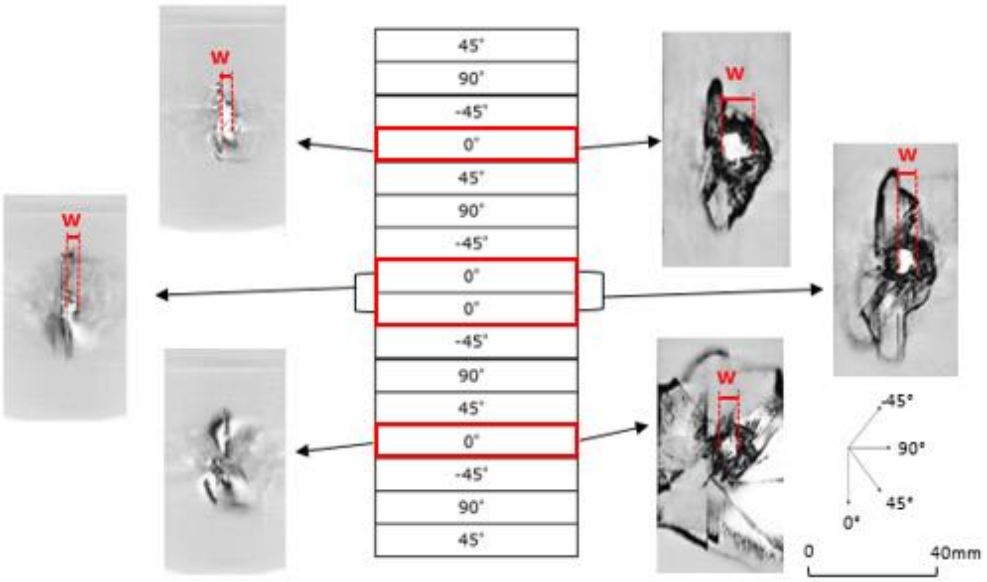

Figure 3.10: Extent of broken fibres in centre-impacted laminates at 200 m/s (left) and 350 m/s (right) [111].

Table 3-3: Fibre fracture width values for edge and centre impacts [111].

	Edge Impacts		**Centre Impacts**	
Impact velocity (m/s)	No. of 0° plies broken	Fibre fracture width (mm)	No. of 0° plies broken	Fibre fracture width (mm)
100	1	1.33	0	-
150	1	1.83	0	-
200	4	2.49	3	1.40
250	4	3.46	3	3.22
300	4	4.64	3	3.90
350	4	7.53	4	6.95

Table 3-4: Comparing the fibre fracture widths for edge and centre impacts based on 0° plies and all plies.

	Edge Impacts		**Centre Impacts**	
Impact velocity (m/s)	Fibre fracture width (mm)		Fibre fracture width (mm)	
	0° plies	All plies	0° plies	All plies
100	1.33	1.21	-	1.20
150	1.83	1.77	-	1.38
200	2.49	2.48	1.40	1.58
250	3.46	3.34	3.22	3.36
300	4.64	4.62	3.90	3.96
350	7.53	7.32	6.95	7.04

The debonding between plies, also known as delamination, is another important feature of impact damage, and it is represented by the slightly darker patches in *Figure 3.11*, where typical -45°/0° interfaces for edge impacts at 200 m/s and 350 m/s are illustrated. All the interfaces within the laminates were inspected from CT scans. The area enclosed within the region marked in white, shown in *Figure 3.11*, represents the delaminated area for one interface. Using a freehand option available in the ImageJ® software, the white shapes in *Figure 3.11* were drawn. One error associated with this freehand option is the addition or subtraction of material while sketching. Typical image width is 175 pixels, with one pixel corresponding to 228 µm. The image height varies between 265 – 340 pixels as different lengths of impacted specimens from different configurations were utilised for CT scan. The area within the region showing delamination was then determined in terms of its number of pixels and translated to a value equivalent to the area, in mm^2 [111].

The extent of delaminated area for each interface was determined and the delamination area was obtained by averaging over the 15 interfaces within the laminate. Using X-ray CT scan, it is possible to accurately identify each interface by laminate segmentation and for this study, different colours are assigned to every delaminated interface. The projected delamination areas observed in edge- and centre-impacted laminates over a range of velocities are represented in *Figure 3.12* and delamination under impact is discussed in the following section, while the effect of impact position on the delamination area is studied in section 3.2.4.

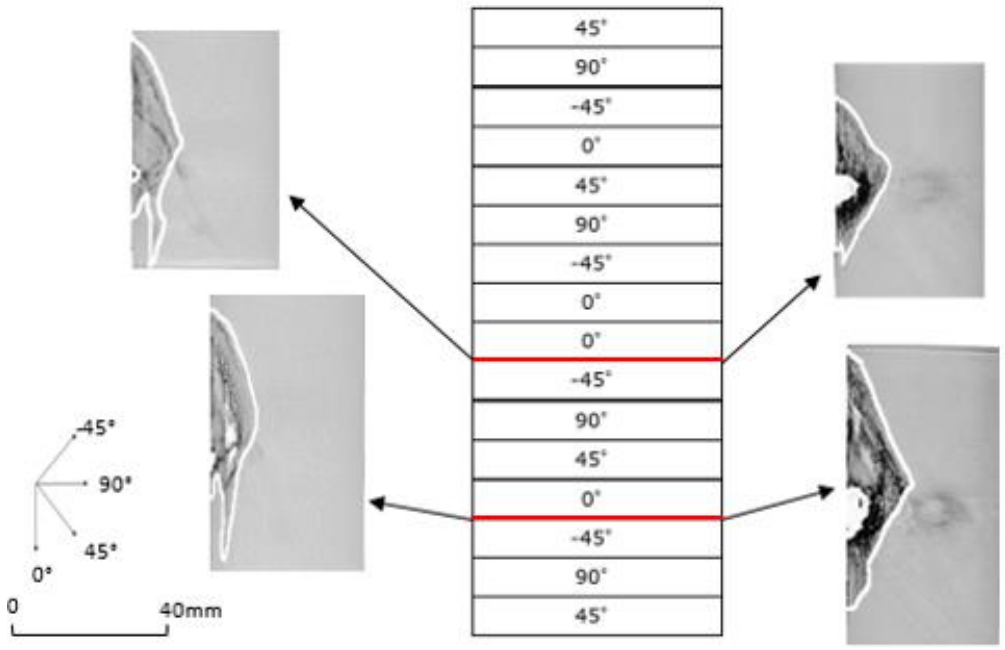

Figure 3.11: Enclosed within the white regions is the extent of delamination at -45°/0° interfaces in edge-impacted laminates at 200 m/s (left) and 350 m/s (right) [99].

3.2.3. Delamination under impact

Delamination is a critical damage mode under impact loading as observed from the characteristic delamination patterns illustrated in *Figure 3.12*. There are two mechanisms driving the delamination. When the projectile strikes the laminate, interlaminar shear arises due to the contact force causing a region of maximum stress near the mid-plane, and the stress decreases away from the impact point. Delamination occurring at the mid-plane causes a large reduction in bending stiffness as there is less material at the neutral plane to resist against bending deformation, which leads to a significant energy-release rate. *Davies et al* [120] proposed a threshold impact force for delamination after showing that the energy-release rate was constant with the delamination size for an axisymmetric case with a point load in a homogeneous quasi-isotropic laminate. As the number of delaminated interfaces increases, the energy-release

rate also increases [121], thus promoting further delamination once the first one has initiated. Through-thickness compressive stresses tend to suppress the delamination right under the impact point. *Figure 3.13* shows a cross-sectional view of an impacted laminates at 200 m/s, where the extent of delamination parallel to the 0° fibres can be analysed through the thickness. Impacted laminates revealed shorter delamination lengths under the impact point, and their sizes grow further away from the impact point.

Transverse tensile cracks which appear towards the back surface of the laminate due to bending is the second mechanism driving delamination [122]. While bending is the dominant mechanism in thin laminates and shear is more important in thicker laminates, both mechanisms occur in practice. The staircase pattern of delaminations observed in edge- and centre-impacted laminates, as shown by the coloured patterns in *Figure 3.12*, are formed when multiple delaminations through the thickness link up via transverse cracks. As the impact velocity is increased, the shapes of the individual delaminations are influenced by the matrix cracks, which tend to be elongated along the direction of the crack.

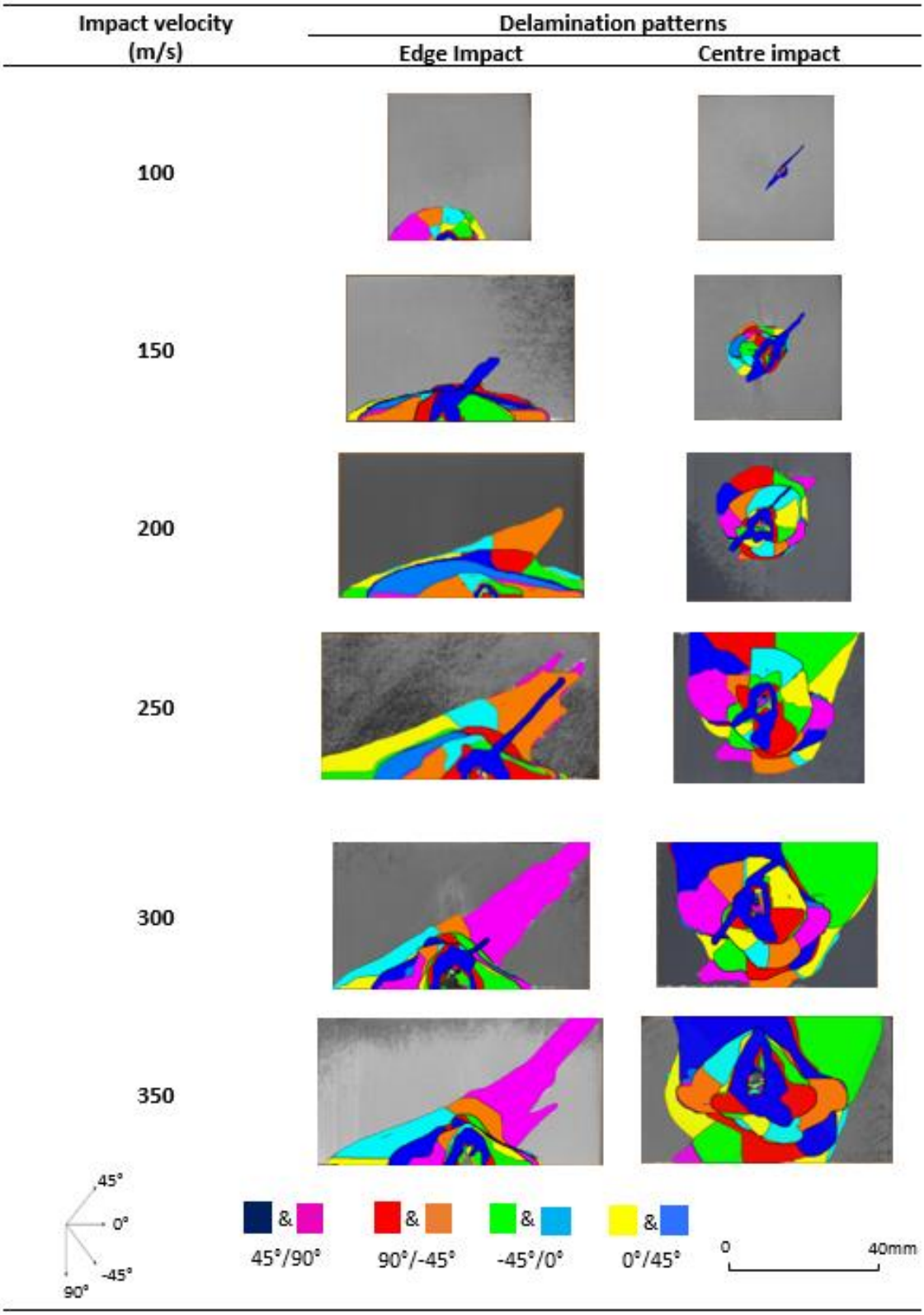

Figure 3.12: Delamination patterns in edge- and centre-impacted laminates over a range of velocities.

Figure 3.13: Cross-section CT image of an impacted laminate at 200 m/s showing fibre failure and delamination.

3.2.4. Effect of impact position

The effect of impact position is represented by the extent of fibre fracture and delamination area in both impact cases. As impact velocity increases, the fibre fracture width of edge-impacted laminates is always larger than the fibre fracture width observed in centre-impacted laminates. Under an impact, the laminate is less prone to bending at the centre than it is at the edge due to the presence of more material. Consequently, a rigid body is more likely to cause extensive fibre failure when penetrating an edge of the laminate than the surface of the laminate [111]. The impact position also affects the extent of delamination area observed for both edge- and centre-impacted laminates.

The variation of delamination area with impact velocity for both edge and centre impacts is graphically represented in *Figure 3.14*. The delamination areas measured from all the interfaces for both impact configurations are provided in *Appendix B*. For both edge- and centre-impacted laminates, the delamination areas were observed to be smallest in the interfaces close to the impact point. Away from the impact point, the delamination area increased in size, as confirmed by the error bars in *Figure 3.14.* At high impact velocities, the delamination area for a centre-impacted laminate is larger than the delamination area observed in an edge-impacted laminate. The larger extent of delamination in centre-impacted laminate compared to edge-impacted laminate at 350

m/s is the result of more splitting under an impact event, as observed from *Figures 3.9* and *3.10*. The large differences in delamination areas for the laminates impacted at the edge and the centre may be due to the different amount of energy absorbed. In addition, for centre impacts, delamination can grow around the impact point in all directions as compared to delamination growth being restricted by the edge for edge impacts. Furthermore, the larger delamination area in centre-impacted specimen can be associated with the greater constraint at the impact point where, due to symmetry of the central impact geometry there is no rotation of the laminate, leading to higher local interlaminar shear stresses whereas for edge impacts, the edge is free to rotate upon impact [111].

The tops of the error bars from *Figure 3.14* can also be interpreted to obtain the maximum delamination area for any impact configuration. Through inspection of all delaminated interfaces, the interfaces showing the maximum delamination area can be studied in reference to detailed results in Appendix B. The bottom 90°/45° interface in edge-impacted laminates revealed the largest delamination area for impact velocities of 300 m/s and beyond. Since laminate perforation occurs at 300 m/s with the projectile going through the target, the top interfaces have much more localised delamination area compared to the bottom interfaces. For centre impacts, the bottom 45°/0° revealed the largest delamination area. Despite all plies in the centre-impacted sample at 350 m/s showing fibre failure, the largest delamination is not observed in the bottom 90°/45° interface. This may be due to the projectile bouncing away from the target after impact instead of going through the target.

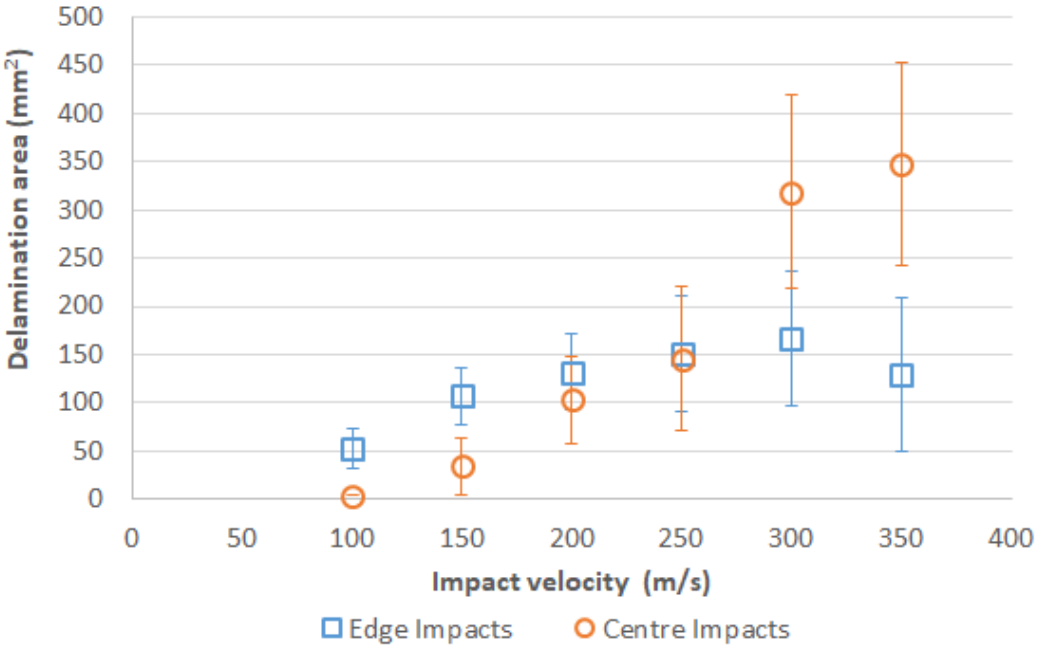

Figure 3.14: Variations in delamination areas in edge- and centre-impacted laminates as impact velocity is increased [99].

For edge impacts in *Figure 3.14*, the delamination area increases with increasing impact velocity until it reaches a maximum value, after which it decreases in size as impact velocity is increased. At impact velocities above 300 m/s, edge-impacted laminates show a larger fibre fracture width with decreasing delamination area. For centre impacts, delamination area increases with increasing impact velocity and the maximum area has not yet been reached at 350 m/s. *Pernas-Sanchez et al.* [109] experimentally investigated the effect of obliquity on carbon/epoxy laminate response, where the extent of damaged area was seen to increase with impact velocity until the laminate was perforated. Beyond the velocity at which laminate perforation was observed, the damaged area decreased with increasing velocity. A similar trend is observed in this work. For edge impacts, complete perforation is observed at an impact velocity of 300 m/s. This is due to much more localised impact damage induced by the

projectile beyond 300 m/s, which may explain why the delamination area decreases with increasing impact velocity.

For centre impacts, further impacts tests for centre impacts at velocities higher than 350 m/s are required to validate the hypothesis of decreasing delamination area with increasing impact velocity. *Figure 3.15* illustrates cross-sectional CT images of edge- and centre-impacted laminates over a range of velocities. Both impacted laminates exhibit fibre breakage along the projectile direction, accompanied by multiple delaminations. The extent of fibre fracture through the thickness can be analysed, where the number of plies showing fibre failure increases with increasing impact velocity. Careful examinations of the centre-impacted laminates considering all broken fibres through the thickness revealed that complete perforation occurs at 350 m/s. As such, a decreasing damaged area may be expected in centre-impacted laminates beyond 350 m/s.

3.2.5. Energy absorption mechanisms

Under high velocity impact events, the mechanisms identified by *Pernas-Sanchez* [109] through which the laminate absorbs the initial kinetic energy of the projectile E_k are:

- Delamination, E_D – the energy absorbed by the laminate through delamination can be estimated as $\mathrm{E_D} = kA_D G_{IIC}$, where the number of delaminated interfaces is represented by k, A_D is the delamination area and G_{IIC} is the critical energy release rate in Mode II, which is a material property. The delamination is assumed to occur in Mode II since there is no tensile load normal to the laminate plane.

- Fibre failure, E_F – the energy consumed in breaking fibres. E_F is dependent on the fibre strength and the extent to which the projectile penetrates the laminate.
- Linear momentum transfer, E_{lm} – the energy required to accelerate the plug from rest to the residual velocity of the projectile. *Hazell et al.* [123] observed a phenomenon termed as 'plug' and the latter refers to a lump of the laminate which is detached from the laminate when the projectile perforates the laminate.

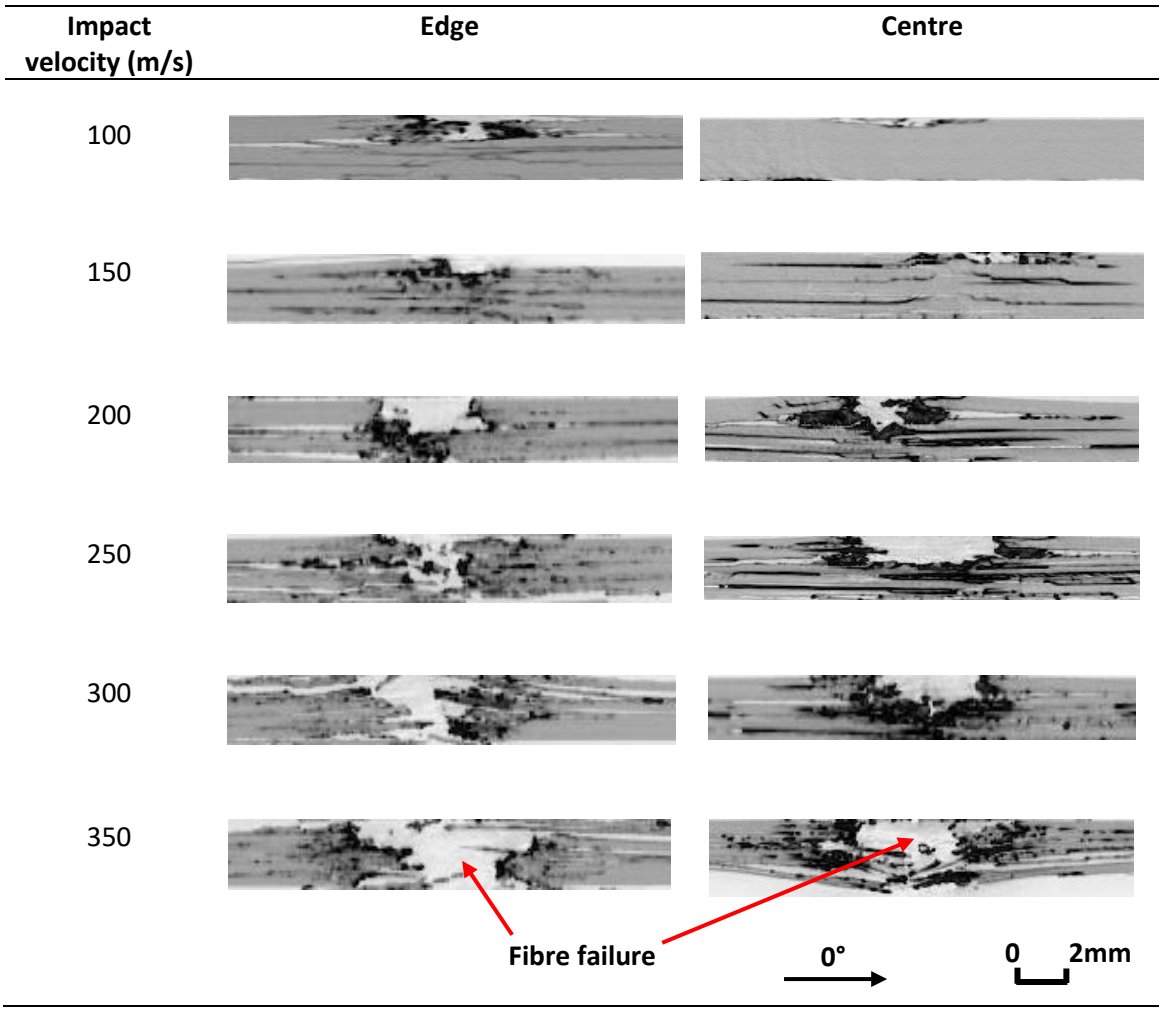

Figure 3.15: Cross-sectional CT scans of impacted laminates over a range of velocities.

Previous impact studies have shown that the residual velocity of the projectile is an important parameter to determine the amount of energy absorbed by the laminate.

However, in this work, it was not possible to capture the trajectory of the projectile after the impact and therefore, it is not possible to calculate the residual kinetic energy.

The delamination areas and number of delaminated interfaces observed in impacted laminates are provided in *Table 3.5*. As such, the energy absorbed due to delamination can be calculated. The ratio, E_D / E_K, between the energy absorbed due to delamination and the initial kinetic energy of the projectile is depicted in *Figure 3.16* for varying impact velocities. Since complete perforation is observed at 300 m/s for edge-impacted laminates, the energy absorbed by the laminate through linear transfer momentum is zero for velocities below 300 m/s. For edge impacts at 100 m/s, more than half of the initial kinetic energy of the projectile is absorbed by the laminate through delamination, and the rest is contributed to fibre breakage. As impact velocity is increased to 150 m/s, the delamination area doubles in size corresponding to an increase in E_D / E_K. As impact velocity is further increased, the delamination area slowly approaches its maximum value and E_D / E_K decreases because the contribution of fibre breakage becomes more significant compared to delamination. Beyond the impact velocity where laminate perforation occurs, it is expected that most of the initial kinetic energy of the projectile will be absorbed in the form of linear transfer momentum and fibre breakage, with some contribution from delamination as well.

Table 3-5: Number of delaminated interfaces and delamination areas for several impact configurations.

	Edge Impacts		Centre Impacts	
Impact velocity (m/s)	Delamination area (mm^2)	No. of delaminated interfaces	Delamination area (mm^2)	No. of delaminated interfaces
100	52.4	12	4.40	1
150	107	15	34.4	15
200	133	15	103	15
250	150	15	146	15
300	166	15	319	15
350	129	15	347	15

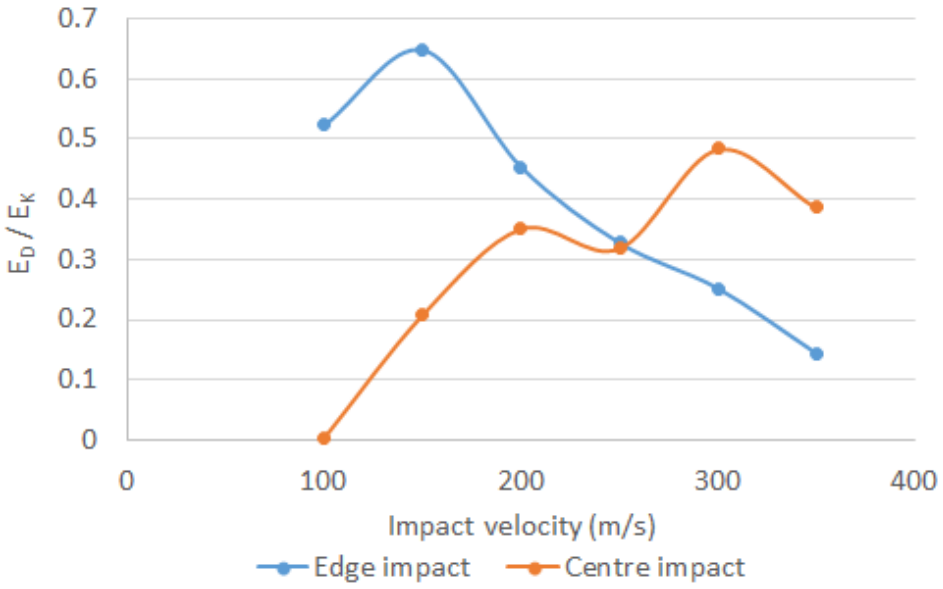

Figure 3.16: The relationship between energy absorbed due to delamination and initial kinetic energy of the projectile over a range of impact velocities.

For centre-impacted laminates, E_{lm} is expected to be negligible for impact velocities lower than 350 m/s since laminate perforation occurs at 350 m/s. From *Figure 3.16*, the ratio E_D / E_K is almost zero at an impact velocity of 100 m/s. This is because centre-impacted laminate at 100 m/s revealed only two broken surface plies and a very small delamination area of 4.4 mm^2 observed in the top 45°/90° interface. As impact velocity is increased up to 200 m/s, the delamination area increases in size with more broken fibres. E_D / E_K is about 35 % at 200 m/s, implying that fibre failure is a dominant mechanism in absorbing the projectile's initial kinetic energy. From 200 m/s to 250 m/s, the number of broken fibres is slightly increased while the fibre fracture width is increased by 130 %, leading to a reduction in E_D / E_K. Between 250 m/s and 300 m/s, the delamination area grows twice in size while the fibre fracture width experiences a slight increase. Consequently, an increase in E_D / E_K is observed between 250 m/s and 300 m/s. Beyond 300 m/s, centre-impacted laminates revealed fibres broken in all plies and the extent of fibre fracture is increased by 80 %, causing a reduction in E_D / E_K.

3.3 Conclusion

An initial impact study was conducted on 1 mm and 2 mm thick carbon/epoxy laminates subjected to high velocity impacts using a gas gun. The delamination areas and extent of fibre fracture observed in C-scan images were studied for different impact configurations. The effect of thickness, impact position and impact angle on the extent of impact damage were investigated. The thickness of the laminate influences the damage extent, where thinner laminates showed larger impact damage than thicker laminates. A larger damage extent was also observed in laminates impacted at the leading edge. The

trajectory of the projectile significantly affects the extent of impact damage, where oblique impacts to the leading edge revealed larger damaged area than normal impacts.

The findings from the initial study allowed the development of a second set of high velocity impact tests, where 2 mm thick carbon/epoxy laminates were impacted at 45° to the edge and centre of the laminates over a range of velocities. For this study, it was desirable to study the impact response with varying velocities and impact damage was characterised through detailed X-ray Computed Tomography (CT). Two impact damage parameters were considered, namely fibre failure and delamination. From the results presented and discussed, the main conclusions are as follows:

- The extent of fibre failure, termed as fibre fracture width, increases with increasing impact velocity for both edge- and centre-impacted laminates.
- Edge-impacted laminates have increasing delamination areas with impact velocities up to 300 m/s. Beyond 300 m/s, the delamination area decreases. Centre-impacted laminates have increasing delamination areas with impact velocities and the maximum delamination area may be expected at 350 m/s.
- For edge impacts, laminate perforation occurs at 300 m/s. This implies that the impact damage becomes much localised beyond impact velocities of 300 m/s. For centre impacts, laminate perforation happens at 350 m/s.
- The initial kinetic energy of the projectile is assumed to be absorbed by the laminate mainly in the form of fibre breakage, delamination and linear transfer momentum. The latter becomes increasingly significant only upon laminate perforation.

- The ratio between energy absorbed by delamination and initial kinetic energy of the projectile for both edge- and centre-impacted laminates was analysed. Edge-impacted laminates revealed a larger ratio for velocities up to 250 m/s. Beyond 250 m/s, centre-impacted laminates showed a larger ratio because the extent of delamination was much larger than in edge-impacted laminates.
- In edge-impacted laminates, the energy absorbed by the laminate in breaking the fibres is the dominant energy absorption mechanism only for impact velocities of 200 m/s and beyond. For centre-impacted laminates over the full range of velocities considered, most of the initial kinetic energy of the projectile is absorbed in breaking the fibres.

Research dissemination

Kristnama AR, Xu X, Nowell D, Wisnom MR, Hallett SR. Experimental investigation of high velocity oblique impact and residual tensile strength of carbon/epoxy laminates. J Comp Sci Technol, 2019;182:107772.

CompTest 2017, Leuven, Belgium

4. High velocity impact modelling

In the previous section, an experimental investigation on the effect of high velocity oblique impacts on carbon/epoxy laminates was carried out. This section focusses on developing appropriate finite element models to simulate the impact tests. The finite model developed is used to predict the impact damage in terms of fibre failure and delamination area over a range of impact velocities and at two impact locations. The predicted impact damage is then compared to the experimental data to assess the reliability of the model.

In this current FE analysis, a Hi-fidelity Finite Element Method (Hi-FEM) method is used, which combines different failure criteria, with multiple split paths and delamination modelled using cohesive elements, together with an automated meshing technique. In the follow, the finite element model developed is explained in depth and the failure criteria employed to predict impact damage are described. The impact damage is characterised in terms of fibre fracture and delamination area, and the effect of impact position on the impact damage is also investigated, which is followed by further improvements to the impact model.

4.1. Description of baseline impact model

The finite element model developed for this chapter is employed to simulate the high velocity impact experiments as described in *Chapter 3*. Simulations are carried out in LS-DYNA using solid and cohesive elements to represent the IM7/8552 laminates. The finite element model consists of a steel cube impactor and a composite plate with suitable boundary conditions. As in the experiments, the mass of the impactor is kept

constant while the velocity is altered for impacts to the edge and centre of the laminates. An eroding type of contact algorithm is used to model the interaction between the impactor and the laminate. A surface-to-surface contact is also defined between each ply to maintain contact between plies after delamination has initiated. The predicted fibre fracture and delamination areas are then validated against the experimental results.

4.1.1. Impactor

In the experiments, a 3 mm steel cube projectile was used to impact the 250 mm x 40 mm laminate at 45° to the edge and the centre. The impact configurations have been described in *Chapter 3*. The impactor was aligned to strike the laminate at 1.5 mm from the edge and at the centre of the laminate, as represented in *Figure 4.1*. For the simulation, the hardness of the steel impactor is assumed to be significantly higher than the target's hardness. Since recovered projectiles from ballistic experiments showed negligible deformation, plastic deformation of the projectile is not considered, and hence the steel cube projectile is assumed linear-elastic and is modelled using MAT 01 in LS-DYNA. The material properties for the impactor are: density (ρ) = 7850 kg/m^3, Young's modulus (E) = 210 GPa and Poisson's ratio (v) = 0.3.

The impactor is modelled with 8-noded constant stress solid elements (TYPE 1 in LS-DYNA). The projectile should have a reasonably fine mesh to capture its true geometry. An overly coarse mesh may result in contact instability. To promote proper distribution of contact forces, the node spacing on the contact surface of the projectile should be no coarser than the mesh of any deformable part which encounters the impactor. Therefore, the impactor is modelled with a mesh size of 0.1 mm.

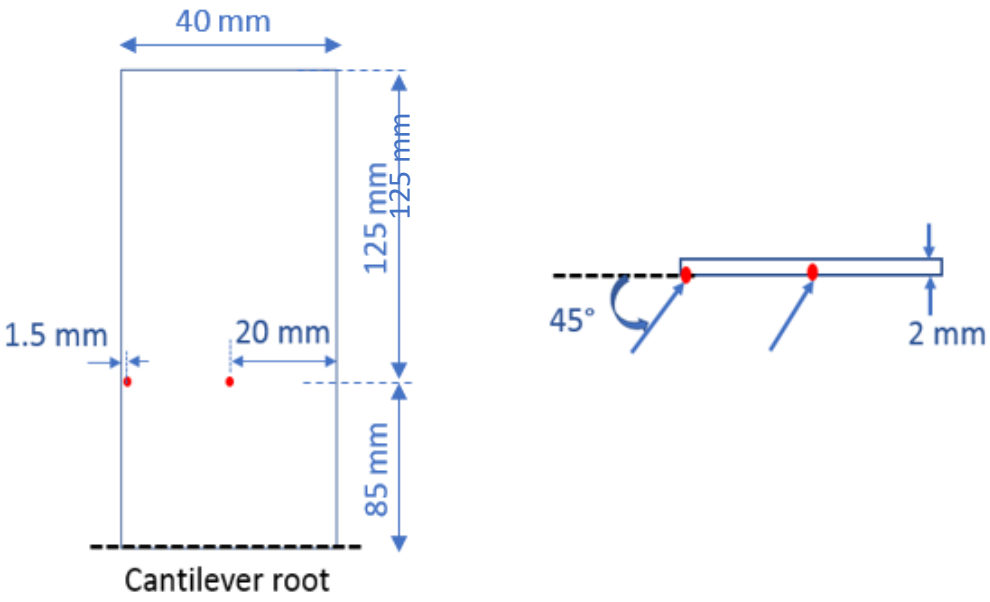

Figure 4.1: Impact positions shown in red on a laminate – front view (left), top view (right).

4.1.2. Penetration mechanisms

There are three stages in the penetration process of a composite laminate by a metal projectile: impact, entry and exit. Shock waves are generated in the projectile and target in the impact phase. The amplitude of these waves is dependent on the impact velocity, shock impedance of the target and projectile. As the laminate bends, delamination arises with the shock waves travelling through the thickness [124]. In the next phase, the composite is subjected to compression in the contact region, where fibre and matrix failure occur around the impact region. A schematic of the damage processes in a composite laminate is presented in *Figure 4.2*.

Shear cutting of the fibres and cavity expansion (radial expansion of the target material) are the dominant failure modes, which are accompanied by local fibre buckling and matrix cracking [125]. There is a transition from compressive to tensile failure in the exit phase, accompanied by multiple delaminations. Delamination is initiated earlier in the impact phase and propagates until the projectile reaches the delaminated interfaces.

The plies are pushed ahead of the impactor and tensile fibre failure occurs away from the impactor. For all phases considered, part of the projectile's energy is dissipated in the form of fibre failure, delamination and matrix cracking, as well as the transfer of kinetic energy to the target.

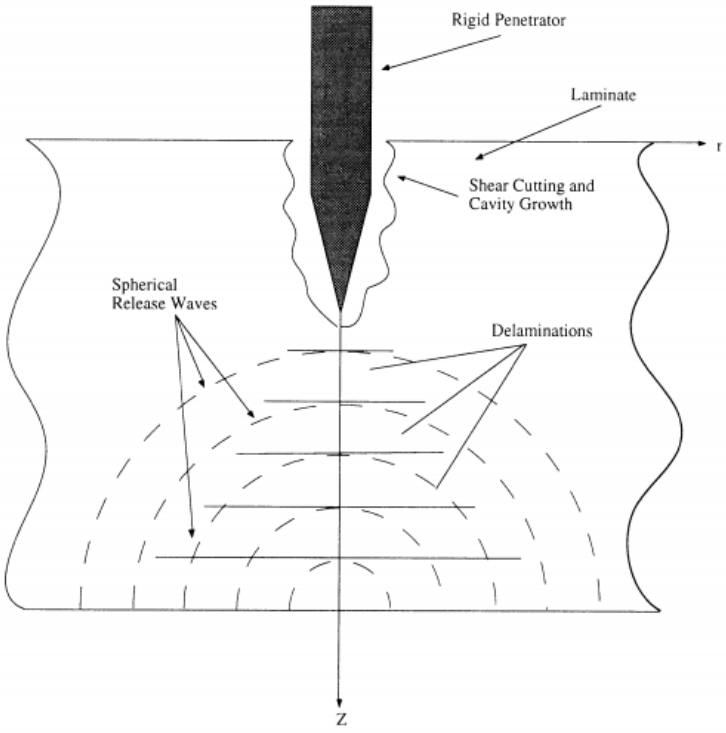

Figure 4.2: Schematic of the delamination in a composite laminate due to penetration by a metal projectile [124].

4.1.3. Failure criteria

During an impact, there are several damage mechanisms which take place (as described in *section 4.1.2*) and it is important that the finite element model developed can capture all failure mechanisms. In this analysis, three types of damage are considered: fibre failure, delamination and matrix cracking. Stress based damage criteria have been commonly used to model the damage mechanisms in composites subjected to high velocity impacts. For example, in a numerical study conducted by *Pernas-Sanchez et*

al. [94] on high velocity impacts on unidirectional laminates, the damage mechanism for fibre failure under tension was given by *Eq (4.1).*

$$e_{f,t}^2 = \left(\frac{\sigma_{11}}{X_T}\right) + \alpha\left(\frac{\sigma_{12}}{S_{12}}\right)^2 - 1 \quad (4.1)$$

where σ_{ij} are the stress tensor components, X_T and S_{12} are the strengths of the composite laminate in tension (in the fibre direction) and under in-plane shear respectively. The parameter α allows to calibrate the shear stress interaction, in order not to overestimate its contribution as the Hashin criterion does (it assumes α = 1). The authors also provided equations for damage mechanisms relating to fibre failure under compression, matrix failure under tension and matrix failure under compression.

4.1.3.1. Fibre failure

The carbon/epoxy plies behave as an orthotropic linear elastic material, with elastic material properties listed in Table 4.1 [72]. In this work, the fibre failure criteria considered relates to fibre failure under tension with a continuous damage process predicted based on Weibull theory. Fibre failure under compression is based on a maximum stress criterion relating to the strength of the laminate in the fibre direction under compression. Weibull proposed a statistical distribution that is extensively used to represent the strength of brittle materials [126]. This statistical method has been widely utilised to model fibre failure in polymer matrix composites [127 – 130]. Weibull theory is based on a weakest-link principle. Assuming a chain consists of several links and the probability of failure at any load applied to a “single” link is found by testing. In order to find the probability of failure of a chain consisting of several links, it is assumed that the chain has failed if any of its parts has

Table 4-1: Properties of lamina elements [72].

E_{11} (GPa)	$E_{22} = E_{33}$ (GPa)	$G_{12} = G_{13}$(GPa)	G_{23} (GPa)
161	11.4	5.17	3.98
$\alpha_{22} = \alpha_{33}$ ($°C^{-1}$)	α_{11} ($°C^{-1}$)	$\nu_{12}=\nu_{13}$	ν_{23}
$3x10^{-5}$	0.0	0.320	0.436

failed. Accordingly, the probability of nonfailure of the chain is equal to the probability of the simultaneous nonfailure of all the links. The weakest link in a chain determines the strength of a material, and as the number of links increases, the strength tends to decrease. The strength of a brittle-like material is related to the stressed volume and is controlled by defects which follow a Weibull distribution. Assuming equal probability of survival between the model and a unit volume of material, fibre failure occurs when the stress on a volume of material reaches the unnotched unidirectional strength. This leads to *Eq. (4.2)*.

$$\int_V (\frac{\sigma}{\sigma_{unit}})^m dV = \sum_{i=1}^{Total\ No.of\ solid\ Elements} (\frac{\sigma_i}{\sigma_{unit}})^m V_i = 1 \quad (4.2)$$

where σ_i is the elemental stress, V_i is the elemental volume, σ_{unit} is the tensile strength of a unit volume of material and m is the Weibull modulus from scaled unnotched unidirectional tensile tests of the same material [131]. In V, we can derive the material constants as m = 41 and σ_{unit} = 3131 MPa for 1 mm^3. When the failure criterion is satisfied after *Eq. (4.2)* is checked at each time step, element deletion occurs. After this, the load is redistributed to the other remaining elements. The continuous fibre breakage process is

achieved when *Eq. (4.2)* is satisfied again as the stresses in the remaining elements increase with increasing applied load [72,132].

The fibre failure under compression is given by *Eq. (4.2).* It is based on a maximum stress criterion relating to the strength of the laminate in the fibre direction under compression. When the parameter associated with the failure criteria $e_{f,c}^2$ is greater or equal to zero, the elements with stresses σ_{11} are removed from the calculations.

$$e_{f,c}^2 = \left(\frac{\sigma_{11}}{X_C}\right)^2 - 1 \tag{4.3}$$

where X_C = 1690 MPa is the strength of the laminate in the fibre direction under compression, as provided by the manufacturer [133].

4.1.3.2. Inter-laminar failure and matrix cracks

Cohesive interface elements were employed to model delamination between plies and intra-ply splitting. Cohesive elements are essentially 2D elements and deformations are typically expressed in terms of displacements and tractions (force per unit area) at the Gauss points rather than strains and stresses. The insertion of cohesive elements between solid elements allows defining the relative opening displacements between the upper and lower faces interpolated at the Gauss points in terms of traction using the cohesive law. Based on the Cohesive Zone Modelling (CZM) approach, cohesive interface elements with finite thicknesses are employed to model the resin-rich regions within the laminate. The cohesive formulation developed by *Jiang et al.* [134] is adopted here and implemented into the non-linear explicit solver, LS-DYNA, via a user material subroutine. A bi-linear traction-separation law (TSL) governs the cohesive formulation, which is associated with the traction and separation of the cohesive element in a mixed-mode

behaviour. The formulation is shown in *Figure 4.3*, where the area under the bi-linear curve corresponds to the critical Energy Release Rate (ERR) of the fracture modes.

The damage onset in mixed-mode loading is governed by a quadratic stress-based failure criterion presented in *Eq. (4.4)*, where σ_I and σ_I^* are the Mode I (opening) stress and strength, σ_{II} and σ_{II}^* are the Mode II resultant shear stress and strength. A fracture energy based mixed-mode power law controls the damage propagation, as presented in *Eq. (4.5).* α is an empirical parameter, whose value is taken as equal to 1.0. G_{IC} and G_{IIC} are the critical ERRs for pure Mode I and II loading, and G_I and G_{II} are the pure mode components of ERR due to the mixed-mode loading.

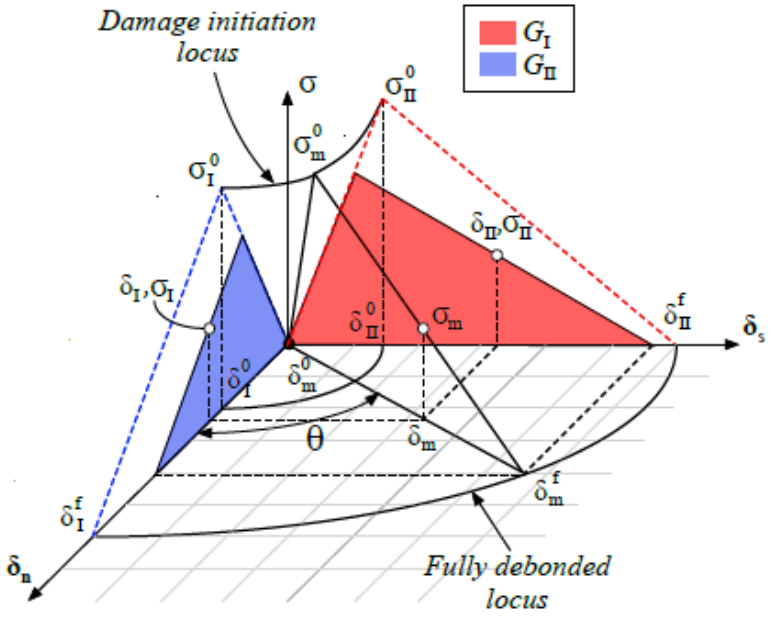

Figure 4.3: Traction-separation law of a cohesive element [134].

To capture the Mode II behaviour in an event such as impact, the enhancement effect of though-thickness compression on the shear behaviour is considered. The cohesive formulation considers a material-dependent enhancement factor (η) through a linear relationship between the shear strength and Mode II critical ERR, as defined by *Eq. (4.6).* This enhancement approach was adopted from *Li et al.* [135] where they looked at

cut-ply and dropped-ply specimens and studied the effect of compressive stress on damage initiation and growth of Mode II delamination. The effect of through-thickness compression on the shear strength was experimentally and numerically investigated by *Gan et al.* [136] using a modified double-notch shear test. For an in-plane loading such as impact, it is important to consider the enhancement effect to accurately capture the Mode II behaviour.

$$\sqrt{(\frac{\sigma_I}{\sigma_I^*})^2 + (\frac{\sigma_{II}}{\sigma_{II}^*})^2} = 1 \tag{4.4}$$

$$(\frac{G_I}{G_{IC}})^\alpha + (\frac{G_{II}}{G_{IIC}})^\alpha = 1 \tag{4.5}$$

$$\begin{cases} \sigma_{II_n}^* = \sigma_{II}^* - \eta\sigma_I \\ G_{IIC_n} = G_{IIC}(\frac{\sigma_{II_n}^*}{\sigma_{II}^*}) \end{cases} \qquad when\ \sigma_I < 0 \tag{4.6}$$

The IM7/8552 material has been characterised at different strain rates with various combinations of stress conditions, including considerable dynamic studies using the split-Hopkinson bar test system in a study and a relatively complete datasheet representing the rate-dependent failure envelope of IM7/8552 laminate can be found in [55]. The cohesive interface elements properties are shown in *Table 4.2* [55,72,137]. The effective elastic properties of the laminate are dependent on the properties of the cohesive surfaces and the bulk constitutive relations of the plies. The purpose of the cohesive surfaces is to simulate fracture, and several guidelines have been proposed to select a value for the interface stiffness. While *Zou et al.* [138] proposed a stiffness value between 10^4 and 10^7 multiplied by the value of interfacial strength per unit length,

Camanho et al. [139] obtained successful predictions of graphite/epoxy laminates with a stiffness of 10^6 N/mm^3. *Turon et al.* [140] derived a new equation to select the interface stiffness, where their approach yielded a stiffness value of 10^5 N/mm^3 to ensure the presence of a stiff connection between two adjacent layers whilst maintaining numerical stability. To represent a physical stiffness between the plies in this impact study, a value of 10^5 N/mm^3 is chosen for the cohesive elements [140].

Table 4-2: Cohesive interface element properties.

G_{IC} (N/mm)	G_{IIC} (N/mm)	σ_I^{max} (MPa)	σ_{II}^{max} (MPa)
0.2 [55]	0.9 [55,137]	60 [72]	90 [72]

4.1.4. Boundary conditions

For the impact tests, a mechanical fixture was employed to clamp the laminate as a cantilever beam. Since the full length of the laminate is modelled, all the nodes through the thickness were selected from one end to represent the mechanical fixture. The distance over which the nodes are fixed measures 40 mm in length. The selected nodes are illustrated in *Figure 4.4* and they are given Single Point Constraint (SPC) boundary conditions in LS-DYNA, i.e. all the three translational degrees of freedom are fixed. The projectile is oriented such that the surface of the cube strikes the target, as depicted in *Figure 4.5*. This orientation was chosen as the projectile was held in this position inside the sabot during the experiments.

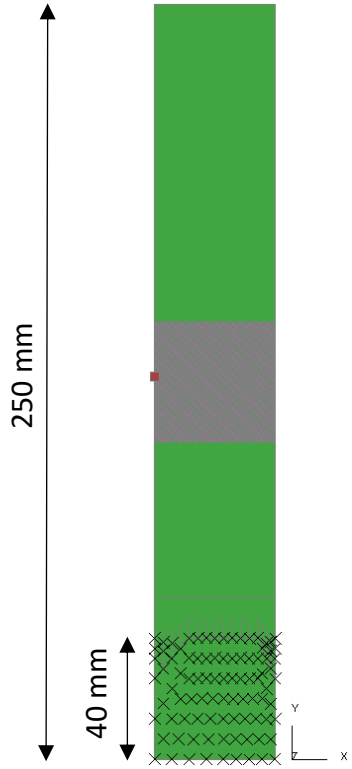

Figure 4.2=4: Finite element model showing boundary conditions applied to one end of the laminate.

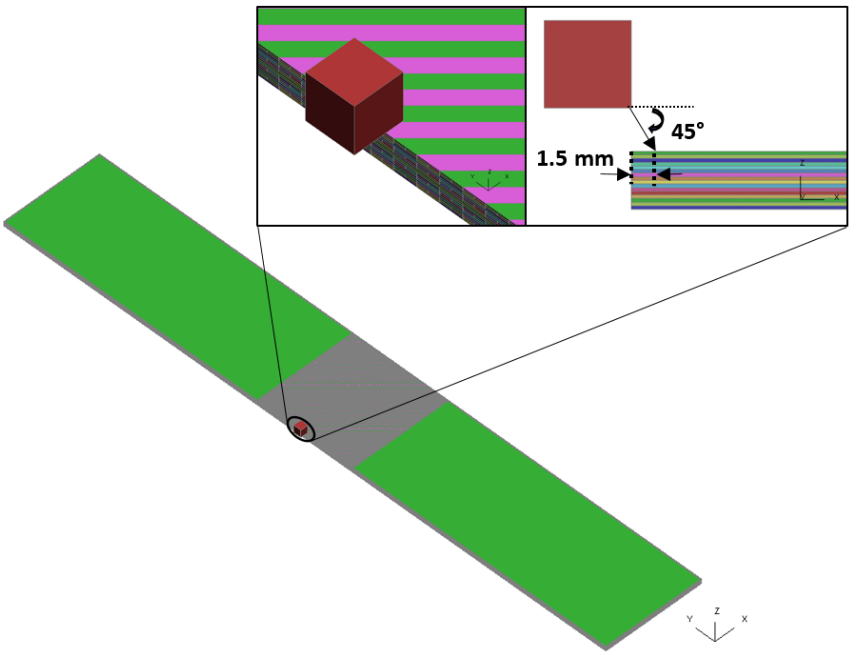

Figure 4.5: Schematic showing projectile orientation before an edge impact.

4.1.5. Finite element model

Detailed ply-by-ply 3D finite element models were constructed in LS-DYNA to represent the targets for edge and centre impacts. The full thickness of the specimen was modelled with each ply having one element in the through thickness direction. A single layer of 8-noded brick elements with reduced integration (TYPE-1 in LS-DYNA) and with elastic orthotropic material properties listed in *Table 4.1* were used to model each ply. Through the thickness, 8-noded cohesive elements (TYPE-19 in LS-DYNA) with zero thickness were assigned to represent the resin-rich regions between the plies, where delamination may arise. Cohesive elements were also employed with the Region of Interest (RoI) to model potential split paths.

The RoI measures 40 mm x 40 mm, which is enclosed within the blue box, as represented in *Figure 4.6*. The mesh for the RoI was based on a unit cell [141], where the average mesh size is equal to 0.23 mm, and the laminate outside the RoI was defined with a coarser mesh size. By inputting the unit mesh size, dimension of each ply, stacking sequences and spacing of predefined splits in the plies, the MATLAB-based meshing tool generates the basic mesh for each oriented ply. Cohesive elements for inter-laminar failure are inserted after every ply and cohesive elements for intra-ply splits are put at interfaces between different areas.

CT scans of impacted laminates revealed multiple matrix cracks around the impact point, and the mesh based on a unit cell allows defining the 0° and 90° splits with 0.71 mm spacing, while the 45° and -45° splits were modelled with 1 mm spacing. The split spacings represent the minimum values allowable based on a unit cell. *Figure* 4.7

illustrates the mesh used for the four possible matrix cracking directions using the unit cell meshing technique.

Generally, the solution accuracy is significantly influenced by hourglass deformation modes that result from the use of reduced-integration elements. Employing fully integrated brick elements can avoid the hourglass problem, but in this case the computation becomes inefficient due to the high computational costs associated to their usage. The hourglass problem can be controlled by either viscosity or stiffness type options in LS-DYNA. In this work, the stiffness based Hourglass control (Type-5 in LS-DYNA) was used for all reduced-integration elements to suppress zero strain energy distortion modes. A thermal load of -160 °C was included in the simulations prior to the tensile loading to model the 'cooling down' of the laminate from 180 °C to room temperature after the curing process and generation of thermal residual stresses. In LS-DYNA, a thermal load curve is defined with thermal expansion coefficients for IM7/8552 provided in Table 4.1 [72]. The nodal temperatures are uniform throughout the model and vary according to the load curve, where the temperature is defined as a function of time.

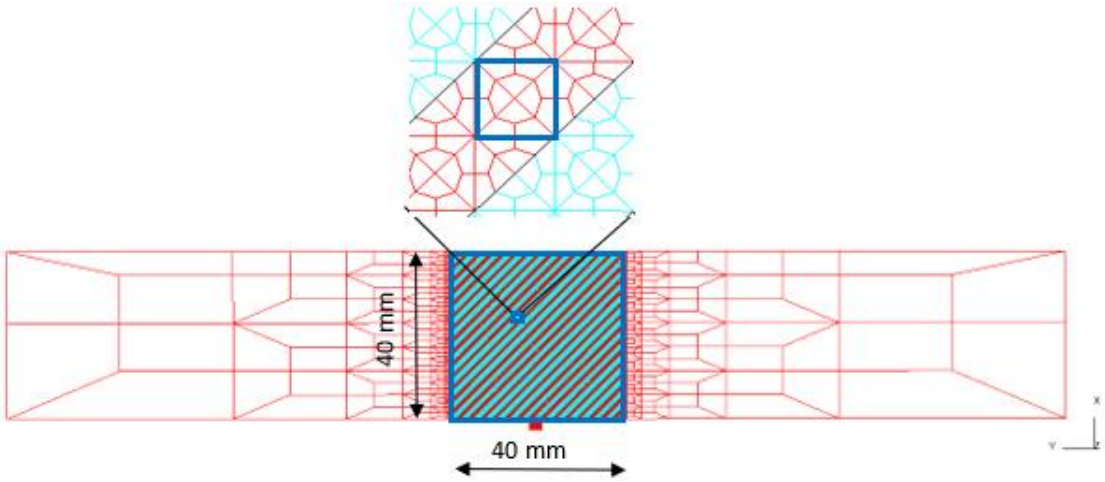

Figure 4.6: Typical FE mesh, showing the mesh defined based on a unit cell enclosed within the smaller blue box.

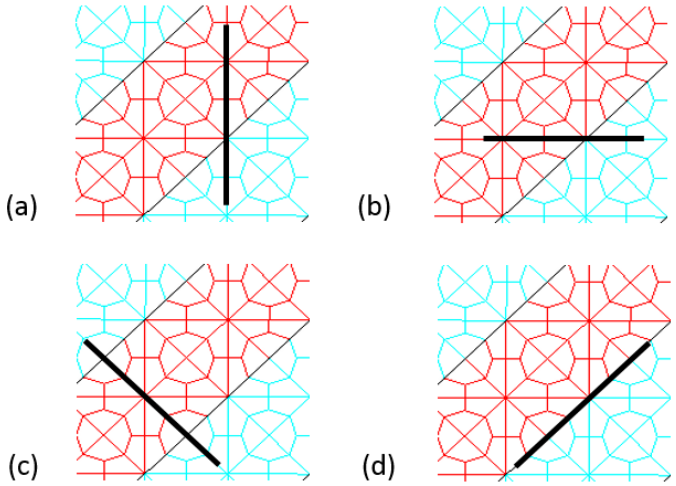

Figure 4.7: A ply-level mesh allowing matrix cracking predictions in four different orientations, where the black lines represent (a) 0°, (b) 90°, (c) 45° and (d) -45° splits.

4.1.5. Contact algorithm

LS-DYNA offers three basic contact types, namely single surface contact, nodes-to-surface contact and surface-to-surface contact. For the problem of high velocity impacts, the surface-to-surface contact type was chosen since the surface of the projectile initially encounters the surface of the target. A high velocity impact represents a penetration

problem and an eroding contact is required when the elements forming one or both exterior surfaces experience material failure during contact. For the laminate and/or projectile which may rupture as a result of the impact, it is important to define a contact formulation which will redefine the contact surfaces to find new contact among elements exposed when adjacent elements are eroded. As such, an Eroding Surface-to-Surface contact algorithm was defined between the laminate and the projectile.

Severe element distortion is likely to occur in high velocity impact simulations, and so an additional Automatic Surface-to-Surface contact was defined between each ply to limit the extent to which solid elements interpenetrate each other after cohesive elements are deleted. Frictional effects between the projectile and target were considered based on a basic Coulomb friction model, which is defined by two contacting surfaces carrying shear stresses up to a critical shear stress that is dependent on the contact pressure [90]. For the steel/composite and composite/composite contacts, the coefficient of friction was set to a value of 0.3 [90].

4.2. High velocity impact simulation

The set of high velocity impact configurations, as illustrated in *Figure 4.1*, has been simulated in LS-DYNA for a duration of 0.5 ms over a range of velocities. Typical runtimes for the simulations vary from 10 hours of analysis time for lower velocities to 48 hours for higher velocities. The impact process for a typical edge impact at 350 m/s is analysed, where the axial strain wave propagation (ε_y) and interlaminar delamination are shown as a function of time in *Figures 4.8* and *4.9* respectively. As the projectile comes into contact with the composite target, the material on either side of the projectile undergoes compression (in green) and the rest of the laminate is in tension (yellow). As the

simulation progresses, the compressive strain waves propagate in the through thickness direction while the bottom part of the laminate is in tension. Fibre failure initiates when the stress exceeds the tensile and compressive fibre strengths.

From *Figure 4.9*, which shows the delamination area within the RoI, delamination initiates at all interfaces as the projectile penetrates the laminate at 10 µs. As the projectile continues penetrating through the laminate, delamination growth continues at all interfaces and the delamination area increases in size with time. While only an impact at 350 m/s is shown in *Figure 4.9*, the sequence of evolution of delamination is the same for all impact velocities. For centre impacts, delamination initiation and propagation is observed on all sides around the impact point. In this work, the modelling accuracy is assessed against the experimental results from impacts tests and post-processing of the impact simulations includes measuring the extent of fibre failure in all plies and the delamination areas at all interfaces within the laminate.

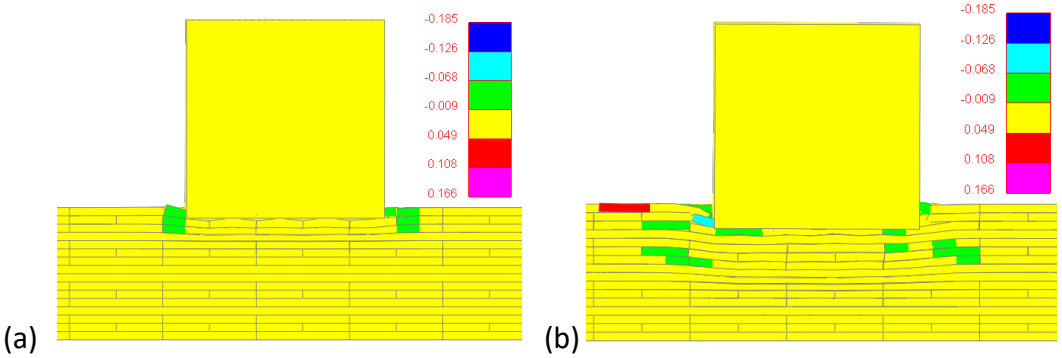

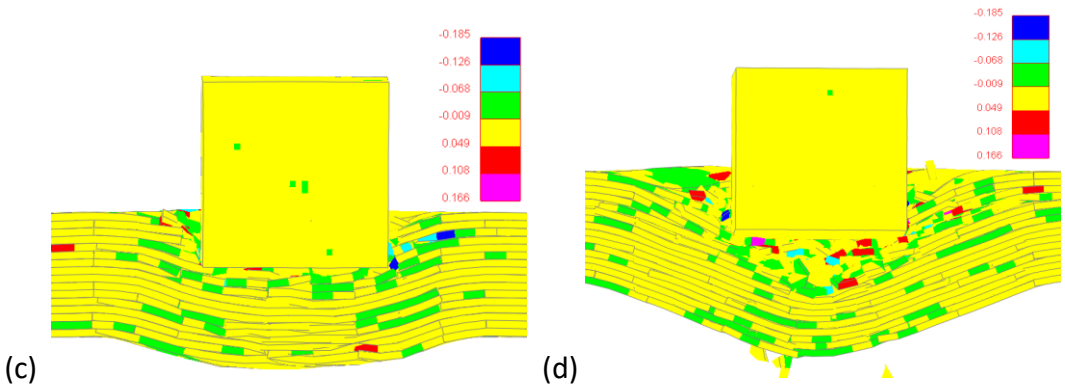

Figure 4.3: Axial strain wave propagation (ε_y) for a typical edge impact at 350 m/s at (a) 1 µs (b) 2 µs (c) 6 µs and (d) 13 µs.

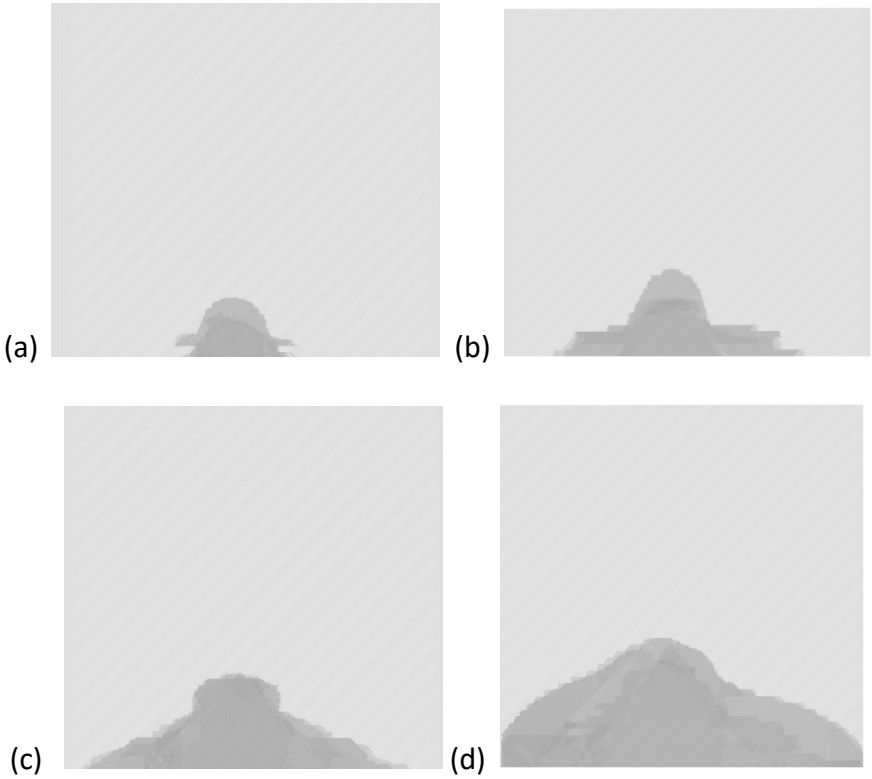

Figure 4.4: Propagated delamination for a typical edge impact at 350 m/s at (a) 10 µs (b) 20 µs (c) 50 µs and (d) 340 µs. All plies superimposed.

4.2.1. Fibre failure

The extent of fibre failure for all impact configurations is characterised by measuring the fibre fracture width from all plies within the laminate. The same method employed in *Chapter 3* for impact damage characterisation is applied here. *Figure* 4.10 shows a typical example of how the width, *w*, of broken fibres is measured post-impact simulation. For edge impacts, the width of broken fibres corresponds to the distance between the edge and the furthest failed solid element from the edge for all the plies. For the centre impacts, the distance between the two furthest failed solid elements for all the plies corresponds to the width of broken fibres.

Once the widths of broken fibres are measured, the fibre fracture width for a laminate impacted at a given velocity is determined as the widths of broken fibres averaged over the number of plies showing fibre failure. The results for all impact configurations, with respect to impact energy, are summarised in *Table 4.3*. From the recorded incident velocities, the impact energies for each configuration can be calculated using the *Eq. (4.7).*

$$E_K = \frac{1}{2} m_p v_p^2 \tag{4.7}$$

where E_k is the incident kinetic energy of the projectile just before impact, m_p is the mass of the projectile and v_p is the recorded impact velocity of the projectile. The extent of fibre failure and number of broken plies observed for a given impact position increase with impact energy. For a laminate, the fibre fracture width is largest in the top plies, and it decreases in size in the through thickness direction.

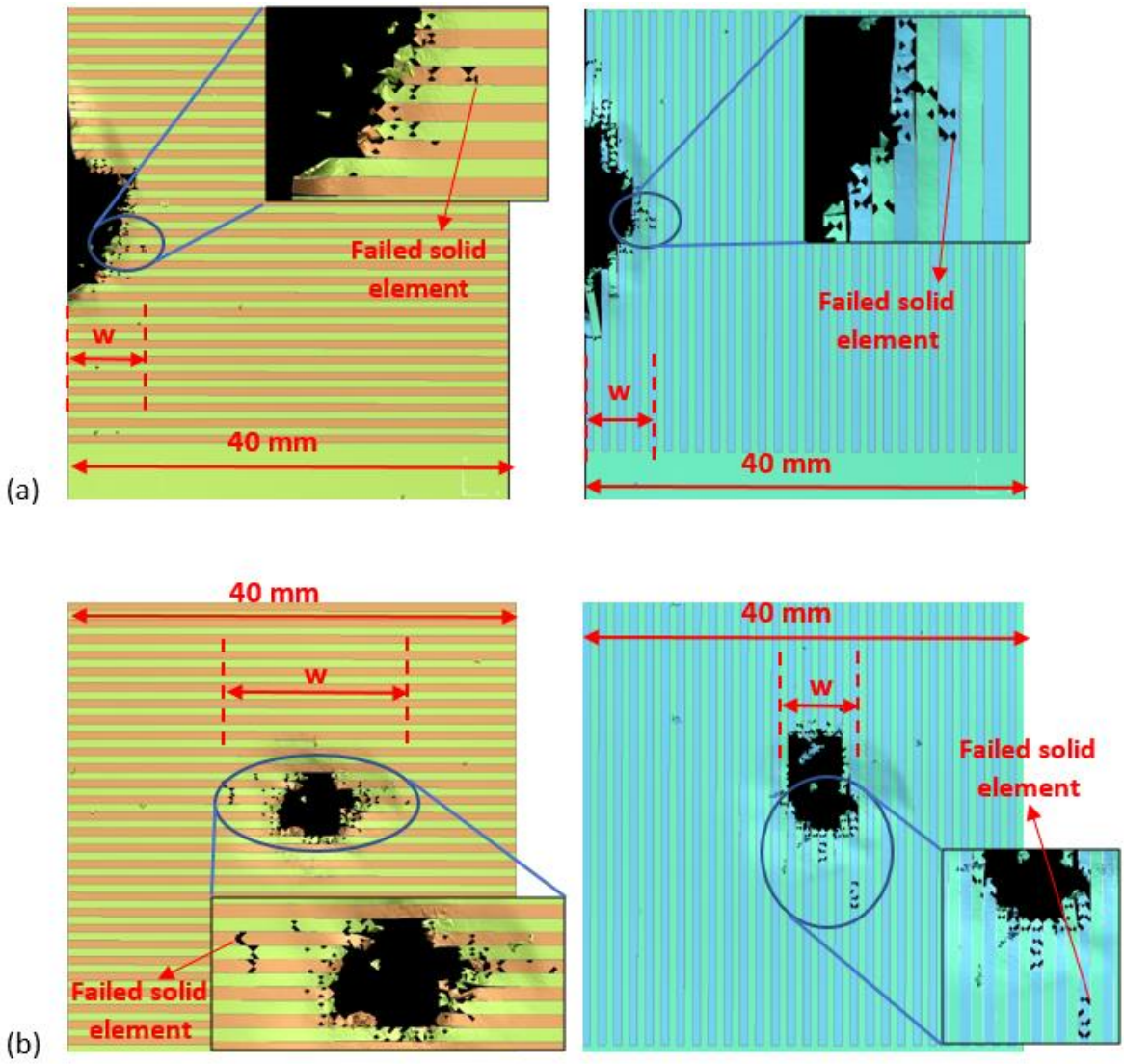

Figure 4.5: Determining the width, w, of broken fibres for (a) edge impact at 350 m/s (90° ply on left and 0° ply on right) and (b) centre impact at 350 m/s (90° ply on left and 0° ply on right).

The fibre fracture widths for all impact configurations are then compared to experimental results from *Chapter 3* and the impact results are illustrated in *Figures 4.11* and *4.12* respectively. Also shown in *Figures 4.11* and *4.12* are the error bars corresponding to the variations in the widths of broken fibres within each ply for a single laminate. Large variations in the widths of broken fibres are observed for most impact

energies, which are due to a larger extent of fibre failure in the plies close to the impact point and a smaller extent of fibre failure in the plies away from the impact point.

At 1.1 J, the edge impact model revealed fibre failure in the top 45° ply only as compared to the first seven plies showing fibre failure from the impact test. Beyond impact energy of 1.1 J, the predicted fibre fracture widths differ from the experimental fibre fracture widths, with an average difference of 26%. A larger discrepancy between test and FE results for low energy edge impacts is observed and this may be associated with the fact that the model fails to cause fibre failure in several plies, i.e. at 2.5 J, the impact model shows fibre failure in 3 plies as compared to the 7 broken plies in the impacted specimen from the experiments. For centre impacts at energy levels beyond 1.1 J, the predicted fibre fracture widths fluctuate from the experimental results by an average difference of 30%. The large differences observed in the predicted and actual fibre fracture widths are believed to be due to the orientation of the cube before impact and the fact that there might be a slight variation in exactly where the cube strikes the target. To further investigate the effect of different projectile orientations on the extent of fibre failure, a parametric study is conducted in *section 4.3*.

Table 4-3: Fibre fracture width values for edge and centre impacts – FE.

	Edge Impacts		Centre Impacts	
Impact energy (J)	No. of broken plies	Fibre fracture width (mm)	No. of broken plies	Fibre fracture width (mm)
1.1	1	2.48	1	0.5
2.5	3	2.71	2	1.06
4.4	6	3.36	3	2.60
6.5	11	3.80	8	2.01
9.9	12	5.03	10	4.55
13.5	15	5.79	13	5.73

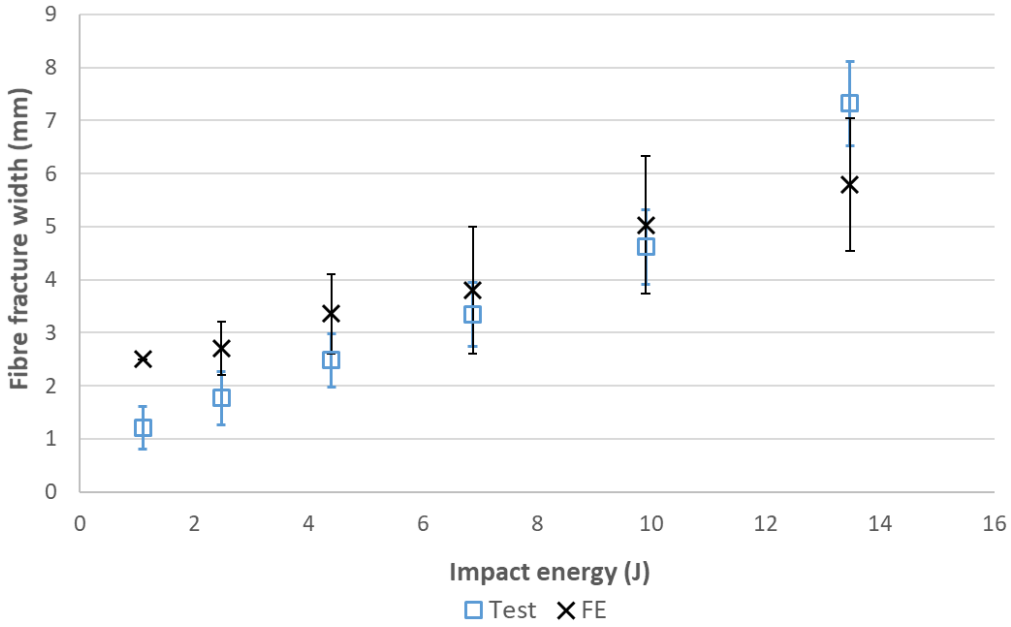

Figure 4.6: Fibre fracture widths for all edge-impacted laminates over a range of impact energies – Test versus FE.

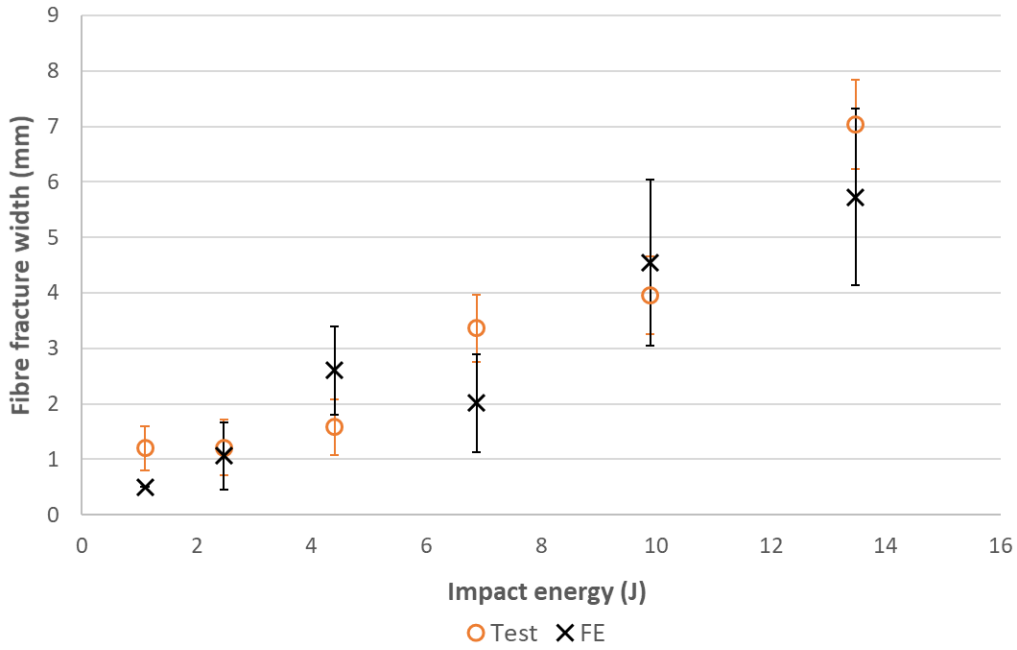

Figure 4.7: Fibre fracture widths for all centre-impacted laminates over a range of impact energies – Test versus FE.

4.2.2. Delamination area

The cohesive interface elements between every ply for all impact configurations are analysed, where fully failed cohesive elements correspond to the delamination area. To measure the delamination area, an image of the cohesive interface is uploaded to the ImageJ® software. Typical 45°/90° interfaces from edge- and centre-impacted laminates at 350 m/s are shown in *Figure 4.13*. The image size is 620 x 620 pixels, corresponding to the Region of Interest (RoI) which measures 40 mm x 40 mm. Using the freehand option available in ImageJ®, the patterns marked in white in *Figure 4.13* are drawn. The area enclosed within the white region is determined in terms of its number of pixels and then translated to an equivalent value in mm^2. This procedure is repeated for all delaminated interfaces from all impact configurations. The delamination area for an impacted laminate was then obtained by averaging over the number of interfaces showing delamination. Detailed results are presented in *Table 4.4*.

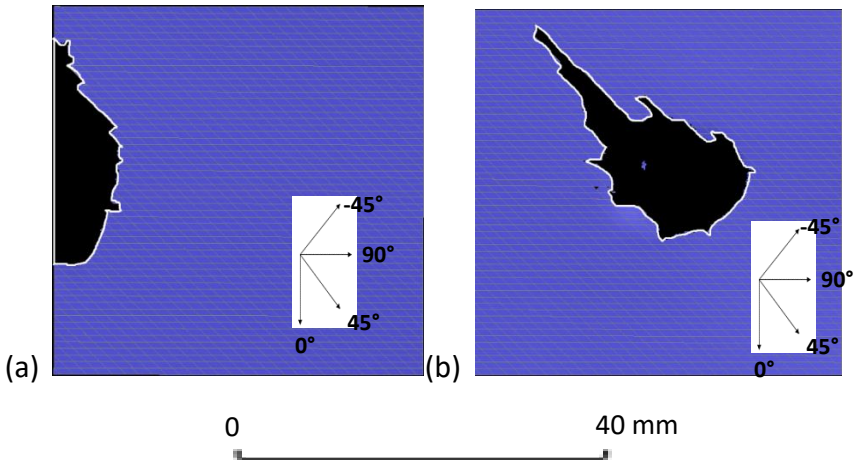

Figure 4.8: Predicted delamination area marked within the white region for typical 45°/90° interfaces as observed in (a) edge-impacted laminate and (b) centre-impacted laminate at 350 m/s.

Table 4-4: Predicted delamination area for all impact configurations.

	Edge Impacts	**Centre Impacts**
Impact energy (J)	Delamination area (mm^2)	Delamination area (mm^2)
1.1	15.8	6.77
2.5	50.3	35.8
4.4	79.9	82.7
6.5	130	134
9.9	177	182
13.5	182	242

The impact model predicts delamination at all interfaces for all impact energies. From *section 3.5*, the CT scanning images revealed delamination in 12 interfaces for an

edge impact at 1.1 J and only one delaminated interface for centre impacts at 1.1 J. As impact energy is increased beyond 1.1 J, the number of delaminated interfaces is correctly predicted by the model. As impact energy is increased, the delamination area increases for both edge and centre impacts. For edge and centre cases, the variations in delamination area with impact energy are plotted in *Figures 4.14* and *4.15* respectively. The delamination areas determined from CT scanning images are also included in *Figures 4.14* and *4.15*. The error bars in *Figures 4.14* and *4.15* are associated with the variations in delamination area of the individual interfaces from the mean in a single specimen.

As impact energy is increased, the predicted delamination area in edge-impacted laminates increases and beyond 9.9 J, increases more slowly. A maximum delamination area and laminate perforation was observed at 9.9 J from the impact tests, and the impact model fails to predict this maximum delamination area, as well as laminate perforation. For centre impacts in *Figure 4.15*, the delamination areas are correctly predicted by the impact model for impact energies between 1.1 J and 6.5 J. However, as impact energy is increased beyond 6.5 J, the predicted delamination areas lie below the experimental results by 46%. The differences in the predicted and experimental delamination areas may be related to the number and positions of interface layers and the fact that the model consists of only one element per ply in the through thickness direction, where the bending stiffness in the through thickness direction is underestimated when using elements with reduced integration. Since the extent of delamination is dependent on the laminate's bending stiffness, the impact model fails to capture the correct the delamination areas for some impact energies. In addition, the smaller predicted delamination areas for some impact cases may be due to the split

spacings used in the impact model. The automated unit cell technique has a limitation since the smallest split spacings vary from 0.71 mm – 1.0 mm.

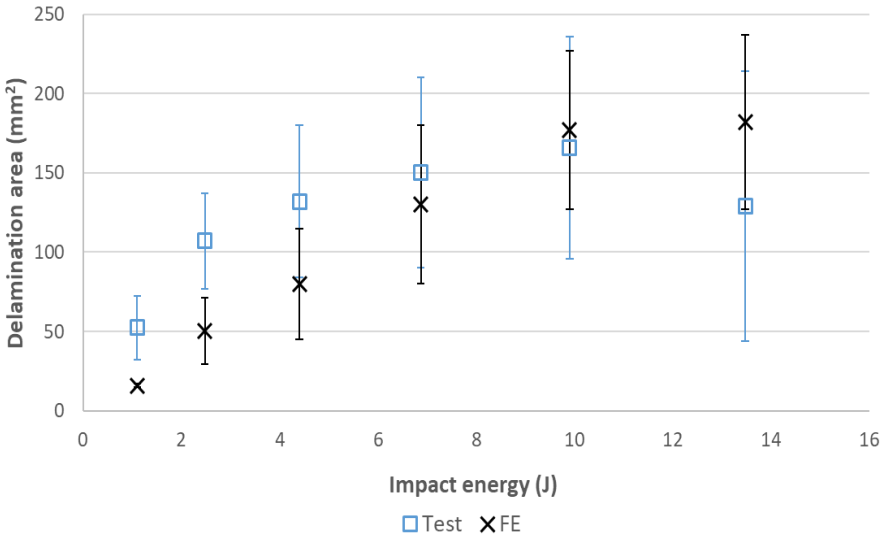

Figure 4.9: Delamination area for all edge-impacted laminates over a range of impact energies – Test versus FE.

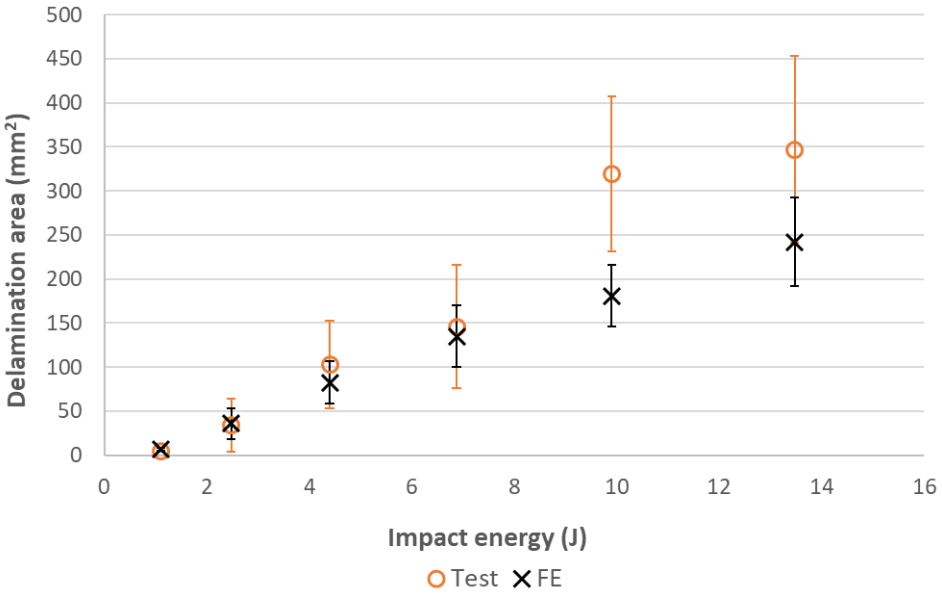

Figure 4.10: Delamination area for all centre-impacted laminates over a range of impact energies – Test versus FE.

4.2.3. Kinetic energy

Post-processing of the finite element simulations allows determining the energy transferred to the system, which is equal to the difference between the initial and the residual kinetic energies of the projectile. The energy is transferred to the system via several failure modes and *Figure 4.16* illustrates the relationship between the transferred energy and the impact energy for edge and centre impacts. As the impact energy increases, the extent of transferred energy increases for both impact configurations, which is why both edge- and centre-impacted laminates show increasing impact damage size with increasing impact energy. For any given impact energy, *Figure 4.16* shows that edge-impacted laminates transfer more kinetic energy to the system than centre-impacted laminates. This implies more energy is available to break the fibres and to contribute to delamination. This agrees with the results from *Table 4.3*, where edge-impacted laminates have a greater number of broken plies and larger extent of fibre failure than centre-impacted laminates.

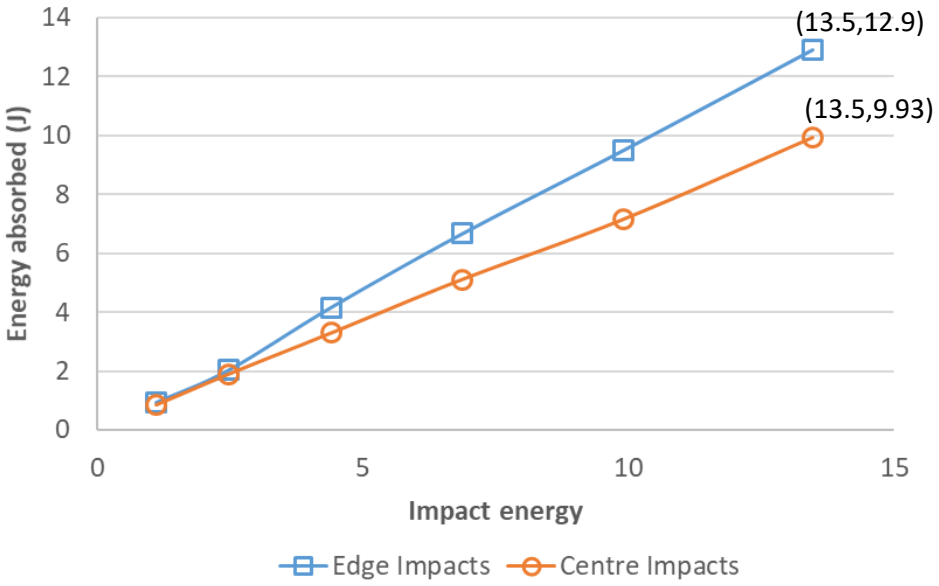

Figure 4.11: Relationship between impact energy and absorbed energy for both impact configurations.

4.2.4. Hourglass energy

As mentioned in *section 4.1.3*, hourglassing is a spurious deformation mode of the finite element mesh, where individual elements are severely distorted. The hourglass energy can be computed in the impact simulations and its value should be small relative to total and internal energy. The accepted rule-of-thumb is that hourglass energy should be less than 10% of internal energy [142]. Here, an investigation into the hourglass and internal energies of the whole system is carried out for different impact energies and the results are illustrated in *Figures 4.17* and *4.18* for edge and centre impacts respectively. Edge and centre impacts at 1.1 J and 13.5 J are considered, and the results show that the hourglass energy is approximately 4% of the internal energy. As such, the use of Flanagan-Belytschko stiffness-based hourglass control is justified, which makes the use of more expensive elements with full integration unnecessary.

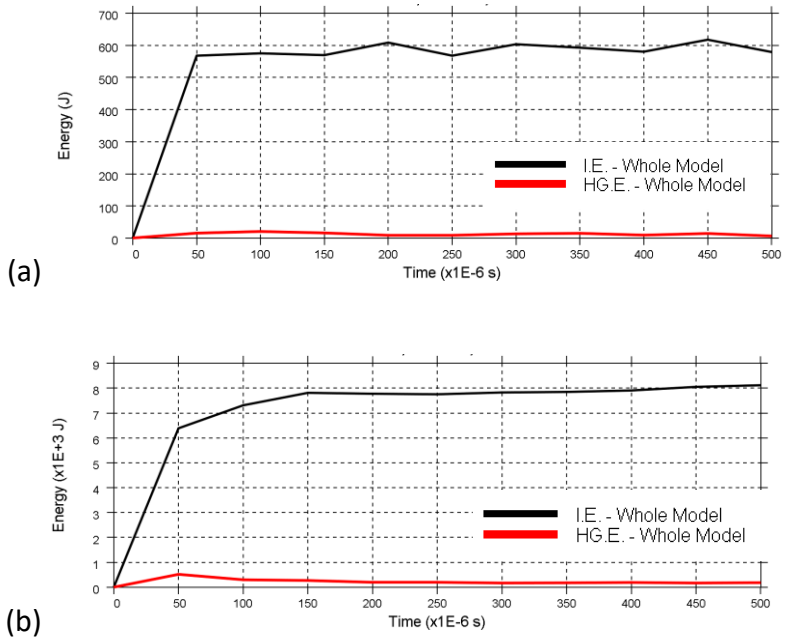

Figure 4.12: Hourglass energy and internal energy of the system for edge impacts at (a) 1.1 J and (b) 13.5 J.

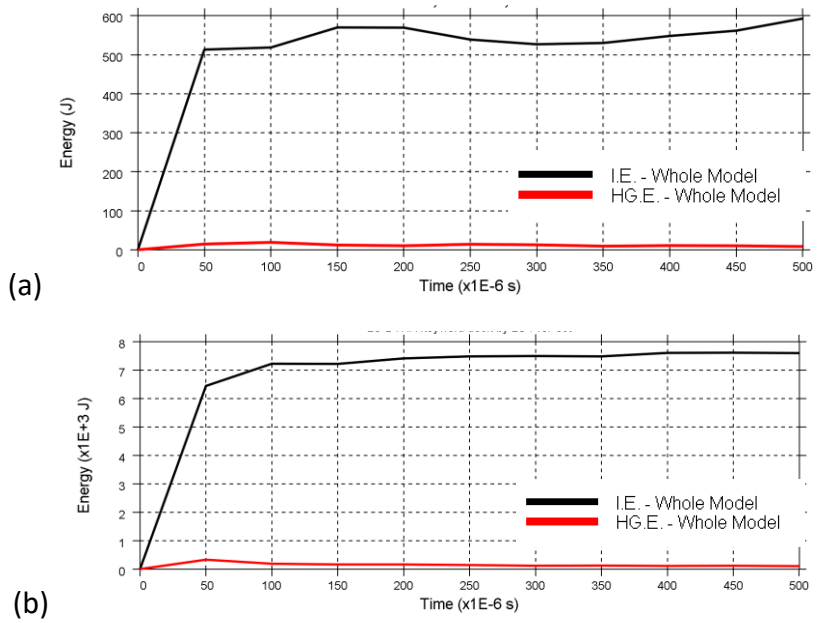

Figure 4.13: Hourglass energy and internal energy of the system for centre impacts at (a) 1.1 J and (b) 13.5 J.

4.2.5. Effect of through thickness compression on shear

As mentioned in *section 4.1.3*, the enhancement effect of through thickness compression is important to consider to accurately capture the Mode II behaviour. The enhancement factor, (η) in *Eq. (4.3)*, is critical in controlling the load corresponding to the delamination initiation, where it serves as an internal friction coefficient that increases the strength in Mode II and the critical energy release rate due to through thickness compression [143]. *Sun et al*. [143] employed an enhancement factor of 0.58 to model barely visible impact damage in scaled composite laminates. As an initial trial and due to the nature of a high velocity impact which occurs in a short period of time, the enhancement factor is set to a higher value equal to 0.7. Because of the strain-rate sensitivity of the friction coefficient [144], a parametric study on the enhancement factor is conducted here, with η set to 0.6 and 1.5. Edge impacts at 100 m/s and 350 m/s are chosen for this parametric study and the predicted impact damage is analysed, where *Figure 4.19* illustrates the sensitivity of the fibre fracture width with varying enhancement factors and *Figure 4.20* refers to the predicted delamination areas as the enhancement factor is altered. For impacts at 100 m/s and 350 m/s, the fibre fracture width decreases as η is set to 0.6 and 1.5, with an average difference of 16%. In comparison to the experimental fibre fracture widths, the closest predictions are obtained with η = 1.5 for 100 m/s and η = 0.7 for 350 m/s. As η is modified, small variations in predicted delamination areas are observed at 100 m/s, where the predicted delamination areas are underestimated irrespective of the value assigned to η. For impacts at 350 m/s, large variations in delamination areas are observed as η is altered, and all predicted areas are overestimated.

The parametric study conducted here shows that the extent of impact damage varies with changes in the enhancement factor and further analysis is required which takes into consideration a wider range of enhancement factors. Otherwise, interlaminar shear strength tests under dynamic conditions using a split-Hopkinson bar test system need to be carried out to determine η. However, for this study, a value of 0.7 for the enhancement factor is considered.

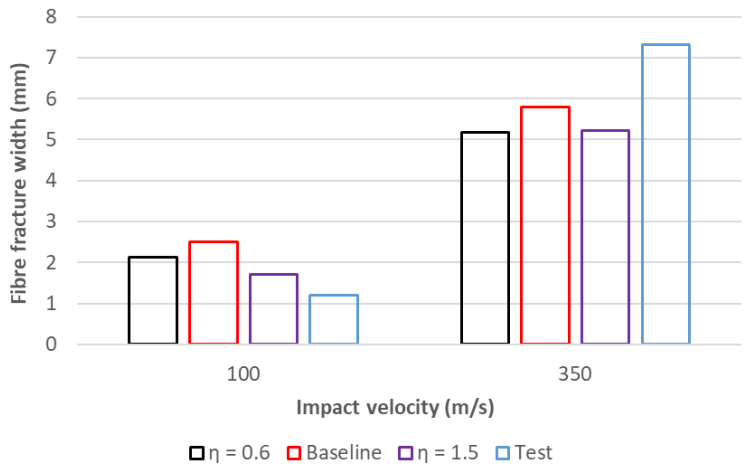

Figure 4.14: Fibre fracture width sensitivity to variations in the enhancement factor.

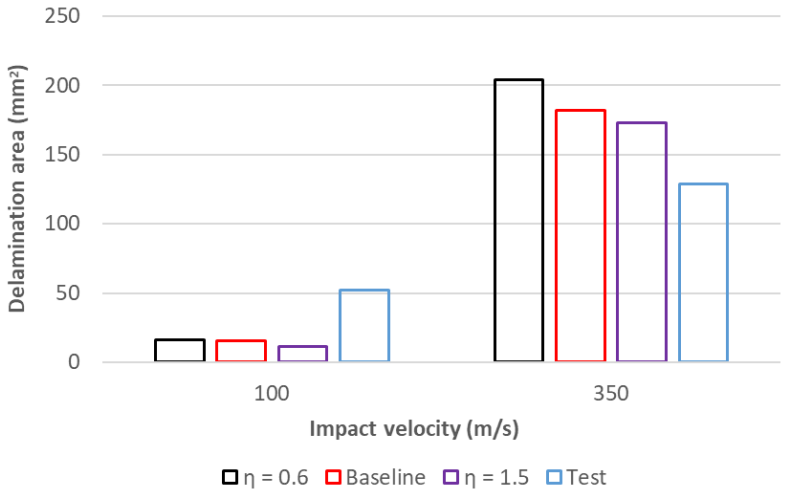

Figure 4.15: Delamination area sensitivity to variations in the enhancement factor.

4.3. Development of baseline impact model

The finite element simulation results for both edge and centre impacts, in terms of extent of fibre failure and delamination area, differ considerably for some impact energy levels. To this extent, this section describes several ways at improving the baseline impact model and at the same time, investigating the parameters which may affect the extent of impact damage. The possible improvements are:

- Finer mesh size
- Different projectile orientations before impact
- Representative sub-laminates, where the number and positions of cohesive layers are varied
- Through thickness mesh density, i.e. number of elements per ply.

4.3.1. Mesh sensitivity

The impact model developed in *section 4.1* has an average mesh size of 0.23 mm in the RoI region, while the region outside the RoI has a much coarser mesh size. To verify how sensitive the extent of impact damage is to mesh size, simulations are carried out with a finer mesh size for the RoI. The refined RoI has an average mesh size of 0.11 mm. Due to a limited of number of elements which can be created for a finite element model with the automated unit cell meshing technique, there is a restriction on the size of the RoI and the latter is 40 mm wide and 25 mm long. The new RoI is illustrated in *Figure 4.21*. High velocity impacts at energy levels of 1.1 J, 4.4 J, 9.9 J and 13.5 J are simulated, and the extent of fibre failure and delamination area are investigated and compared to the FE model with the baseline mesh size.

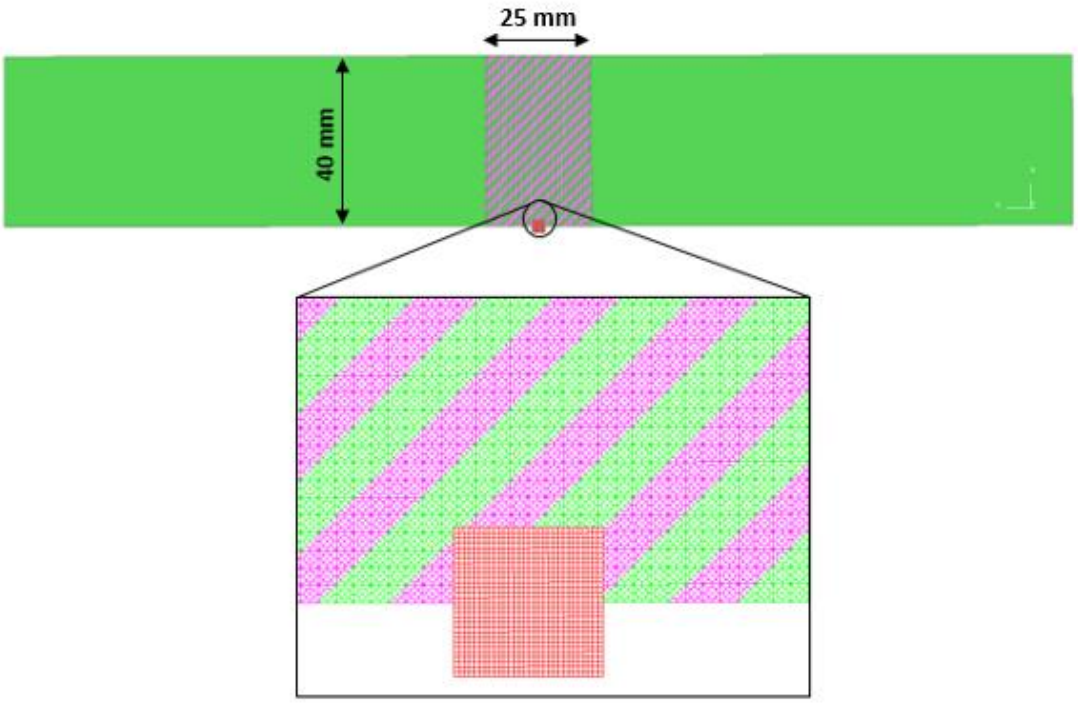

Figure 4.16: FE model illustrating Region of Interest (RoI) with finer mesh.

4.3.1.1. Fibre fracture width

The extent of fibre failure in all plies was inspected for edge and centre impacts at varying energy levels. The fibre fracture widths from CT scans, FE model with baseline mesh and FE model with finer mesh are compared and illustrated in *Figures 4.22* and *4.23* for edge and centre cases respectively. For edge impacts over the range of impact energies considered, the predicted fibre fracture widths using the baseline and fine meshes differ by an average of 4.1%. At an impact energy of 1.1 J, the predicted fibre frature width is lower by 11% as the mesh size is reduced. As impact energy is increased, the fine and baseline mesh results converge.

For centre impacts over the range of impact energies, the predicted fibre fracture widths using the baseline and fine meshes differ by an average of 28%. At an impact energy of 1.1 J, the predicted fibre fracture width is significantly higher as the mesh size is

reduced. With increasing impact energy, the fine and baseline mesh results converge. In comparsion to the experimental fibre fracture widths, it is observed that there is no significant improvement in the fibre failure predictions as the mesh size is reduced. In addition, there are high computational costs associated with using a finer mesh. The baseline mesh employed in the impact model is considered adequate.

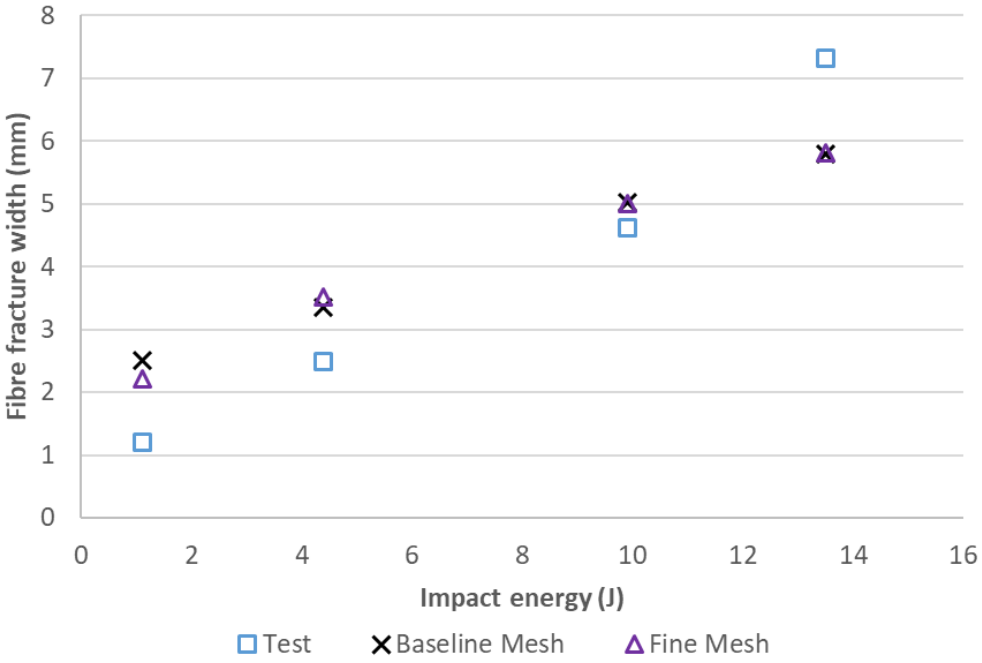

Figure 4.17: Effect of mesh size on fibre fracture widths for edge impacts.

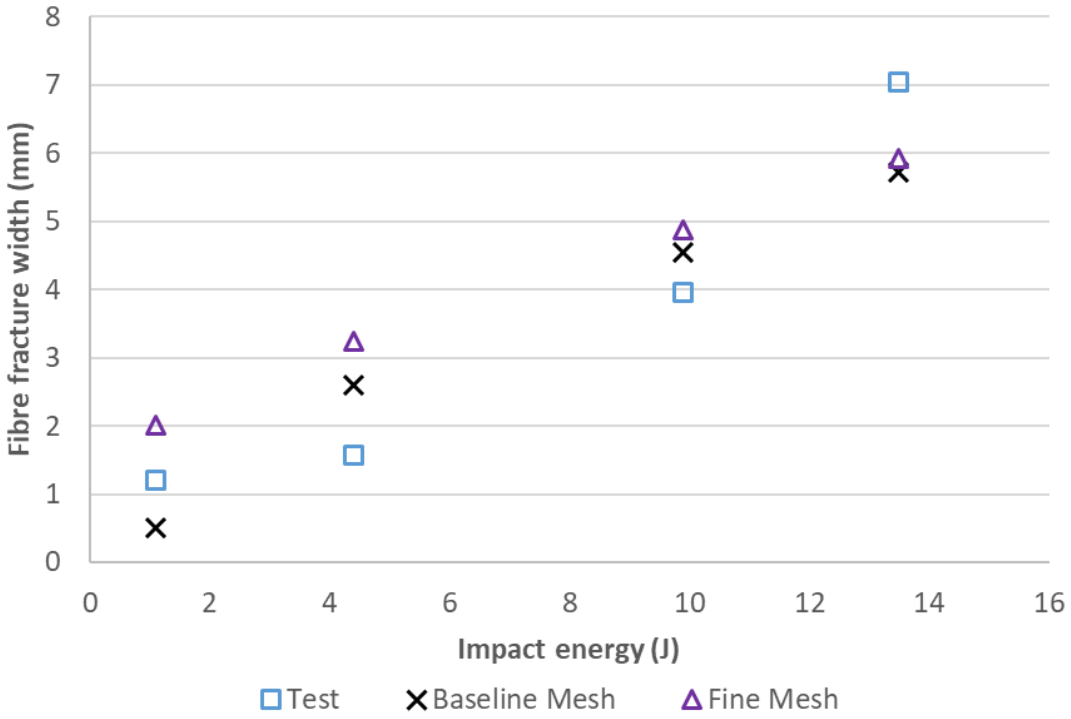

Figure 4.18: Effect of mesh size on fibre fracture widths for centre impacts.

4.3.1.2. Delamination area

The predicted delamination areas for edge and centre impacts over a range of impact energies obtained from models with the baseline and fine mesh sizes are compared and illustrated in *Figures 4.24* and *4.25*. The predicted delamination areas differ by an average of 5% over the range of impact energies considered. At lower impact energies, the fine and baseline mesh results converge. However, as impact energy is increased to 13.5 J, the delamination area is higher by 9% as the mesh size is reduced. The predicted delamination areas for centre impacts from *Figure 4.25* show that the fine and baseline mesh results converge over the range of impact energies considered. In comparison to the experimental results, an impact model with a finer mesh does not yield significant improvements in the predicted delamination areas. As such, for this numerical

study, the baseline mesh is assumed sufficient in addition to its lower computational costs.

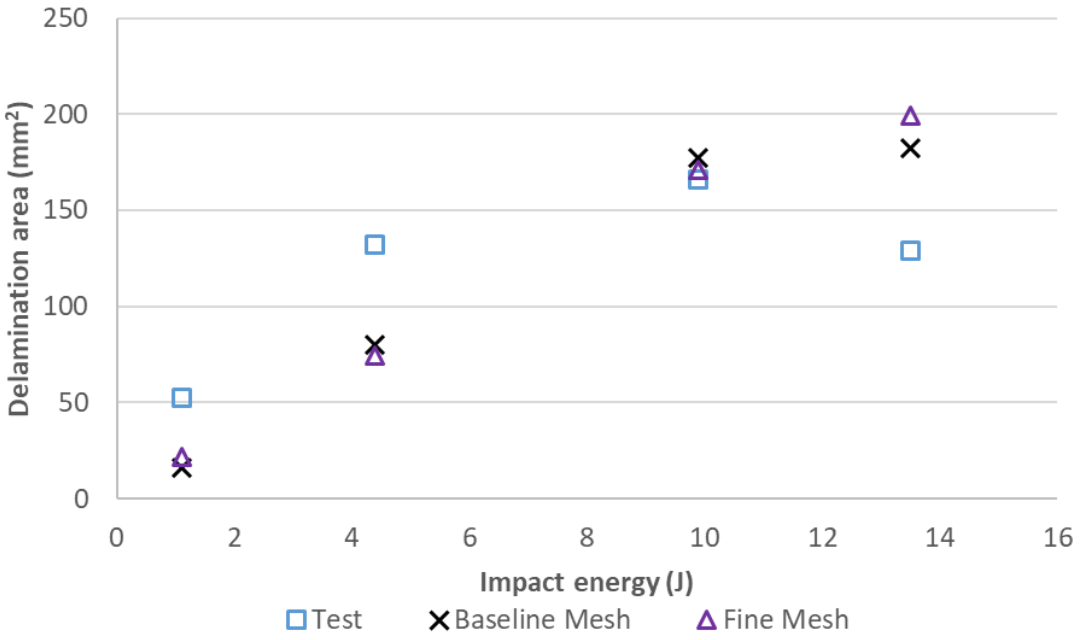

Figure 4.19: Effect of mesh size on delamination areas for edge impacts.

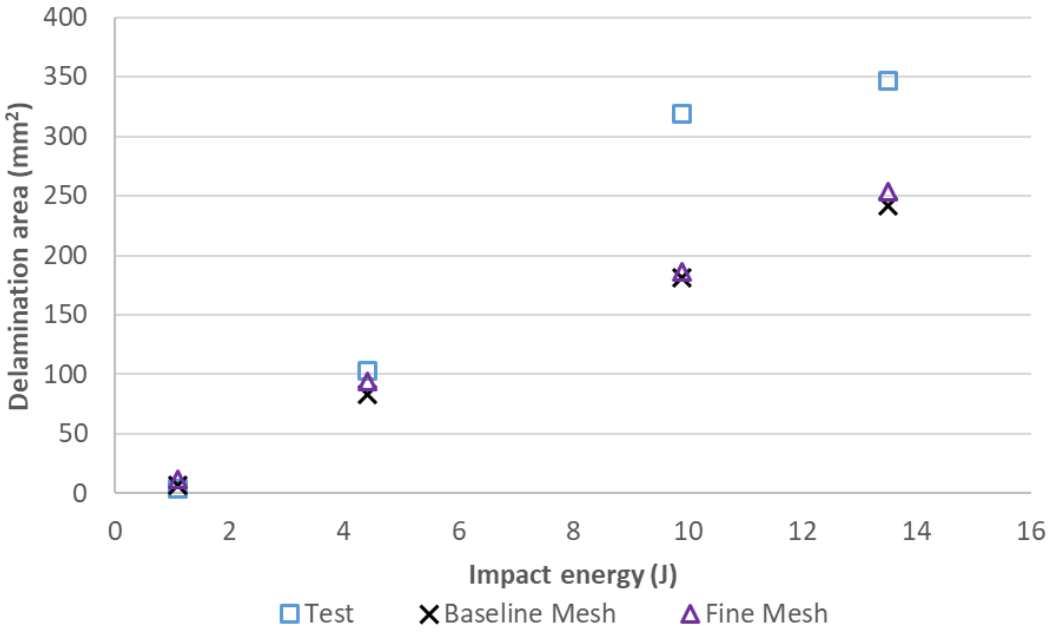

Figure 4.20: Effect of mesh size on delamination areas for centre impacts.

4.3.2. Effect of projectile's orientation

The differences observed in the extent of impact damage between the FE and experimental results for edge- and centre-impacted laminates could be due to different orientations of the projectile before impact and possible variation in exactly where the laminate was struck. In the impact test setup, the mechanical fixture was positioned such that the projectile strikes the target at 1.5 mm and 20 mm from the edge for the edge and centre impacts respectively. However, as mentioned in *Chapter 3*, it was not possible to control the projectile's rotation once it leaves the sabot. To this end, it is interesting to investigate the effect of different projectile orientations on the predicted extent of impact damage.

The baseline orientation of the projectile in the baseline impact model, as shown in *Figure 4.3*, relates to the surface of the projectile impacting the target. The first variation in the projectile's orientation considered is where the projectile strikes the target in a 'point first' configuration, which is referred to as 'Point'. The second one relates to an edge of the projectile striking the target and is referred to as 'Edge'. As before, an oblique impact is to be simulated, where the projectile strikes the target at 1.5 mm and 20 mm from the edge. *Figure 4.26* illustrates the two different projectile orientations for a typical edge impact. The finite element model with different orientations is simulated for edge and centre impacts at impact energy levels of 1.1 J, 4.4 J, 9.9 J and 13.5 J. Post-processing includes determining the fibre fracture widths and delamination areas.

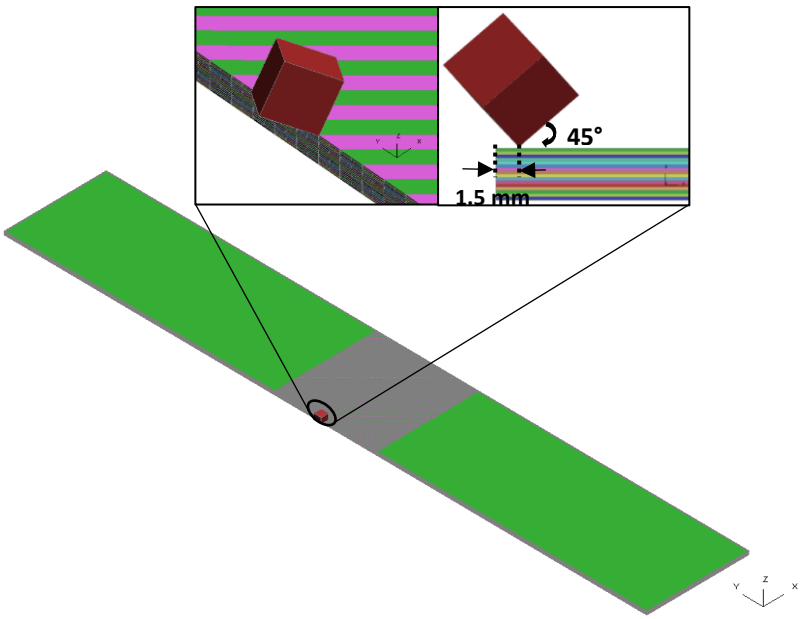

(a)

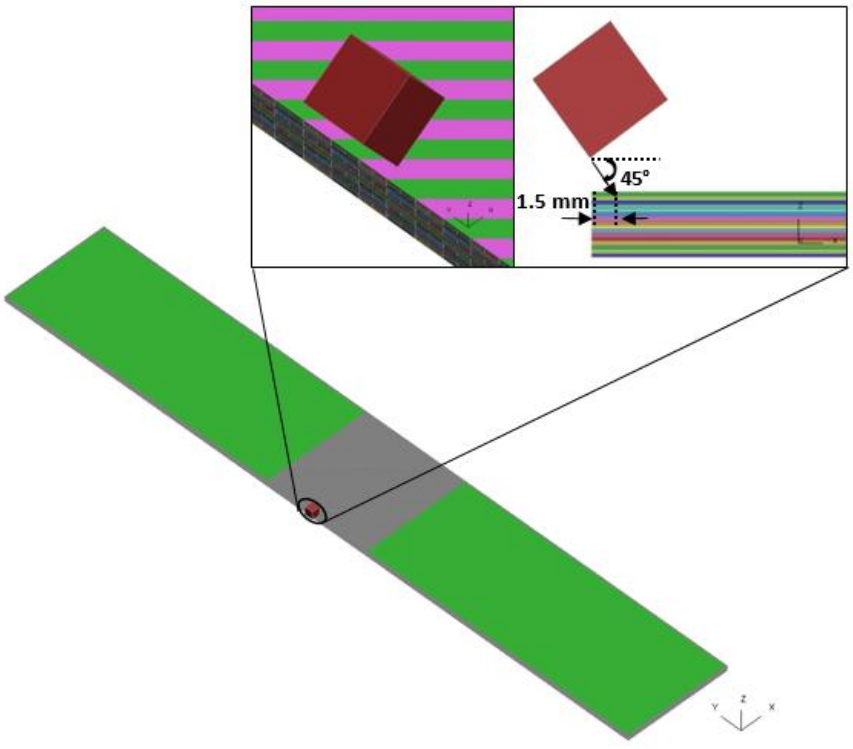

(b)

Figure 4.21: FE model showing the two projectile orientations considered where (a) shows a 'Point' of the projectile striking the target and (b) shows an 'Edge' of the projectile striking the target.

4.3.2.1. Fibre fracture width

The extent of fibre failure in all plies was measured using the ImageJ® software. *Figures 4.27* and *4.28* illustrate the predicted fibre fracture widths for edge and centre impacts respectively. Also included on the plots are the results from the impact tests. For edge impacts at 1.1 J and 4.4 J, changes in the orientations of the projectile before impact do not result in large variations in the predicted fibre fracture widths. However, as the impact energy is increased beyond 4.4 J, the predicted fibre fracture widths are significantly influenced by the changes in projectile orientations. Between 4.4 J and 13.5 J, the orientation 'Point' yields the largest fibre fracture width. An interesting observation is made at 13.5 J, where the experimental fibre fracture width lies within the range of predicted fibre fracture widths with different orientations.

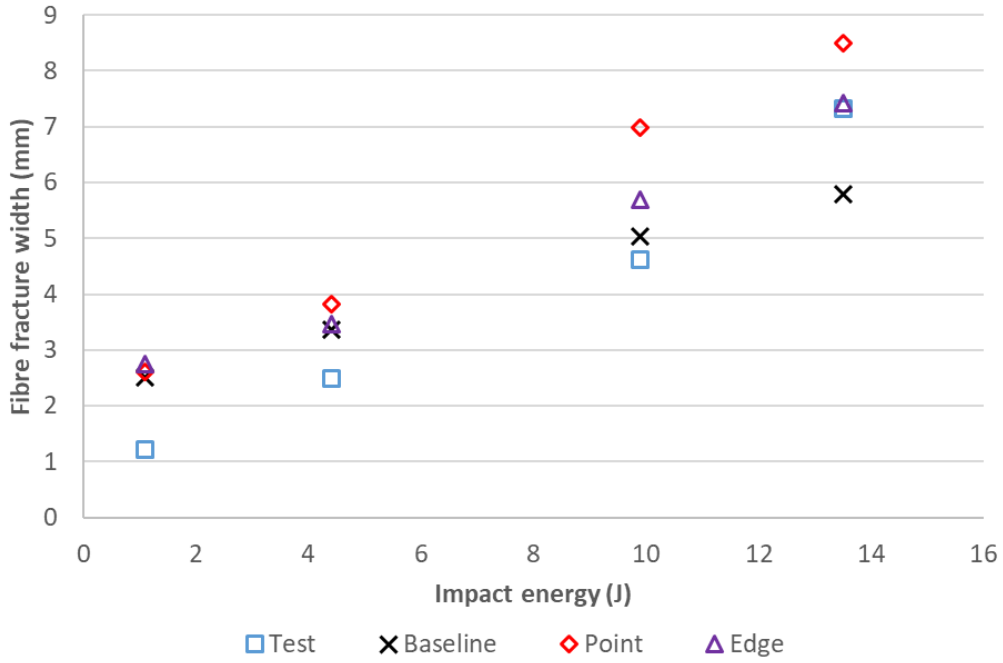

Figure 4.22: Predicted fibre fracture widths for different projectile's orientations and experimental fibre fracture widths for varying energy levels in edge-impacted laminates.

As the orientations are altered for centre impacts, the variations in predicted fibre fracture width become larger beyond 1.1 J. The 'Point' configuration produces the largest extent of fibre fracture at any given impact energy and at 1.1 J, the predicted fibre fracture width is spot on with the 'Point' configuration. At impact energy of 13.5 J, the experimental fibre fracture again lies within the range of predicted fibre fracture widths with varying orientations. For both edge and centre impacts, it is shown that the predicted fibre fracture widths are affected by changes in projectile orientations. While the projectile has a mesh size of 0.1 mm and the laminate within the RoI has an average mesh size of 0.23 mm, there is a possibility that the effect of sharp contact in the 'Point' and 'Edge' configurations is not simulated as it should be. A finer mesh size for the projectile and the laminate represents a possible improvement, however, it is computationally expensive.

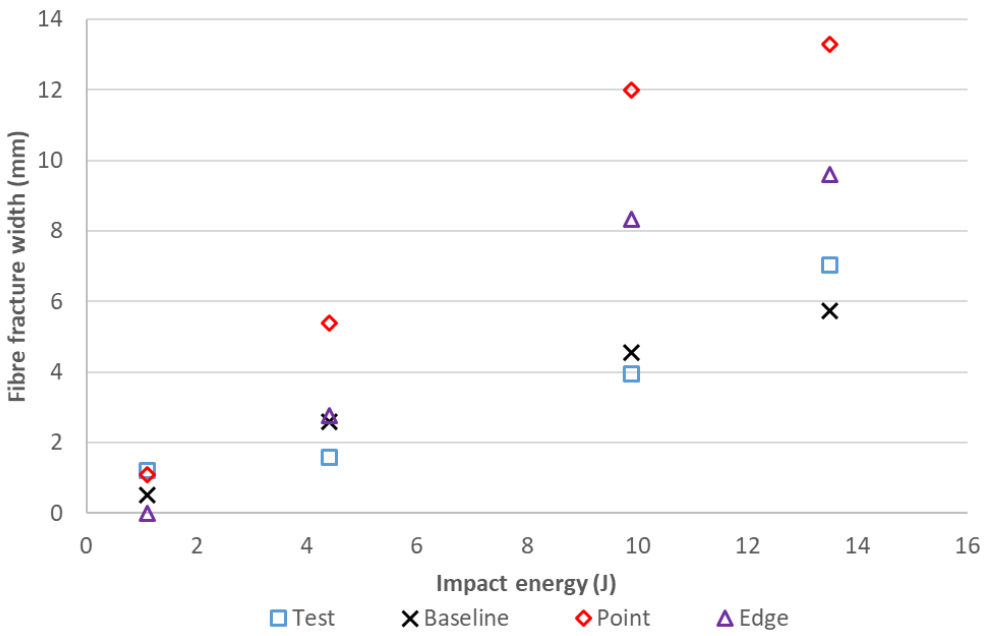

Figure 4.23: Predicted fibre fracture widths for different projectile's orientations and experimental fibre fracture widths for varying energy levels in centre-impacted laminates.

4.3.2.2. Delamination area

The delamination areas for different projectile orientations are predicted and compared to the experimental results. The findings are illustrated in *Figures 4.29* and *4.30* for edge and centre impacts respectively. For lower impact energies, the extent of delamination area is less affected by changes in the orientation of the projectile as compared to impacts at higher energies. For an edge impact at 9.9 J, the experimental delamination area lies within the range of predicted areas as the orientations are varied. For a centre impact at 13.5 J, the 'Point' configuration yields the closest value with the experimental result, however, its associated fibre fracture width is significantly higher than the experimental fibre fracture width.

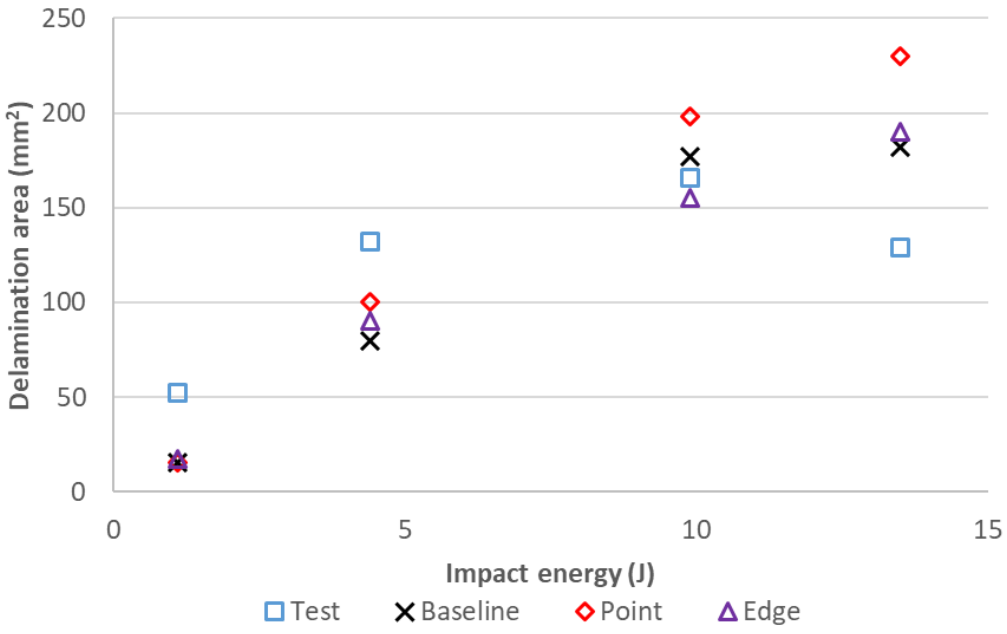

Figure 4.24: Predicted delamination areas for different projectile's orientations and experimental delamination areas for varying energy levels in edge-impacted laminates.

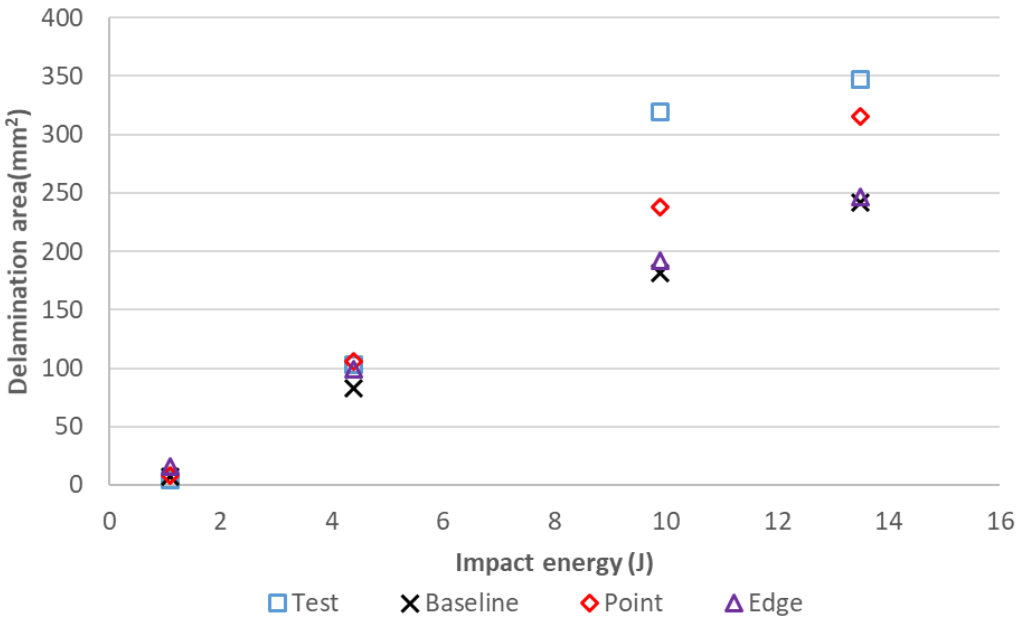

Figure 4.25: Predicted delamination areas for different projectile's orientations and experimental delamination areas for varying energy levels in centre-impacted laminates.

4.3.2.3. Contact force

The changes in the orientation of the projectile before impact have been shown to yield large variations in the extent of fibre failure. These variations in the fibre fracture width can be associated with the contact force on impact and the area of contact between the projectile and the laminate. Typical force-time histories obtained from the numerical models for various projectile orientations and impact energies are illustrated in *Figures 4.31* for typical centre impacts at 4.4 J and 13.5 J. The time duration of the impact event is similar for the impact cases considered and the contact force increases with impact energy. For impacts at 4.4 J and 13.5 J, the model with the 'Point' orientation shows the highest contact force. Given the 'Point' configuration has the smallest contact area upon impact, the 'Point' configuration results in the largest fibre fracture widths as shown in *Figure 4.28*. As the orientation is varied from 'Point' to 'Edge', the contact force decreases and the contact area increases. As such, the predicted fibre fracture widths are

smaller compared to the predicted values from the 'Point' orientation. The baseline orientation has the smallest contact force upon impact, as seen in *Figure 4.31*, which can be associated with the smallest fibre fracture widths observed for this particular orientation.

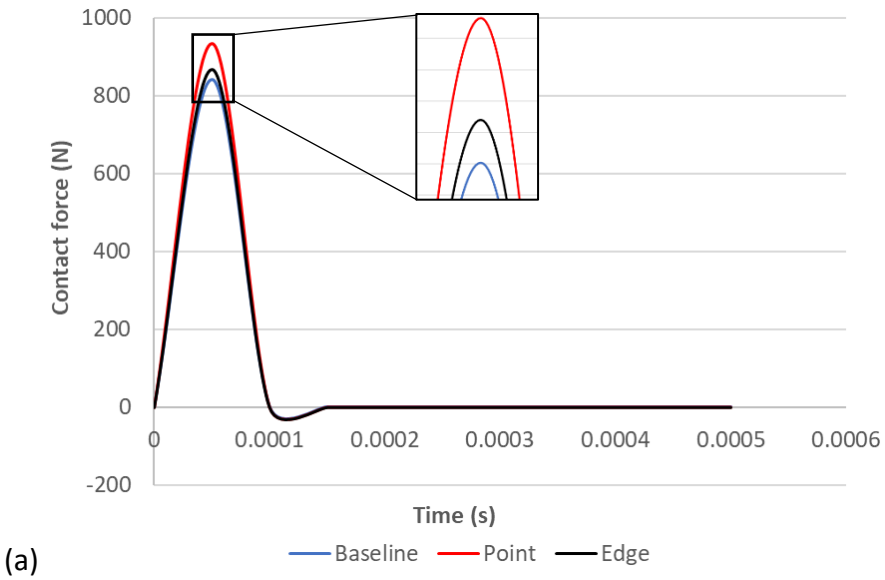

(a)

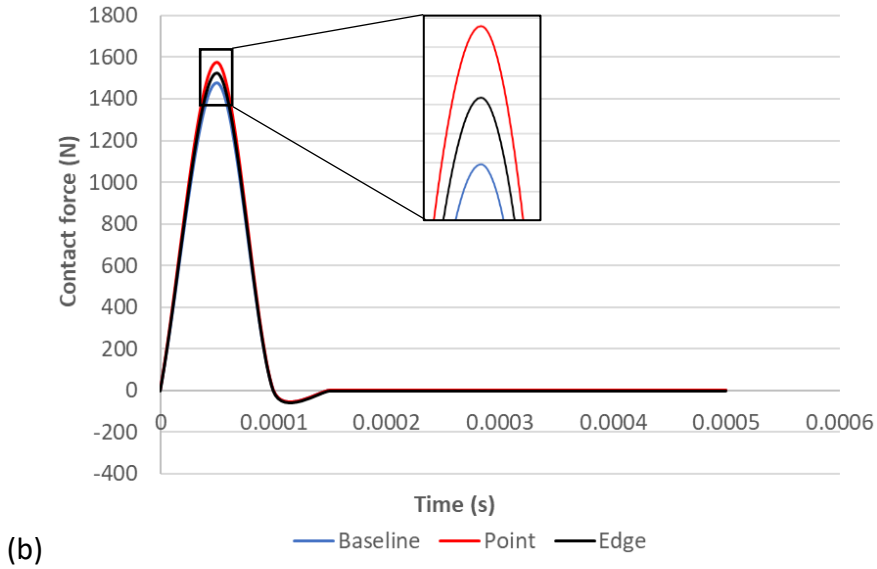

(b)

Figure 4.26: Contact force-time histories for centre impacts with varying projectile orientations at impact energy of (a) 1.1 J and (b) 13.5 J.

4.3.3. Representative sub-laminates

Inter-laminar load transfer between plies of different orientations (Mode II) and through thickness tensile stress waves (Mode I) lead to interface stresses, which drive delamination in impacted laminates [90]. Local delamination mainly occurs close to the impact point and further away from the impact point, interface cracks accumulate. While cohesive interface elements were defined between every ply in the baseline impact model, it is of interest to investigate the effect on the extent of delamination area when the position and number of interface layers are reduced. In doing so, the computational costs are significantly reduced as the number of equations to be solved is decreased. Additionally, since each ply is made up of one layer of single integration point elements, once it has delaminated either side, its bending stiffness is incorrect. Therefore, once the laminate is separated into layers of multiple elements, the delamination area is expected to increase as the extent of delamination is dependent on the local bending stiffness of the sub-laminate as discretised. Based on the failure behaviour observed in an experimental study conducted by *Johnson et al.* [145], four sub-laminates each consisting of four plies were used to simulate a 16-ply laminate. While *Heims et al.* [146] studied the effect of using two, three, four and six cohesive layers for a 24-ply laminate to simulate low velocity impact, *Pickett et al.* [147] employed eight layers of shell elements to simulate a 16-ply laminate. Only the number of interfaces was changed in the above studies [145-147], and each single ply was defined by one element with single point integration. The authors observed that the amount of energy absorbed by the system is significantly influenced by the number of interface layers and an increase in the number of interface layers contributed to a reduction in lateral bending stiffness.

From the baseline impact model, the delamination area was underpredicted for edge impacts at lower impact energies and for centre impacts at higher impact energies. This section investigates the effect of the number and position of interface layers on the extent of impact damage. Finite element models are created with similar boundary conditions, failure criteria, lamina and cohesive properties as in the baseline impact model, and the number of elements per ply is kept at one. The number and positions of cohesive interface layers are illustrated in *Figure 4.32*, which shows cohesive elements inserted after every two and four plies. The variation in delamination area with impact energy for edge-impacted laminates are shown in *Figure 4.33*, and the delamination patterns observed for the different sub-laminate configurations within the RoI are illustrated in *Figure 4.34*. While *Figure 4.35* depicts the relationship between delamination area and impact energy for centre-impacted laminates, *Figure 4.36* shows the damage patterns in centre-impacted laminates within the RoI over a range of impact energies. To assess the effect of the number of cohesive layers on the delamination area, the delamination areas and patterns from the baseline impact model and impact tests are also included in *Figures 4.33, 4.34*, *4.35 and 4.36*.

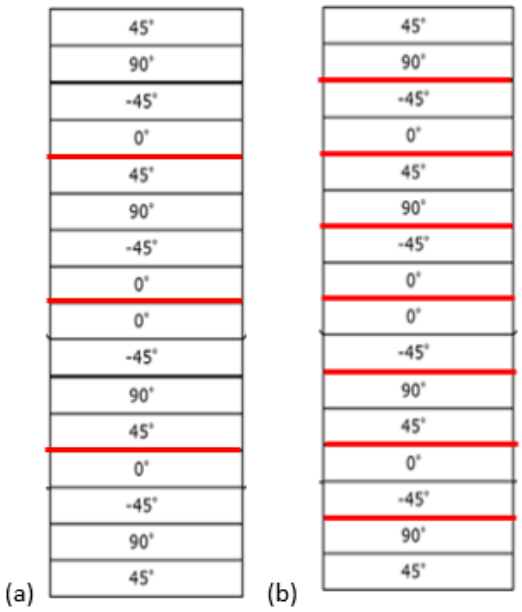

Figure 4.27: Definition of cohesive interfaces (a) after every 4 plies and (b) after every 2 plies. The cohesive interfaces are represented by the red lines.

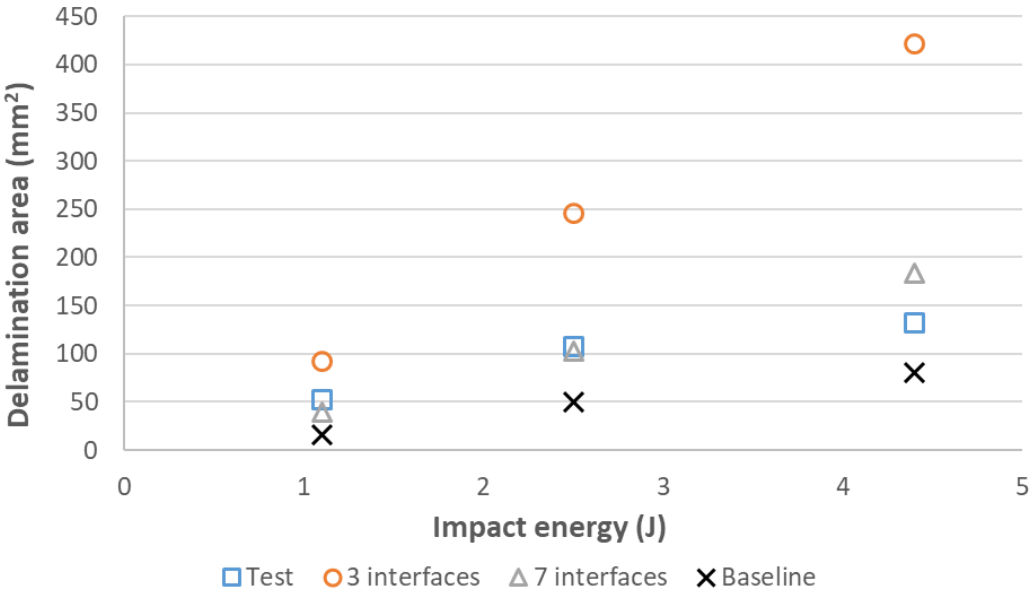

Figure 4.28: Delamination area versus impact energy for different sub-laminate configurations in edge-impacted laminates.

The results reveal that the changes to the number of interfaces have significant effects on the predicted delamination areas. For edge impacts in *Figure 4.33*, the extent of delamination is largest when interface elements are inserted after every 4 plies. At lower impact energies, there is a smaller variation in the delamination area compared to the variations in the area at higher impact energies as the number of interface layers are varied. The predicted delamination patterns from *Figure 4.34* when interface layers are inserted between all plies differ considerably from the CT scan images. As the number of interface layers is decreased, the delamination patterns approach those from CT scans. In addition, at 4.4 J, all sub-laminate configurations fail to capture the delamination pattern observed in the bottom 45°/90° interface, which extends across more than half of the laminate's width. Similar observations can be made for centre impacts at higher impact energies, where the delamination area varies significantly as the number of interface layers is increased.

Throughout this numerical study, delamination areas have been characterised as an average value as it clearly represents the extent of internal damage within an impacted laminate. Nevertheless, the total delamination area and the projected delamination area were also considered. However, neither total delamination area nor projected delamination area have yielded closer predictions to the experimental results.

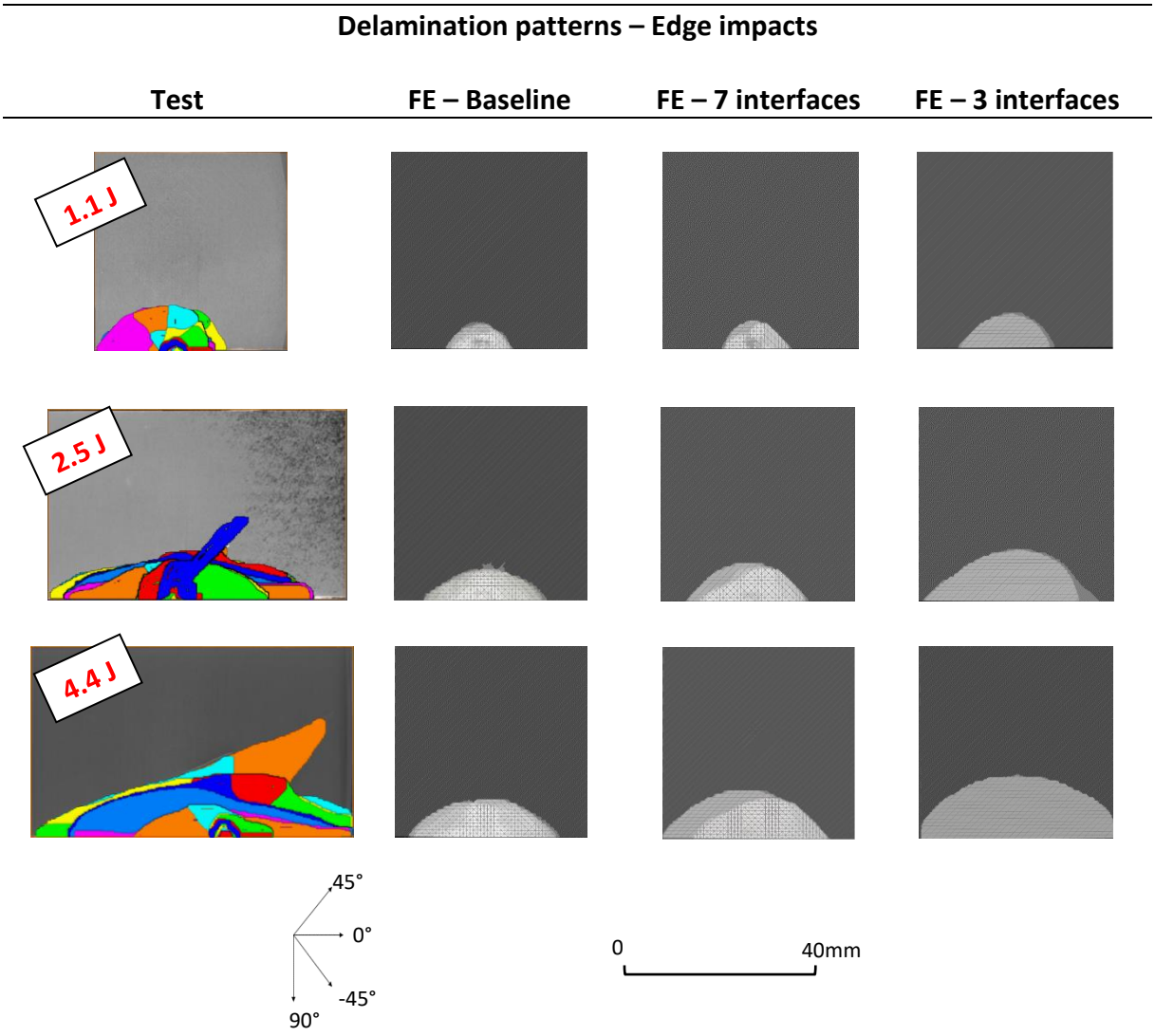

Figure 4.29: Delamination patterns over a range of impact energies for different sub-laminate configurations in edge-impacted laminates.

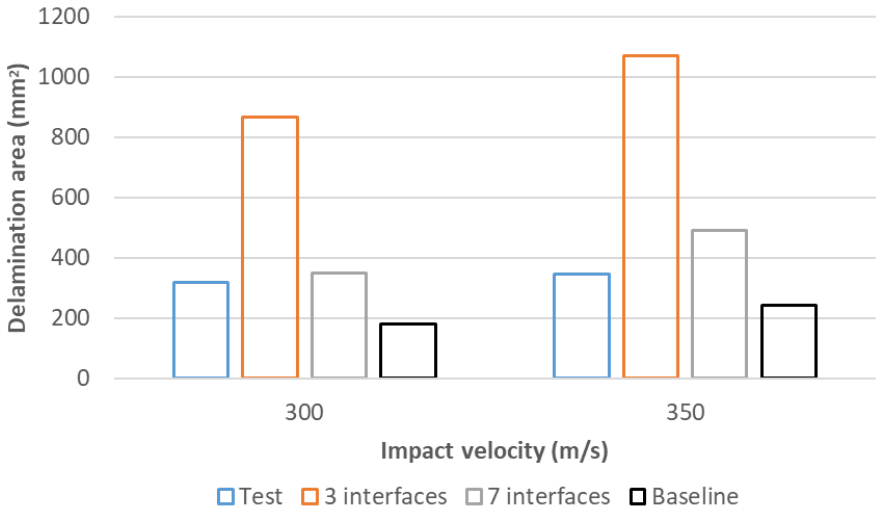

Figure 4.30: Delamination area versus impact energy for different sub-laminate configurations in centre-impacted laminates.

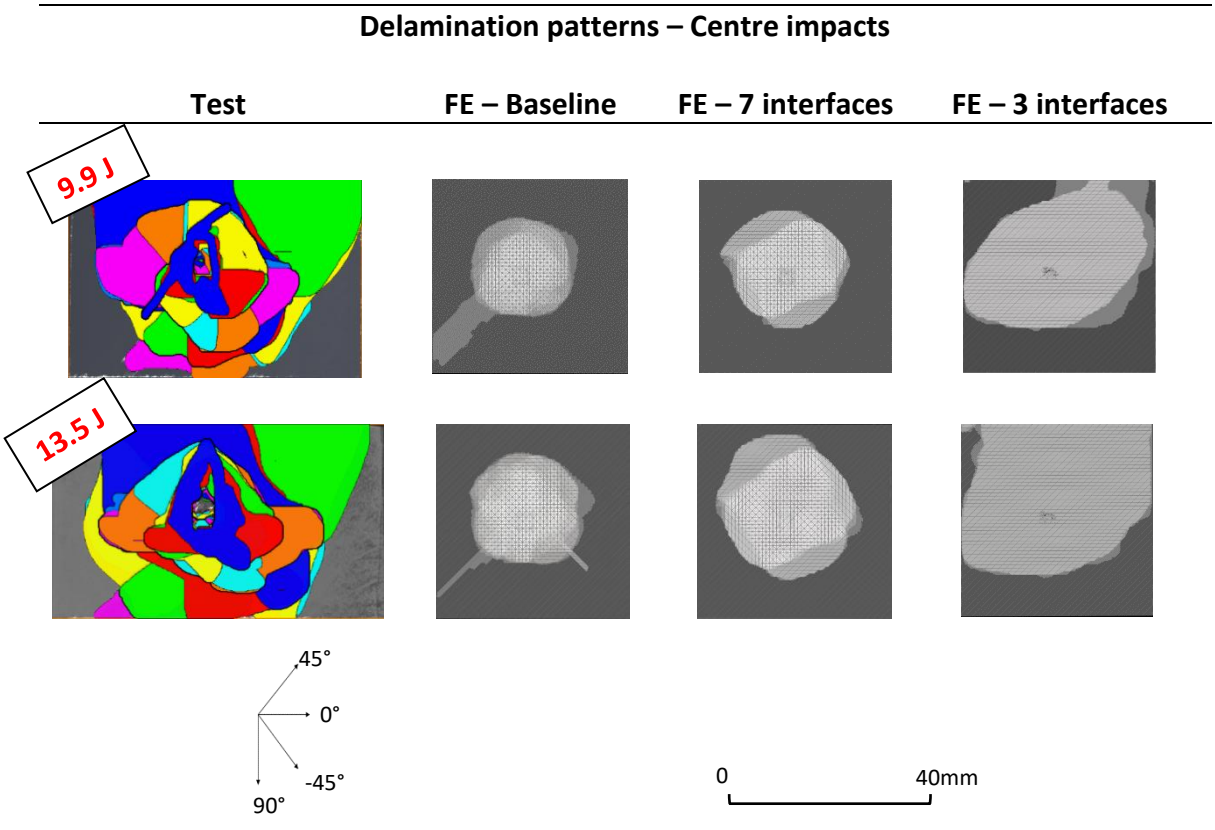

Figure 4.31: Delamination patterns over a range of impact energies for different sub-laminate configurations in centre-impacted laminates.

The extent of fibre failure observed in the impacted laminates with the varying sub-laminate configurations are investigated and the results for edge and centre impacts are presented in *Figures 4.37* and *4.38* respectively. For edge impacts, the laminates show large differences in the extent of fibre failure as the number of interface layers in decreased. In addition, the impact model with different sub-laminate configurations overestimates the experimental fibre fracture widths. Likewise, for centre impacts, there are large variations in fibre fracture widths as the number of interface layers is decreased.

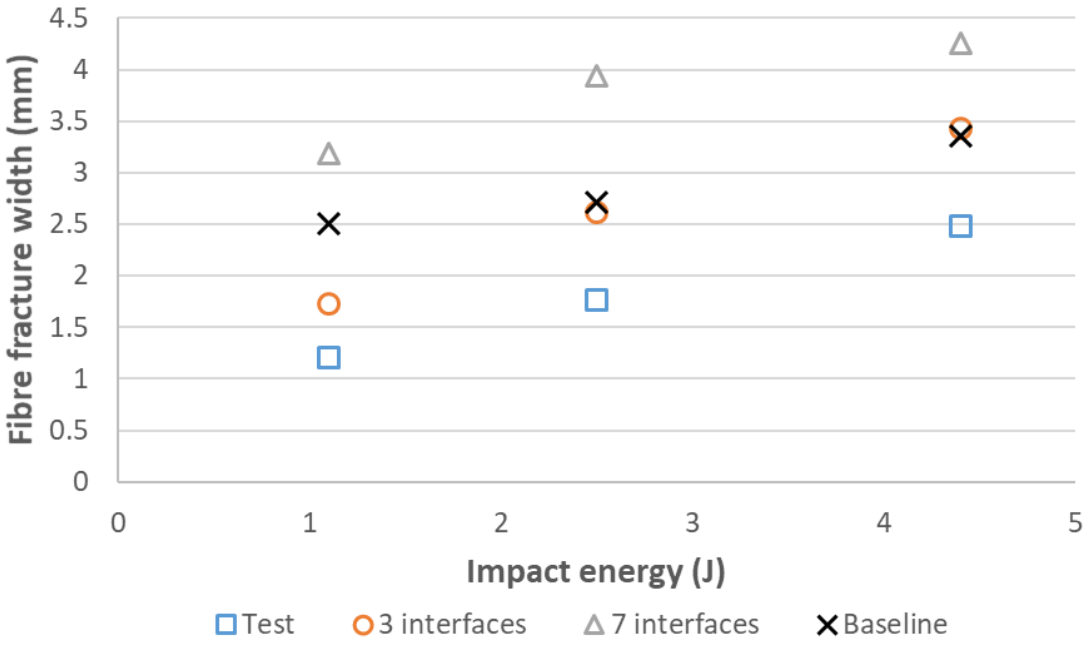

Figure 4.32: Extent of fibre failure over a range of impact energy with varying sub-laminate configurations for edge impacts.

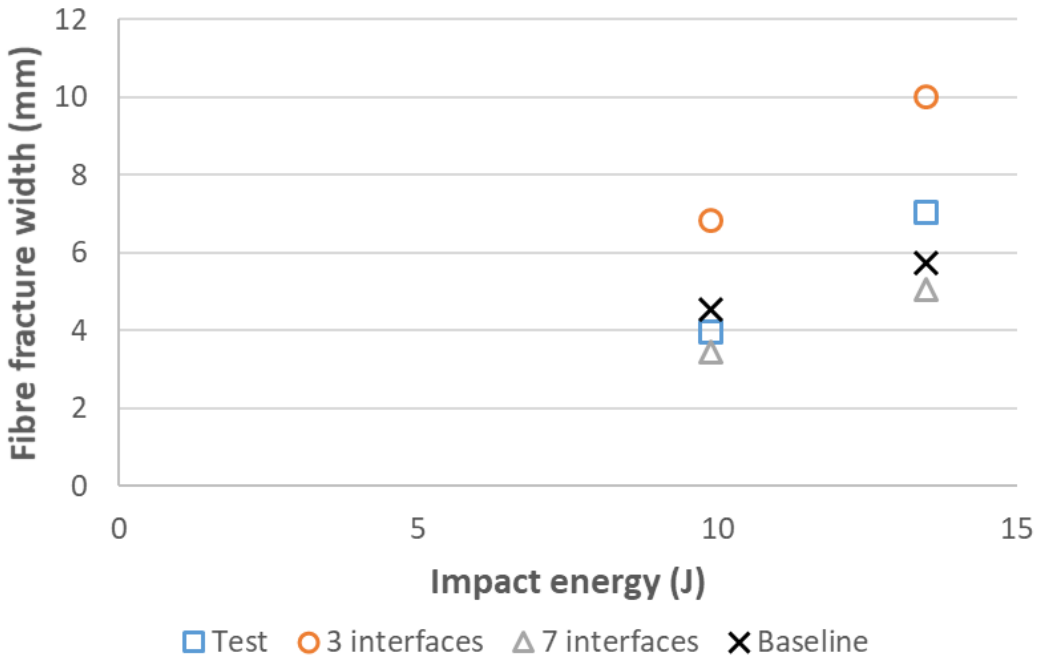

Figure 4.33: Extent of fibre failure over a range of impact energy with varying sub-laminate configurations for centre impacts.

4.3.4. Through-thickness mesh density

Previous numerical works on high velocity impact [55,84,87,94,148] have reported the use of one element per ply in the through-thickness direction. While the baseline impact model consists of one element per ply, it is expected that increasing the through-thickness mesh density will lead to a more accurate load distribution and deformation throughout the model, but the run time costs would be significantly higher. It is expected that to obtain better delamination area predictions for the different impact configurations, each ply needs to be modelled with more than one solid element in the through-thickness direction. A simple numerical study is conducted to investigate the effect of the through-thickness mesh density on the extent of delamination. The baseline impact model has been modified to include two elements per ply in the through-thickness direction and all cohesive elements representing potential split paths have been

removed. The centre impact case at 350 m/s is considered and *Figure 4.39* depicts the propagated delamination within the RoI for the two mesh densities considered. An increase in the number of elements per ply in the through-thickness direction results in an improved delamination area by 5%. With the addition of potential split paths, an increase in the delamination area can be expected as delamination spreads via matrix cracks. Further numerical analysis using more than two elements per ply in the through-thickness direction is also required. It is worth mentioning that the run time for the model with two elements per ply was approximately 96 hours of analysis time. With more elements in the through-thickness direction and multiple split paths, the run time can be expected to be greater than 100 of analysis time. Since the aim of this numerical study is to obtain a computationally efficient impact model, even though increasing the through-thickness discretisation may be a potential avenue for obtaining better impact damage predictions, it is not considered in this work as it may be less practical for industrial application.

(a) 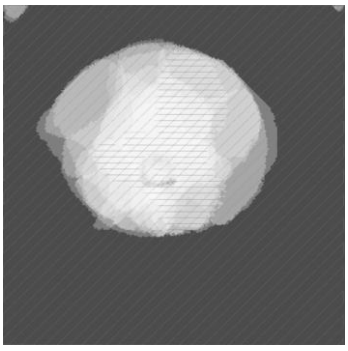 (b) 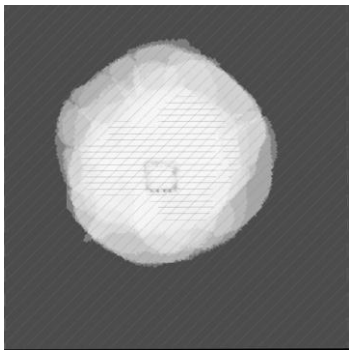

Figure 4.34: Propagated delamination area for centre-impacted laminate at 350 m/s using (a) one element per ply and (b) two elements per ply in the through thickness direction.

4.4. Conclusion

A Hi-fidelity Finite Element Method has been employed to simulate high velocity impacts over a range of impact energies. The predicted impact damage was validated against experimental results from *Chapter 3* and the FE model yielded good predictions, in terms of fibre fracture width and delamination areas, for some impact energies. In order to obtain better impact damage predictions, whilst maintaining the robustness and efficiency of the impact model, several improvements were investigated.

A mesh sensitivity study was conducted, where impact damage predictions were not significantly mesh sensitive as impact energy was increased and therefore, the automated unit cell meshing technique with an average mesh size of 0.23 mm is deemed adequate for this numerical study. It was shown that changes in the projectile's orientation before impact significantly influence the extent of fibre failure. This can be associated with the contact force and the contact area during the impact event. Another improvement to the impact model was the number and positions of interface layers within the laminate. As the number of interface layers is increased, the numerical representation of delamination damage becomes less accurate as it is dependent on the local bending stiffness of the sub-laminate discretisation. In modelling terms, cohesive layers inserted after every ply are an accurate representation of the laminates utilised for the impact tests. In order to obtain a single FE model which can accurately predict the impact damage over a range of impact velocities, an optimisation study in sub-laminate definitions needs to be carried out. This optimisation study will consider a range of number and position of interface layers, where plies that were previously neighbours and of equal or similar orientation can be grouped together. A fourth plausible enhancement

for the impact model is the through-thickness discretisation, however, it was not investigated in this study due to its high computational cost.

The Hi-fidelity Finite Element Method used for the impact study does have some limitations, such as the omission of shear stress interactions with the compressive fibre failure, restrictions on the split spacings using the automated unit cell meshing technique, single integration points for solid elements and a single projectile orientation before impact. Since it is unlikely to use different impact models with different projectile orientations and different number of interface layers to simulate high velocity impacts over a range of velocities, the baseline impact model developed in this work is considered for further numerical analysis on the residual tensile strength.

Journal paper – Review process in Composite Structures

Kristnama AR, Xu X, Wisnom MR, Hallett SR. Numerical analysis of high velocity oblique impacts on carbon/epoxy laminates and tension after impact.

5. Residual Tensile Strength – Experimental work

As mentioned in *section 2.3*, there are some studies published in the literature on the relationship between extent of damage due to localised high velocity impacts and residual strength. While most authors investigated residual strength of laminates subjected to low velocity impacts, some have studied the residual strength of high velocity impacted laminates, where Compression After Impact (CAI) has been the standardised strength measurement for impacts conducted with large and heavy projectiles. However, tension after impact is also important for structural components subjected to high tensile forces.

The effects of fibre fracture and delamination area on the residual strength are considered through quasi-static tensile tests on high velocity impacted laminates and this chapter explains the methodology behind the tests carried out and investigates the reduction in residual tensile strength. In the first instance, the impacted laminates from the initial impact study carried out in *section 3.1* are loaded under tension. Then, the residual tensile strength of impacted laminates from the second impact study (*section 3.2*) over a range of velocities is investigated. The relationship between residual tensile strength and characterised impact damage is studied. In addition, the residual tensile strength of machined notches is investigated experimentally and compared to the residual tensile strength of impacted laminates in order to assess the equivalence in strength reduction.

5.1. Test method

Quasi-static tensile tests, according to the ASTM D3909 standard [149], were carried out in the University of Bristol laboratory, using the Instron 100 kN hydraulic-driven test machine, shown in *Figure 5.1*. Quasi-isotropic laminates with no impact were used as a baseline to determine the reduction in residual strength. With no end tabs being used, all specimens were gripped with a pressure of 12 MPa, to minimise the risk of slippage.

All specimens were positioned between the grips and were ensured to be well aligned in the test machine before testing. A length of 50 mm on both sides of the specimens was allocated for gripping. All specimens were loaded vertically in the 0° fibre orientation under displacement control with a loading rate of 1 mm/min. The bottom part of the machine is fixed, and the top head moves vertically. The position of the top head is recorded during the test through a load cell.

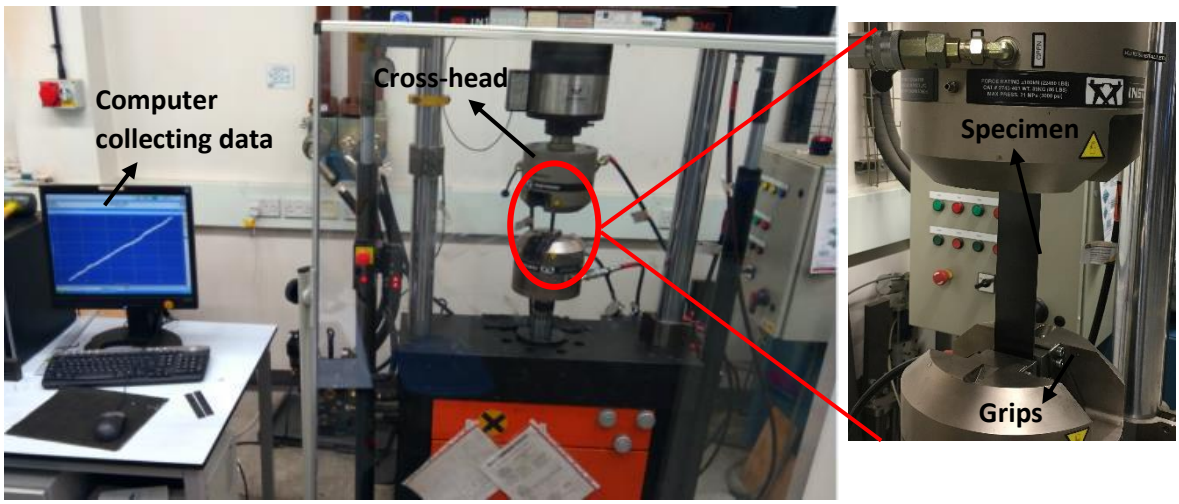

Figure 5.1: Quasi-static tensile test set up.

5.2. Initial impact study

This section investigates the residual tensile strength of the impacted laminates considered in *section 3.1* (refer to *Figure 3.1* for impact configurations). Out of the five specimens tested for high velocity impacts, one from each configuration was used for C-scan and the remaining four were tested for quasi-static tension. *Figure 5.2a* and *5.2b* illustrate typical load-crosshead displacement curves for 1 mm and 2 mm thick laminates, corresponding to laminates with no impact and laminates impacted at 45° to the leading edge (LE). As seen from *Figures 5.2a* and *5.2b*, there is an initial stiffness mismatch between impacted and non-impacted laminates. From these load-crosshead displacement responses, the highest load level is taken as the failure load, from which the tensile strength is calculated using *Eq. 5.1*.

$$\sigma = \frac{P_{failure}}{A_{total}} \tag{5.1}$$

where, σ is the tensile failure stress, $P_{failure}$ is the average peak load recorded at failure and A_{total} is the total cross-sectional area of the laminate, obtained from the measured widths and thicknesses of the laminates. The residual tensile strength data for all laminates is provided in *Table 5.1.* Due to some slippage observed in the unnotched specimens, the use of an extensometer would have improved the accuracy of the displacement readings. However, as strain values of the specimens loaded in tension are not investigated, the crosshead displacements are adequately accurate to determine the tensile failure strength.

The effect of thickness, impact position and angle of impact on the tensile strength are represented on the histograms shown in *Figure 5.3*. The largest reduction in

residual tensile strength is observed for impact at 45° to the LE on 1 mm thick laminates. This represents the most severe impact case with a 60% reduction in strength. Doubling the thickness of the laminate, a reduction of 47% in residual tensile strength is observed for the most severe impact case. It is also possible to compare the effect of impact position on the residual strength. An oblique (45°) impact to the leading edge of the laminate induces a larger extent of impact damage compared to impacts at the trailing edge (refer to *Section 3.1.3*). Consequently, the reduction in residual tensile strength is larger for laminates impacted at 45° to the LE. A 45° impact to the LE results in a lower residual tensile strength compared to a 90° impact at the same edge. This is because the oblique trajectory of the projectile induces a larger extent of damage at the edge of the laminate. For 2 mm thick laminates, the residual tensile strengths of laminates impacted at 45° and 90° to the LE differ by 4%. A larger difference of 16% was observed for 1 mm thick laminates. As such, the oblique trajectory of the projectile does not significantly influence the strength degradation when the laminate's bending stiffness is increased.

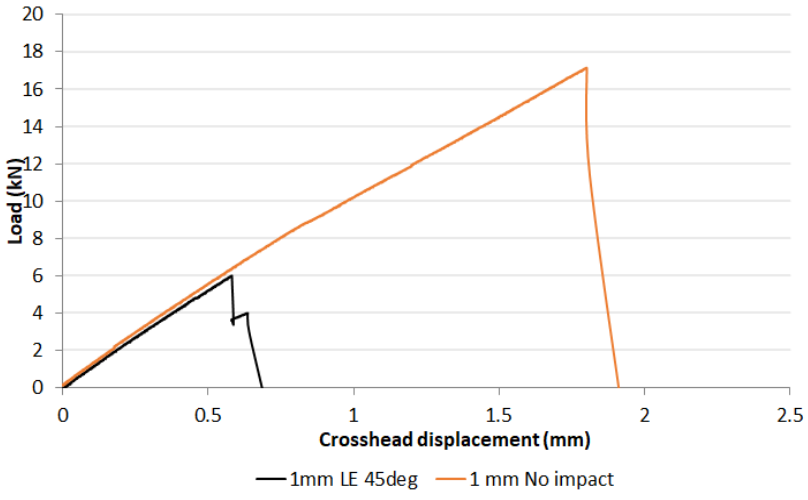

(a)

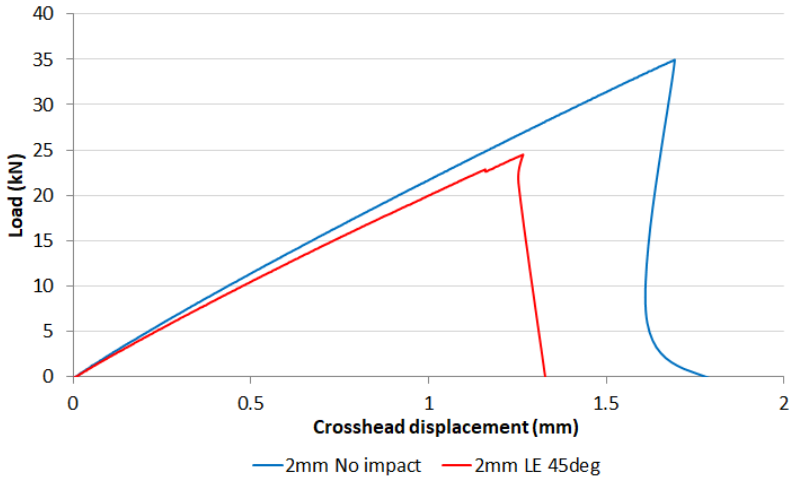

(b)

Figure 5.2: Typical load vs crosshead displacement responses of non-impacted and impacted laminates, where (a) is for 1 mm thick laminates and (b) is for 2 mm thick laminates.

Table 5-1: Residual tensile strength of impacted laminates from Extended Project [96].

Thickness (mm)	Impact position	Impact angle (°)	Impact Velocity (m/s)	Residual Tensile Strength (MPa) (C.V. %)
1	-	-	-	824 (2.7)
2	-	-	-	939 (3.0)
High velocity impacts				
1	Leading edge	45	300	331 (2.3)
1	Leading edge	90	301	392 (3.1)
1	Trailing edge	45	304	506 (2.2)
2	Leading edge	45	304	494 (1.8)
2	Leading edge	90	302	514 (2.7)
2	Trailing edge	45	300	594 (2.7)

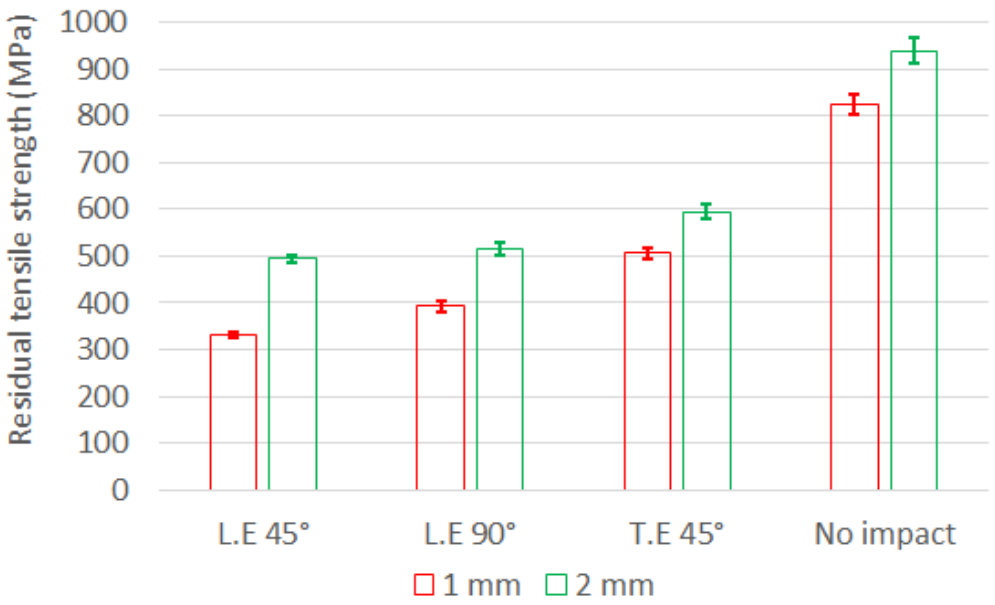

Figure 5.3: High velocity impacts – Effect of varying thickness, impact position and impact angle on the residual tensile strength.

5.3. High velocity impact

As mentioned previously, there have been several works in the literature which looked at residual strength of laminates under low velocity impact. While studies of the residual strength of laminates subjected to high velocity or ballistic impacts are few, some works looked at oblique impacts on thin laminates over a range of impact velocities, where the analysis of normal and oblique ballistic impacts on thin carbon/epoxy woven laminates was carried out, for example by *Lopez-Puente et al.* [54]. However, the extension of the latter's work to investigate residual strength has not been published yet.

The laminates subjected to high velocity impacts between 100 m/s and 350 m/s with impacts carried out at two specific points on the laminates were investigated for

residual strength through quasi-static tensile tests [111]. The residual strength study was extended further to analyse the effect of impact position.

5.3.1 Load vs. displacement response

Typical load crosshead-displacement responses of the unnotched, edge- and centre-impacted laminates at an impact velocity of 350 m/s are shown in *Figure 5.4*. Edge- and centre-impacted laminates show an almost linear response up to failure, where a fibre pull-out mechanism is identified near the impact damage front at the failure load. The non-impacted laminate shows failure close to the gripping region and its non-linearity is due to slippage at the grips during the test [111]. From these load crosshead-displacement responses, the highest load level is taken as the failure load and the residual tensile strength is calculated using *Eq. (5.1). Table 5.2* provides details on the residual tensile strength for all laminates tested. The tensile strength for unnotched laminates is 909 MPa (C.V. 2.2%), which is similar to the unnotched tensile test results for a quasi-isotropic laminate with similar lay-up and volume of 0° plies [150].

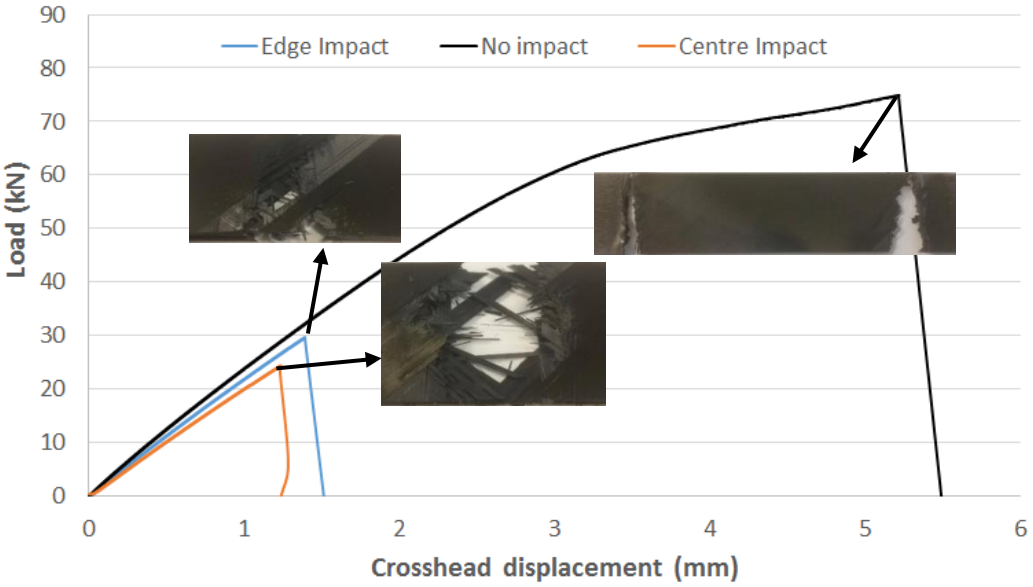

Figure 5.4: Typical load-displacement curves of non-impacted laminates and laminates impacted at the edge and centre [111].

Table 5-2: Calculated values for the tensile strength of baseline and impacted laminates [111].

Impact velocity (m/s)	Residual tensile strength (MPa) (C.V%)			
	Edge	No. of specimen	Centre	No. of specimen
100	741 (6.0)	3	908 (3.8)	4
150	604 (15)	3	846 (5.8)	3
200	525 (12)	3	728 (2.8)	4
250	463 (4.0)	3	578 (2.7)	4
300	435 (13)	4	498 (4.3)	4
350	358 (7.1)	3	318 (9.4)	4
Non-impacted laminate (5 specimens) = 909 MPa (2.2 %)				

The projectile was aimed to strike the target at 1.5 mm from the edge, and at the centre of the laminate's width. Some of the high C.V values in *Table 5.2* may be due to

some variability in exactly where the laminates were impacted and possible projectile rotation once it leaves the sabot [111]. At 350 m/s, a centre-impacted laminate represents the worst impact case with a reduction of 65% in residual tensile strength. For lower impact velocities, edge-impacted laminates show larger reductions in residual tensile strength. Out of the four specimens tested for residual strength with impact carried out at 100 m/s to the centre of the laminate, some specimens either have only one surface ply (45°) with broken fibres or no broken fibres at all. Therefore, the reduction in residual strength for that impact case is insignificant. The reduction of 7% in residual strength for centre-impacted laminates at 150 m/s is due to fibre failure in the top 45°, 90° and -45° plies.

From the recorded incident velocities, the impact energies for each configuration were calculated using the previously described Eq. (4.7) in *Chapter 4*, *section 4.2.1*. The relationship between the residual strength and the impact energy for edge and centre impacts is illustrated in *Figure 5.5*. The trendlines drawn on the plot in *Figure 5.5* indicate a steeper reduction in residual tensile strength for centre-impacted laminates as the impact energy is increased. This may be due to the large delamination areas that accompany the fibre fracture widths observed in centre-impacted laminates at high velocities.

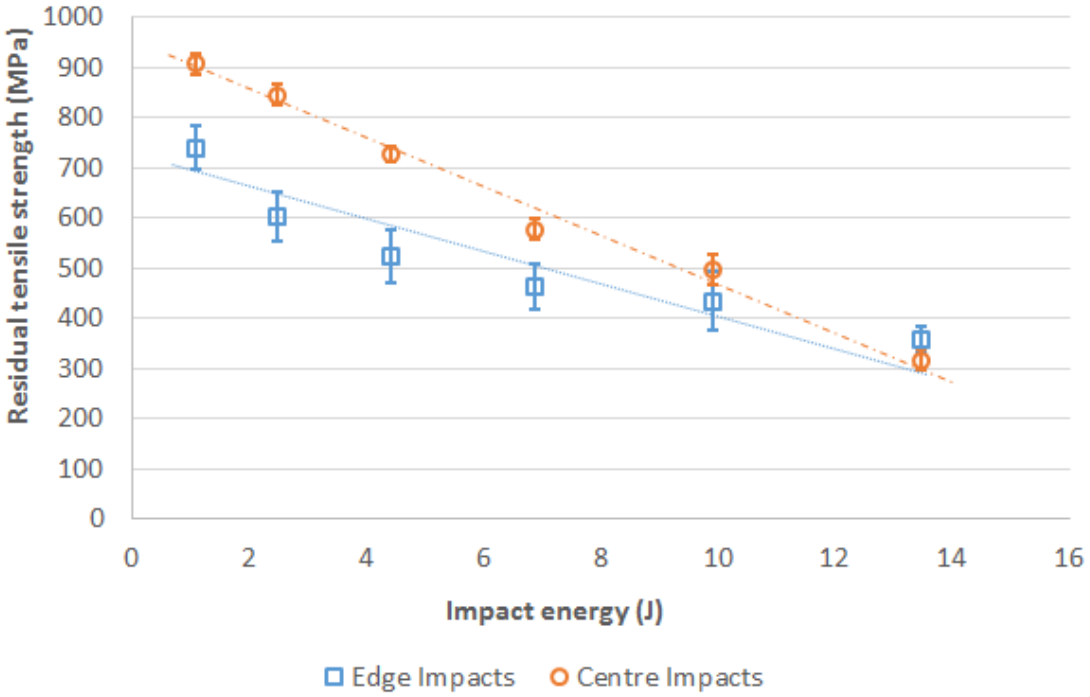

Figure 5.5: The relationship between residual strength and impact energy in edge- and centre-impacted laminates.

While the residual tensile strength has been determined per convention, i.e. using the total cross-sectional area of the impacted coupons, it is interesting to consider the net cross-sectional area of the impacted coupons. Hence, the extent to which the remaining fibres can achieve their undamaged strength may be investigated. The net cross-sectional area of the impacted coupons is determined using *Eq. (5.3)* hereunder

$$A_{net} = A_{total} - A_{ff} \tag{5.3}$$

where A_{net} is the net cross-sectional area, A_{total} is the total cross-sectional area, obtained from the measured width and thickness of the coupons and A_{ff} is the area of fractured fibres. From CT scans images, the area of fractured fibres can be accurately obtained using the measured fibre fracture widths and coupons' thicknesses. The residual tensile strength of the remaining fibres can then be determined using *Eq. (5.4).*

$$\sigma = \frac{P_{failure}}{A_{net}} \tag{5.4}$$

The extent to which the remaining fibres can achieve the undamaged strength is represented in *Figure 5.6.* The percentage of undamaged strength retained by coupons impacted at the edge decreases with impact energy for both edge and centre impacts. For edge impact at an energy level of 1.1 J, the coupon strength drops by 18% of the undamaged tensile value. As the impact energy is increased to 13.5 J, the coupon can achieve 48% of the undamaged strength. For centre impacts, the coupon can achieve 99.5% of the undamaged strength at an impact energy of 1.1 J. This is because of the stress concentration at the grips which is more significant than the top 45° ply showing fibre failure. The extent of fibre failure and delamination area in the centre-impacted laminate is significantly increased at an energy level of 13.5 J, and the coupon can only achieve 42% of the undamaged strength.

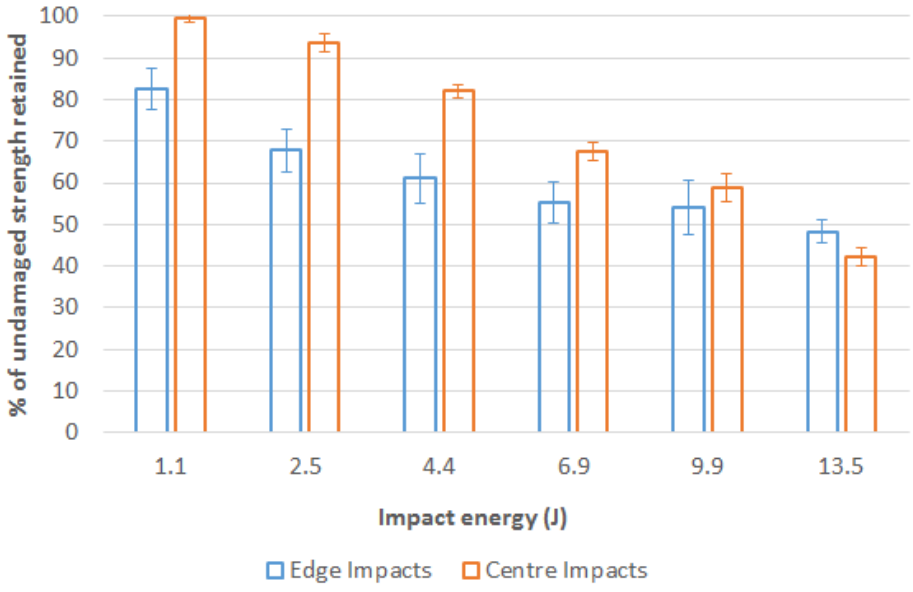

Figure 5.6: Percentage of undamaged strength retained by impacted coupons for different energy levels.

5.3.2 Effect of impact position

Figure 5.6 shows the relationship between the residual tensile strength and delamination area for both impact cases. In *section 3.2.4*, it was shown that edge-impacted laminates have a decreasing delamination area as impact velocity increases above 300 m/s (impact energy = 9.9 J). From *Figure 5.7*, the residual tensile strength of edge-impacted laminates decreases as impact velocity increases beyond 300 m/s. As such, it can be deduced that the reduction in tensile strength is mainly governed by the amount of fibre failure and the influence of delamination area, if any, on the residual strength is insignificant. The same cannot be said for centre impacts because the impact velocity after which the delamination area would be expected to decrease has not been reached.

The variation in residual tensile strength with the extent of fibre fracture due to edge and centre impacts is shown in *Figure 5.8.* The residual tensile strength of all impacted laminates decreases with increasing fibre fracture width. At the maximum velocity of 350 m/s (impact energy = 13.5 J), an edge-impacted laminate shows a larger extent of fibre fracture than a centre-impacted laminate. However, a centre-impacted laminate shows a delamination area which is more than twice the area observed for an edge-impacted laminate at 350 m/s. Although larger fibre fracture and smaller delamination area are observed in the edge-impacted laminates at 350 m/s, the residual tensile strength of edge-impacted laminates is higher than centre-impacted laminates. This difference can be accounted for by the asymmetry of the test. Furthermore, the very large delamination areas observed in centre-impacted laminates may affect the residual tensile strength and this will be discussed in the following sections. As such, it is

important to characterise impact damage in terms of fibre fracture extent and delamination area [111].

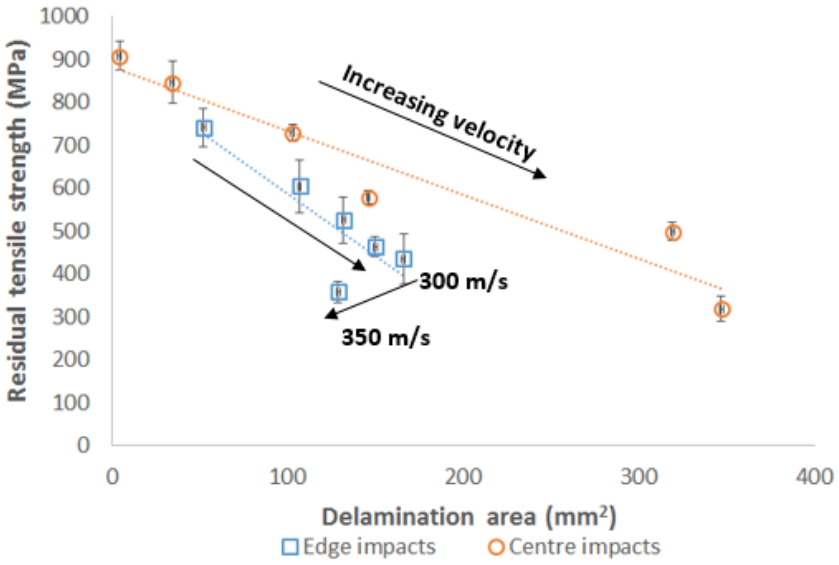

Figure 5.7: The relationship between residual strength and extent of delamination in edge- and centre-impacted laminates [111].

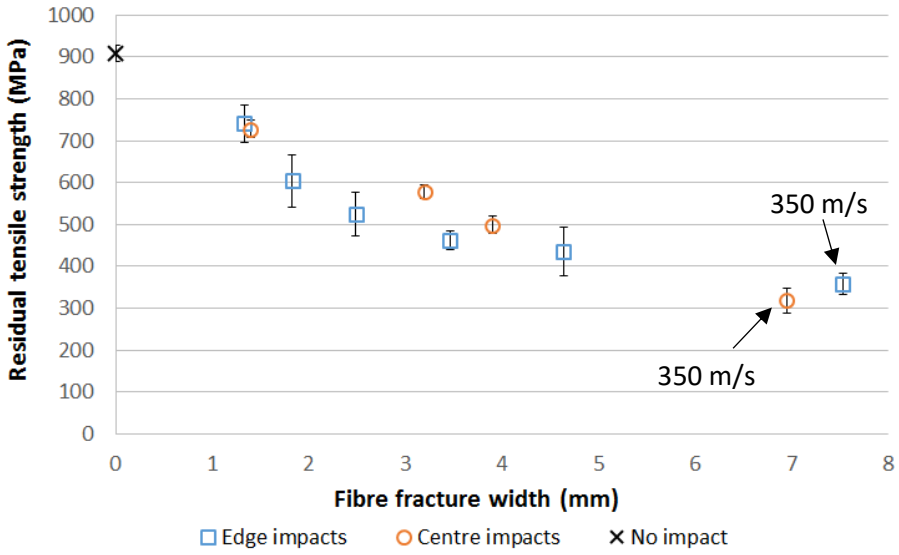

Figure 5.8: The relationship between residual strength and extent of fibre failure in edge- and centre-impacted laminates [111].

5.3.3. Effect of delamination

To investigate the contribution of delamination area to the residual tensile strength, a comparison between some of the delaminated interfaces from edge- and centre-impacted laminates at 350 m/s is shown in *Figure 5.9*. As the 0° plies carry most of the post-impact tensile load, the delaminated interfaces close to the 0° plies are examined. The edge-impacted laminate does not show delamination extending across the full width. On the other hand, the centre-impacted laminate shows delamination extending across the full width in some interfaces close to the 0° plies.

The amount of the initial kinetic energy of the projectile absorbed due to delamination was analysed in *section 3.2.5*, where the ratio of energy absorbed by delamination to initial kinetic energy of the projectile for edge-impacted laminates is smaller than centre-impacted laminates at 350 m/s, and this is consistent with the extent of delamination observed in *Figure 5.9*. At the maximum impact velocity, the delamination is much more localised around the impact point for edge cases, but for centre impacts the delamination spreads across the full width in some interfaces close to the 0° ply. Schematics of edge- and centre-impacted laminates showing 0° plies and the adjacent -45°/0° interface are provided in *Figure 5.10* to assess the effect of delaminated interfaces under tensile loading. For both laminates, splits are expected to grow as the applied load is increased. As the load is further increased, fibre failure occurs, and the crack tip is expected to be at the boundary up to which delamination has propagated across the width. While fibre failure propagates in a single direction across the width in an edge-impacted specimen under tension, centre-impacted laminate has fibre failure propagation in both directions. In addition to the very large delamination areas, the fibre

failure propagation across the whole width happens sooner in centre-impacted laminates than in edge-impacted laminates.

Hence, only when the delamination area is large enough and extends across the full width at several interfaces that its contribution to the residual strength may become significant. When its value is small and does not extend across the full width at more than one interface, the reductions in residual tensile strength can be accounted for by the fibre fracture width.

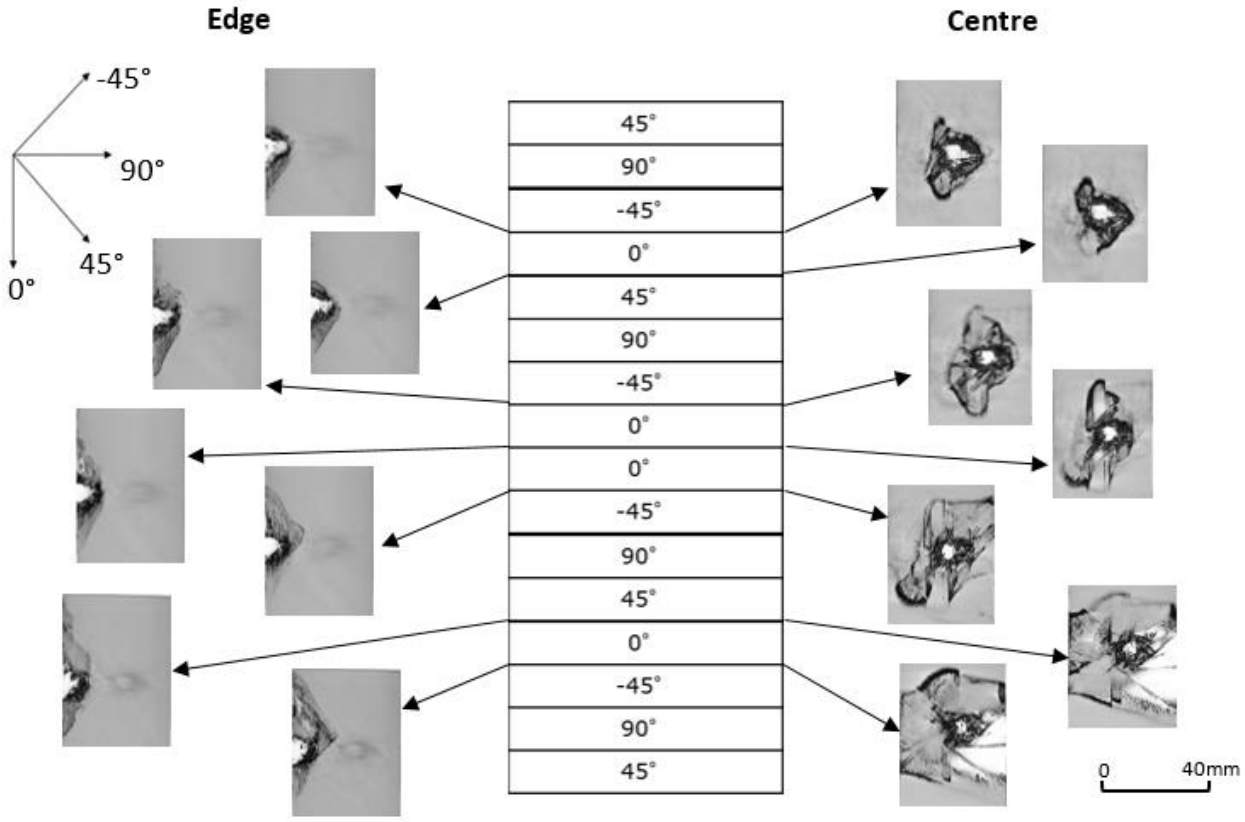

Figure 5.9: Comparison between delaminated interfaces for edge and centre impacts at 350 m/s.

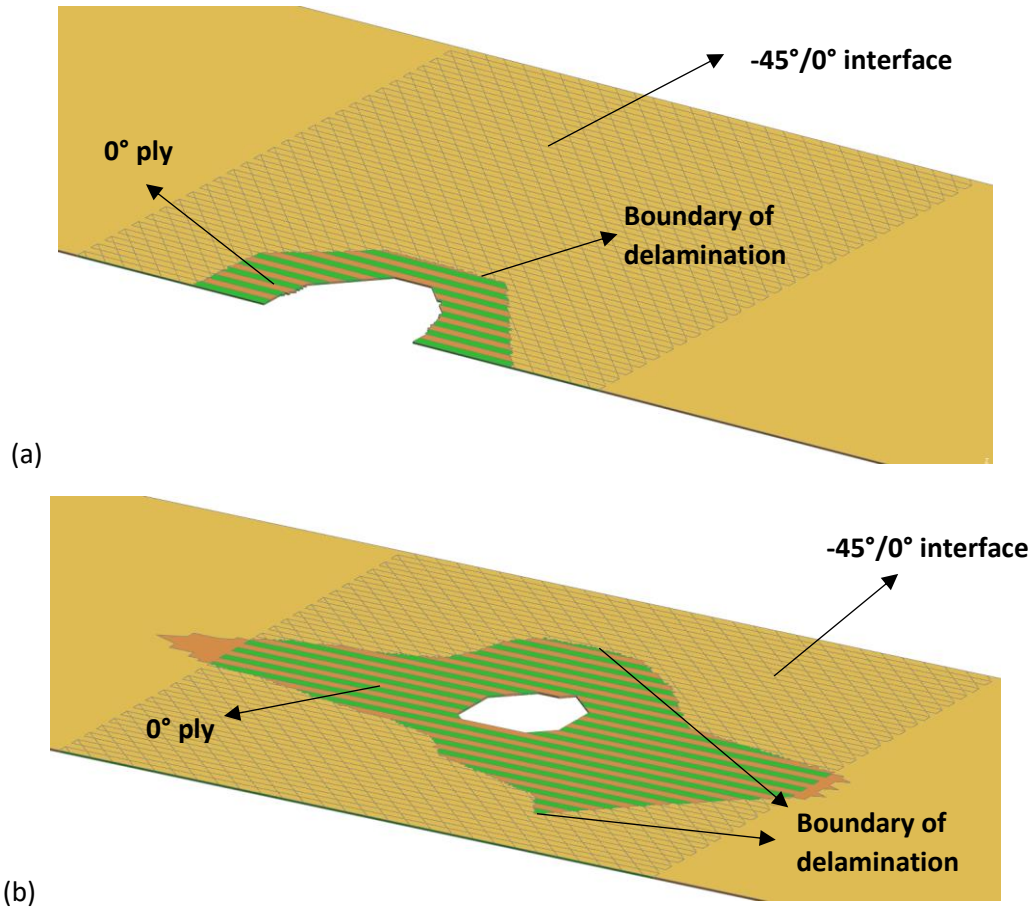

Figure 5.10: Schematic showing 0° ply, -45°/0° interface and delamination boundary in (a) edge- and (b) centre-impacted laminates.

5.4. Machined notches

The residual strength of composites subjected to any kind of impact is a critical design driver. Generally, it is mandatory to carry out impact tests, and then tension or compression tests to investigate the residual strength. Carrying out high velocity impact testing for several configurations can be an expensive test programme, especially during the preliminary design phase. As such, it is interesting to investigate the equivalence in strength degradation between impacted and notched laminates to see if this might offer a simpler and quicker way to assess the effect of impact damage [111]. In addition, the equivalence study aids in analysing the contribution of large delamination areas to the

residual tensile strength, as extensive delamination is not present in notched laminates prior to strength tests. Quasi-isotropic open-hole and centre-notched specimens have been extensively tested, for example to study strength scaling [151-153] and some studies have looked at tensile strength comparison between open-hole and equivalent centre-notched specimens [154,155]. Several studies exist which investigated the equivalence in strength degradation between impacted laminates and laminates with a circular hole [156-158] or an elliptical hole [159]. The studies conducted in [156-159] referred to Compression After Impact (CAI) where drop weight impact tests were carried out.

Components found in aircraft engines may be subject to compression, tension and cyclic loads. While CAI has been the standardised strength measurement of post-impact, it is also important to determine the residual strength of impacted components which may undergo high tensile forces, where the strength reduction is expected to be strongly dependent on the extent of fibre failure. Currently, there are no available studies from the literature which looked at comparing the tensile strength of impacted laminates to that of notched specimens of equivalent sizes. Therefore, machined notches were made at the edge and at the centre of the laminate, as shown in *Figure 5.11*. The width of the notch was 1 mm as it is sharp enough not to affect the measured fracture toughness, as concluded by *Camanho and Catalanotti* [160] who tested quasi-isotropic IM7/8552 carbon/epoxy laminates. Laminates with the same notch length were stacked together and then cut on a Computer Numerical Control (CNC) machine using a 1 mm diameter end mill. For centre-notched laminates with small notch length, holes were made at the notch tips using a 0.5 mm diameter drill bit prior to cutting on the CNC machine. The configurations for the machined notches are detailed in *Table 5.3*. The laminates with

machined notches were tested for residual strength through quasi-static tensile tests (according to the ASTM D3909 standard) using a 100 kN Instron hydraulic machine under displacement control, with a loading rate of 1 mm/min.

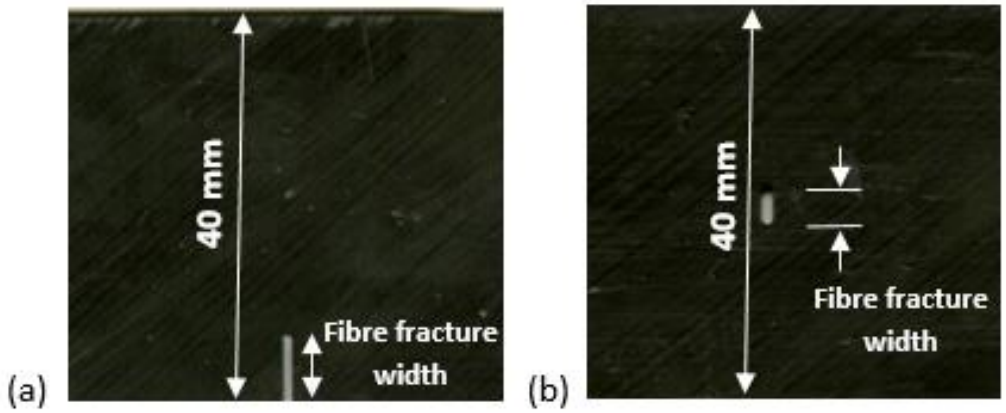

Figure 5.11: Machined notch at the (a) edge and (b) centre of the laminate.

Table 5-3: Machined notch configurations [111].

Edge		**Centre**	
Notch length (mm)	No. of specimens	Notch length (mm)	No. of specimens
1.33	5	1.40	5
2.49	5	3.22	5
4.64	5	3.90	5
7.53	5	6.95	5

5.4.1. Residual tensile strength comparison

The residual tensile strength is plotted against the fibre fracture width for edge and centre cases, as shown in *Figures 5.12* and *5.13* respectively [111]. The residual tensile strength of impacted laminates is strongly dependent on the impact velocity up to a certain limit, after which it reaches a plateau. As the impact velocity increases, the

extent of fibre fracture observed in the two impact cases increases, which leads to a decrease in the residual tensile strength. From *Figure 5.12,* there is a good correlation between the results for large fibre fracture widths, where the edge-notched laminates slightly overpredict the residual tensile strength by an average 5.4%. For the fibre fracture width equal to 1.33 mm, the difference in the residual strengths between edge-impacted and edge-notched laminates is due to there being only one 0° ply broken for the edge impact case, while edge-notched laminates have all four 0° plies with broken fibres through the thickness.

For centre-impacted laminates with small fibre fracture widths, where impacted laminates have three out of four 0° plies broken, the residual tensile strengths are quite close to centre machined notches of equivalent sizes, with an average difference of 7%. However, as the fibre fracture width is increased at higher impact velocities, centre machined notches are unconservative due to the large delamination areas in the impacted laminates. As such, the reduction in residual tensile strength of centre-impacted specimens at high impact velocities is governed by the extent of fibre failure and delamination.

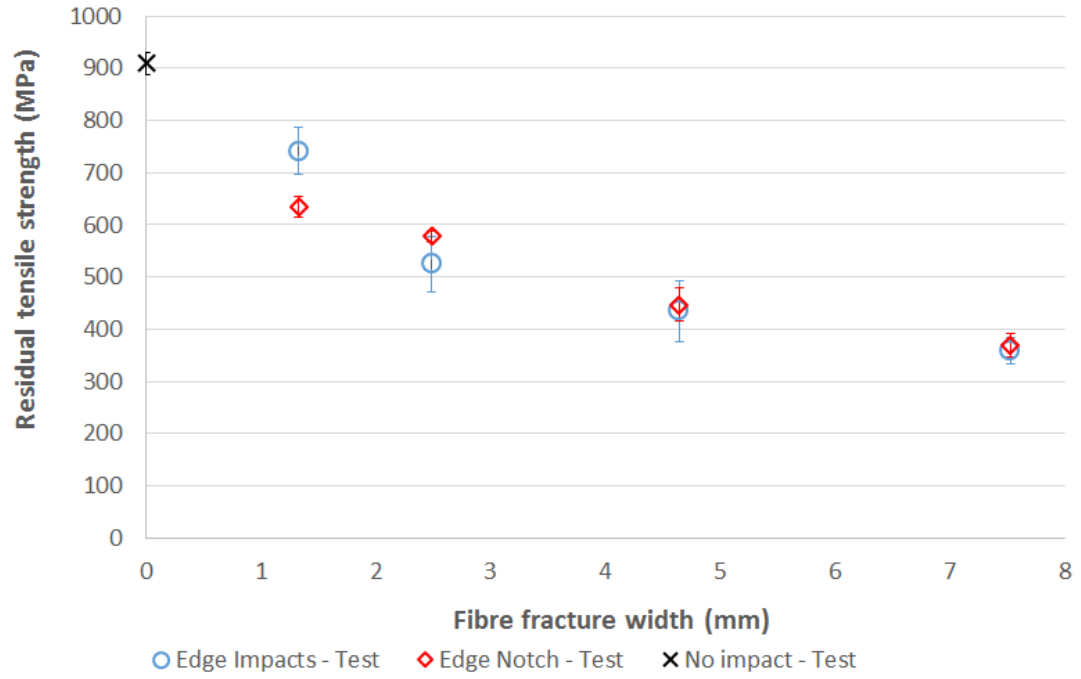

Figure 5.12: The relationship between residual strength and extent of fibre failure in edge-impacted and edge-notched laminates [111].

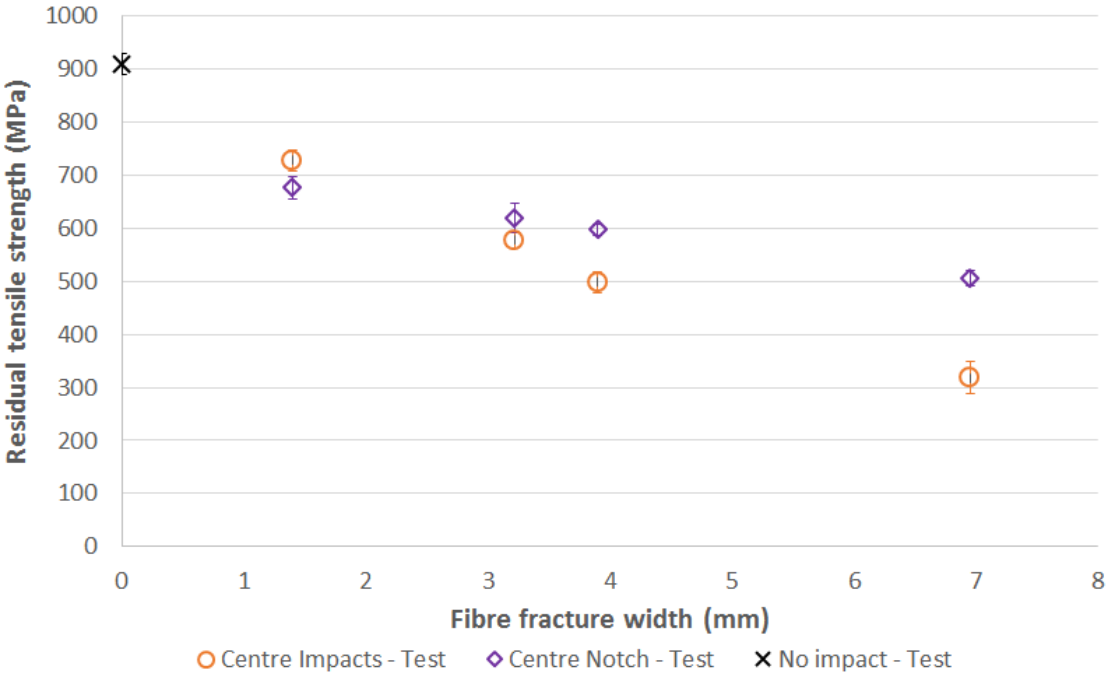

Figure 5.13: The relationship between residual strength and extent of fibre failure in centre-impacted and centre-notched laminates [111].

5.4.2. Damage zones in notched specimens

In addition to the tensile tests on notched specimens, interrupted tests of notched specimens in which the tests were stopped at 95% of the average failure load together with CT scanning were carried out. Interrupted tests with CT scanning can provide promising images of the damage zones at the crack tips with a large amount of detail [155]. All notched specimens tested under tension have a mean C.V. value of 3.9% on strength, which indicates a high consistency of the test results. Therefore, the damage zones at 95% of the failure load in the other specimens should be similar to the CT scan images of the specimens from the interrupted tests.

There is a double 0° ply block at the central symmetry plane through the thickness and only single 0° plies outboard. Typical CT scans of 0° plies in edge- and centre-notched specimens are shown in *Figures 5.14* and *5.15* respectively, where the CT images were enlarged around the notches to better illustrate the damage zone. For edge notch of 1.33 mm and centre notch of 1.40 mm, there is no fibre failure in the central double 0° ply block. By comparison, local fibre failure occurs at the crack tips in the outboard single 0° plies. This is because the thicker 0° ply block has more energy available to cause the splits to propagate than the outboard single 0° plies [155] and this is consistent with the longer 0° splits in the central 0° ply block compared to the outboard single 0° plies. In the central double ply block, local fibre breakage is delayed as the longer 0° splits blunt the stress concentration. In the outboard single 0° plies, local fibre failure is arrested, and other splits start to grow at the new crack front. For the rest of the notched specimens, the central double 0° ply block has longer splits than the single outboard 0° plies. However, local fibre

Edge-notched laminates		
Notch length (mm)	Outboard single 0° ply	Central double 0° ply block
1.33	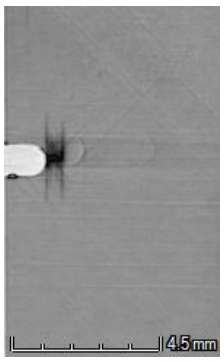	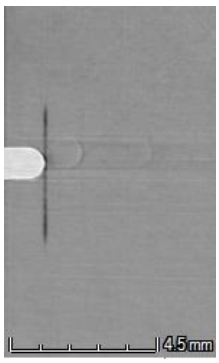
2.49	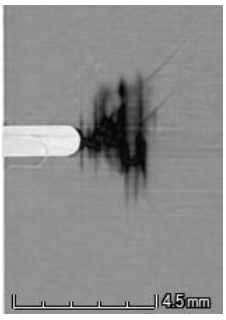	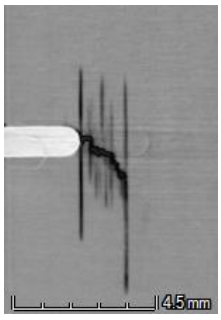
4.64	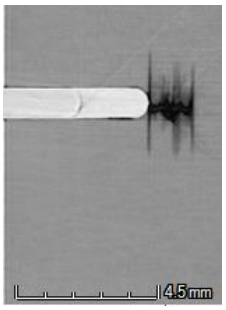	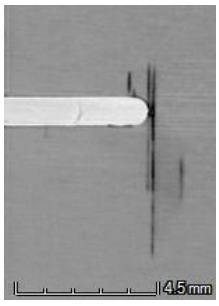
7.53	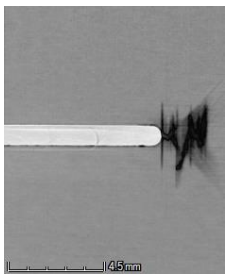	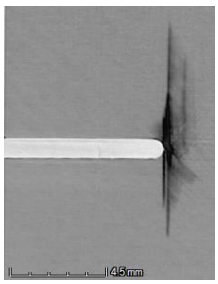

Figure 5.14: CT scanning images showing damage zones in edge-notched laminates for several notch lengths.

Centre-notched laminates		
Notch length (mm)	Outboard single 0° ply	Central double 0° ply block
1.40	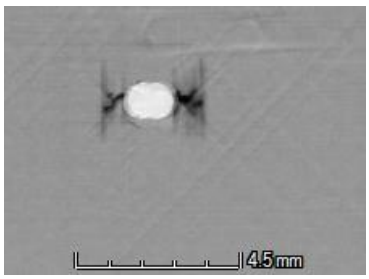	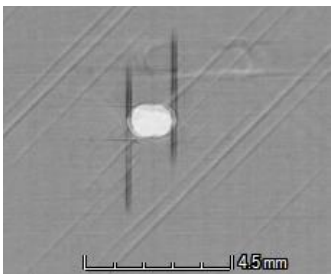
3.22	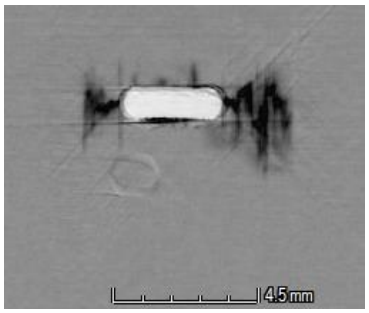	
3.91	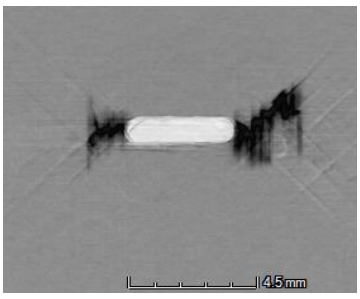	
6.95	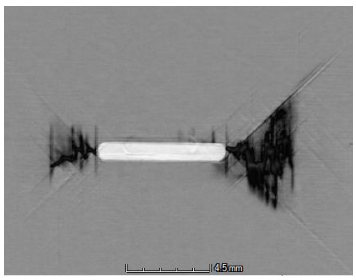	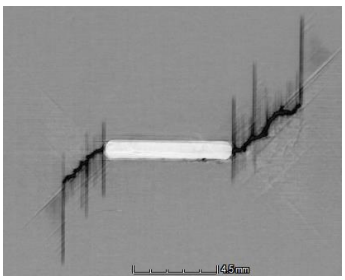

Figure 5.15: CT scanning images showing damage zones in centre-notched laminates for several notch lengths.

failure is already present in the central double 0° ply block. All other 0° plies show similar damage except the differences in the central double 0° ply block.

5.4.3. Damage zones comparison

It was shown that for large fibre fracture widths, an edge notch is a reasonable representation of edge-impacted laminate in terms of residual tensile strength. However, for larger fibre fracture widths, centre-notched laminates have higher residual strength compared to centre-impacted laminates. The damage zones in impacted and notched laminates are analysed to explain the similarities and differences observed in their residual tensile strengths.

In notched specimens, the damage zone is defined as the average distance between the notch tip and the last split in the 0° plies. For impacted laminates, the damage zone is quantified as the average distance ahead of the impact damage front up to the furthest split in the 0° plies. The damage zones in the outboard single 0° plies and central double 0° ply block of the impacted and notched laminates are studied. While *Figure 5.16* illustrates the comparison of damage zones between a laminate impacted at the edge at 350 m/s (fibre fracture width = 7.53 mm) and an edge-notched laminate with notch length 7.53 mm, *Figure 5.17* shows the comparison of damage zone between a laminate impacted at the centre at 350 m/s (fibre fracture width = 6.95 mm) and a centre-notched laminate with notch length 6.95 mm. The residual tensile strengths of the impacted and notched laminates can be explained by the sizes of the damage zones in the impacted laminates prior to tensile loading and in the notched laminates at 95% of the failure load. *Table 5.4* provides details on the sizes of the damage zones within the 0° plies in the impacted and notched laminates.

The size of the damage zone within the 0° plies in an edge-impacted laminate corresponding to an impact velocity of 200 m/s is 1.92 mm, which is 20% smaller than the size of the damage zone within the 0° plies in the laminate with an edge notch of length 2.49 mm. Consequently, an edge-impacted laminate at 200 m/s has a residual tensile strength which is about 14% higher than an edge-notched laminate for the same extent of fibre fracture. From *Figure 5.12*, the residual strength of an edge-impacted laminate at 350 m/s is slightly higher by 3% compared to an edge-notched laminate with the same extent of fibre fracture. The similarity in residual strength between these two laminates can be explained by the damage zone sizes, where an edge-impacted laminate at 350 m/s has a damage zone of 2.21 mm, while an edge-notched laminate with a notch length of 7.53 mm has a damage zone of 2.23 mm.

For small fibre fracture widths in *Figure 5.13*, centre-impacted laminates have approximately similar residual tensile strength as centre-notched laminates, differing by 7%. This difference in residual strengths was previously explained by the difference in the number of 0° broken plies observed between these two laminates. In addition, the sizes of damage zones observed in these two laminates which differ by 14% may also explain the difference in their residual strengths. However, as the extent of fibre fracture is further increased, the damage zones observed in centre-impacted laminates are much larger than those observed in centre-notched laminates, differing by 55%. As such, the lower residual tensile strength of centre-impacted laminates compared to centre-notched laminates can be explained by the much larger damage zone.

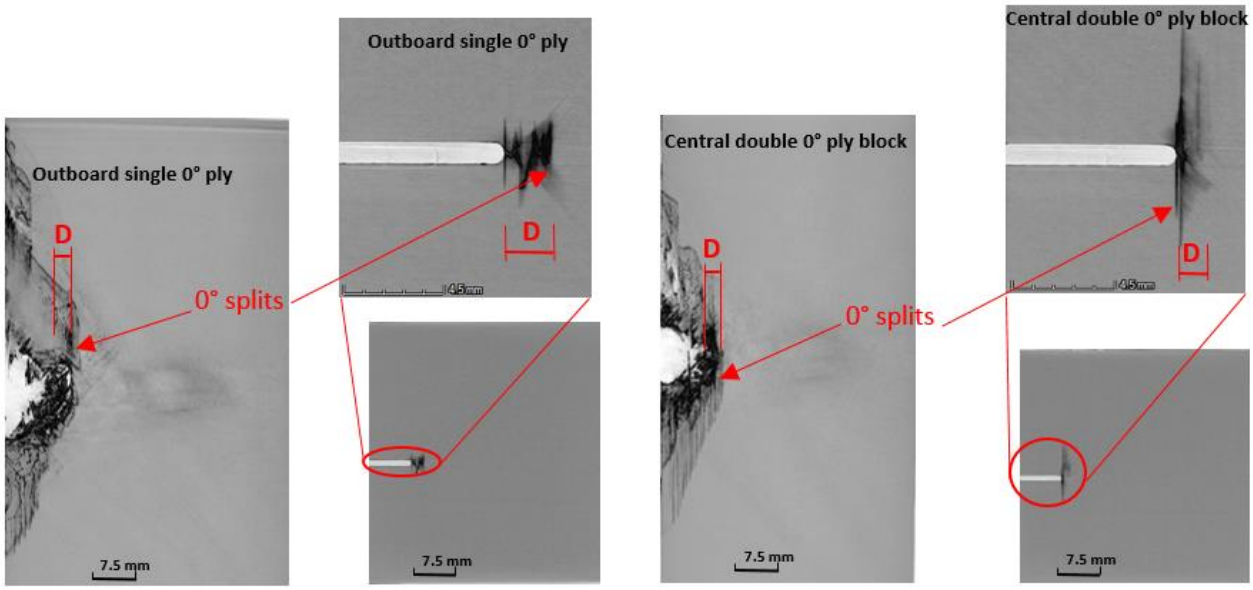

Figure 5.16: Comparison in damage zones, D, between a laminate impacted at the edge at 350 m/s (fibre fracture width = 7.53 mm) and a laminate with an edge notch of 7.53 mm.

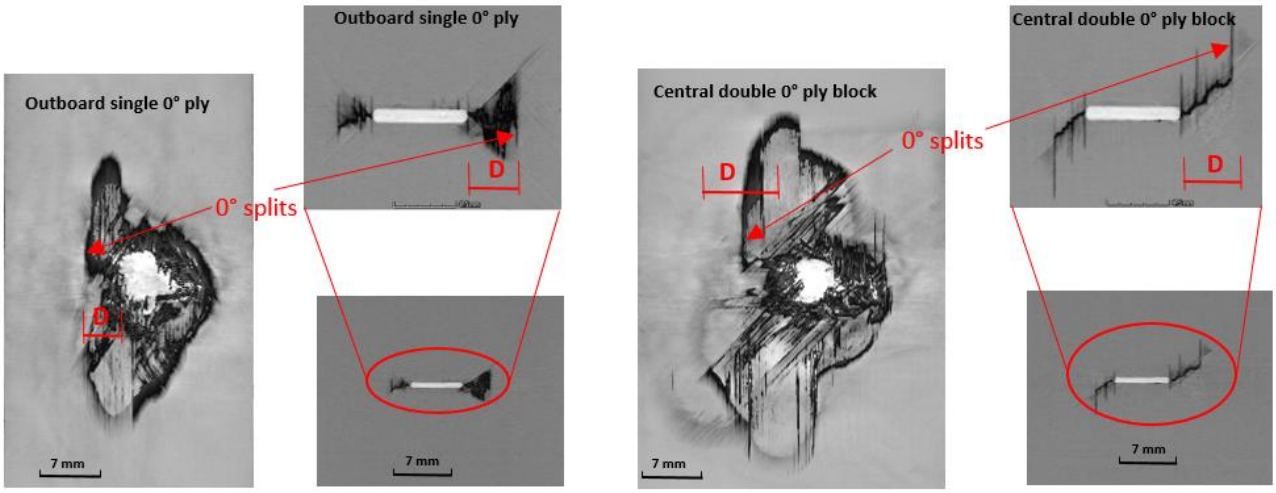

Figure 5.17: Comparison in damage zones, D, between a laminate impacted at the centre at 350 m/s (fibre fracture width = 6.95 mm) and a laminate with a centre notch of 6.95 mm.

Table 5-4: Damage zone sizes measured in impacted and notched laminates.

Configurations	Damage zone size, D (mm)
Edge impact 200/s (fibre fracture width = 2.49 mm)	1.92
Edge Notch (Notch length = 2.49 mm)	2.32
Edge impact 350/s (fibre fracture width = 7.53 mm)	2.21
Edge Notch (Notch length = 7.53 mm)	2.32
Centre impact 200/s (fibre fracture width = 1.40 mm)	1.12
Centre Notch (Notch length = 1.40 mm)	0.98
Centre impact 350/s (fibre fracture width = 6.95 mm)	8.38
Centre Notch (Notch length = 6.95 mm)	3.76

5.4.4. Comparison with open-hole laminates

Whilst machined notches provide a reasonable approximation to impacted laminates in terms of residual strength for some impact configurations, it is also of interest to look at open-hole test data available from the literature [161]. This is to investigate whether open-hole laminates can provide a better equivalence to centre-impacted laminates than centre-notched laminates. *Figure 5.18* shows the tensile strength results for centre-impacted, centre-notched and open-hole laminates, with the dashed lines as trendlines. The fibre fracture widths for open-hole laminates are equivalent to the hole diameters. The plot indicates that most open-hole results have

lower strength than centre-impacted laminates, except for the largest fibre fracture width (6.95 mm). For small fibre fracture widths, the centre-impacted laminates have residual strength close to the centre-notched laminates. As the fibre fracture width increases, the residual strength of centre-impacted laminates deviates from the centre-notched laminates and approaches the trendline of the open-hole laminates. With further increase in fibre fracture width, the strength of centre-impacted laminate falls below the trendline of the open-hole laminates.

Xu et al. [155] looked at a comparison in damage zones in open-hole and centre-notched laminates at 95% of the failure load. The authors stated that the 0° splits in notched laminates can grow longer compared to open-hole laminates, where longer 0° splits blunt stress concentrations, and therefore result in higher tensile failure stresses. When the fibre fracture width is equal to 1.4 mm, centre-impacted laminates have higher residual strength than centre-notched and open-hole laminates. This may be associated with a significant growth of the 0° splits in impacted laminates and thus, blunting the stress concentrations. At the maximum fibre fracture width of 6.95 mm, centre-impacted laminates have lower residual strength than centre-notched and open-hole laminates. This may be linked to the 0° splits in impacted laminates which are restricted to grow longer with increasing applied stress and thus, the lower tensile failure stresses. Further discussions on the growth of the 0° splits under tension in impacted laminates are provided in *Chapter 6.* While Figure 5.18 is applicable to smaller structural components, a study on size effects is important for application on a higher structural level.

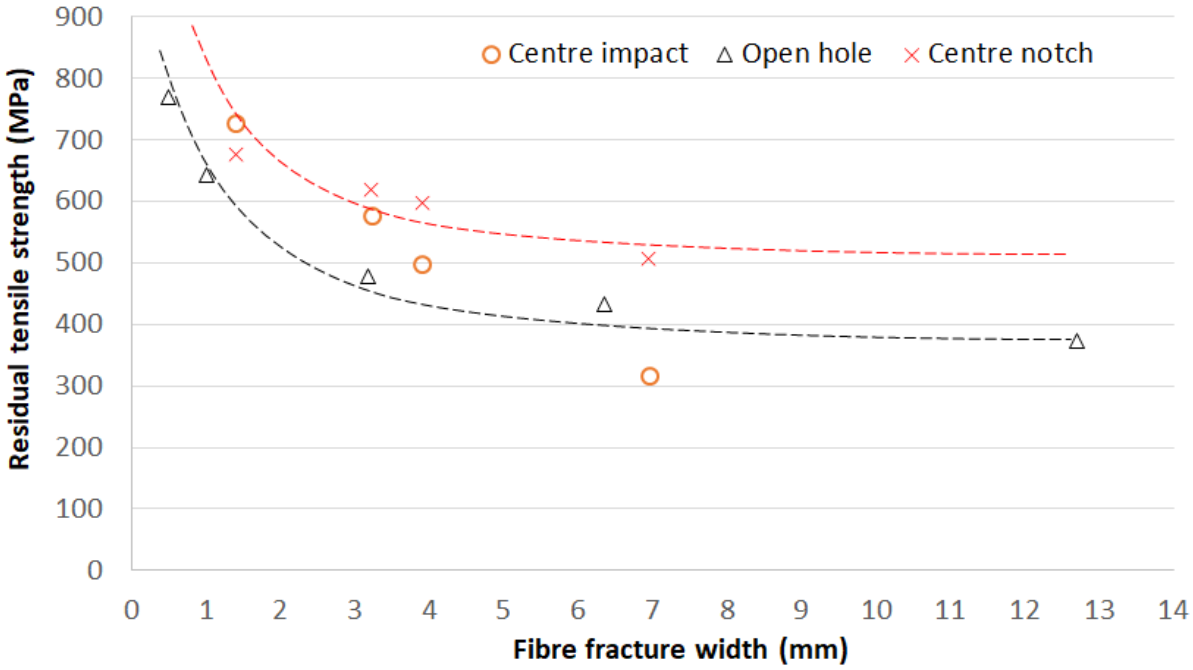

Figure 5.18: Residual tensile strength data for centre-impacted, centre-notched and open-hole laminates.

5.5 Conclusion

The residual tensile strength of impacted laminates is driven by the impact velocity. Increasing impact velocity leads to an increase in both fibre fracture width and delamination area, except for edge impacts beyond 300 m/s which show decreasing delamination area. For most impact cases, where the delamination areas are not large and do not propagate across the full width of the specimen, the degradation in tensile strength is mainly governed by the extent of fibre fracture. For centre impacts at higher velocities, if the residual tensile strength was governed by the extent of fibre fracture only, then the residual strength of centre-notched and impacted laminates would have been expected to be approximately similar. Therefore, the residual strength of centre-impacted laminates at higher velocities is driven by the extent of fibre failure and delamination area.

For edge-impacted laminates, it is only when the fibre fracture widths are large that edge machined notches are a reasonable approximation. The same can be said for small fibre fracture widths in centre-impacted and notched laminates. The similarities in damage zone sizes observed in impacted and notched laminates make this approximation apt. Further comparisons in residual strength between centre-impacted, centre-notched and open-hole laminates were carried out. The results reveal that both centre-notched and open-hole laminates fail to match the residual strength of centre-impacted laminates for large fibre fracture widths. Due to the occurrence of numerous failure modes under high velocity impact, it is unlikely to find a suitable substitute for impacted laminates in terms of residual tensile strength for the range impact velocities considered in this study.

Research dissemination

Kristnama AR, Xu X, Nowell D, Wisnom MR, Hallett SR. Experimental investigation of high velocity oblique impact and residual tensile strength of carbon/epoxy laminates. J Comp Sci Technol, 2019;182:107772.

CompTest 2017, Leuven, Belgium

6. Predicting residual tensile strength

The finite element (FE) commercial code LS-DYNA was employed to predict the residual tensile strength of impacted and notched laminates, and to understand the damage development under tension. A Hi-FEM is employed for this numerical study, with an automated unit cell meshing technique, a cohesive formulation based on a bi-linear traction-separation law and a fibre failure criterion based on the Weibull statistics. Two approaches for residual strength prediction are considered and are as follows:

a. Method 1 (M1): Post-process impact model from *Chapter 4* for tensile simulations.
b. Method 2 (M2): Incorporate the characterised impact damage from CT scans (*Chapter 3*) into the FE model before quasi-static tensile simulations,

Since the predicted impact damage (from *Chapter 4*) differs from the experimental impact damage for some impact energies, the second approach is of interest to examine the differences in tensile strength predictions. All the tensile strength predictions from both approaches are then discussed in comparison with the experimental results from *Chapter 5*.

6.1 FE model setup

The laminate model, cohesive formulation and the failure criterion have been presented in detail in *Chapter 4*, and pertinent information will not be repeated except for the description of some key features of the laminate and tensile simulation setup.

6.1.1. Cohesive law formulation

The cohesive formulation developed by *Jiang et al.* [134] was implemented into LS-DYNA, via a user-material subroutine. The formulation is based on a bi-linear traction-separation law, where cohesive elements are deleted when the critical Energy Release Rate (ERR) of the fracture modes is reached. Damage initiation is governed by a quadratic stress-based failure criterion and a fracture energy based mixed-mode power law controls the damage propagation. Damage initiation and damage propagation are given by *Eq. (6.1)* and *Eq. (6.2)* respectively. Detailed descriptions of the parameters can be found in Chapter 4 (*Section 4.1.6*).

$$\sqrt{(\frac{\sigma_I}{\sigma_I^*})^2 + (\frac{\sigma_{II}}{\sigma_{II}^*})^2} = 1 \tag{6.1}$$

$$(\frac{G_I}{G_{IC}})^\alpha + (\frac{G_{II}}{G_{IIC}})^\alpha = 1 \tag{6.2}$$

6.1.2. Laminate model

Detailed ply-by-ply 3D FE models with 8-node constant stress solid elements (Type-1 in LS-DYNA) and 8-node cohesive elements (Type-19 in LS-DYNA) were constructed in LS-DYNA for the impacted and notched laminates. The full thickness of each specimen was modelled with one element per ply. For M1 simulations, a keyword file was written from the LS-DYNA impact simulations after the damage had fully formed. The keyword file includes all nodal coordinates with constraints and element topology and *Figure 6.1a* illustrates an example FE model post-impact simulation. All failed elements were removed from the model and the latter is shown in *Figure 6.1b*.

From CT scan images, impact damage was characterised in terms of fibre fracture width and delamination area. For M2, these two parameters were included in the FE models to represent the impacted laminates. For edge and centre impacts, solid elements were deleted to represent the fibre fracture widths, as characterised in *Chapter 3*. The fibre fracture width corresponding to an edge impact at 350 m/s is illustrated in *Figure 6.2*. To represent the impact-induced delamination between plies, only cohesive elements between plies were deleted. The extent of deleted cohesive elements was determined from the X-ray CT scan results. In *Figure 6.2*, the delaminated area at each interface within the laminate is represented by several coloured patterns, while the 45° blue striped pattern in the background represents the laminate within the Region of Interest (RoI). For machined notches at the edge and centre of the laminates, solid and cohesive elements were removed through the full thickness to represent the notch, where a typical edge notch equivalent to the fibre fracture width due to an edge impact at 350 m/s is shown in *Figure 6.3*.

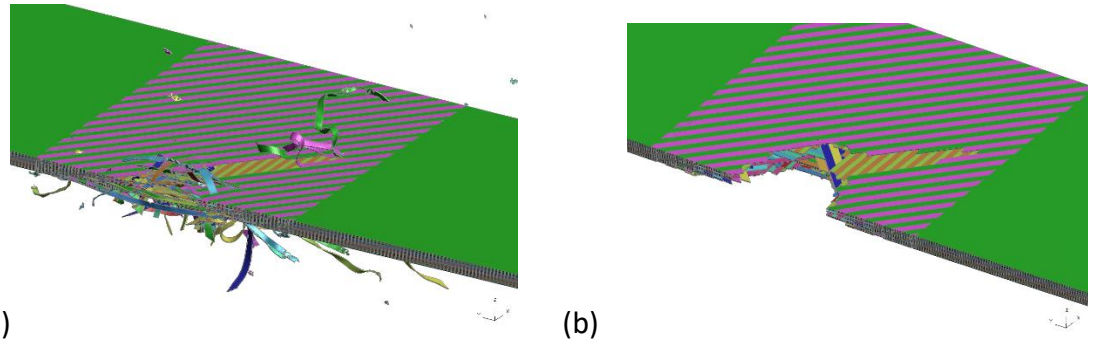

(a) (b)

Figure 6.1: Finite element model of an edge-impacted laminate at 350 m/s (a) post-impact and (b) after removal of all distorted elements.

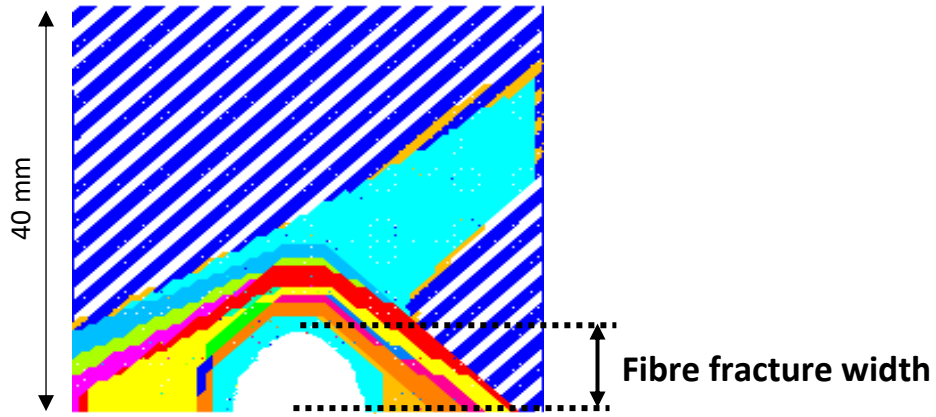

Figure 6.2: Fibre fracture width and delamination definitions for FE model in an edge impact at 350 m/s case. Note that the blue striped region is the background laminate and that coloured areas are delamination.

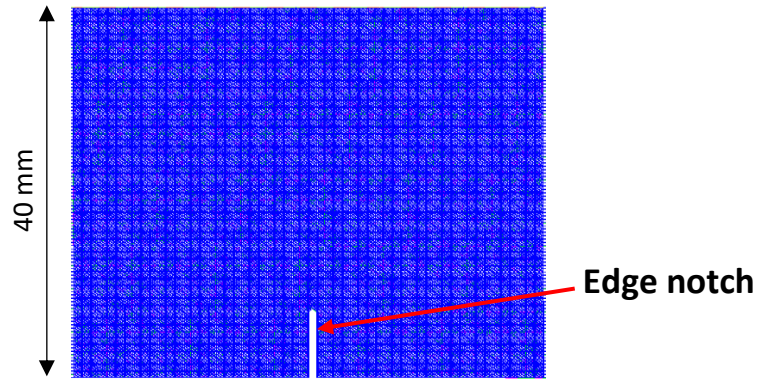

Figure 6.3: Machined notch representation in FE model.

In order to minimise the computational time whilst maintaining the accuracy of the results, the densities of all materials were scaled up by three orders of magnitude to increase the minimum time step size in the residual tensile strength models [143]. Hourglass control (Type-6 in LS-DYNA) was used for all reduced-integration elements to suppress zero strain energy distortion modes. In addition, an initial thermal load of -160 °C was included in the simulations prior to the tensile loading to model the 'cooling down' of the laminate from 180 °C to room temperature after the curing process and generation of thermal residual stresses.

6.1.3. FE mesh

As described in *section 4.1.3*, while the RoI was defined with a fine mesh size of 0.23 mm, a coarser mesh density was used for the rest for the laminate outside the ROI. The mesh for the ROI was done based on a unit cell [141]. The automated unit cell meshing technique allows 0° and 90° splits with 0.71 mm spacing and 45° and -45° splits with 1 mm spacing. The split spacings represent the minimum values based on a unit cell. In addition, the split spacings are considered sufficient based on the observation made by *Xu et al.* [72], who demonstrated that the predicted stress-strain curves for notched tensile tests were not sensitive to the density of the split paths for a spacing of 1 mm or less.

6.1.4. Boundary conditions

During quasi-static tensile tests, the laminate was gripped over a length of 50 mm in the test machine, and the specimen was loaded with a displacement rate of 1 mm/min. To represent the boundary conditions of the quasi-static tests, all the nodes through the thickness at both ends of the laminate were given Single Point Constraints (SPC) and Prescribed Motion boundary conditions in LS-DYNA. *Figure 6.4* illustrates the nodes used to implement the boundary conditions for a typical edge-impacted laminate. All nodes were allowed to translate in the 0° fibre direction corresponding to the loading direction and SPCs were applied to the other directions. For the Prescribed Motion, the sets of nodes were assigned a displacement translational degree of freedom in the loading direction. The sets of nodes were given Prescribed Motion boundary conditions in opposite directions to represent tension.

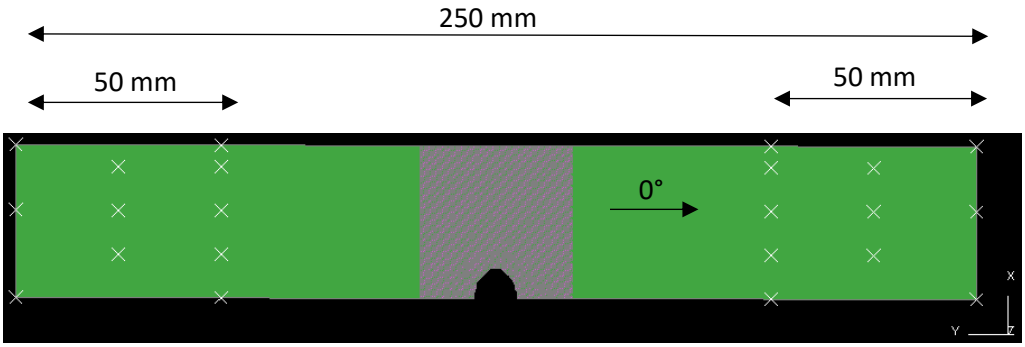

Figure 6.4: Selected nodes, represented by 'X', which are employed to define the boundary conditions for quasi-static tensile test simulation.

6.2. Residual tensile strength

In this section, the residual tensile strength of laminates with impact damage is predicted and compared against experimental results together with the predicted residual tensile strength of machined notches. The residual strength of machined notches is investigated mainly to provide a quicker and simpler way to assess the effect of impact damage on the residual strength.

6.2.1. Laminate response

By examining the reaction forces on the selected groups of nodes where the boundary conditions were applied, typical load-strain curves can be obtained once the tensile simulations are completed and these curves are shown in *Figures 6.5a* and *6.5b* for edge and centre impacts respectively at an impact velocity of 300 m/s. The load-strain curves from both approaches considered for strength predictions and from experimental results are included in *Figure 6.5*. Impacted laminates show a linear response up to failure both experimentally and numerically. For both edge and centre impacts, there is a stiffness mismatch between test and FE results. This is believed to be due to the different

extent of impact damage in the FE models, as illustrated in *Figure 6.6*. From these curves, the highest load level is taken as the failure load, from which the failure stress can be determined by averaging over the width and thickness of the specimen. This procedure is repeated for all impacted and notched laminates.

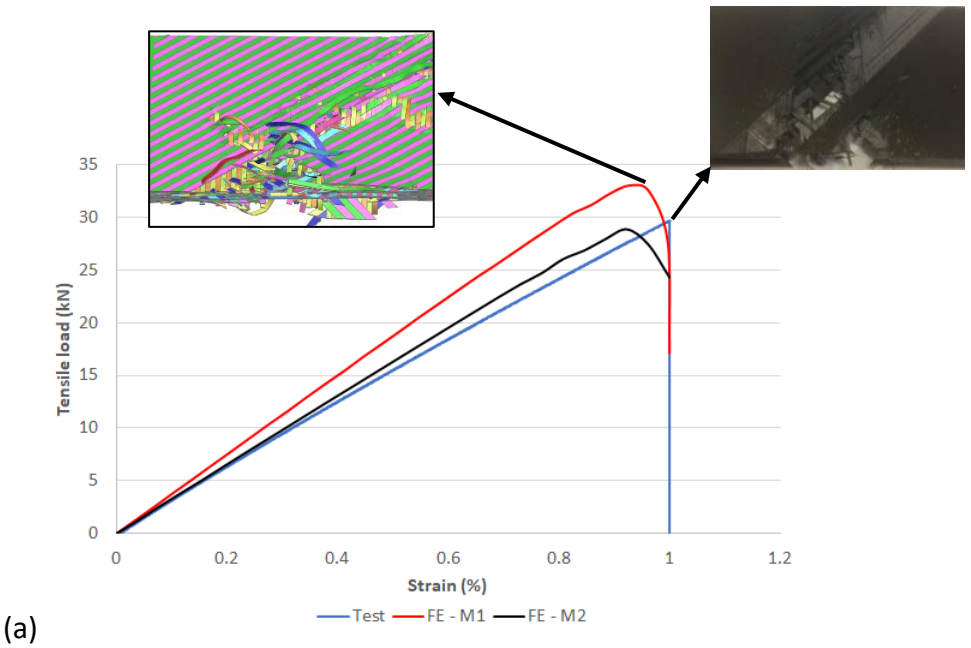

(a)

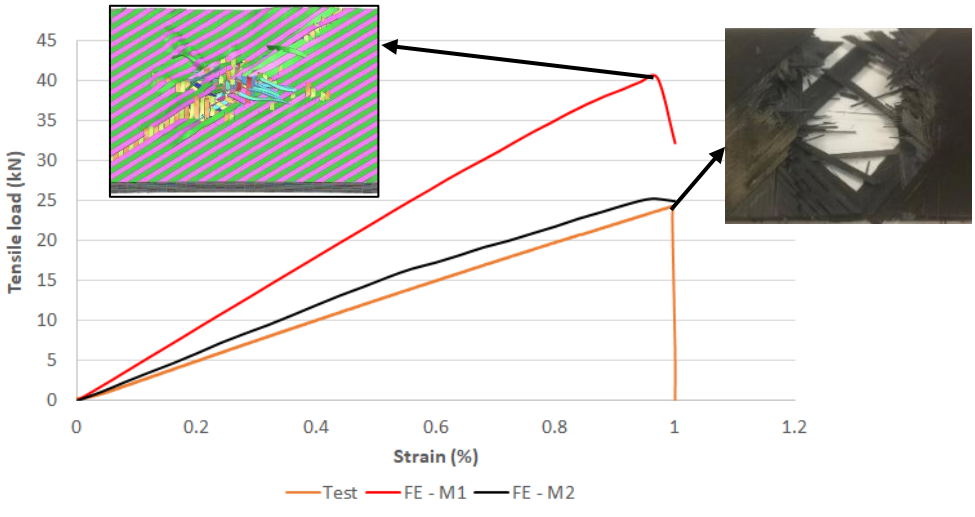

(b)

Figure 6.5: Load-strain curves from simulations and test for (a) edge impact at 350 m/s and (b) centre impact at 350 m/s.

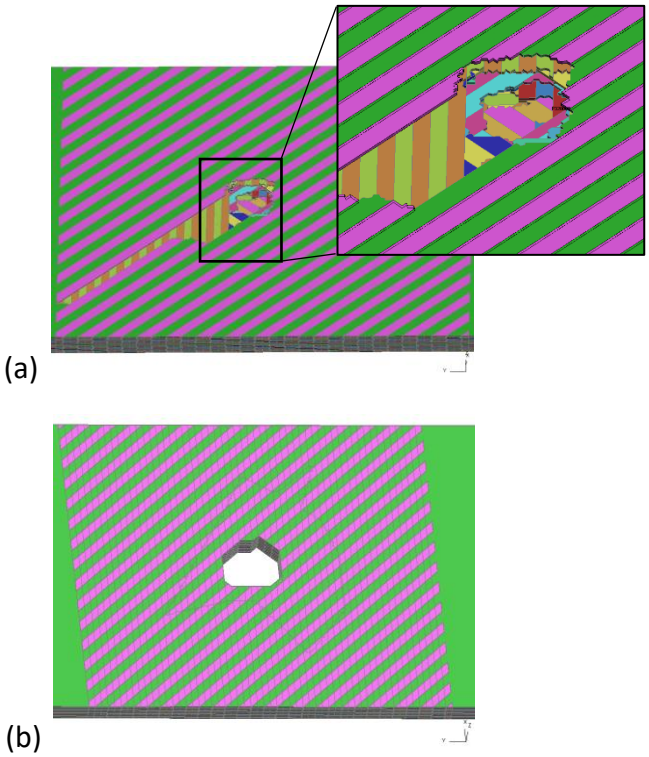

Figure 6.6: Differences in the extent of fibre fracture for FE model from (a) M1 and (b) M2.

6.2.2. Mesh sensitivity

The mesh size of 0.23 mm has been used for all the finite element models created for diverse impact cases. To verify how sensitive the residual strength model is to mesh size, the current mesh density is almost doubled to form a mesh size of 0.11 mm for the Region of Interest (ROI). The number of splits and the split spacings are unchanged in the fine mesh model. FE models with finer mesh in the RoIs from approach M2 were created to represent edge impact scenarios at 100 m/s and 350 m/s. The resulting stress versus strain plots in *Figure 6.7* show the effect of mesh refinement on the post edge impact tensile stress for 100 m/s and 350 m/s cases.

For an edge impact at 100 m/s, there is an increase of 3% in the tensile failure stress for the finer mesh compared to the baseline mesh. At 350 m/s, there is a difference of 7.8% in tensile stress at failure between the fine mesh and baseline mesh. This rather

large difference in the tensile stress at failure is due to the differences the extent of impact damage that was manually included in the FE models prior to tensile simulations, where the fibre fracture width in the standard mesh model is slightly larger by 4% than that in the fine mesh model. Further mesh refinement was not considered as the size of the RoI would be too small, due to a limitation in the number of elements associated with the automated unit cell meshing technique. While the finer mesh does give a slightly improved result by an average of 5.4%, typical simulations are approximately 140 hours of analysis time which are twice the duration using the standard mesh. As such, to minimise the computational time whilst maintaining the efficiency of the FE models, the baseline mesh density is considered to be sufficiently refined.

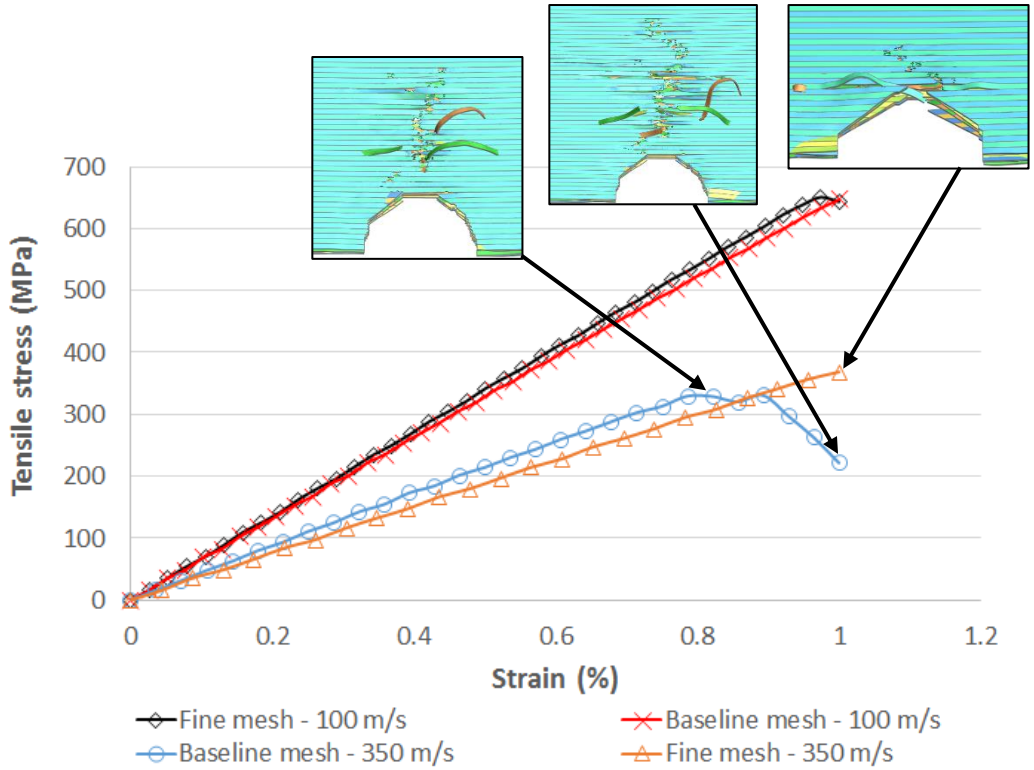

Figure 6.7: Effect of mesh density on the residual tensile stress for edge impact cases of 100 m/s and 350 m/s. The 0° plies are also shown at different points on the stress-strain curve.

6.2.3. Residual strength comparison

The predicted residual tensile strength using both approaches and the strength data from the quasi-static tensile tests is illustrated in *Figures 6.8* and *6.9*, for edge and centre cases respectively. The strength results are plotted against impact velocity. From *Figure 6.8*, the strength predictions using M1 and M2 differ by an average of 12%. For M1, the predicted results vary from the experimental results by an average difference of 8%. Using M2, there is an average difference of 5% between predicted strengths and experimental results.

For centre impacts in *Figure 6.9*, the predicted strength using M1 and M2 differ by an average of 17%. The predicted residual strength using Method 1 show large deviations from the experimental results at 100 m/s, 150 m/s and 350 m/s, with an average difference of 27%. However, at an impact velocity of 200 m/s, 250 m/s and 300 m/s, the predicted strength using M1 differs from the experimental value by an average of 5%. Using M2, there is a good correlation between test and FE results where the predicted strengths differ from the tests by an average of 3%.

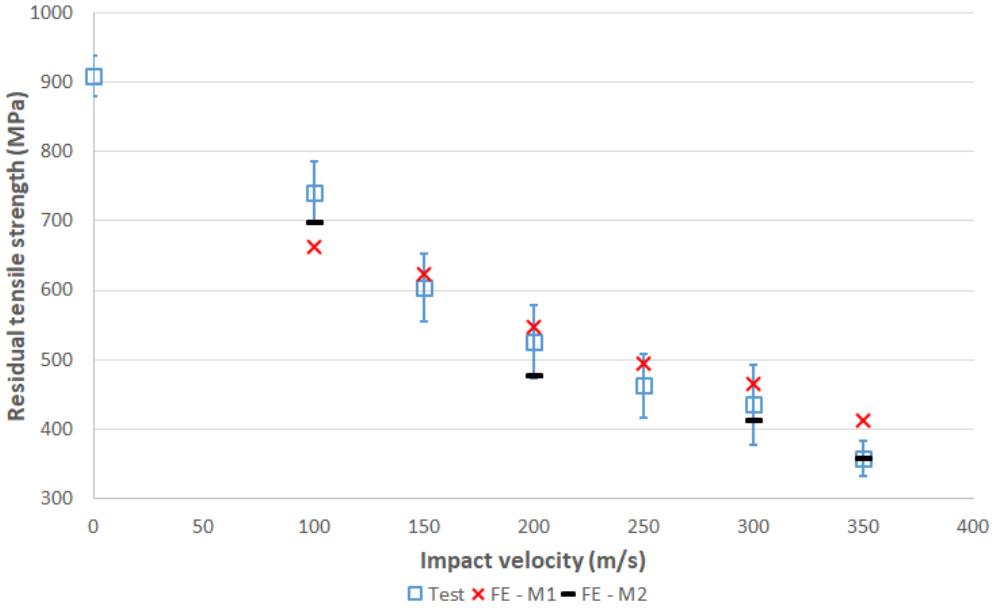

Figure 6.8: Residual tensile strength versus impact velocity for edge impacts – Test and FE.

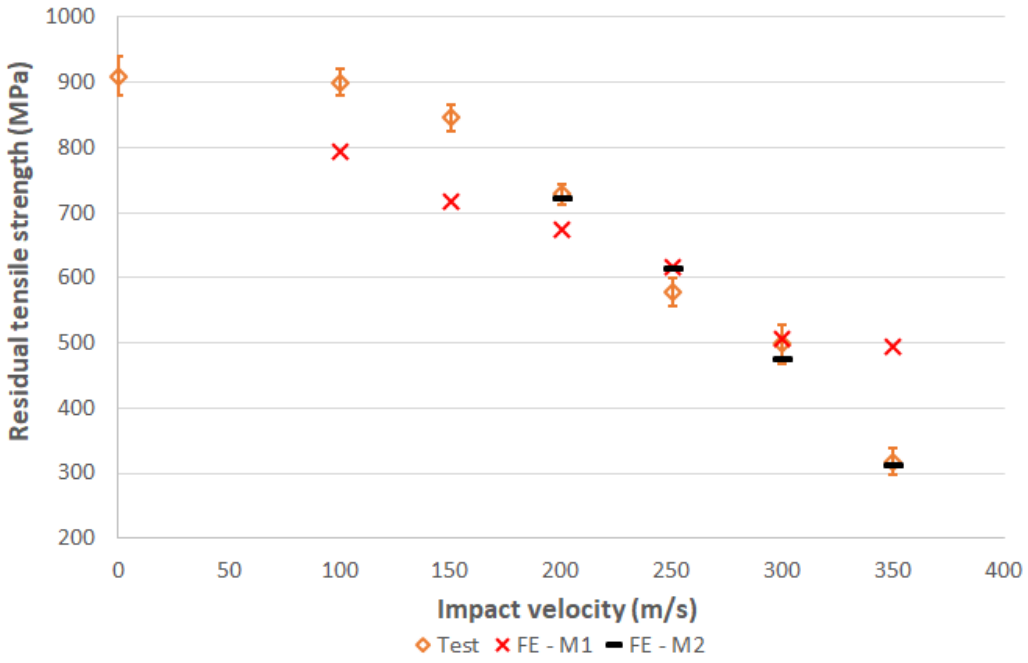

Figure 6.9:Residual tensile strength versus impact velocity for centre impacts – Test and FE.

The strength predictions using Method 1 differ from the experimental results due to the differences in the actual and predicted extent of impact damage. The differences between the predicted residual strengths using M1 and M2 are believed to be due to the different extent of predicted fibre failure and differences in the growth of 0° splits when the impacted laminates are loaded in tension. Further investigation into 0° split development is provided in section 6.4.

The predicted residual tensile strengths of machined notches of equivalent sizes corresponding to the fibre fracture widths observed in the impacted laminates are presented in *Tables 6.1* and *6.2*, together with experimental results from *Chapter 5 – section 5.4.1*. For edge notches, the predicted strengths differ from the experimental results by an average difference of 5.6%. For centre notches, the predicted strengths vary from the experimental results by an average difference of 4.6%. In *Chapter 5*, it was

shown that while edge notches are reasonable approximations for edge-impacted laminates at impact velocities of 300 m/s and above, centre notches have residual strength close to centre-impacted laminates for impact velocities below 250 m/s. These approximations were previously validated by comparing the damage zones in impacted and notched laminates under tension. Further validations are provided in *section 6.4* by analysing the growth of 0° splits in impacted and notched laminates under tension.

Table 6-1: Residual strengths of edge-impacted and edge-notched laminates.

Impact velocity	Residual tensile strength (MPa) (C.V%)		
(m/s)	Edge impact - Test	Edge notch - Test	Edge notch - FE
100	741 (6.0)	634 (3.3)	619
150	604 (15)	-	-
200	525 (12)	578 (1.9)	555
250	463 (4.0)	-	-
300	435 (13)	447 (7.2)	482
350	358 (7.1)	370 (6.1)	399

Table 6-2: Residual strengths of centre-impacted and centre-notched laminates.

Impact velocity (m/s)	Residual tensile strength (MPa) (C.V%)		
	Centre impact - Test	Centre notch - Test	Centre notch - FE
100	908 (3.8)	-	-
150	846 (5.8)	-	-
200	728 (2.8)	676 (3.1)	747
250	578 (2.7)	619 (4.4)	591
300	498 (4.3)	597 (1.9)	603
350	318 (9.4)	506 (3.0)	516

6.3. Numerical damage development

The damage development of edge- and centre-impacted laminates under quasi-static tension is numerically investigated and compared against the numerical damage development in laminates with machined notches. Further investigation of fibre failure initiation and growth of 0° splits in impacted and notched laminates under tension is carried out. This is to understand the damage process under tensile loading and to validate the equivalence drawn between impacted and notched laminates.

6.3.1. Edge-impacted laminates under tension

The damage development is investigated at different load levels up to failure. The damage development in a typical edge-impacted laminate under tension for M1 is illustrated in *Figure 6.10* using the 350 m/s case. For M2, which corresponds to defining the impact damage characteristics from CT scans into the FE model, the damage development observed in a typical edge-impacted laminate corresponding to an impact

velocity of 350 m/s is shown in *Figure 6.11*. The degraded elements representing fibre failure are marked as small patches over the striped background, which represents the superimposed 0° plies. The failed cohesive interface elements where the critical strain energy release rate has been exceeded are marked as shown in *Figures 6.10* and *6.11*. The failed cohesive elements correspond to the growth of the impact-induced delamination area. Prior to tensile simulations, there is a fundamental difference between the models obtained using M1 and M2, which is related to the split lengths. The 0° splits are represented by the white lines in *Figure 6.12* for a typical edge-impacted laminate corresponding to 350 m/s.

For M1, the damage develops in the following sequence: The initial 0° splits are long due to the impact induced damage, as depicted in *Figure 6.12*. As the simulation begins, 0° splits are restricted to grow around the impact damage zone. With increase in applied stress, fibre failure occurs at the impact damage front. Fibre failure propagates across the width with the crack tip reaching the boundary of the impact-induced delamination area before it is arrested. As the stress is further increased, secondary 0° splits start to grow at the crack tip and the impact-induced delamination area starts to grow slowly. Fibre breakage continues to grow, and the simulation is terminated when fibre failure has propagated unstably across the width.

Stress (MPa)	Fibre failure in 0° plies	Delamination
304	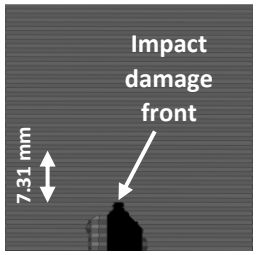	
379	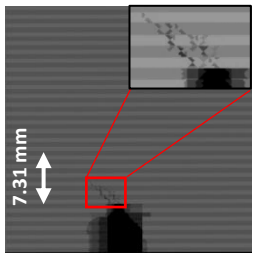	
412	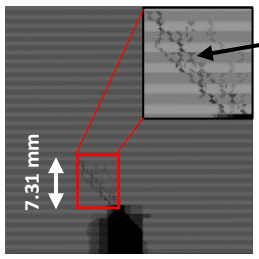	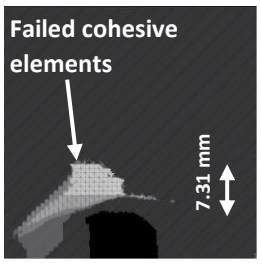

Figure 6.10: Damage development in an edge-impacted laminate corresponding to an impact velocity of 350 m/s (all layers superimposed) – M1 case. Tensile failure stress = 412 MPa.

For M2, the damage due to tensile loading develops in the following sequence: Around the damage zone, splits grow in all plies with increasing applied stress. Around the damage zone, splits grow in all plies with applied stress. The impact-induced delamination area starts to grow slowly, and splits of different fibre orientations can join up. With an increase in applied stress, fibre failure and further delamination occur ahead of the impact damage front at the boundary of the impact-induced delamination area. The crack tip, defined by the fibre failure at the boundary of the impact-induced

delamination area, is then arrested and when the applied stress is increased again, secondary 0° splits grow at the new crack front, and fibre breakage continues to grow. The simulation is terminated after fibre failure has propagated unstably across the full width. The damage process for centre-impacted laminates subjected to tensile loading (considering both M1 and M2) follows the sequences described in *section 6.3.1*. The only obvious difference is related to the fibre failure propagation in both directions as applied stress is increased.

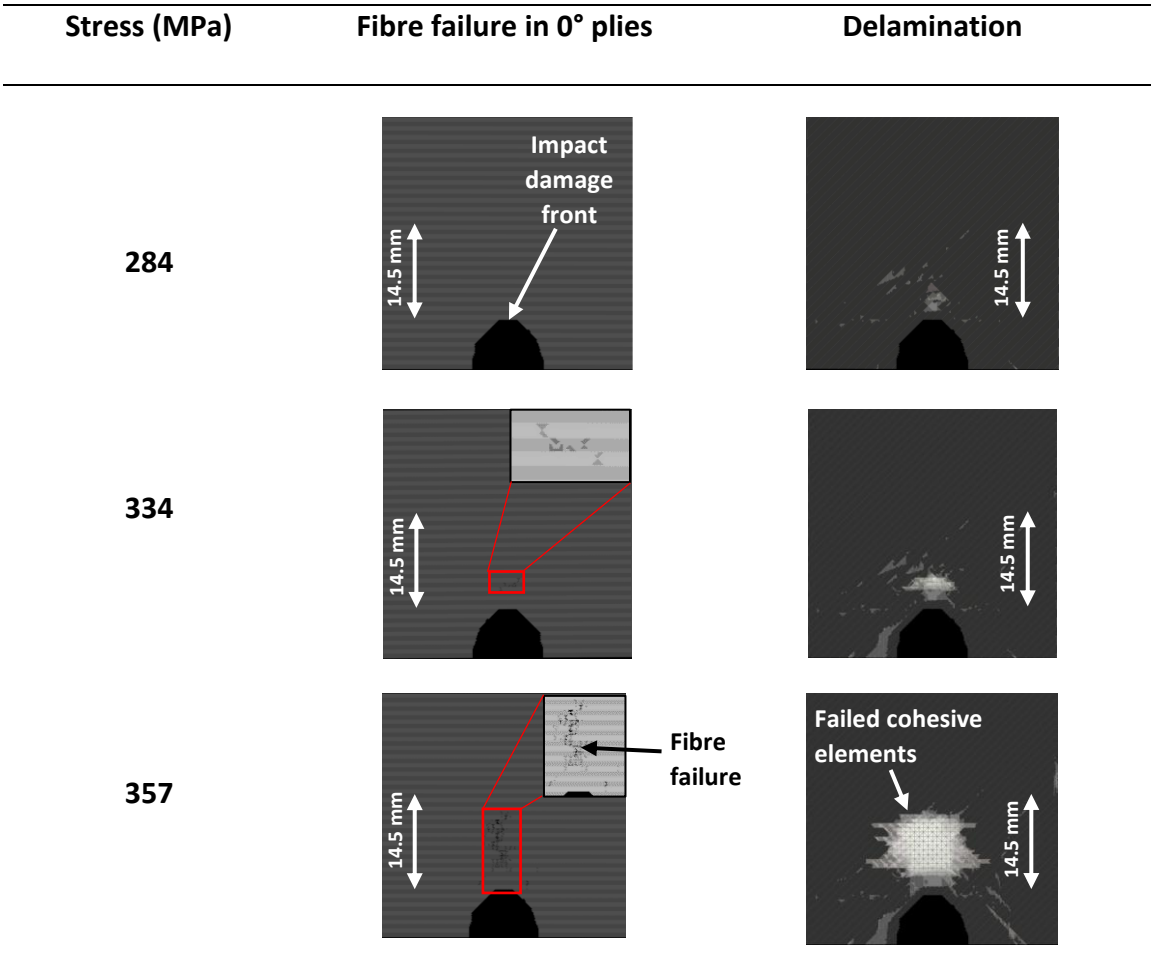

Figure 6.11: Damage development in an edge-impacted laminate corresponding to an impact velocity of 350 m/s (all layers superimposed) – M2. Tensile failure stress = 357 MPa.

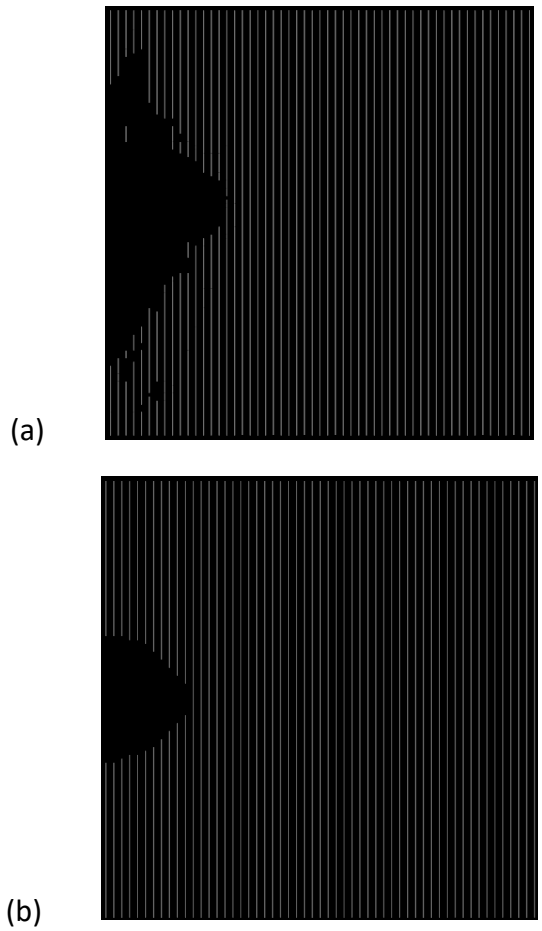

Figure 6.12: Difference in split lengths within the RoI in models using (a) approach M1 and (b) approach M2 prior to tensile simulations. All 0° splits are superimposed and represented by the white lines.

6.3.2. Notched laminates under tension

With the numerical model, it is possible to study the damage development in edge- and centre-notched laminates under tension at different load levels up to failure, as shown in *Figures 6.13* and *6.14.* The notch lengths considered correspond to the fibre fracture widths observed in edge- and centre-impacted laminates at an impact velocity of 350 m/s. The damage sequence is as follows: Initial splits grow in all plies with increase in applied stress. At a higher stress level, delamination starts to grow, and splits of different fibre orientations can join up. Fibre failure occurs in some 0° plies as the applied stress is

increased and the crack is arrested. With further increase in applied stress, secondary 0° splits grow at the new crack front and fibre failure in 0° plies occur until the simulation is terminated as fibre propagates unstably across the full width.

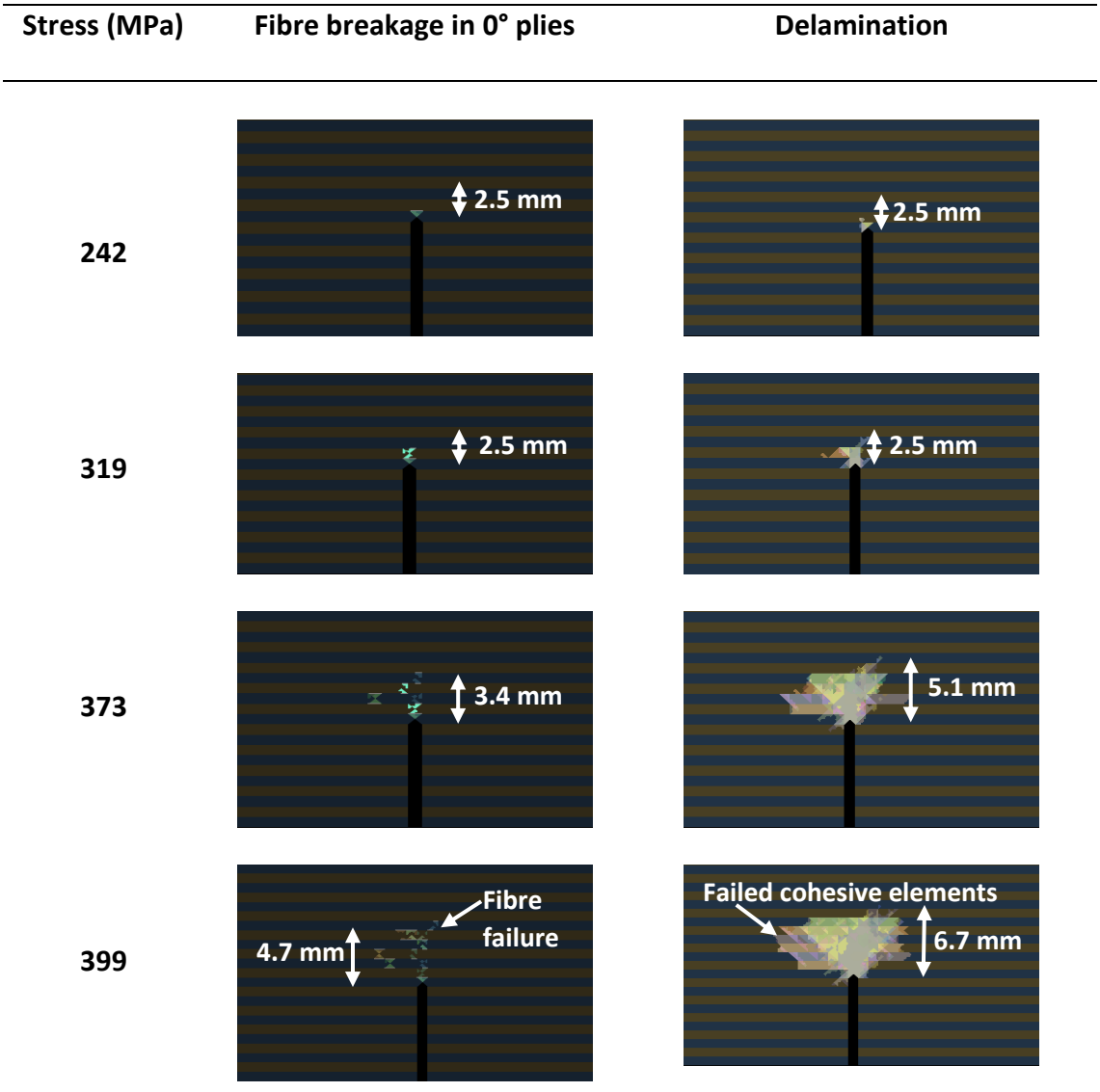

Figure 6.13: Damage development in an edge-notched laminate (fibre fracture width = 7.32 mm) with all layers superimposed. Tensile failure stress = 399 MPa.

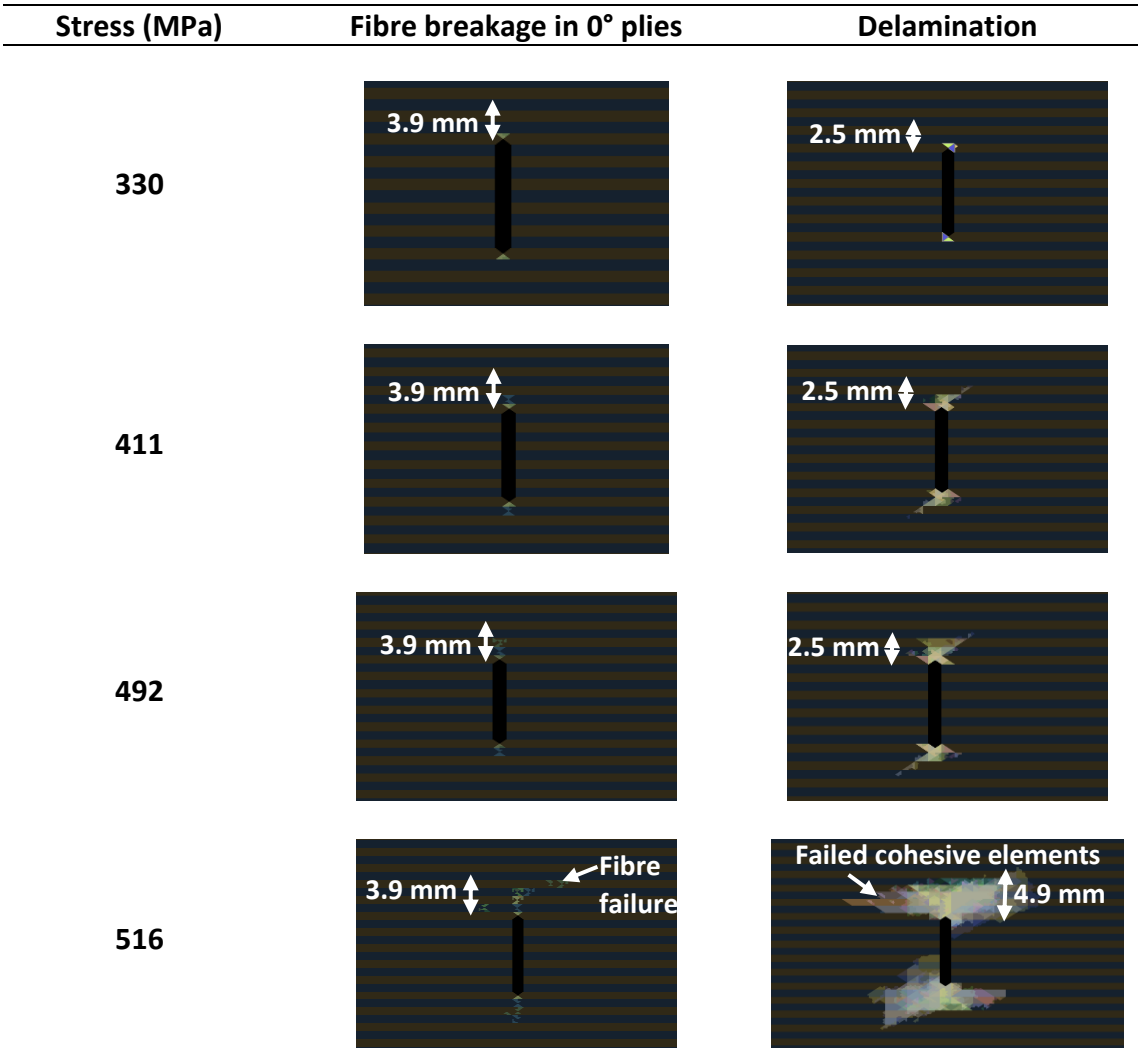

Figure 6.14: Damage development in centre-notched laminate (fibre fracture width = 7.04 mm) with all layers superimposed. Tensile failure stress = 516 MPa.

In *section 5.4.2*, the damage zones in notched specimens at 95% of the tensile failure load were analysed. Here, a comparison is made between the damage zones in the 0° plies from the model and the test data, as shown in *Figures 6.15* and *6.16* for edge and centre notches respectively. The notch cases considered are equivalent to impacted laminates at 350 m/s. The damage zone, D, is defined as the distance from the notch tip to the furthest 0° split in the test, while in the model, it is defined as the distance between the notch tip to the furthest fibre failure. For the edge notch case, the damage

zone in the single outboard 0° ply is larger by 6% in the model compared to the test. The damage zones in the double central 0° ply block from the test and the model are similar. For the centre notch case, the damage zone in the single outboard 0° ply is larger by 6% in the model compared to the test. For the central double 0° ply block in centre-notched laminates, the damage zone in the model is smaller by 11% compared to the damage zone in the test. The predicted damage zones are in good agreement with the CT scans at 95% of the failure load, except for the central 0° ply block in the centre notch case, where the damage is underpredicted.

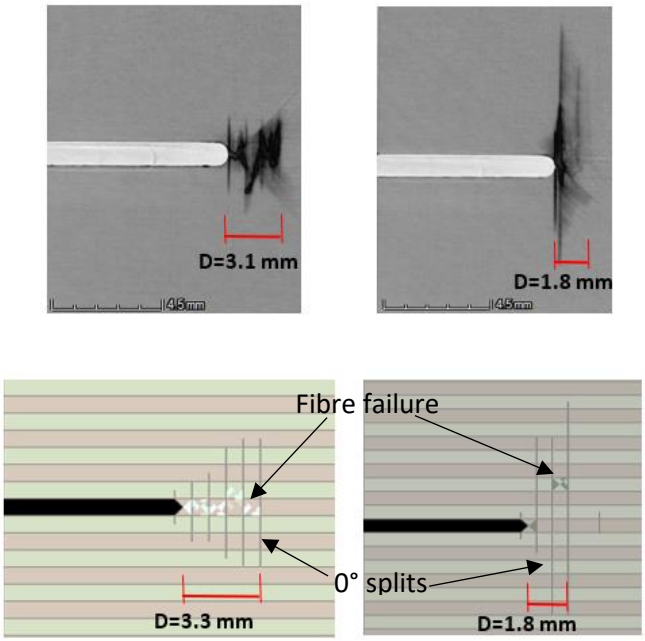

Figure 6.15: Damage zone, D, comparisons at 95% of the failure load in edge-notched laminates from single outboard 0° ply in test (top left), central double 0° plies in test (top right), single outboard 0° ply in model (bottom left) and double central 0° plies in model (bottom right).

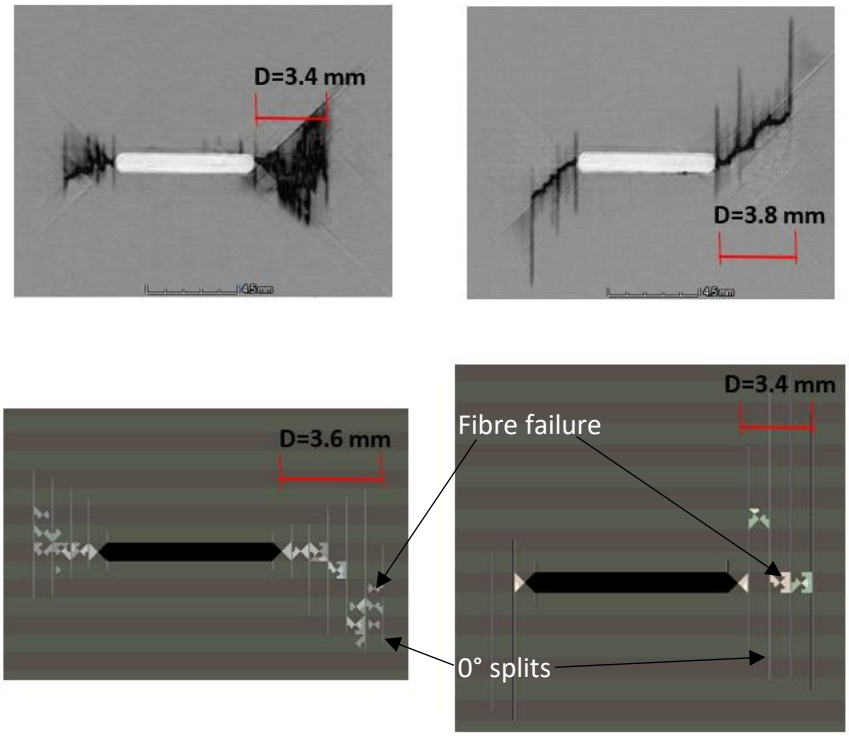

Figure 6.16: Damage zone comparisons at 95% of the failure load in centre-notched laminates from single outboard 0° ply in test (top left), central double 0° plies in test (top right), single outboard 0° ply in model (bottom left) and double central 0° plies in model (bottom right).

6.3.3. Fibre failure initiation

With the available FE data, it is possible to investigate the stress concentrations in the 0° plies up to failure. *Figure 6.17* shows the axial stress (σ_y) plots for edge-impacted and edge-notched laminates under tension (at same scale on each row). The models using approaches M1 and M2 are considered. The stress plots provided in *Figure* 6.17 are for laminates with fibre fracture width and notch length corresponding to an impact velocity of 350 m/s. Also shown in *Figure 6.17* are the regions of maximum stress concentrations, enclosed within the black box. For M1, there is a region of maximum stress concentrations at the impact damage front. As the stress is further increased, fibre failure

occurs at the impact damage front and the region of maximum stress concentration is situated at the crack tip. With further increase in applied stress, the region of maximum stress concentration shifts across the width as fibre failure propagates.

For M2, an edge-impacted laminate shows a region of maximum stress concentration at the impact damage front. 0° splits start to grow with applied stress. As the stress is further increased, the region of maximum stress is concentrated ahead of the impact damage front at the impact-induced delamination area boundary, where fibre failure initiates. The region of maximum stress travels across the width as fibre breakage continues. For the notched case, stress concentrations build up at the notch tip and 0° splits grow. With further increase in applied stress, fibre failure occurs, and the region of maximum stress is located where the crack tip is arrested, thus promoting the growth of secondary 0° splits. While edge cases have been shown here, it is expected that centre cases will follow similar trends with the regions of maximum stress concentrations located on both sides of the impact damage and notch.

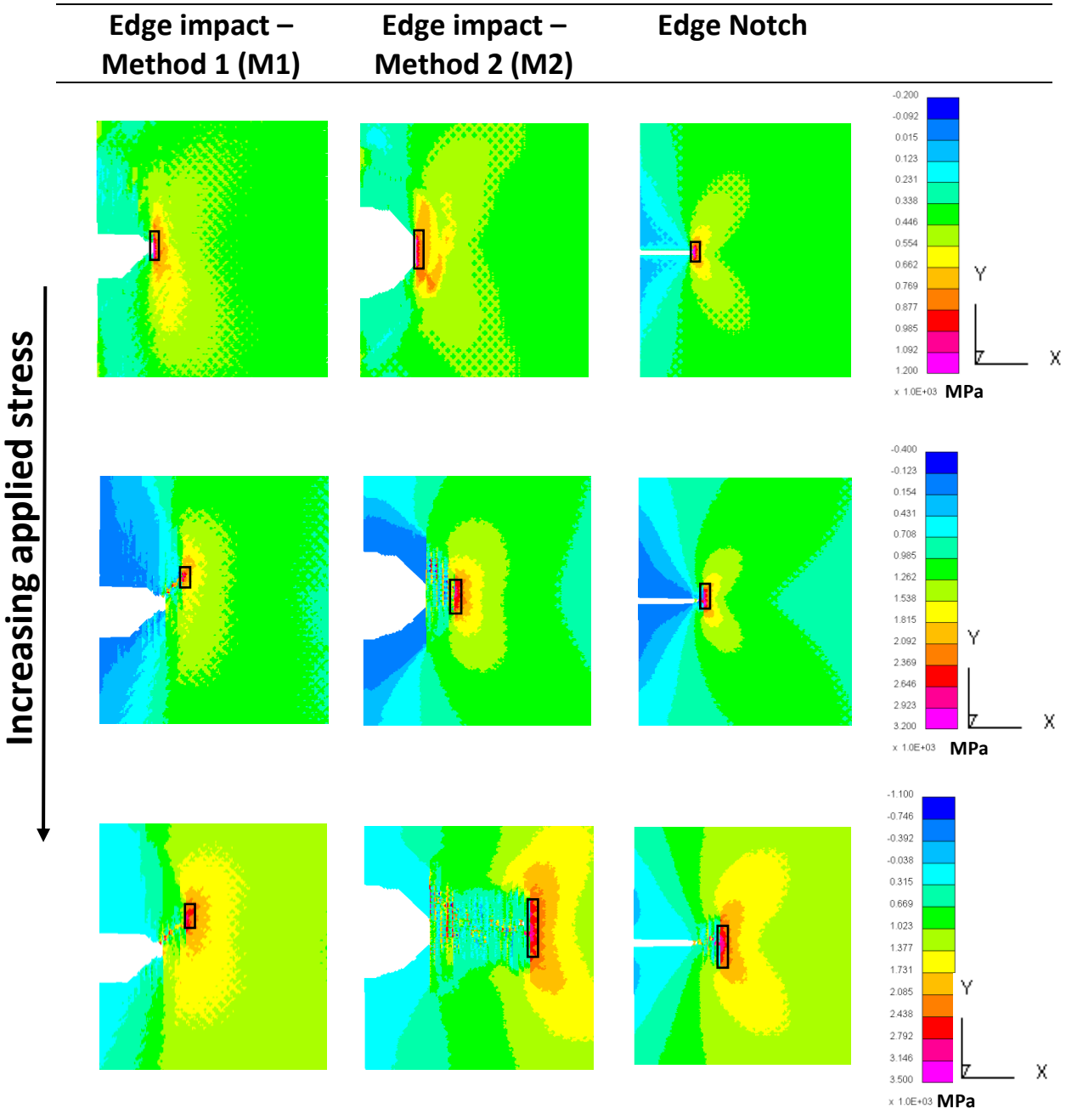

Figure 6.17: Axial stress (σ_y) plots of superimposed 0° plies in edge-impacted and edge-notched laminates. Impact velocity = 350 m/s and fibre fracture width = 7.32 mm.

6.4. Propagation of 0° splits

In *section 6.2*, for edge impacts, it was shown that the residual tensile strengths predicted using both Method 1 (M1) and Method (M2) differ by an average of 12%. While the predicted strength using M1 is higher by 15% from the experimental result at 350 m/s, the predicted strength using M2 is spot on. For the centre impact at 300 m/s, while the predicted residual strength using M1 is closest to the experimental value, the predicted strength using M2 is within 5% of the experimental value. In addition, it was shown that the tensile strength of an edge-notched laminate approaches the strength of an edge-impacted laminate at higher velocities. For centre cases at higher velocities, there is a large difference in tensile strength between notched and impacted laminates. With the fibre failure criterion switched off in the model, an investigation into the growth of 0° splits is conducted for the impacted laminates, using results from both M1 and M2 in order to explain the similarities and differences observed in the predicted tensile strengths. Furthermore, the development of 0° splits in notched laminates is analysed to validate the equivalence drawn between edge-impacted and edge-notched laminates.

The growth of 0° splits is analysed against the strain energy release rate, G. The strain energy release rate, G is calculated according to *Eq. (6.3)* [162], which is valid for quasi-isotropic laminates ignoring ply level effects such as free edge stresses and damage.

$$G = \frac{\pi C f^2 \sigma_g^2}{2E} \tag{6.3}$$

where σ_g is the applied gross section stress, f is a geometric parameter to account for the effect of finite width and with f = 1.38 for edge cases, while f = 1.02 for centre cases. C is the fibre fracture width and E = 61.6 GPa is the in-plane Young's modulus.

The equivalent Stress Concentration Factors (SCFs) in the 0° plies were also studied for the impacted and notched laminates. The maximum elemental stress in the 0° plies is divided by a factor of 2.61 to obtain an equivalent value for the laminate. This factor represents the ratio between the stress in the 0° ply and the average stress in the laminate according to Classical Laminate Theory (CLT). The equivalent SCF is then calculated using the equivalent laminate stress divided by the applied gross section stress.

The growth of 0° splits together with the length of the splits at failure influence the equivalent SCF under tensile loading [72]. The equivalent SCFs at failure are investigated and the argument is that if the equivalent SCFs between any two comparable laminates do not differ by more than 10%, the predicted residual tensile strengths are expected to be similar within 10% unless there is a significant difference in the fibre fracture prior to tensile simulations. The development of 0° splits for edge impact at 350 m/s, centre impacts at 150 m/s and 300 m/s and edge machined notch equivalence are considered hereunder.

6.4.1. Edge impact at 350 m/s

The development of 0° splits based on models from M1 and M2 is presented against G in *Figure 6.18*. Before the tensile simulation begins, the initial 0° splits are much longer in M1 than those in M2. The 0° splits in M2 grow as the simulation begins. As G is increased, the 0° splits in both M1 and M2 show a negligible growth in length. For both M1 and M2, the central double 0° plies have longer splits than the outboard single 0° plies.

The equivalent SCFs in the double central and single outboard 0° plies were analysed against applied nominal stress and the results are shown in *Figure 6.19*. For M1

and M2, the equivalent SCF increases with applied stress because there is very small or negligible growth in the 0° splits. At the failure point, the equivalent SCFs in the 0° plies from M1 are lower than those from M2, which is due to longer 0° splits in M1. In addition, the central double 0° plies have a lower SCF than the outboard single 0° plies at failure point, which is due to the splits being longer in the central 0° plies than those in the outboard single 0° plies. Since the equivalent SCFs at failure for both M1 and M2 differ by 13%, in addition to the smaller fibre fracture width in M1, the predicted residual tensile strength using M1 is higher by 15%. While an edge impact at 350 m/s is considered here, the predicted strength when using M1 and M2 differ by 55% for centre impact at 350 m/s. This is because of the differences in the extent of impact damage and the development of 0° splits between the models from M1 and M2.

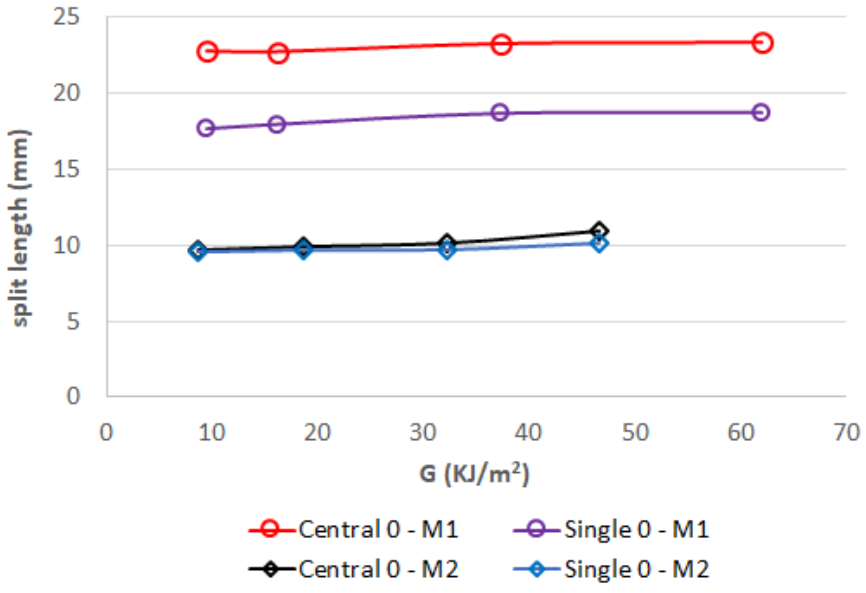

Figure 6.18: Development of the initial splits in the 0° plies for models from Methods 1 and 2. Edge impact at velocity of 350 m/s.

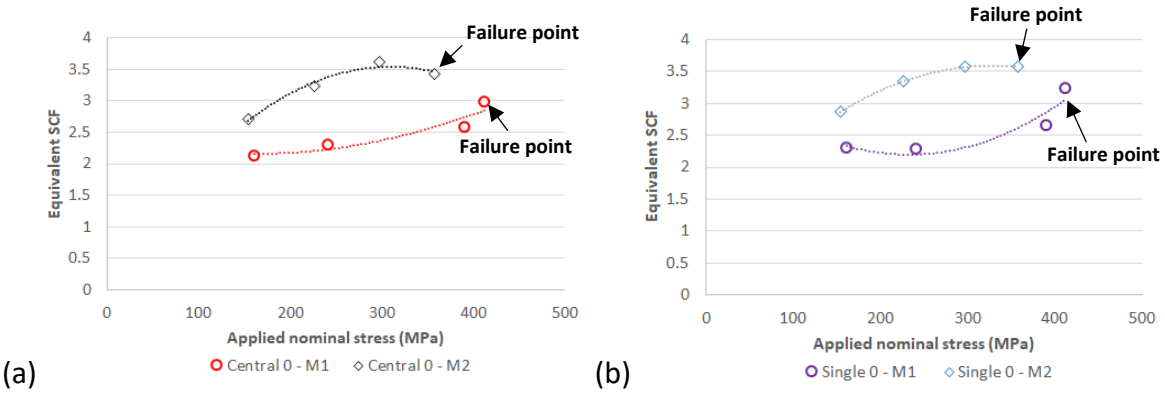

Figure 6.19: Development of equivalent SCFs in (a) central double and (b) single outboard 0° plies for models from Methods 1 and 2. Edge impact at a velocity of 350 m/s.

6.4.2. Centre impact at 300 m/s

From *Figure 6.9*, the predicted strength using M1 is very close to the experimental value. On the other hand, the predicted strength using M1 is higher by 6% compared to the predicted strength using M2. This small difference is due to dissimilar extent of fibre fracture widths, number of broken plies and the development of 0° splits. The latter is studied here and the equivalent SCFs in the central double and single outboard 0° plies from the models using M1 and M2 are presented in *Figure 6.20*. For M1, the equivalent SCFs increase with applied nominal stress. This is due to small or negligible growth in the 0° splits as G is increased. For M2, the equivalent SCFs decrease with applied stress in both the central double and outboard single 0° plies as the 0° splits grow with increasing G. At failure, the equivalent SCFs in the 0° plies from M1 is lower than those from M2, by an average difference of 7%. The lower equivalent SCF from M1 at failure, due to the longer 0° splits, explains why the 0° plies in M1 break at a stress level higher by 6%. In addition, the central double 0° plies have a lower equivalent SCFs at failure than the outboard single 0° plies, which is due to longer 0° splits in the central 0° plies.

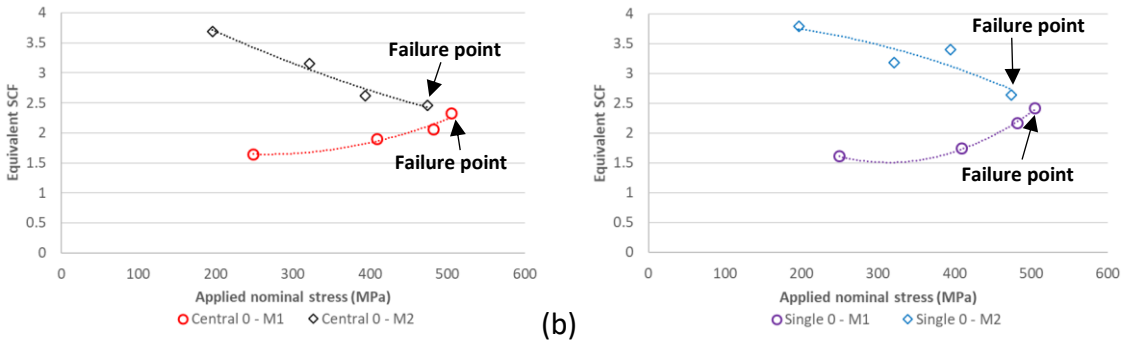

(a) (b)

Figure 6.20: Development of equivalent SCFs in (a) central double and (b) single outboard 0° plies for models from Methods 1 and 2. Centre impact at a velocity of 300 m/s.

6.4.3. Centre impact at 150 m/s

To further investigate the influence of the development of 0° splits on the tensile strength, the centre impact case at 150 m/s is considered. The predicted impact damage from the baseline impact model yielded fibre fracture width and delamination area values very close to the experimental results. However, the tensile failure stress using M1 is lower than the experimental results by 15%. This difference is believed to be due to the growth of 0° splits. In M1, the 0° splits are initially long and as G is increased, the 0° splits show very small or negligible growth. As such, the equivalent SCFs increase with applied stress. For the impacted laminate from the experiment, it is believed that the 0° splits are able to grow longer as G is increased and consequently, the equivalent SCFs decrease with applied stress. At failure, it is believed that the equivalent SCFs in the 0° plies from M1 and the specimen differ, which may explain the lower tensile failure stress in M1.

6.4.4. Machined notch equivalence

Machined notches were investigated to see if they offer a quicker way to assess the effect of impact damage in terms of residual strength. Edge notches were found to be good approximations to edge-impacted laminates at high velocities. However, the residual strength of centre notches was found to be unconservative when compared to the residual strength of centre-impacted laminates at high velocities, and therefore centre notches are not useful as approximations. To further investigate why edge notches are good approximations, the development of 0° splits and equivalent SCFs are provided hereunder. Predicted strength data from M2 and only the central double 0° plies are considered as *Xu et al.* [74] observed longer 0° splits in the central double 0° plies than in the outboard single 0° plies.

The development of 0° splits in the edge-notched laminate are compared to those from M2 (edge-impacted laminate), as shown in *Figure 6.21a*. *Figure 6.21b* illustrates the comparison in equivalent SCFs for the two laminates considered. In the notched laminates, the initial 0° split lengths increase with increasing G. For the impacted laminates, the initial 0° splits are long and there is then only a small growth in the 0° splits as G is further increased. The 0° splits in notched laminates, by comparison, grow significantly with further increase in G.

For notched laminates, the equivalent SCF decreases with applied stress because 0° splits grow with increasing G. For impacted laminates, the equivalent SCF increases with applied stress due to very small or negligible growth of the 0° splits with increasing G. At failure, the equivalent SCFs of edge-impacted and edge-notched laminates differ by 7%, which is due to the 0° splits being longer in the impacted laminate. Since the

difference in equivalent SCFs is less than 10%, an edge notch can represent an edge-impacted laminate corresponding to an impact velocity of 350 m/s.

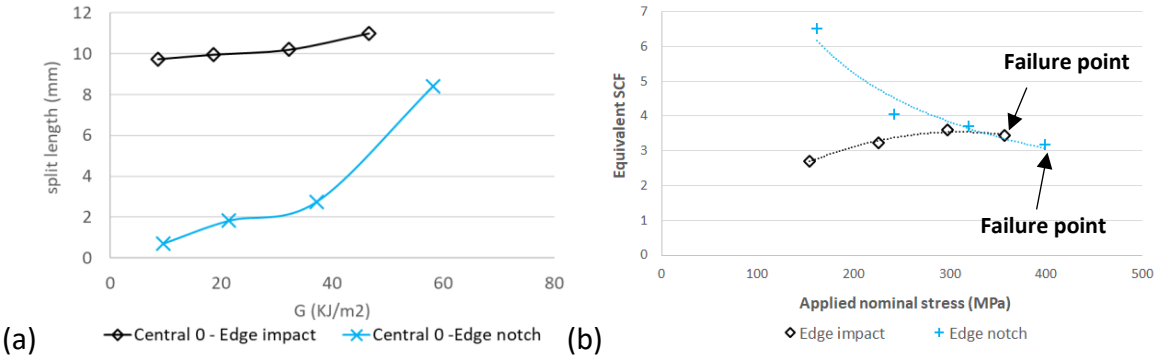

Figure 6.21: (a) Development of the initial splits in the central double 0° plies. (b) Development of SCFs in the central double 0° plies. The results are for edge-impacted and notched laminates, corresponding to an impact velocity of 350 m/s.

6.5. Conclusion

The Hi-FEM modelling technique allows representing the delamination shapes, split lengths and continuous fibre breakage process within the damage zone through pre-defined multiple split paths and the Weibull criterion for fibre failure. By employing cohesive interface elements, the interactions between fibre failure, delamination and splitting can be simulated. The Hi-FEM also provides a powerful tool for understanding the damage development and growth of 0° splits in impacted and notched laminates under quasi-static tension.

In terms of predicting the residual tensile strength of impacted laminates, two approaches were considered. Firstly, the proposed impact models from Chapter 4 were post-processed and then loaded under tension. Secondly, characterised impact damage from CT scans was manually inserted into FE models prior to tensile simulations. For edge and centre impacts, the predicted strengths from the two different approaches considered vary for some impact velocities, with the largest difference observed for a centre impact at 350 m/s. The first approach (M1) has been shown to yield reasonable strength predictions for intermediate velocities, however, the predictions are unconservative for edge impacts at 100 m/s and 350 m/s, and centre impacts at 100 m/s, 150 m/s and 350 m/s. Although the process in the second approach (M2) is not as computationally efficient as M1, the predicted strengths were found to be closest to the experimental strengths, where it is possible to assess the interactions of different failure modes under tensile loading. The strength predictions obtained when using these two approaches are affected by the extent of impact damage and by the development of 0° splits. It was found that the growth of 0° splits when the laminates are subjected to

tensile loading significantly affects the stress levels at which the 0° plies break. If further improvements in the baseline impact model in *section 4.4* could be made, then the M1 approach could become more suitable than M2 for tensile strength predictions, since impact tests will not have to be conducted.

Machined notches were also investigated for their residual strengths. While edge notches provide a reasonable approximation for edge-impacted laminates at high impact velocities, the residual strengths of centre-notched laminates are unconservative in comparison to centre-impacted laminates at higher velocities. The equivalence was validated by inspecting the growth of 0° splits in impacted and notched laminates. The edge machined notch approach can be very useful in the early design stages, where development costs can be reduced by reducing the number of impact tests to be carried out.

Journal paper – Review process in Composite Structures

Kristnama AR, Xu X, Wisnom MR, Hallett SR. Numerical analysis of high velocity oblique impacts on carbon/epoxy laminates and tension after impact.

7. Effect of edge shield under impact

In aircraft structures such as blades, stator vanes and nozzle guide vanes, the edges are usually protected with metal sheet in order to act against impact and erosion. This chapter experimentally investigates the importance of an edge shield under impact, where a thin sheet of metal is bonded to the edge of the carbon/epoxy laminate. Several high velocity oblique impacts are carried out to the edge of the laminates. The effect of the shield on the impact damage and residual tensile strength is investigated via X-ray Computed Tomography (CT) scans and quasi-static tension tests.

7.1. Introduction

Foreign object damage (FOD) is a significant threat to gas turbine components. Such engines generate powerful suction, which can draw in small hard objects. The hard body particles can hit the rotating blades and travel further down the engines with high speeds. Therefore, any engine components downstream of the blades may be impacted at high velocity by these small hard body particles. The impacts can occur over a range of velocity and anywhere on the components. As such, when manufacturing these components from composite materials or even metal, a protective layer is typically applied onto the surface of the components to prevent significant impact damage or erosion. While aluminium coatings are not good for erosion and due to potential galvanic corrosion with composite components, the addition of platinum to the aluminium coating, through electroplating, has become popular over the years despite the high costs associated to it.

Core materials (honeycomb, foam, hollow spheres) are of great interest as they have good specific resistance and enhanced energy absorption capabilities. For protection against bird strikes, some aircraft cockpits have a layer of aluminium honeycomb covered by a skin of aluminium to improve energy absorption capacity. The energy absorption increases when the relative density of the honeycomb cores is increased [163-166]. *Li et al.* [167] conducted hypervelocity velocity impacts on different types of sandwich, which involved several material systems: - fabric-reinforced silicon carbide ceramic-matrix composite as impact-facing sheet, hollow sphere energy absorption materials, carbon fabric and Kevlar fabric reinforced epoxy matrix composites as pressure walls. They investigated the energy absorption capability of the sandwich materials which were subjected to 1 – 7 km/s impact loading. Of interest, when stainless metal fibre reinforced silicon carbon matrix composites were used as impact-facing sheets, they absorbed and translated energy in a much better way than polymer matrix composites as the projectiles disintegrated into smaller particles on impact. *Hart and Ubels* [168] used protective layers consisting of epoxy filled with glass microballoons covered with one or more layers of aluminium gauze. Their work has shown that the protective surface layer improved the resistance to impact damage. *Rahme et al.* [169] used a low-density energy absorbent material (hollow spheres) of a certain thickness and a thin layer of Kevlar for the protective surface against low velocity impacts. This concept of protective layers has been shown to be a good candidate against impact, and despite some weight addition to the whole structure, the concept is applicable to components that are expensive to replace or repair. The use of a thermal protection layer, such as cork, in a study conducted by *Petit et al.* [170] showed good mechanical protection resistance against impact and the use of such protection increases the residual compressive strength after impact tests.

In this experimental study, the protective layer considered is a thin mild steel sheet bonded to the edges of the carbon/epoxy laminates. The effect of the shield on the extent of impact damage is investigated, and the impacted laminates are examined for residual tensile strength through quasi-static tension. As such, the residual strength of impacted laminates with protective layers can be compared with the residual strength of impacted laminates without the protective layers.

7.2. Material, manufacture and test set-up

The laminates are made of Hexcel HexPly® IM7/8552 carbon-epoxy pre-preg with ply thickness of 0.125 mm. A quasi-isotropic stacking sequence $[45/0/-45/\ 90]_{2s}$ is used and the cured laminates have a nominal fibre volume fraction of about 60%. A 0.1 mm steel shim is employed for the shield and the metal shim is bonded to the edges of the laminates using Redux®319 adhesive. Redux®319 is a high-performance modified epoxy film adhesive which has a curing temperature of 175 °C.

The surface of the laminate to be bonded is grid-blasted to provide a rough surface such that there is good adhesion between the bonding interfaces. A fixture was manufactured which allows aligning the protective layer, the adhesive film and the laminate together. A schematic of the procedure is shown in *Figure 7.1*. The adhesive film is placed over the laminate and the protective layer is folded manually over the adhesive film. The fixture is positioned on a vice tool which allows the alignment of five specimens at a time, by applying pressure at the top and pushing downwards until the laminate is completely slotted into the fixture. The laminates are removed from the slots and the process is repeated. The laminates with protective layers and adhesive films are then carefully bagged, keeping enough space between them to avoid contact with the

adhesive overflow when curing in the oven for 5 hours. *Figure 7.2* shows an image of a laminate with the protective layer bonded to the edge over three-quarter of the chord. After curing, the laminates showed an overflow of adhesive to the sides.

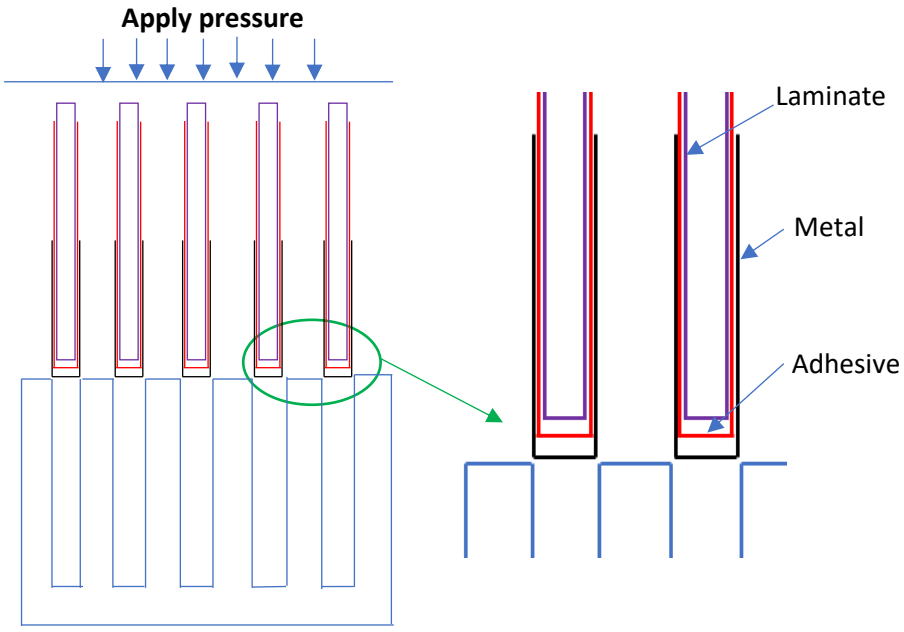

Figure 7.1: Schematic of laminate preparation for metal sheet addition to the edge.

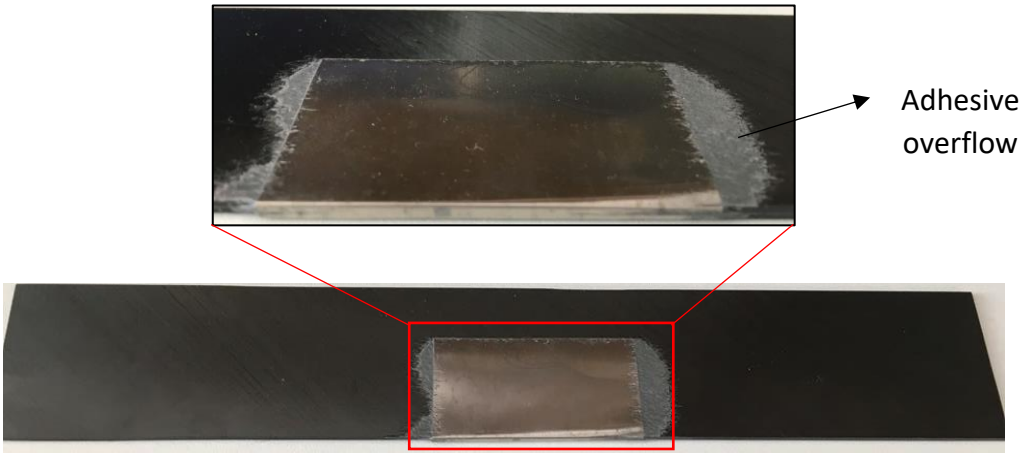

Figure 7.2: Bonded metal sheet over the edge of the laminate.

To ensure that the adhesive was properly cured and to check for any irregularities in the bonding interface, one specimen was inspected using the ultrasonic full-matrix

capture (FMC) [171], where B-scan slices were reconstructed using the total focusing method (TFM) [172]. This was accomplished using a 5MHz array probe connected to a Diagnostic Sonar 'FIToolbox' array controller working with the proprietary Matlab-based BRAIN software developed at the University of Bristol [173]. In array imaging, FMC refers to how the array collects and stores raw data, while TFM is a high-resolution imaging technique which is only feasible as a post-processing operation on the FMC data. The inspection setup is illustrated in *Figure 7.3*. Two different locations on a single surface of the laminate were chosen to inspect for the quality of the bonding interface, namely location 1 with the probe close to the edge and location 2 with the probe further away from the edge.

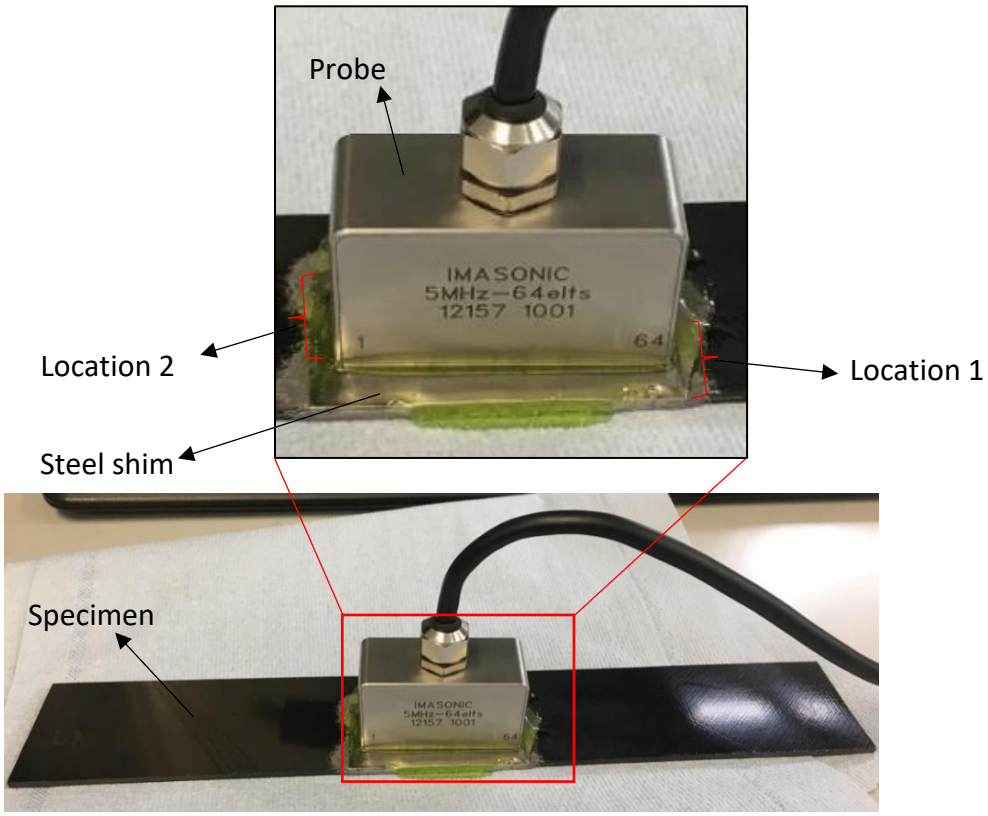

Figure 7.3: Inspection setup with probe positioned at location 2.

The instantaneous amplitudes obtained when positioning the probe at the two different locations are shown in *Figure 7.4*. The positions of the steel sheet and the top surface of the laminate are also indicated in *Figure 7.4*. As the waves emitted from the probe travel through the inspected area, the amplitude of the wave varies from red (highest) to blue (lowest). From *Figure 7.4a*, the regions enclosed within the black ellipses indicate voids between the steel sheet and the top surface of the laminate. There are several voids identified at location 1 compared to location 2. Therefore, the inspected laminate showed relatively poorer bonding interface at the edge of the laminate than further away from the edge.

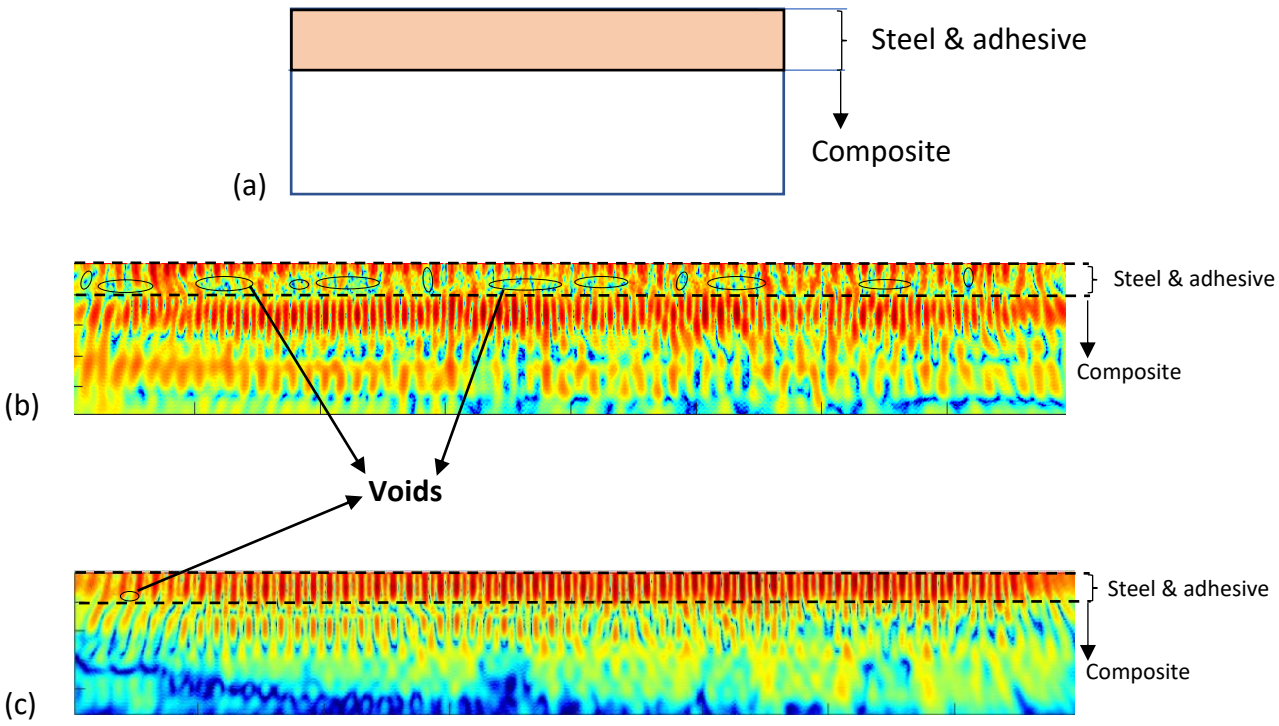

Figure 7.4: The schematic shown in (a) illustrates the region of interest, in shaded colour, corresponding to the region with the steel and the adhesive. The instantaneous amplitudes at 5MHz of the specimen are provided for (b) location 1 and (c) location 2.

Due to unavailability of the gas gun at Oxford, arrangements were made to conduct high velocity impact tests at Imperial College London. As in the previous impact tests carried out in *Chapter 3*, a 3 mm steel cube of mass 0.22 g was used as projectile, the same mechanical fixture which holds the target was utilised and impacts were carried out at 45° to the edge. The test set up is shown in *Figure 7.5* and impacts were carried out for impact velocities of 125 m/s, 226 m/s and 301 m/s, equivalent to 1.72 J, 5.62 J and 9.9 J. A cylindrical sabot of diameter 24.9 mm is used to support the projectile during the acceleration along the barrel. A stopper is fitted at the end of the barrel, which stops the sabot and allows the projectile to travel and exit via the nozzle. It is important to mention that it was not possible to control the rotation of the cube once it leaves the sabot. Two sensors placed 10 mm apart along the barrel records the time as the sabot travels through these two points. The edge of the target was aligned carefully with the axis of the nozzle and the impacts made at a point on the target which is 1.5 mm from the edge, to ensure contact between the projectile and the target. The target is clamped over a length of 40 mm from one end onto the fixture, which is rigidly fixed during the tests. A high-speed camera (Photron Ultima APX-RS) was used to record the impact process. A lamp was also utilised to ensure enough lighting and the camera was configured to obtain 39000 fps.

Post impact, impact damage was characterised using X-ray Computed Tomography (CT), and quasi-static tests (according to the ASTM D3909 standard) were carried out to determine the residual strength of the impacted laminates. The procedures for impact damage characterisation and tensile tests, as described in Chapter 3 and 5, are applied here.

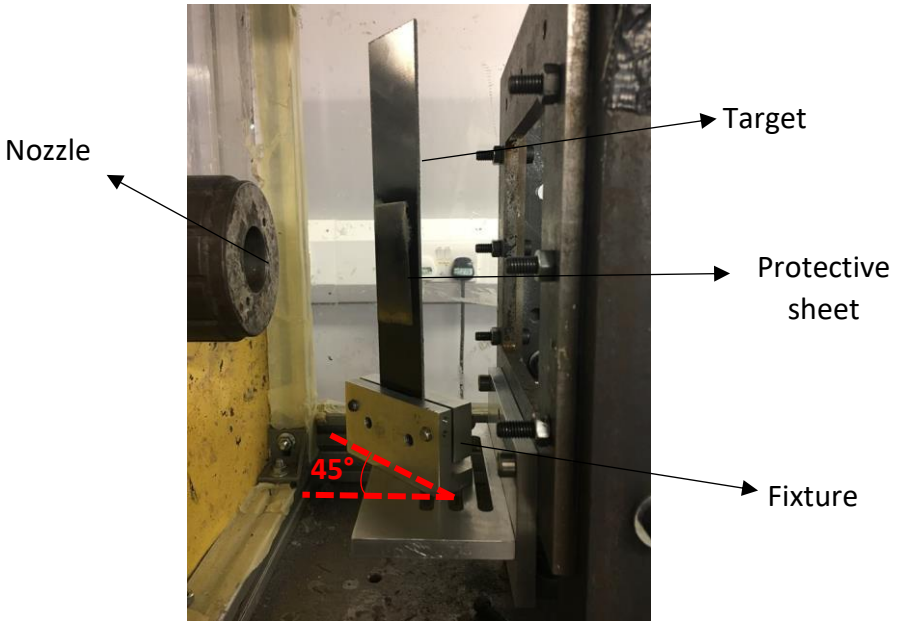

Figure 7.5: Impact test setup showing target in desired position before impact.

7.3. High velocity impact tests

This section describes the impact process by inspecting images from the high-speed video camera. In addition, the impact damage is characterised in terms of fibre fracture width and delamination area. The relationship between impact damage and residual tensile strength is further investigated.

7.3.1. Impact process

At impact velocity of 125 m/s, the projectile indents the edge of the laminate and the protective layer remains bonded to the edge. For impacts at 226 m/s and 301 m/s, the shield is detached from the laminate after the projectile strikes the target. *Figure 7.6* illustrates captured images from video sequences for impacts at 226 m/s and 301 m/s, and the far-right images in *Figure 7.6* show the shield being detached from the laminate. This may be because, as the impact velocity is increased, the shock waves upon impact

also increase in intensity. With high-intensity shock waves propagating through weaker bonding interfaces, the shield is more prone to become detached from the laminate.

The recorded velocities for this experimental study are provided in *Table 7.1*. From *Table 7.1*, the consistency of velocities at 226 m/s and beyond can be confirmed by the low C.V values in the recorded impact velocities. To operate the gas gun, the applied pressure was increased to the desired level using a 'push' button and the readings dropped quickly up to the desired value. During the tests, the gas gun was activated with some fluctuations around the desired pressure value and this error is associated with the high C.V value for impact velocity of 125 m/s. To further verify the consistency of the impact tests, the orientation of the cube just before impact and/or on impact was inspected as shown in *Figure 7.7*. The images show some variations in the orientation of the cube before or on impact, which may influence the extent of impact damage and the residual tensile strength.

(a) 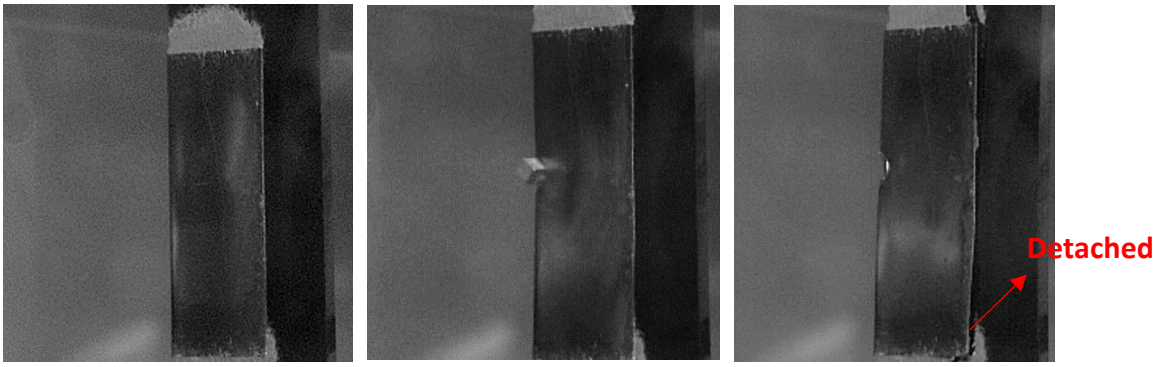

(b)

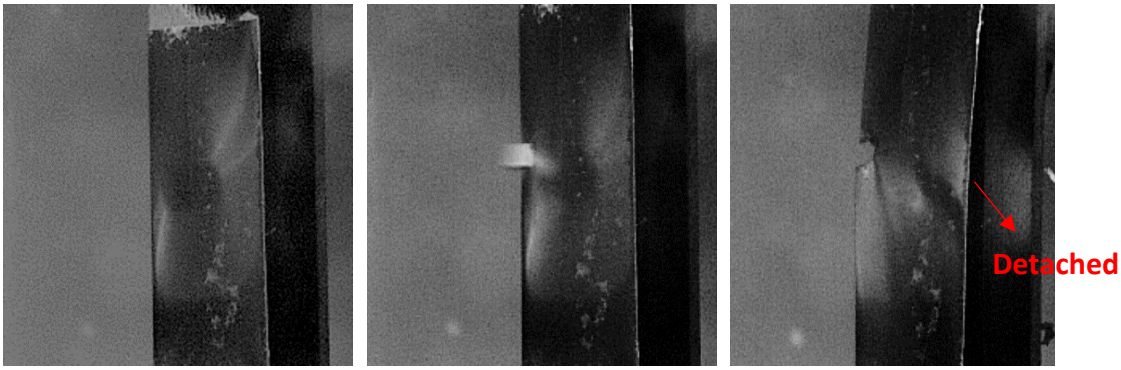

Figure 7.6: Impact sequences from impacts at (a) 226 m/s and (b) 301 m/s.

Table 7-1: Recorded impact velocities before impact.

No. of specimens	Recorded impact velocity (m/s) (C.V %)
5	125 (9.2)
4	226 (4.0)
4	301 (3.4)

(a)

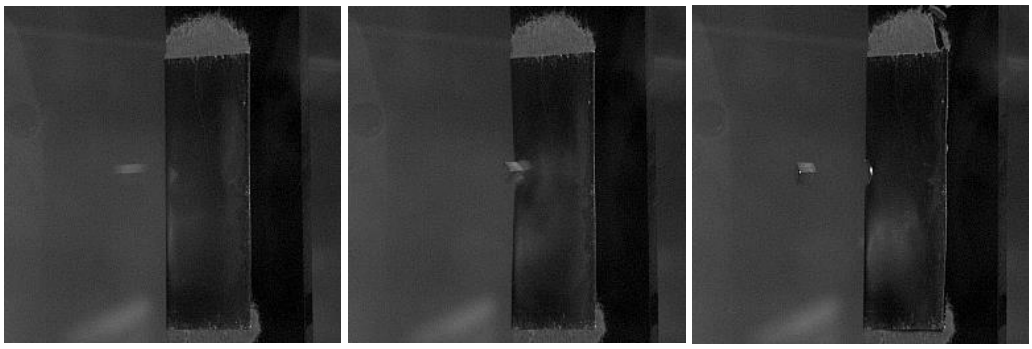

(b) 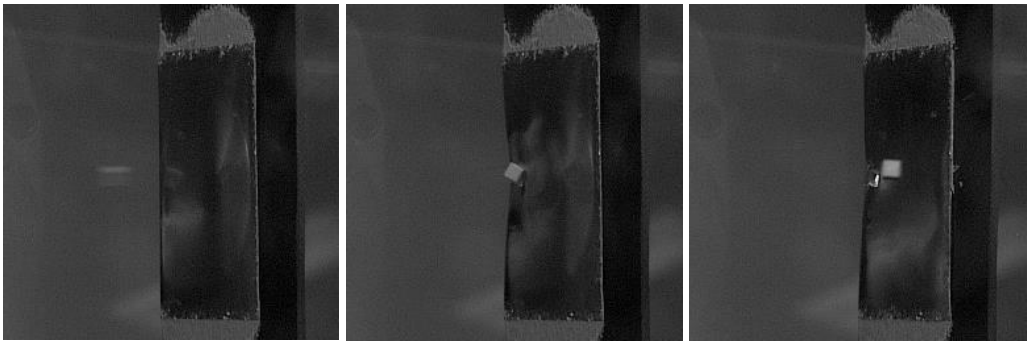

Figure 7.7: Typical images from high speed camera showing orientation of the cube before and/or on impact for impact velocity of (a) 125 m/s and (b) 226 m/s.

7.3.2. Fibre failure

The extent of fibre failure in all the plies for all impact configurations was determined based on the CT scan images. *Figure 7.8* illustrates CT images of impacted laminates at 125 m/s and 301 m/s. Using the method of measuring the width, *w*, of broken fibres in all plies and averaging over the number of plies showing broken fibres, the fibre fracture width was determined, and the results are illustrated in *Figure 7.9*. Through the thickness, there is a double 0° ply block at the central symmetry plane with single 0° plies outboard. For impact velocity of 125 m/s, the top three plies showed fibre failure. As the impact velocity was increased to 226 m/s, fibre failure was observed in the top five plies. With further increase in impact velocity, the laminate showed perforation with fibre failure in all the 16 plies.

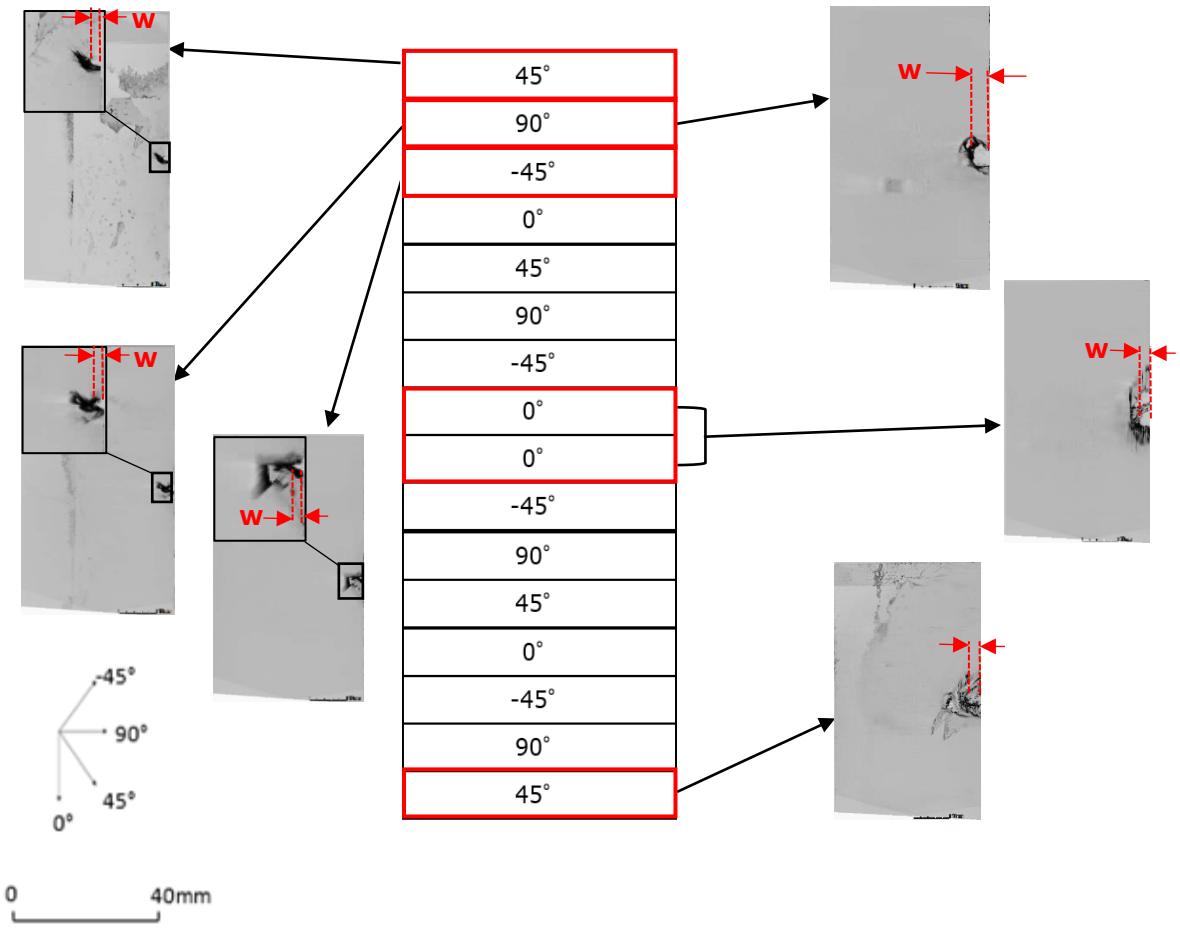

Figure 7.8: Widths of broken fibres, w, observed in different plies for impacted laminates at velocities 125 m/s (left) and 301 m/s (right).

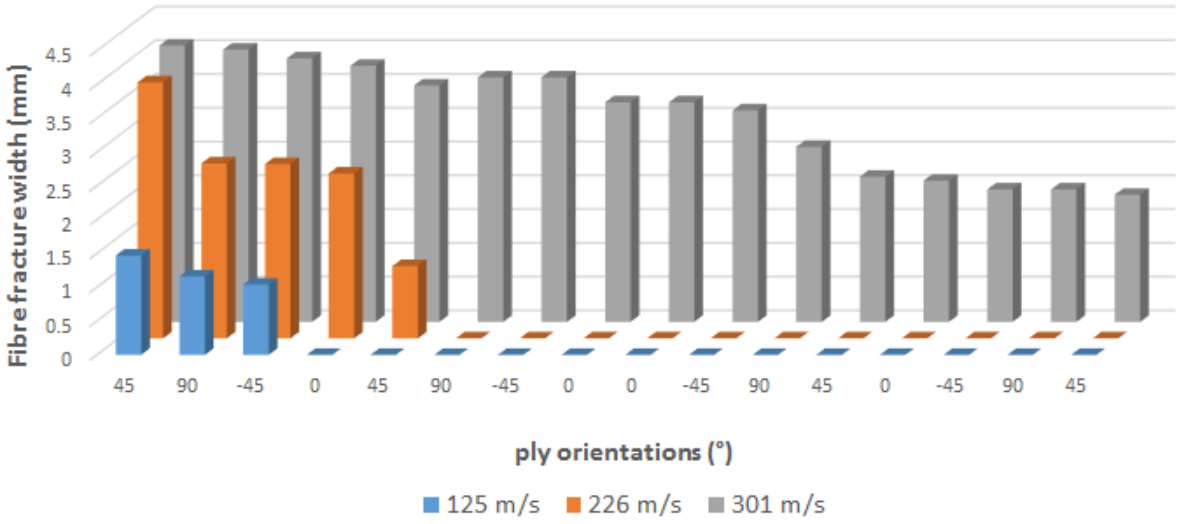

Figure 7.9: Measured fibre fracture widths in all plies.

From *Figure 7.9*, the extent of fibre failure measured in some of the plies is larger than the size of the projectile. This is because of the oblique trajectory of the projectile during penetration which promotes a larger extent of fibre fracture. In addition, the interactions between different failure modes, different ply orientations and local bending around the impact point cause a larger extent of fibre fracture than just the area under the impactor. Due to the projectile's oblique trajectory, the top 45° ply showed the largest extent of fibre failure for all impact velocities and the fibre fracture width decreases in size in the through thickness direction.

7.3.3. Delamination

The extent of the damaged area in the impacted laminates was inspected from CT scans. *Figure 7.10* illustrates typical -45°/0° interfaces observed in laminates impacted at 125 m/s and 226 m/s. The methodology behind determining the delamination area using the ImageJ® software has been explained in detail in *section 3.2.2*. The measured area from all interfaces for all impact configurations are provided in *Figure 7.11*. For all laminates impacted at velocities of 125 m/s, 226 m/s and 301 m/s, every interface is delaminated. The delamination area was observed to be smallest at the interfaces close to the impact point, and its size increased away from the impact point. Just beneath the impact point, the delamination area is smallest because of the effect of through-thickness compressive stresses which suppress delamination. The largest delamination area was observed at the -45°/0° interfaces, adjacent to the central 0° ply block. When the projectile strikes the laminate, interlaminar shear arises due to the contact force and the stress reaches a maximum value near the mid-plane, hence inducing a larger

delamination area. The stress decreases further away from the impact point, thus leading to smaller delamination area away from the central 0° ply block.

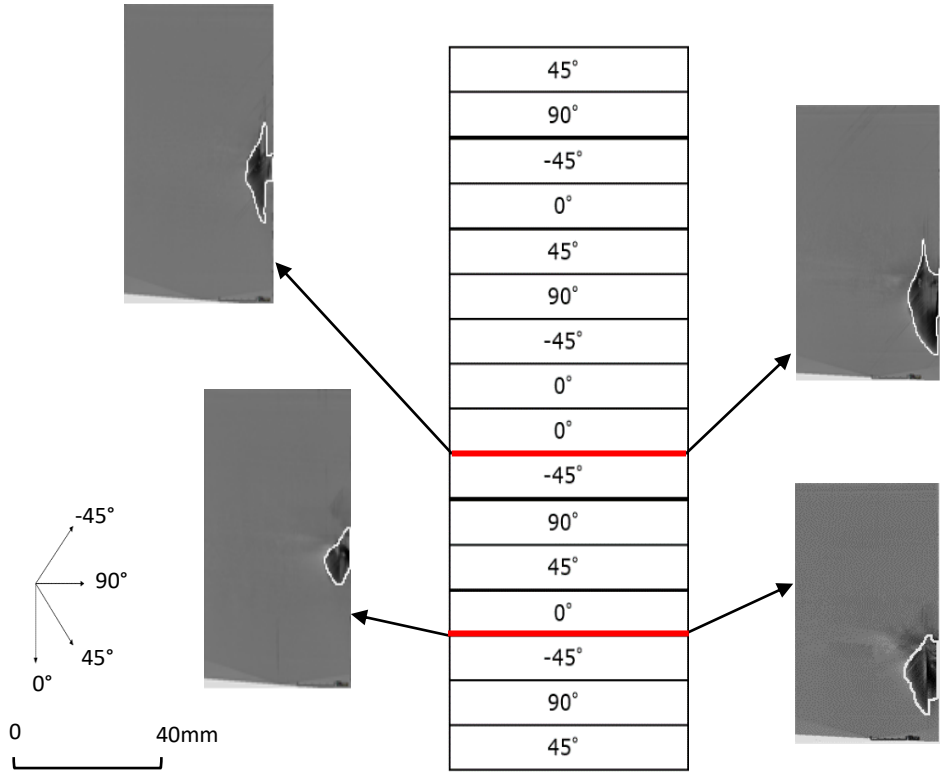

Figure 7.10: Delamination area at different -45°/0° interfaces in the through thickness direction represented within the white region for impacts at 125 m/s (left) and 226 m/s (right).

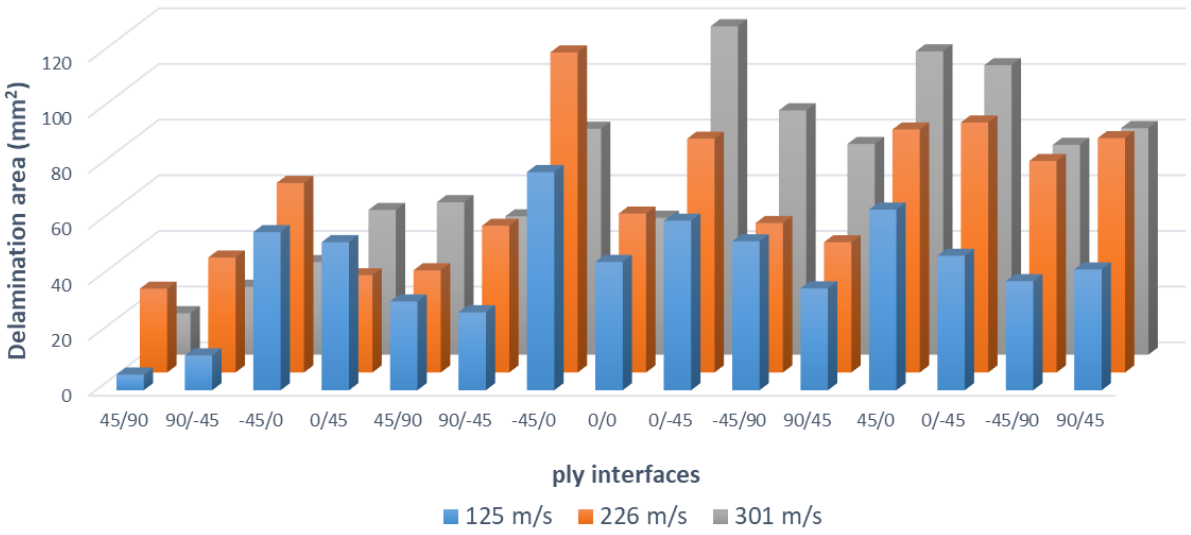

Figure 7.11: Measured delamination areas for all interfaces.

Cross-sectional CT images are provided in *Figure 7.12*, where the locations of delamination through the thickness can be observed. Impacted laminates exhibit fibre breakage in different plies through the thickness, which is accompanied by several delaminations. The damaged area is much more localised just beneath the impact point. Away from the impact point, the laminates revealed longer extent of delamination, as confirmed from *Figure 7.11*. The delamination area determined from all interfaces within the laminate increases with impact velocity. Beyond 226 m/s, the delamination area increases at a slower rate and laminate perforation is observed at 301 m/s. Beyond 301 m/s, as a result of laminate perforation, the impact damage is expected to be much more localised around the impact point and hence, the delamination area may decrease. Further impact tests beyond 301 m/s are required to verify this hypothesis.

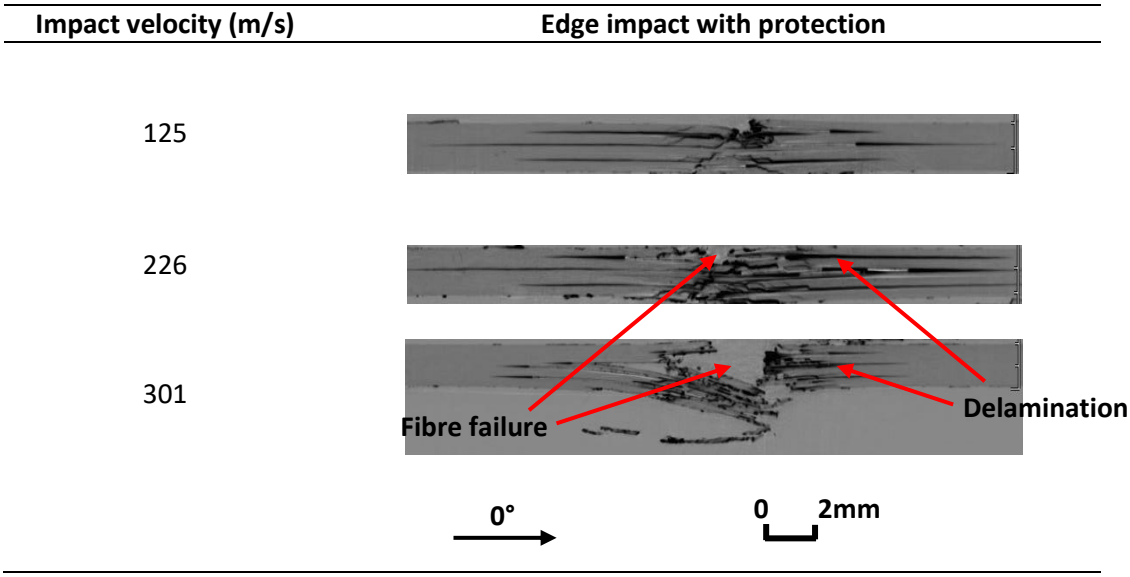

Figure 7.12: Cross-sectional CT scans of impacted laminates over a range of velocities.

7.3.4. Residual tensile strength

A non-impacted laminate without the edge shield was chosen as the baseline because it was shown that non-impacted laminates fail at the grips, and hence the residual strength of non-impacted laminate is expected to be unaffected by the edge shield. Typical load crosshead-displacement responses of non-impacted and impacted laminates are illustrated in *Figure 7.13*. The non-impacted laminate has a non-linear response and failure occurs at the grips. The non-linearity in the non-impacted specimen is due to slippage at the grips during the tests. Impacted laminates show a linear response up to failure, where a fibre pull-out mechanism is identified around the impact damage front at the failure load. From the load crosshead-displacement responses, the highest load level is taken as the failure load and the residual tensile strength is calculated using *Eq. (7.1). Table 7.2* provides details on the residual tensile strength for all laminates tested.

$$\sigma = \frac{P_{failure}}{A} \tag{7.1}$$

where σ is the tensile failure stress, $P_{failure}$ is the peak load recorded at failure and A is the total cross-sectional area of the laminate, obtained from the measured widths and thicknesses of the laminates.

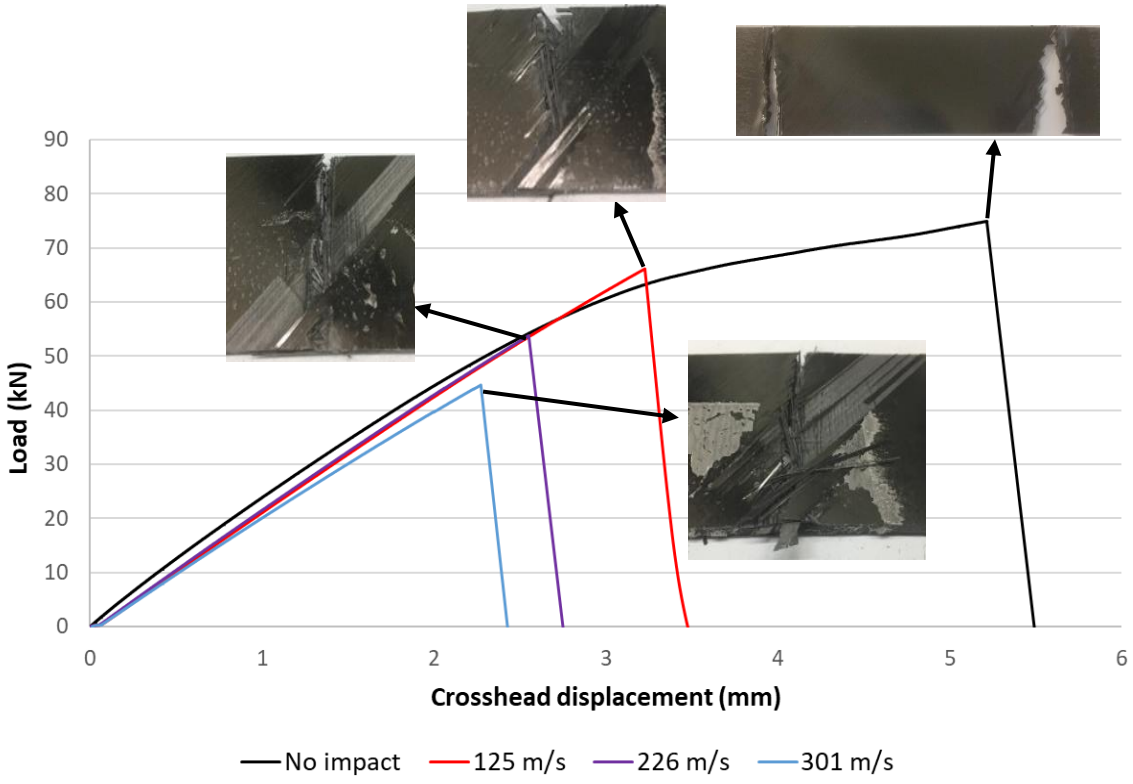

Figure 7.13: Load vs crosshead-displacement responses of laminates under tension.

The fibre fracture width and delamination area in the impacted laminates increase with increasing velocity, and hence the residual tensile strength decreases. At 125 m/s, there is a reduction of 7.9% in residual strength, which is mainly governed by the extent of fibre failure. For an impact at 301 m/s, a reduction of 38% in residual tensile strength is observed. The projectile was aimed to strike the target at 1.5 mm from the edge, and the high C.V values in *Table 7.2* may be due to some variability in exactly where the samples were impacted. In addition, the fact that the projectile can rotate before impact may be linked with the high C.V values.

Table 7-2: Residual tensile strength of laminates with edge protection and the baseline laminate.

No. of specimens	Residual tensile Strength (MPa) (C.V. %)
4	837 (2.9)
3	683 (7.4)
3	562 (11.0)
Un-notched (5 samples) = 909 MPa (2.2 C.V. %)	

7.4. Importance of edge shield

The importance of the protective layer on the edge of the laminate is investigated in this section and comparison is drawn against results from *Chapter 3* and *5*, where impacts were carried out on laminates without the shield.

7.4.1. Effect on impact damage

For laminates with and without the edge protection, the extent of fibre failure observed increases with increasing impact energy and *Figure 7.14* shows the comparison of the extent of fibre failure with varying impact energy between laminates with and without the edge shield. The impact energy is equal to the incident kinetic energy of the projectile, which was determined using the previously described *Eq. (5.2).* For lower impact energies, there is only a slight difference in the fibre fracture widths between laminates with and without the protective layer. However, as the impact energy is increased to 9.9 J, the presence of the protective layer on the edge results in a fibre fracture width which is 35% lower than the fibre fracture width observed in the laminate

without the protective layer. The general trend drawn on *Figure 7.14* for laminates with edge shields also indicates that the extent of fibre failure is slowly approaching a constant value as the impact energy increases.

Figure 7.15 depicts the relationship between the extent of delamination with impact energy for laminates with and without the edge shield. From *Figure 7.15*, the importance of the protective layer is clearly shown by the large reductions in delamination areas for all impact energies. At an impact energy of 9.9 J, the presence of the protective layer attenuates the extent of delamination by 60%. A further comparison between all the superimposed delaminated surfaces in the laminates with and without the edge protection is shown in *Figure 7.16*. For the specimen without the edge shield at impact energy of 9.9 J, the delamination is seen to extend across the whole width in the bottom 90°/45° interface and across half of the width in some of the other lower interfaces. For the same impact energy, the laminate with edge shield reveals a delamination area which propagates across approximately 40% of the width of the laminate in the bottom 90°/45° interface, while most of the remaining interfaces showed delamination extending across nearly a quarter of the width.

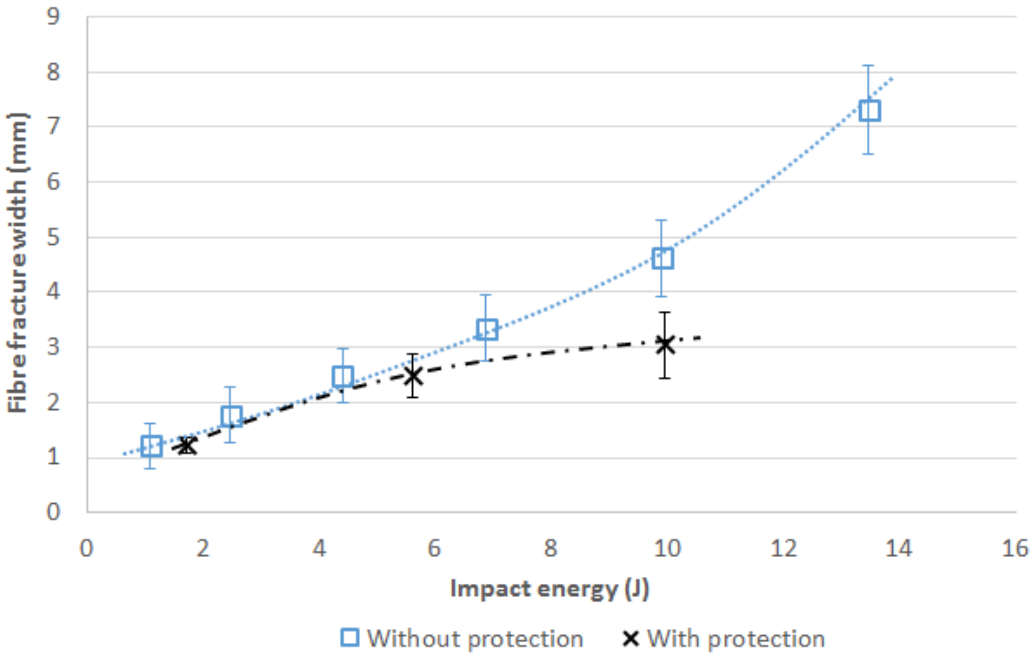

Figure 7.14: Extent of fibre fracture with varying impact energy for laminates with and without edge protection.

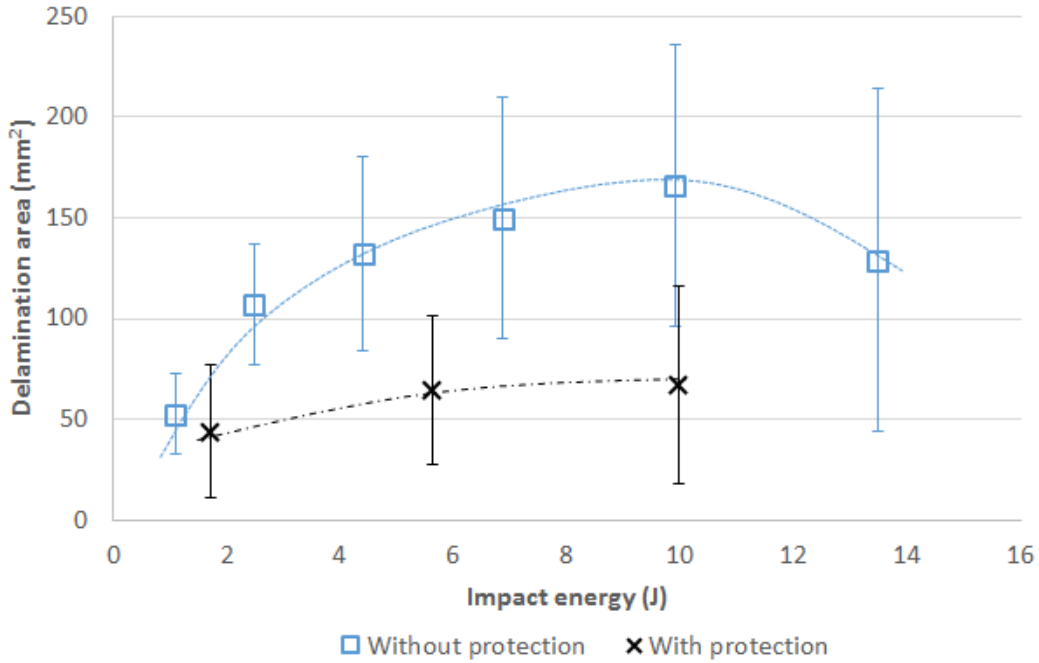

Figure 7.15: Variations in delamination area with respect to impact energy for laminates with and without edge protection.

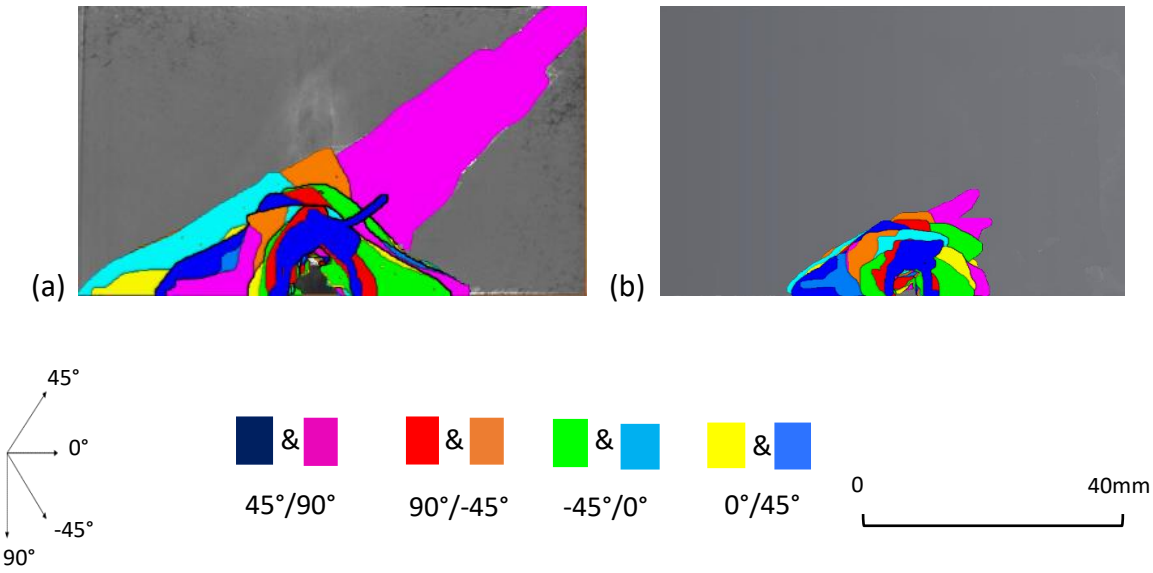

Figure 7.16: Delamination patterns observed in impacted laminates (a) without edge shield and (b) with edge shield, at an impact energy of 9.9 J.

During an impact event, shock waves propagate in the impacted bodies. The shock wave transfers the impact energy [174], which is absorbed by the composite mainly as a result of the failure modes, such as fibre failure and delamination, and by the steel through plastic deformation. As the presence of the steel sheet acts as a supplement to the laminate in absorbing part of the impact energy, the extent of impact damage on laminates with edge protection is smaller than that observed in laminates without the edge protection. In addition, although the impact force has not been determined in this current study, it can be argued that the differences in delamination areas between laminates with and without the edge shield may be associated with the impact force being reduced by the steel sheet at the edge, hence promoting a smaller extent of impact damage in laminates with the edge shield.

7.4.2. Effect on residual strength

The relationship between the residual tensile strength and impact energy of impacted laminates with the edge shield is shown in *Figure 7.17*. *Figure 7.17* also includes the residual tensile strength of impacted laminates without the edge shield. For any impacted laminates, tensile strength reduction increases with increasing impact energy.

The effect of the edge shield can be observed in *Figure 7.17*, where the residual strength of laminates with the shield is approximately 30% higher than laminates without the shield for all impact energy levels between 1.7 J and 9.9 J. The reduction in tensile strength is mainly governed by the extent of fibre failure provided that the delamination areas are not large and does not extend across the width of the specimen (as discussed in Chapter 5). The presence of the protective layer on the edge of the laminate restricts the extent of impact damage, and therefore, the reduction in residual strength is more significant in laminates without the edge protection for any given impact energy.

While the edge shield was ripped off the laminate for impacts at 5.6 J and 9.9 J, it is of interest to investigate the contribution of the steel in carrying additional tensile load after it yielded. The impact at 1.7 J is considered here, and the 0.2% proof strength of steel is used, which is typically around 250 MPa. A = (2 x 0.1 x 25) mm^2 is the total cross-sectional area of the edge shield subjected to tensile loading. Beyond 0.2% proof strength of steel, the edge shield can carry an additional load of 1.25 kN. The additional load carried by the edge shield is approximately 2% of the tensile failure load for the impacted laminate at 1.7 J.

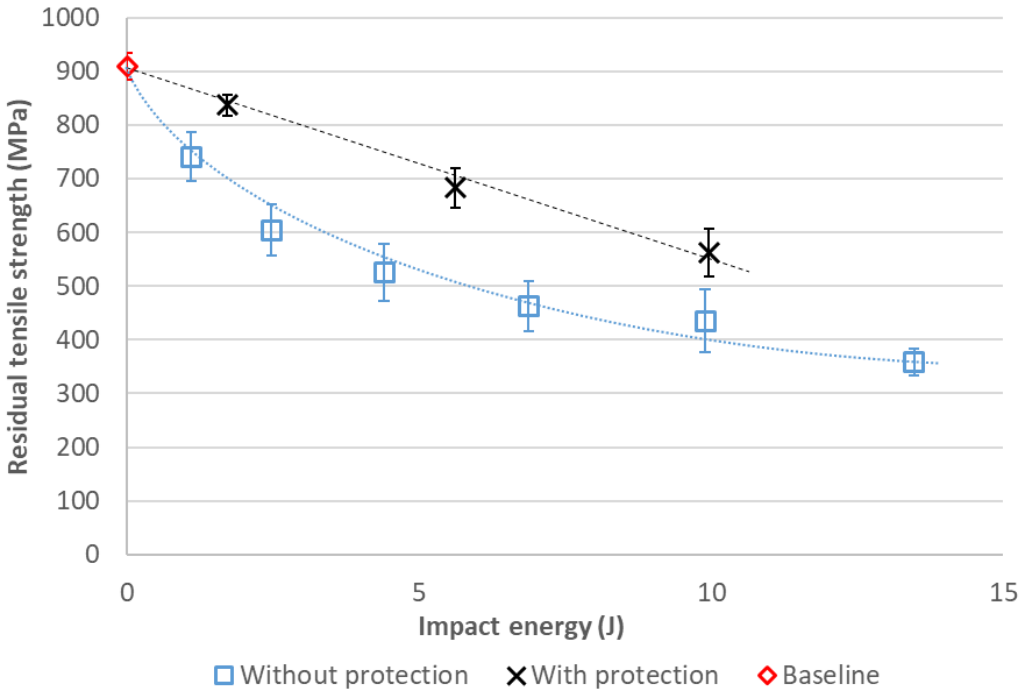

Figure 7.17: Residual tensile strength versus impact energy for impacted laminates with and without edge protection.

7.5. Conclusion

An experimental study investigating the effect and importance of having a protective layer bonded to the edge of the laminate before high velocity oblique impacts has been carried out. A 0.1 mm steel shim was used as the shield and impact tests were carried out for velocities of 125 m/s, 226 m/s and 301 m/s. Increasing the impact velocity results in increases in extent of fibre failure and delamination and laminate perforation was observed at 301 m/s.

The extent of impact damage was compared against experimental results from previous chapters, where impacts were conducted at the edge of the laminate with no protective layer. The protective layer at the edge of the laminate reduces the extent of

fibre failure and significantly reduces the extent of delamination. For impact velocities between 125 m/s – 301 m/s, the residual strength of laminates with the edge shield is enhanced by 30% in comparison to the strength for laminates without the edge shield, which is due to the smaller extent of impact damage with the edge shield. On its own, the edge shield carries only a small amount of the tensile load due to its small cross-sectional area compared to the laminate. Nonetheless, the edge protective layer is important in the design of composite components which may be subject to high velocity impacts.

8. Conclusions and Perspectives

This chapter presents the conclusions extracted from this work as well as the recommendations for future work.

8.1. Conclusions

High velocity impact events represent a serious threat to laminated composite structures and can reduce load bearing capacity severely. The resulting failure modes are complex and not intuitive. The research presented in this work has thus allowed a better understanding of the development of different failure modes and their interactions under two scenarios, namely impact and tension after impact. The key outcomes and points of learning from this work are:

- For composite laminates which are FOD prone, it is important to assess the impact damage in terms of fibre failure and delamination. The use of non-destructive testing is essential for internal damage detection.
- The trajectory of the projectile significantly affects the extent of impact damage, where oblique impacts revealed larger damaged area than normal impacts.
- Ballistic limits for 2 mm thick edge- and centre-impacted IM7/8552 laminates can be deduced based on the impact velocity at which laminate perforation is observed.
- The Hi-FEM employed in this work provides a powerful tool for understanding and predicting the damage development of carbon/epoxy laminates under high velocity impacts and tension after impact. As such, it can be recommended to simulate the dynamic and quasi-static responses of IM7/8552 laminates.

- Impacted laminates at 350 m/s were found to retain between 35 – 39% of the unnotched tensile strength.
- From a residual tensile strength point of view, edge machined notches are very good equivalents to composite laminates impacted on the edge at very high velocities as the reduction in strength is mainly driven by the extent of fibre fracture. However, centre notches are not good approximations to centre-impacted laminates because the reduction in strength is influenced by the large impact-induced delamination areas which restrict the growth of 0° splits under tensile loading.
- The use of a protective shield on the edge of composite structures is vital as the extent of impact damage is significantly reduced at higher impact velocities.

Small, hard body and sharp-edged fragments which may be ingested in aircraft engines are a significant threat to composite components. This limits the insertion of composite material components in engine applications and increases the cost of inspection, repair and replacement. The work in this thesis was motivated to address high velocity impact loading scenario using a 3 mm cube projectile. Since the damage area generally extends to a larger area that is very difficult to detect by visual inspection, the use of non-destructive testing (Ultrasonic C-scan and X-ray CT scan) is critical for internal damage detection. Following impact tests at 300 m/s at two different angles on flat rectangular quasi-isotropic laminates, oblique (45°) impacts were the more severe impact scenario in terms of the extent of damage induced. As such, a second set of oblique impact study was conducted where a range of impact velocities between 100 m/s and 350 m/s were considered and impacts close to the edge (referred to as edge) and away

from the edge (referred to as centre) were investigated. The impact damage was characterised in terms of fibre fracture width and delamination area using X-Ray CT scan images. The extent of fibre failure was seen to increase with impact velocity. For edge impacts, the delamination area was observed to initially increase but then decrease beyond 300 m/s as a result of laminate perforation, where the impact damage becomes much more localised around the impact point. For centre impacts, the delamination area was observed to increase with impact velocity. CT scan images for the centre-impacted laminate at 350 m/s revealed fibre failure in all plies and the delamination area is therefore expected to decrease beyond 350 m/s. Based on the boundary conditions applied to the high velocity impact tests in this work and laminate perforation, ballistic limits of 300 m/s and 350 m/s can be defined for 2 mm thick IM7/8552 laminates impacted at the edge and centre of the laminate respectively.

The findings from the experimental impact study have led to the validation of the high velocity oblique impact models. A High-fidelity Finite Element Method (Hi-FEM) was employed to capture the dynamic response of carbon/epoxy laminates subjected to oblique impacts over a range of velocities. This Hi-FEM takes a new approach in modelling high velocity impacts, where fibre failure was modelled using the Weibull theory and a maximum stress criterion, and multiple split paths and delamination were modelled using cohesive interface elements, together with an automated unit cell meshing technique. In comparison to the experimental results, the impact model yielded good predictions for some impact energies. For most impact energies, the delamination area was underpredicted. To investigate the reason behind the differences between predicted and experimental results, the baseline impact model was further studied by changing the orientation of the projectile before impact and by varying the number and position of

interface layers. While the changes in the projectile's orientation were observed to significantly affect the extent of fibre failure, the delamination area was influenced to a greater extent by the number of interface layers. Several limitations of the baseline impact model were identified, such as restrictions in the split spacings, the omission of shear stress in the fibre failure criterion under compression, single projectile orientation before impact and the use of single integration point for solid elements in the through thickness direction. The ability of the Hi-FEM to model different failure modes and their interactions under a high velocity impact makes it suitable for investigating the dynamic response of IM7/8552 laminates over a range of impact velocities.

The combination of visible and internal impact damage can severely degrade the strength of a composite structure. While most works in the literature have focused on CAI, the residual tensile strength is considered equally important as structural components in aircraft engines are required to withstand high tensile forces. The residual tensile strength, both from an experimental and numerical point of view, was investigated and reductions of 61 – 65% in the residual strength were observed for carbon/epoxy laminates impacted at 350 m/s. The residual tensile strength of impacted laminates was observed to be strongly dependent on the extent of fibre failure. For centre impacts at higher velocities, the large delamination areas may affect the residual tensile strength. This is because the 0° splits show restricted growth in the presence of the large impact-induced delamination areas. The strength predictions using characterised damage from CT scan images were in very good agreement with the experimental results although it was a time-consuming process. The strength predictions based on the baseline impact model agreed with experimental results for some impact velocities. The lack of agreement for the other impact velocities is associated with the

differences in the extent of fibre fracture prior to tensile simulations and the development of 0° splits from the two approaches. The length of 0° splits is an important driving factor for tensile failure stress, where longer 0° splits blunt the stress concentrations, resulting in higher tensile failure stress. The Hi-FEM modelling technique is excellent at predicting the quasi-static tensile response of IM7/8552 laminates. This strength study can be applied to industrial inspection and replacement procedures, where the residual tensile strengths of edge- or centre-impacted IM7/8552 components over a range of impact damage dimensions can be extracted from this work. Hereby, making the process efficient and more cost effective.

Generally, it is mandatory to carry out impact tests and then tension or compression tests to determine the residual strength of an impacted composite structure. This work has taken a new approach for a simpler and quicker way to assess the effect of impact damage, where machined notches were studied as a potential equivalent for tension after impact tests. The damage zones in notched laminates at 95% of the tensile failure load and in impacted laminates prior to tensile tests were studied. For large fibre fracture widths, edge-impacted and edge-notched laminates have relatively similar damage zone sizes. Furthermore, investigations on the propagation of 0° splits and the equivalent Stress Concentration Factors at failure have led to draw the equivalence between edge machined notches and edge-impacted laminates at high velocities. On the other hand, centre notches are not good approximations to centre-impacted laminates as the damage zone sizes in centre-impacted and centre-notched laminates differ by 55% due to the large impact-induced delamination areas in the centre-impacted specimen. Modelling impact damage initiation and its progression under load can be particularly expensive in the preliminary design phase. Consequently, simplified

damage models with edge notches can avoid the high costs associated with intensive computational analysis.

An experimental study was conducted to investigate the influence of a steel edge shield on the extent of impact damage and the residual tensile strength. Although the edge shield was observed to carry a small amount of the tensile load beyond the yielding point of the steel, it significantly reduced the extent of impact damage and hence, provided an enhancement in the residual tensile strength as compared to impacted laminates without the edge shield. Therefore, for a greater lifetime, composite structures benefit from being protected by a shield against the effects of FOD.

8.2. Future work

Whilst maintaining the aim for a robust and computationally efficient FE model, the baseline impact model could be refined by including the interactions of shear stresses to the compressive fibre failure and a further investigation into an optimisation study, related to the number and position of cohesive interface layers, could be carried out. As the automated unit cell meshing technique is limited in its minimum allowable split spacings, investigation on the FE mesh with smaller split spacings may represent suitable avenue for further numerical analysis. In doing so, better delamination area predictions may be obtained for a range of impact velocities.

With the intensive usage of composite materials, it is often asked whether small coupon tests can yield reliable results for the behaviour of large structures. In this work, high velocity impacts have been carried out on small scale coupons and for future work, it is of interest to investigate the influence of size effects on the extent of impact damage. While carrying out impact tests and non-destructive testing on larger structural

components can be both very expensive and difficult, numerical investigation on size effects may be an appropriate avenue. By understanding the relationship between the impact damage of small coupons and that of large structures, the gap between small-scale and large-scale can be bridged. Another serious concern for an impacted structure in service is related to its life and by carrying out a fatigue investigation, it would be possible to determine how long an impacted structure can be further utilised until it must be replaced or repaired. Therefore, experimental and numerical investigation of impacted laminates under cyclic loads could be the subject for future studies.

9. References

[1] Hellard G. Composites in airbus – a long story of innovations and experiences. Technical report, Airbus, 2008.

[2] Soutis C. Fibre reinforced composites in aircraft construction. Progress in aerospace Sciences,2005;41(2): 143-151.

[3] MAAXIMUS. Description of work dow3.5. Technical report, SEVENTH FRAMEWORK PROGRAMME – THEME: FP7-AAT-2007-RTD-1, 2010.

[4] Shadbolt PJ, Corran RS, Ruiz C. A preliminary investigation of plate deformation by projectiles in the subordonance range. Report No 1372/81. University of Oxford, UK, 1981.

[5] Bradshaw FJ, Dorey G, Sidey SR. Impact resistance of carbon reinforced plastics. RAE TR 72240, MOD, 1972.

[6] Avery JG. Design manual for impact damage tolerant aircraft structures, AGARDograph No 238, NATO, 1981.

[7] Manders PW, Harris WC. A parametric study of composite performance in compression after impact testing. SAMPE Journal, 1986;22:47-51.

[8] Rotem A. Residual flexural strength of FRP composite specimens subjected to transverse impact loading. SAMPE Journal, 1988;22(2):19-25.

[9] Abrate S. Impact on laminated composites. Applied Mechanics Review Jan 1991;44(4),155-190.

[10] Langdon G, Cantwell WJ, Guan Z, Nurick G. The response of polymeric composite structures to air-blast loading: A state-of-the-art. Int Mat Reviews, 2014; 59(3):159-177.

[11] Safri SNA, Sultan MTH, Yidris N, Mustapha F. Low velocity and high velocity test on composite materials – A review, The International Journal of engineering and Sciences, 2014; 3(9), p. 50-60.

[12] Razali N, Sultan MTH, Yidris N, Ishak MR, Mustapha F. Impact damage on composite structures – A review, The International Journal of engineering and Sciences, 2014; 3(7), p. 8-20.

[13] Cantwell W, Morton J. The impact resistance of composite materials – A review. Composites,1991;22(5):347-362.

[14] Cantwell WJ, Morton J. Comparison of the low and high velocity impact response of CFRP. Composites, 1989, 20, p.545–551.

[15] Fawcett AJ, Oakes GD, Boeing composite airframe damage tolerance and service experience. Technical report, Boeing Commercial Airplanes – 787 Program, 2012.

[16] Richardson MOW, Wisheart MJ. Review of low-velocity impact properties of composite materials. Composites Part A: Applied Science and Manufacturing, 1996, 27(12), p. 1123-1131.

[17] Dashin L, Malvern LE. Matrix cracking in impacted glass/epoxy plates. Journal of Composite Materials, 1987, 21:594-609.

[18] Joshi SP, Sun CT. Impact-induced fracture initiation and detailed dynamic stress field in the vicinity of impact. In Proc. American Society of Composites 2nd Tech. Conf, 1987.

[19] Choi IH. Low-velocity impact analysis of composite laminates under initial in-plane load. Composite Structures, 2008, 86(1-3):251-257. Fourteenth International Conference on Composite Structures - ICCS/14.

[20] Robinson R, Davies GAO. Impactor mass and specimen geometry effects in low velocity impact of laminated composites. International Journal of Impact Engineering, 1992, 12(2):189-207.

[21] Jiang DZ, Shen W, Wang Xw. Simulation of Impact Deformation, Damage and Fracture in Composite Delaminates". Proceedings of ICCM–11, Gold Coast, Australia, pp 583-592, 14th-18th July (1997).

[22] Shyr TW, Pan YH. Impact resistance and damage characteristics of composite laminates, Journal of Composite Structures, 2003;62(2):193-203.

[23] Sun XC, Wisnom MR, Hallett SR, Interaction of inter- and intralaminar damage in scaled quasi-static indentation tests: Part 2 – Numerical simulation, Journal of Composites Structures, 2016, 136, p. 727-742.

[24] Abrate S. Impact on Composite Structures. Camb Univ Press, 1998.

[25] Choi HY. A model for predicting damage in graphite/epoxy laminated composites resulting from low-velocity point impact. Journal of composite materials,1992;26(14):2134-2169.

[26] Jih CJ. Prediction of delamination in composite laminates subjected to low velocity impact. Journal of composite materials,1993;27(7):684-701.

[27] Joshi SP. Impact induced fracture in a laminated composite. Journal of composite materials, 1985;19(1):51.

[28] Cantwell WJ. Detection of impact damage in CFRP laminates. Composite Structures,1985;3(3-4):241-257.

[29] Freitas M, Silva A, Reis L. Numerical evaluation of failure mechanisms on composite specimens subjected to impact loading. Composites Part B: Engineering, 2000;31(3):199 - 207.

[30] Shyr TW, Pan YH. Impact resistance and damage characteristics of composite laminates. Composite Structures, 2003;62(2):193 - 203.

[31] Berthelot JM. Transverse cracking and delamination in cross-ply glass-fiber and carbon-fiber reinforced plastic laminates: Static and fatigue loading. Applied Mechanics Reviews,2003;56(1):111-147.

[32] Puck A, Schürmann H. Failure analysis of FRP laminates by means of physically based phenomenological models. Composites Science and Technology,2002;62(12-13):1633-1662.

[33] Williams KV, Vaziri R, Poursartip A. A physically based continuum damage mechanics model for thin laminated composite structures, International Journal of Solids and Structures,2003;40(9):2267-2300.

[34] Chang F. A model for predicting damage in graphite/epoxy laminated composites resulting from low-velocity point impact, Journal of Composite Material, 1992;26:2134–2169.

[35] Sridharan S. Delamination behaviour of composites, 1st ed. Woodhead Publishing, 2008.

[36] Olsson R. Analytical prediction of large mass impact damage in composite laminates. Composites Part A: Applied Science and Manufacturing,2001;32(9):1207-1215.

[37] Moura MFSF, Gonçalves JPM. Modelling the interaction between matrix cracking and delamination in carbon-epoxy laminates under low velocity impact. Composites Science and Technology,2004;64(7-8):1021-1027.

[38] Liu D. Impact-induced delamination: a view of bending stiffness mismatching. Journal of composite materials,1988;22(7):674.

[39] Takeda N, Sierakowski R, Malvern LE. Transverse cracks in glass/epoxy cross-ply laminates impacted by projectiles. Journal of materials science, 1981;16(7):2008-2011.

[40] Sheng L. Delamination and matrix cracking of cross-ply laminates due to a spherical indenter. Composite Structures,1993;25(1-4):257-265.

[41] Renault M. Compression strength after impact of a carbon epoxy laminate: failure mechanisms and numerical modelling. Technical report, EADS CCR, 1994.

[42] Lammerant L, Verpoest I. Modelling of the interaction between matrix cracks and delaminations during impact of composite plates. Composites Science and Technology,1986;56(10):1171-1178.

[43] Zou Z, Reid Sr, Li S, Soden PD. Application of a delamination model to laminated composite structures. Composite Structures, 2002;56(4):375-389.

[44] Sjögren A, Krasnikovs A, Varna J. Experimental determination of elastic properties of impact damage in carbon/epoxy laminates. Composites Part A: Applied Science and Manufacturing,2001;32(9):1237-1242.

[45] Davies GAO, Olsson R. Impact on composite structures. Aeronautical Jour-nal, 2004;108:541_563.

[46] Davies GAO, Zhang X. Impact damage prediction in carbon composite structures. International Journal of Impact Engineering, 1995;16(1):149-170.

[47] Davies GAO, Robinson P. Predicting failure by debonding/delamination. In AGARD: 74th Structures & Materials Meeting, Debonding/Delamination of Composites, 1992;108:541-563.

[48] Cantwell WJ, Yang FJ. Impact damage initiation in composite materials, Journal of Composites Science and Technology, 2010;70:336-342.

[49] Schoeppner GA, Abrate S. Delamination threshold loads for low velocity impact on composite laminates. Composites Part A: Applied Science and Manufacturing, 2000;31(9):903-915.

[50] Ahmadi H, Liaghat, GH, Sabouri H, Bidkhouri, E, Investigation on the high velocity impact properties of glass-reinforced fibre metal laminates, Journal of Composite Materials, 2012;47(13), p. 1605-1615.

[51] Gower HL, Cronin DS, Plumtree A. Ballistic impact response of laminated composite panels, International Journal of Impact Engineering, 2008:35:1000-1008.

[52] Kursun A, Senel M, Enginsoy HM, Bayraktar E. Effect of impactor shapes on the low velocity impact damage of sandwich composite plate: Experimental study and modelling, Journal of Composites: Part B, 2016;86:143-151.

[53] Fuoss E, Straznicky PV, Poon C, Effects of stacking sequence on the impact resistance in composite laminates – Part 1: parametric study, Journal of Composite Structures, 1998;41:67-77.

[54] López-Puente J, Zaera R, Navarro C, Experimental and numerical analysis of normal and oblique ballistic impacts on thin carbon/epoxy woven laminates, Composites Part A, 2008; 39: 374-87.

[55] Cui H, Thomson D, Eskandari S, Petrinic N. A critical study on impact damage simulation of IM7/8552 composite laminate plate. Int J Impact Eng 2019; 127:100-109.

[56] Yashiro S, Ogi K, Nakamura T, Yoshimura A, Characterisation of high-velocity impact in CFRP laminates: Part – Experiments, Compopistes: Part A, 2013;48:93-100.

[57] Kärger L, Baaran J, Gunnion A, Thomson R. Evaluation of impact assessment methodologies. part ii: Experimental validation. Composites Part B: Engineering,2009;40(1):71-76.

[58] Pietropaoli E, Riccio A. On the robustness of finite element procedures based on Virtual Crack Closure Technique and fail release approach for delamination growth phenomena. Definition and assessment of a novel methodology, Journal of Composite Science and Technology, 2010;70 (8):1288-1300.

[59] Hasin Z. Failure criteria for unidirectional fibre composites. J Appl Mech, 1980;47:671-694.

[60] Chang FK, Chnag KY. A progressive damage model for laminated composites containing stress concentrations. J Compos Mater, 1987,21:834.

[61] Pinho ST, Davila CG, Camanho PP, Iannucci L, Robinson P. Failure criteria for FRP under in-plane or three-dimensional stress states including shear non-linearity. Research report. NASA/TM-2005-213530. NASA Langley Research Center;2005.

[62] Martinez X, Rastellini F, Oller S, Flores F, Onate E. Computationally optimised formulation for the simulation of composite materials and delamination failures. Compos B: Eng, 2011;42:134-44.

[63] Riccio A, Raimondo A, Fragale S, Camerlingo F, Gambino B, Toscano C, Tescione D. Delaminations buckling and growth phenomena in stiffened composite panels under compression. Part I: an Experimental Study, Journal of Composite Materials, 2014;48(23):2843-2855.

[64] Riccio A, Raimondo A,Caprio FD, Scaramuzzino F. Delaminations buckling and growth phenomena in stiffened composite panels under compression. Part II: a Numerical Study, Journal of Composite Materials, 2014;48(23):2857-2870.

[65] Riccio A, Russo T, Scaramuzzino F. Impact Damage Management of Composite Laminated Structures by a Probabilistic Approach, The Open Materials Science Journal, 2013;7:8-22.

[66] Talreja RA. Continuum mechanics characterization of damage in composite materials, Proc Royal Soc London, 1985;399:195–216.

[67] Ladeve‘ze P. A damage computational method for composite structures, Journal of Computers and Structures, 1992;4:79–87.

[68] Riccio A, Felice GD, Saputo S, Scaramuzzino F. A Numerical Study on Low velocity impact induced damage in stiffened composite panels, Journal of Computational Simulation and Modeling, 2013;3(1):44-47.

[69] Caputo F, Gennaro FD, Lamanna G, Lefons A, Riccio A. Numerical procedures for damage mechanisms analysis in CFRP composites, Journal of Key Engineering Materials, 2013;569:111-118.

[70] Orifici Ac, Herszberg I, Thomson RS. Review of methodologies for composite material modelling incorporating failure. Composite Structures, 2008;86(1-3):194-210. Fourteenth International Conference on Composite Structures -ICCS/14.

[71] https://en.wikipedia.org/wiki/Fracture_mechanics, Accessed: 28/4/2018.

[72] Xu X, Wisnom MR, Li X, Hallett SR. A numerical investigation into size effects in centre-notched quasi-isotropic carbon/epoxy laminates, Journal of composites Science and Technology, 2015;111:2-39.

[73] ASTM International. D5528-13 Standard test method for mode I interlaminar fracture toughness of unidirectional fiber-reinforced polymer matrix composites; West Conshohocken, PA; ASTM International, 2013.

[74] ASTM International. D7905/D7905M-19e1 Standard test method for determination of the mode II interlaminar fracture toughness of unidirectional fiber-reinforced polymer matrix composites; West Conshohocken, PA; ASTM International, 2019.

[75] ASTM International. D6671/D6671M-19 Standard test method for mixed mode I-mode II interlaminar fracture toughness of unidirectional fiber-reinforced polymer matrix composites; West Conshohocken, PA; ASTM International, 2019.

[76] Thomson DM, Cui H, Erice B, Hoffmann J, Wiegand J, Petrinic N. Experimental and numerical study of strain-rate effects on the IFF fracture angle using a new efficient implementation of Puck's criterion. Compos Struct, 2017;181:325-33.

[77] Cui H, Thomson D, Pellegrino A, Wiegand J, Petrinic N. Effect of strain rate and fibre rotation on the in-plane shear response of ±45° laminates in tension and compression tests, Compos Sci Technol,20165; 135:106-115.

[78] Cui H, Melro AR, Yasaee M. Inter-fibre failure of through-thickness reinforced laminates in combined transverse compression and shear load, Compos Sci Technol,2018; 165:48-57,

[79] Hoffmann J, Cui H, Petrinic N. Determination of the strain-energy release rate of a composite laminate under high-rate tensile deformation in fibre direction, Compos Sci Technol, 2018l;164:110-119.

[80] Ploeckl M, Kuhn P, Grosser J, Wolfahrt M, Koerber H. A dynamic test methodology for analyzing the strain-rate effect on the longitudinal compressive behavior of fiber-reinforced composites, Compos Struct,2017; 180:429-438.

[81] Czabaj Mw, Ratcliffe JG. Comparison of intralaminar and interlaminar mode-I fracture toughness of unidirectional IM7/8552 graphite/epoxy composite, 2012:1-18. NASA Tech Rep.

[82] Koerber H, Camanho PP. High strain rate characterisation of unidirectional carbon–epoxy IM7-8552 in longitudinal compression, Compos Part A, 2011;42:462-470.

[83] Koerber H, Xavier J, Camanho PP. High strain rate characterisation of unidirectional carbon-epoxy IM7-8552 in transverse compression and in-plane shear using digital image correlation, Mech Mater, 2010;42:1004-1019.

[84] Hallett SR, Jiang WG, Khan B, Wisnom MR. Modelling the interaction between matrix cracks and delamination damage in scaled quasi-isotropic specimens, Journal of Composites Science and Technology,2008; 68:80-89.

[85] Li Y, Sridharan S. Investigation of delamination caused by impact by using a cohesive-layer model, AIAA Journal, 2005;43:2243-2251.

[86] Aymerich F, Dore F, Priolo P. Prediction of impact-induced delamination in cross-ply composite lamiantes using cohesive interface elements, Journal of Composite Science and Technology, 2008;68:2383-2390.

[87] Johnson AF, Pickett AK. Impact and crash modelling of composite structures: A challenge for damage mechanics. In Proceedings of the European Conference on Computational Mechanics (ECCM '99), Munich, 1999.

[88] Johnson AF, Pickett AK, Rozycki P. Computational methods for predicting impact damage in composite structures. Composites Science and Technology,2001;61(15):2183-2192.

[89] Sebastian H. Bird strike simulations on composite aircraft structures. In SIMULIA Customer Conference, 2011.

[90] Schueler D, Toso-Pentecote N, Voggenreiter H. Simulation of high velocity impact on composite structures – model implementation and validation, Applied Composite Materials, 2016; 23:857-878.

[91] Xiao JR, Gama BA, Gillespie Jr JW. Progressive damage and delamination in plain weave S-2 glass/SC-15 composites under quasi-static punch-shear loading, Composite Structures, 2007;78:182-96.

[92] Gama BA, Gillespie Jr JW. Finite element modelling of impact, damage evolution and penetration of thick-section composites, Int J Impact Engineering, 2011; 38:181-197.

[93] LS-DYNA Keyword User's Manual, Livermore Software Technology Corporation. Version 971, May 2017.

[94] Pernas-Sanchez J, Artero-Guerrero JA, Vinuela JZ, Varas D, Lopez-Puente J. Numerical analysis of high velocity impacts on unidirectional laminates, Journal of Composite Strucutres, 2014; 107:629-634.

[95] Nishikawa M, Hemmi K, Takeda N. Finite-element simulation for modelling composite plates subjected to soft-body, high velocity impact for application to bird-strike problem of composite fan blades, Journal of Composite Structures, 2011; 93:1416-1423.

[96] Xiao S, Chen P, Ye Q. Prediction of damage area in laminated composites plates subjected to low velocity impact, Journal of Composites Science and Technology, 2014;98:51-56.

[97] Topac OT, Tasdemir B, Gozluklu B, Gurses E, Coker D. Experimental and Computational Investigation of Out-of-Plane Low Velocity Impact Behaviour of CFRP Composite Plates. Fracture, Fatigue, Failure and Damage Evolution, 2016;8:9-16.

[98] Christensen RM. The numbers of elastic properties and failure parameters for fibre composites, Journal of Engineering Materials and Technology, 1998;120(2):110-113.

[99] Reifsnider KL, El-Zein M. On the prediction of tensile strength after impact of composite laminates. Comp Sci Tech. 1990; 3:147-154.

[100] Lekhnitskii SG. Anistropic plates. Gordon and Breach Science Publishers. 1968.

[101] Dorey G, Sidey GR. Residual strength of CFRP laminates after ballistic impact. Mechanical properties high rates strain. In: Proceedings of the conference, Oxford; 1974, 344-351.

[102] Horsfall I, Watson CH, Boswell C. Residual strength of composite laminates after ballistic impact, 23rd International symposium on ballistics, Tarragona, Spain; 16-20 April 2007.

[103] Wang J, Callinan. Residual strengths of composite structures subjected to ballistic impact, Composite Structures, 2014; 117: 423-432.

[104] Zhou G. Effect of impact damage on residual compressive strength of GFRP laminates, Journal of Composites Structures, 1996; 35:171-181.

[105] Koo JM, Choi JH, Seok CS. Prediction of residual strength after impact of CFRP composite structures, International Journal of Precision Engineering and Manufacturing, 2017; 15: 1323-1329.

[106] Kannan VK, Rajadurai A, Nageswara Rao B. Residual strength of laminated composites after impact, Journal of Composite Materials, 2010; 45:1031-1043.

[107] Waddoups ME, Eisenman JR, Kaminski BE. Macroscopic fracture mechanics of advanced composite materials, J Compos Mater, 1971;5:446–451.

[108] Extended project, Kristnama AR, November 2015, ACCIS, University of Bristol (Internal).

[109] Pernas-Sanchez J, Artero-Guerrero JA, Varas D, Lopez-Puente J. Experimental analysis of normal and oblique high velocity impacts on carbon/epoxy tape laminates, J Composites: Part A, 2014;60:24-31.

[110] Nowell D, Duo P, Stewart IF. Prediction of fatigue performance in gas turbine blades after foreign object damage. Int J Fatigue, 2003;25:963-969.

[111] Kristnama AR, Xu X, Nowell D, Wisnom MR, Hallett SR. Experimental investigation of high velocity oblique impact and residual tensile strength of carbon/epoxy laminates. J Comp Sci Technol, 2019;182:107772.

[112] Summerscales J. Non-destructive testing of fibre-reinforced plastics composites, London: Elsevier applied Sciences, 1987;1.

[113] Aymerich F, Meili S. Ultrasonic evaluation of matrix damage in impacted composite laminates: Composite Part B, 2000;31(1):1-6.

[114] Safri SNA, Chan TY, Sultan MTH. A novel method for detecting and characterising low velocity impact (LVI) in commercial composite, Int Journal of Research in Engineering & Technology, 2014; 3(8):101-106.

[115] Summerscales J. Non-destructive testing of fibre-reinforced plastics composites, London: Elsevier applied Sciences, 1990; 2.

[116] Schilling PJ, Karedla BR, Tatiparthi AK, Verges MA, Herrington PD. X-ray computed microtomography of internal damage in fibre reinforced polymer matrix composites. Compos. Sci. Technol, 2005;65:2071–2078.

[117] Lambert J, Chambers A, Sinclair I, Spearing S. 3D damage characterisation and the role of voids in the fatigue of wind turbine blade materials. J Composite Science Technology. Technol. 2012; 72:337–343.

[118] Nixon-Pearson OJ, Hallett SR. An investigation into the damage development and residual strengths of open-hole specimens in fatigue, J Composites: Part A, 2015;69:266-278.

[119] Wright P, Moffat A, Sinclair I, Spearing SM. High resolution tomographic imaging and modelling of notch tip damage in a laminated composite, J Composite Science Technology, 2010; 40(10):1444-52.

[120] Davies GAO, Robinson P, Robson J, Eady D. 1997 Shear driven delamination propagation in two dimensions, Compos. A,1997; 28: 757–765.

[121] Suemasu H, Majima O. Multiple delaminations and their severity in circular axisymmetric plates subjected to transverse loading, J. Compos. Mater, 1996;30: 441–453.

[122] Davies GAO, Zhang X, Zhou G, Watson S. Numerical modelling of impact damage, J. Composites; 1994;25: 342–350.

[123] Hazell PJ, Kister G, Stennett C, Bourque P, Cooper G. Normal and oblique penetration of woven CFRP laminates by a high velocity steel sphere, Composites Part A, 2008; 39: 866-874.

[124] Chandra N, Rajendran AM. Micromechanics based modelling of damage in composites under high velocity impacts – a review. In: 5th International Conference on Structures under shock and impact. Thessaloniki, Greece, June 1998.

[125] Rajendran AM. An approach to analytical modelling of metal projectile into composite laminates. University of Dayton, Research Institute Technical report. Jan 1992.

[126] Weibull W. A statistical distribution function of wide applicability, Journal of Applied Mechanics, 1951;18:293-7.

[127] Wisnom MR. Size effects in the testing of fibre-composite materials, Journal of Composite Science & Technology, 1999; 59:1937–57.

[128] Ling S, Wagner HD. An energy-based interpretation of interfacial adhesion from single fibre composite fragmentation testing. J Mater. Sci., 1993;28:623-633.

[129] Favre JP, Sigety P, Jacques D. Stress transfer by shear in carbon fibre model composites. J. Mater. Sci., 1991,26(1):189-195.

[130] Phoenix SL. Statistical issues in the fracture of brittle-matrix fibrous composites. 1993,48(4):65-80.

[131] Wisnom MR, Khan B, Hallett SR. Size effects in unnotched tensile strength of unidirectional and quasi-isotropic carbon/epoxy composites, Journal of Composite Structures, 2008; 84:21–8.

[132] Xu X, Wisnom MR, Hallett SR. Deducing the R-curve for trans-laminar fracture from virtual Over-height Compact Tension (OCT) test, Composite Part A, 2019;118:162-170.

[133] HexTow® IM7 Carbon Fiber Datasheet, Hexcel®.

[134] Jiang W-G, Hallett SR, Green BG, Wisnom MR. A concise interface constitutive law for analysis of delamination and splitting in composite materials and its application to scaled notched tensile specimens, International J Numer Meth Eng, 2007; 69:1982–95.

[135] Li X, Hallett SR, Wisnom MR. Predicting the effect of through-thickness compressive stress on delamination using interface elements, Composite Part A, 2008; 39:218–30.

[136] Gan KW, Hallett SR, Wisnom MR. Measurement and modelling of interlaminar shear strength enhancement under moderate through-thickness compression, Composite Part A, 2013;49:18-25.

[137] Yasaee M, Mohamed G, Pellegrino A, Petrinic N, Hallett SR. Strain rate dependence of mode II delamination resistance in through thickness reinforced laminated composites, Int J Impact Eng, 2017;107:1-11.

[138] Zou Z, Reid SR, Li S, Soden PD. Modelling interlaminar and intralaminar damage in filament wound pipes under quasi-static indentation, 2002, J Compos Mater, 36:477-499.

[139] Camanho PP, Dávila CG, De Moura MF. Numerical simulation of mixed-mode progressive delamination in composite materials,2003, J Compos Mater, 37 (16):1415-1438

[140] Turon A, Davilla CG, Camanho PP, Costa J. An engineering solution for mesh size effects in the simulation of delamination using cohesive zone models, 2007, Engineering Fracture Mechanics, 74(10):1665-1682.

[141] Li X, Hallett SR, Wisnom MR. Modelling the effect of gaps and overlaps in automated fibre placement (AFP) – manufactured laminates, 2015, Sci Eng Compos Matter, 22(2): 115-129.

[142] Hourglass, LS-DYNA Support. LS-DYNA®. https://www.dynasupport.com/howtos/element/hourglass Last accessed on: 20/8/2019

[143] Sun XC, Hallett SR. Barely visible impact damage in scaled composite laminates: Experiments and numerical simulations, 2017, Int J Imp Eng, 109:178-195.

[144] Ramesh R, Kishore RRMVGK. Dry wear studies on glass fibre reinforced epoxy composites, 1983, Wear, 89:131-136.

[145] Johnson AF, Pickett AK, Rozycki P. Computational methods for predicting impact damage in composite structures, 2001, Compos. Sci. Technol, 61(15): 2183–2192.

[146] Heimbs S, Heller S, Middendorf P, Hähnel F, Weiße J. Low velocity impact on CFRP plates with compressive preload: test and modelling, International Journal of Impact Engineering, 2009, 36(10):1182–1193.

[147] Pickett AK, Fouinneteau MRC, Middendorf P. Test and modelling of impact on pre-loaded composite panels, 2009, Appl. Compos. Mater, 16(4):225–244.

[148] Kim YA, Woo K, Cho H, Kim IG, Kim JH. High velocity impact damage behaviour of carbon/epoxy composite laminates, Int J of Aeronautical & Space Sci, 2015;16(2):190-205.

[149] Jacobsen G. Mechanical Performance Characterization of Stretch Broken Carbon Fiber Materials. In: Proceedings of SAMPE '09 Spring Symposium Conference Proceedings, 18th-21st May 2009.

[150] Xu X, Wisnom MR, Chang K, Hallett SR. Unification of strength scaling between unidirectional, quasi-isotropic, and notched carbon/epoxy laminates. Compos Part A 2016; 90:296-305.

[151] Hallett SR, Green BG, Jiang WG, Wisnom MR. An experimental and numerical investigation into the damage mechanisms in notched composites. Compos Part A: Appl Sci Manuf 2009;40(5):613–24.

[152] Harris CE, Morris DH. Effect of laminate thickness and specimen configuration on the fracture of laminated composites. In: Composite materials: testing and design (seventh conference). ASTM STP 893; 1986. p. 117–95.

[153] Kortschot MT, Beaumont PWR, Ashby MF. Damage mechanics of composite materials. III: Prediction of damage growth and notched strength. Compos Sci Technol 1991;40(2):147–65.

[154] Daniel IM. Strain and failure analysis of graphine/epoxy plates with cracks. Exp Mech 1978;18(7):246–52.

[155] Xu X, Wisnom MR, Li X, Hallett SR. An experimental investigation into size effects in quasi-isotropic carbon/epoxy laminates with sharp and blunt notches, 2014, J Composites Science and Technology, 100:220-227.

[156] Romano F, Di Caprio F, Mercurio U. Compression after impact analysis of composite panels and equivalent hole method. Procedia Eng 2016; 167:182-189.

[157] Nettles AT. Notched compression strength of 18-ply laminates with various percentages of 0 plies. Compos Mater 2014;49(4):495-505.

[158] Puhui C, Zhen S, Junyang W. A new method for compression after impact strength prediction of composite laminates. Compost Mater 2002; 36:589-610.

[159] Wallin M, Saarela O. Compression strength of notched and impact damaged composite laminates. In: Proceedings of 26th Congress of the International Council of the Aeronautical Sciences. Achorage, Alaska, USA, 14th – 19th Sept 2008.

[160] Camanho PP, Catalanotti G, On the relation between the mode I fracture toughness of a composite laminate and that of a 0 ply: analytical model and experimental validation, 2011, Eng Fracture Mech,78(13):2535-46.

[161] Green BG, Wisnom MR, Hallett SR. An experimental investigation into the tensile strength scaling of notched composites, 2007, composites: Part A, 40(5):613-24.

[162] Edwards HL, Wanhill RJH. Fracture mechanics: Edward Arnold, Delftse Uitgevers Maatchappij; 1984.

[163] Wang D. Impact behaviour and energy absorption of paper honeycomb sandwich panels, Int J Impact Eng, 2009;36(1):110–4.

[164] Ha NS, Lu G, Xiang X. Energy absorption of a bio-inspired honeycomb sandwich panel. J Mat Sci, 2019;54:6286-6300.

[165] Alantali A, Alia RA, Umer R, Cantwell WJ. Energy absorption in aluminium honeycomb cores reinforced with carbon fibre reinforced plastic tubes. J Sandwich Structures & Materials, 2019;21(8):2801-2815.

[166] Zhou H, Xu P, Xie S, Feng Z, Wang D. Mechanical performance and energy absorption properties of structures combining two Nomex honeycombs. Compos Struc, 2018;185:524-536.

[167] Li Y, Li JB, Zhang R. Energy-absorption performance of porous materials in sandwich composites under hypervelocity impact loading, Compos Struct, 2004;64(1):71-78.

[168] Hart WGJ, Ubels LC. Impact energy absorbing surface layers for protection of composite aircraft structure, In: 8th European conference on composite materials, Naples, June 1998.

[169] Rahme P, Bouvet C, Rivallant S, Fascio V, Valembois G. Experimental investigation of impact on composite laminates with protective layers, Compos Sci Technol, 2012;72:182-189.

[170] Petit S, Bouvet C, Bergerot A, Barrau JJ. Impact and compression after impact experimental study of a composite laminate with a cork thermal shield, Compos Sci Technol, 2007;67(15–16):3286–99.

[171] Holmes C, Drinkwater BW, Wilcox PD. Post-processing of the full matrix of ultrasonic transmit-receive array data for non-destructive evaluation. NDT&E International 2005; 38:701-711.

[172] Zhang J, Drinkwater BW, Wilcox PD, Hunter AJ. Defect detection using ultrasonic arrays: The multi-mode total focusing method. NDT&E International 2010; 43:123-133.

[173] Array Imaging, University of Bristol : http://www.bris.ac.uk/engineering/research/ndt/research/array-imaging/ , last assessed on 08/05/19.

[174] Thaumaturgo C, Da Costa Jr AM. Shock-waves on polymer composites. Material Science Letters. 1997; 16: 1480-1482.

A. Appendix A

The extent of fibre failure, termed as fibre fracture width, in all the plies corresponding to edge- and centre-impacted laminates over a range of impact velocities are presented in the tables below.

Table A-1: Measured fibre fracture widths for all plies in edge impacts (100 – 200 m/s).

	100 m/s	150 m/s	200 m/s
Ply angle (°)	Fibre fracture width (mm)	Fibre fracture width (mm)	Fibre fracture width (mm)
45	1.72	3.31	3.34
90	1.67	2.29	3.17
-45	1.54	1.97	3.01
0	1.33	1.83	3.02
45	1.29	1.27	2.85
90	0.69	1.11	2.77
-45	0.24	0.62	2.68
0	-	-	2.65
0	-	-	2.65
-45	-	-	2.18
90	-	-	1.94
45	-	-	1.74
0	-	-	1.64
-45	-	-	1.01
90	-	-	-
45	-	-	-
Average:	**1.21**	**1.77**	**2.48**

Table A-2: Measured fibre fracture widths for all plies in edge impacts (250 – 350 m/s).

	250 m/s	300 m/s	350 m/s
Ply angle (°)	Fibre fracture width (mm)	Fibre fracture width (mm)	Fibre fracture width (mm)
45	4.32	6.80	9.49
90	4.16	6.34	8.28
-45	4.01	5.65	8.21
0	3.83	5.45	8.16
45	3.81	5.12	8.01
90	3.76	4.83	7.98
-45	3.69	4.75	7.98
0	3.67	4.60	7.93
0	3.67	4.60	7.93
-45	3.52	4.38	7.43
90	2.99	4.19	6.74
45	2.71	3.97	6.18
0	2.67	3.91	6.10
-45	1.98	3.51	5.82
90	1.33	3.08	5.79
45	-	2.81	5.13
Average:	**3.34**	**4.62**	**7.32**

Table A-3: Measured fibre fracture widths for all plies in centre impacts (100 – 200 m/s).

	100 m/s	150 m/s	200 m/s
Ply angle (°)	Fibre fracture width (mm)	Fibre fracture width (mm)	Fibre fracture width (mm)
45	1.31	1.61	2.57
90	1.06	1.05	2.42
-45	-	0.99	2.26
0	-	-	2.18
45	-	-	1.49
90	-	-	1.32
-45	-	-	1.08
0	-	-	1.03
0	-	-	1.03
-45	-	-	0.45
90	-	-	-
45	-	-	-
0	-	-	-
-45	-	-	-
90	-	-	-
45	-	-	-
Average:	**1.20**	**1.21**	**1.58**

Table A-4: Measured fibre fracture widths for all plies in centre impacts (250 – 350 m/s).

	250 m/s	300 m/s	350 m/s
Ply angle (°)	Fibre fracture width (mm)	Fibre fracture width (mm)	Fibre fracture width (mm)
45	6.49	7.47	13.4
90	5.23	5.81	11.6
-45	4.05	4.56	9.99
0	4.07	4.37	9.60
45	3.61	4.02	8.50
90	3.23	3.73	8.12
-45	2.99	3.70	7.03
0	2.77	3.67	6.85
0	2.77	3.67	6.85
-45	1.22	1.47	5.66
90	0.69	1.12	4.94
45	-	-	4.76
0	-	-	4.51
-45	-	-	4.04
90	-	-	3.75
45	-	-	3.07
Average:	**3.36**	**3.96**	**7.04**

B. Appendix B

The extent of delamination at all interfaces within the laminates corresponding to edge and centre impacts over a range of velocities are presented in the tables below.

Table B-1: Measured delamination areas for all interfaces in edge impacts (100–200 m/s).

	100 m/s	150 m/s	200 m/s
Interface	Delamination area (mm^2)	Delamination area (mm^2)	Delamination area (mm^2)
45°/90°	9.40	52.0	8.60
90°/-45°	12.1	60.9	8.80
-45°/0°	22.8	79.5	45.2
0°/45°	59.8	89.0	16.9
45°/90°	63.8	35.9	23.3
90°/-45°	70.8	41.4	110
-45°/0°	164	104	84.7
0°/0°	-	115	61.0
0°/-45°	22.2	184	295
-45°/90°	41.1	130	122
90°/45°	52.7	88.2	273
45°/0°	58.1	308	234
0°/-45°	-	182	335
-45°/90°	-	84.1	152
90°/45°	-	64.4	225
Average:	**52.4**	**107**	**133**

Table B-2: Measured delamination areas for all interfaces in edge impacts (250–350m/s).

	250 m/s	300 m/s	350 m/s
Interface	Delamination area (mm^2)	Delamination area (mm^2)	Delamination area (mm^2)
45°/90°	55.7	51.2	26.0
90°/-45°	56.3	64.6	49.0
-45°/0°	58.3	97.8	81.0
0°/45°	60.1	94.0	127
45°/90°	64.0	87.4	85.0
90°/-45°	102	88.1	53.0
-45°/0°	161	172	103
0°/0°	138	134	147
0°/-45°	221	260	213
-45°/90°	160	178	127
90°/45°	92.7	154	80.6
45°/0°	245	251	116
0°/-45°	313	315	250
-45°/90°	193	213	129
90°/45°	281	328	383
Average:	**150**	**166**	**129**

Table B-3: Measured delamination areas for all interfaces in centre impacts (100–200 m/s).

	100 m/s	150 m/s	200 m/s
Interface	Delamination area (mm^2)	Delamination area (mm^2)	Delamination area (mm^2)
45°/90°	4.40	37.0	46.8
90°/-45°	-	35.9	50.3
-45°/0°	-	18.3	92.2
0°/45°	-	29.7	85.6
45°/90°	-	28.3	123
90°/-45°	-	39.6	106
-45°/0°	-	82.4	131
0°/0°	-	15.3	53.7
0°/-45°	-	40.4	163
-45°/90°	-	26.8	191
90°/45°	-	40.8	129
45°/0°	-	55.2	128
0°/-45°	-	29.7	52.2
-45°/90°	-	23.5	58.2
90°/45°	-	12.4	136
Average:	**4.40**	**34.4**	**103**

Table B-4: Measured delamination areas for all interfaces in centre impacts (250 – 350 m/s).

	250 m/s	300 m/s	350 m/s
Interface	Delamination area (mm^2)	Delamination area (mm^2)	Delamination area (mm^2)
45°/90°	57.0	129	175
90°/-45°	46.8	165	191
-45°/0°	78.7	210	184
0°/45°	103	288	161
45°/90°	128	324	238
90°/-45°	147	374	344
-45°/0°	122	421	412
0°/0°	187	457	582
0°/-45°	163	255	493
-45°/90°	283	459	420
90°/45°	392	343	305
45°/0°	137	543	552
0°/-45°	109	138	423
-45°/90°	65.2	213	311
90°/45°	177	460	409
Average:	**146**	**319**	**347**